SURFACE PHENOMENA IN LIQUID METAL ALLOYS

WITH APPLICATION TO

DEVELOPMENT OF A LIQUID METAL ION SOURCE OF B AND AS

Michael J. Bozack
B.S., Michigan State University, 1975
M.S., Michigan State University, 1977
M.A., Western Conservative Baptist Seminary, 1979

A thesis submitted to the faculty
of the Oregon Graduate Center
in partial fulfillment of the
requirements for the degree
Doctor of Philosophy
in
Applied Physics

January 14, 1985

The thesis "Surface Phenomena in Liquid Metal Alloys with Application to Development of a Liquid Metal Ion Source of B and As" by Michael J. Bozack has been examined and approved by the following Examination Committee:

PAUL R. DAVIS
Associate Professor
Thesis Research Advisor

LYNWOOD W. SWANSON
Professor
Thesis Research Advisor

ANTHONY E. BELL
Research Scientist

JACK H. DEVLETIAN
Associate Professor

ROBERT L. MARTIN
Professor
Lewis and Clark College

ACKNOWLEDGMENTS

Recognition is due to a number of individuals who have contributed to my scientific career. First, I wish to thank the members of my thesis committee for their guidance and stimulation, and for providing a superb education in experimental surface physics. Each has contributed in his own unique way: Lyn Swanson has allowed me to benefit from his considerable expertise in the field, Paul Davis has been a genuine friend and colleague whose door has always been open, Tony Bell has helped me discover the value of a good newspaper in scientific work, Jack Devletian has contributed invaluable criticism from the materials perspective, and Bob Martin has been a source of uncommon wit and advice.

Second, I am thankful to the physics department at Michigan State University and the staff of the National Superconducting Cyclotron Laboratory, who are responsible for my general education in physics.

Generous use of the high resolution scanning Auger microprobe was afforded by Dr. Gerald J. Lapeyre, director of the Center for Research in Surface Science and Submicron Analysis (CRISS) at Montana State University, and Mr. Doug Jones of the Materials Analysis Laboratory at Tektronix. The materials science and technology group at Los Alamos National Laboratory, headed by Dr. Robert G. Behrens, was responsible for manufacture of many of the B and As alloys in the

later stages of the project, and Dr. Robert L. Seliger and the ion beam technology group at Hughes Research Laboratories provided the prime motivation for this study.

The emission characteristics of the sources were generously supplied through the labor of Mr. G. A. Schwind.

A year at Carnegie-Mellon University was productive due to many enjoyable conversations with Dr. Hugh D. Young, who showed me how difficult a task textbook writing can be. Dr. Sherwood K. Haynes of Michigan State was instrumental in pointing me toward high standards in physics education.

I would like to acknowledge several scholarship programs that have financially supported me during my education: the State of Michigan Competitive Scholarship Program (1970-75), the Junior College Honors Scholarship Program (1973-74), the Michigan State University Scholarship Program (1972-76), the Student Aid Grant Program (1973-77), and the Clark Foundation Fellowship Award Program (1982-83).

Finally, I wish to thank my parents and family who have consistently supported me along this long academic road. In particular, my wife Carol has steadfastly stood beside me with unfailing humor and a common appreciation for good ice cream.

This work was supported by Hughes Research Laboratory (S1-202065-2) and the U.S. Government (83F854800).

DEDICATION

This dissertation is dedicated to the memory of my father (Joseph J. Bozack) and my stepfather (Eugene R. Roblee), whom I lost during its completion.

TABLE OF CONTENTS

LIST OF TABLES

LIST OF FIGURES

ABSTRACT

Surface Phenomena in Liquid Metal Alloys

with Application to

Development of a Liquid Metal Ion Source of B and As

Michael J. Bozack, Ph.D.
Oregon Graduate Center, 1985

Supervising Professors: Lynwood W. Swanson
Paul R. Davis

Liquid metal ion (LMI) sources are currently the subject of active investigation due to their potential application in microcircuit fabrication, focused beam technology, and surface analytical instruments. A LMI source is defined as a low volatility liquid metal film which flows to the apex of a solid needle support structure. Subsequent application of a high electric field deforms the liquid and results in ion emission.

Considerable interest has been shown in development of LMI sources capable of producing a variety of technologically important ions. For implantation of silicon, for example, B is the preferred p-type dopant, while As and P are the preferred n-type dopants. It has been difficult to construct long-lived ion sources based upon these species because B possesses a high melting point and reacts

strongly with most refractory metal supports, while As and P have high vapor pressures. Further, little is known about the surface behavior of high temperature liquid metal alloys.

To overcome these difficulties, the material and thermochemical properties of liquid metal alloy surfaces have been studied. A number of successful contact systems have been identified for B, while the development of a LMI source of As has been completely solved. To lower the chemical reactivity of B alloys, it has been necessary to utilize nonmetallic support structures, but then problems with wettability arise because wetting is dependent upon sufficient chemical reaction between alloy and substrate. The wettability of B-based alloys to nonmetallic substrates is governed by surface segregation of low-level, low surface tension impurities within the alloys. At melting, the molten alloy surface possesses a large concentration of segregated material (e.g., C and N) which inhibits reaction between alloy and substrate. This results in a poorly-wetted droplet of alloy with a large contact angle. Coating the substrate with a material having a high affinity to carbon (e.g., B or Si) acts to tie up the segregated material and promote wetting. When purified in this way, the alloy subsequently wets the virgin substrate.

Suppressing the high vapor pressure of As has been accomplished by constructing a liquid compound with a low (i.e., strongly negative) Gibbs free energy of formation. For a given arsenic compound, $AsX_n(l)$, where X is a low volatility element, the equilibrium condition between vapor and liquid is $AsX_n(l) = n\ X(g) + As(g)$. The equilibrium constant for this reaction is $K = P(As)\ P^n(X)$ and the Gibbs free energy is $dG = -RT \ln K$. When dG is strongly negative, K and P(As) will typically be smaller than the case of an ideal solution (no compound formation) of the same elemental constituents. Since the vapor pressure of As at the relatively low temperature of 600 C is nearly 1 atmosphere, it is necessary to lower the vapor pressure by over 10 orders of magnitude. This technique has been successful because the increased stability of the alloy results in a situation where it is energetically more favorable for As to exist in the liquid than in the gaseous state.

CHAPTER 1

INTRODUCTION

The goal of this research effort is to investigate the material and thermochemical properties of liquid metal alloy surfaces. The specific application to liquid metal ion sources is only one of many possible uses of this information. Interfacial phenomena between a molten metal and the solid surface of a high-melting material occur in many important technological processes, and constitute an integral part of the structure of materials. These processes include liquid phase sintering, crystalline growth from the melt, impregnation of porous solid materials by liquid binders, wetting, detergency, adhesion, wear, and catalysis. Two recent studies by the National Academy of Sciences have emphasized the importance of fundamental studies on the subject of interfaces, and have placed high priority on further research in this area [1-2]. The prime directive addressed in the present work is the development of a liquid metal ion source of boron and arsenic.

Liquid metal ion (LMI) sources are currently the subject of active investigation [3-8] due to their potential application in microcircuit fabrication, focused beam technology, and surface analytical instruments. A LMI source is defined as a low volatility liquid metal film which flows to the apex of a solid needle support

structure (see Figure 1-1). Subsequent application of a high electric field deforms the liquid and results in formation of a conical protrusion known as the Taylor cone [9-10]. Taylor [11] showed that the balance of liquid surface tension and electrostatic stress results in a stablized cone of half angle 49.3 degrees. Emission of singly charged ions occurs through field evaporation, whereby singly charged species are evaporated over the Schottky barrier formed by field deformation of the potential well [12]. Higher charged states are thought to arise by postionization, according to a theory developed by Kingham [13].

Considerable interest has been shown in development of ion sources capable of producing a variety of technologically important ions. For implantation of silicon, for example, B is the preferred p-type dopant, while As and P are the preferred n-type dopants. It has been difficult to construct ion sources based upon these species because B possesses a high melting point and strongly corrodes most metals, while As and P have high vapor pressures. Further, little is known about the critical properties of the liquid metal and substrate which provide reasons for improper source operation and guidance for successful source development.

The development of a useful LMI source of B and As ions involves the construction of a low melting alloy of B and As and a compatible solid support. The study of liquid alloy surfaces under conditions of high or ultrahigh vacuum is essential to verify required liquid and support properties. There presently exist but few published

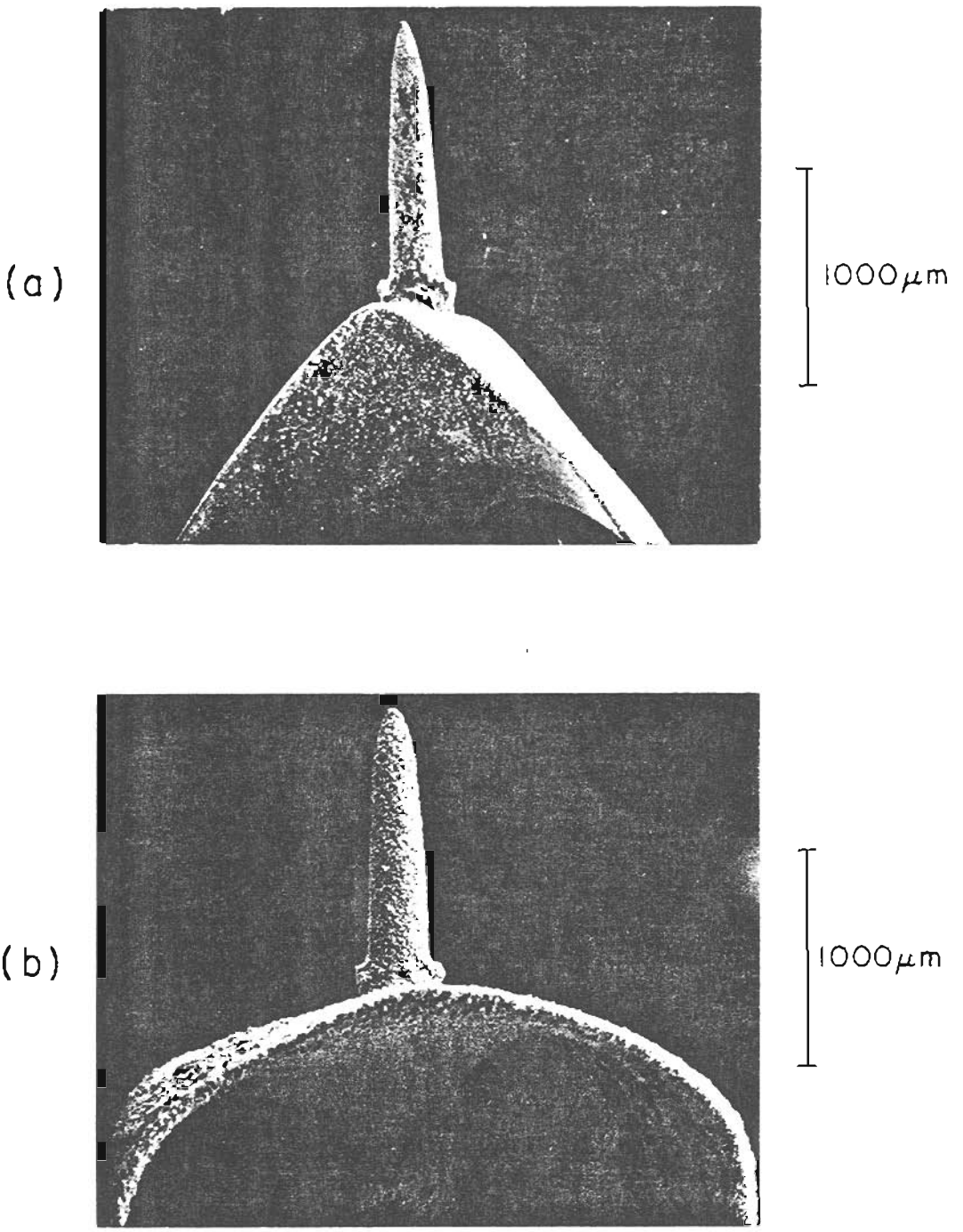

Figure 1-1. The appearance of a typical liquid metal ion source. (a) Source structure with loaded alloy; (b) Source structure after alloy exhaustion.

reports of the application of surface analytical techniques to the study of liquid metal alloys and the liquid-gas interface. This is particularly evident for Auger electron spectroscopy. Hardy and Fine [14], for example, in a 1982 paper remark that they were aware of only two previous applications of Auger spectroscopy to the study of liquid surfaces. One of the earliest studies was done by Berglund and Somorjai [15], who investigated surface segregation in Pb-In alloys. More recently, Goumiri and Joud [16] studied the effect of oxygen coverage on the surface tension and contact angle of the Al-Sn system. In light of the limited number of studies of the liquid surface, this dissertation represents the first treatment of the properties of B and As based liquid metal contact systems.

The experimental work presented in this dissertation represents part of a concerted effort by three laboratories in the United States to overcome the challenging gaps in fundamental understanding and existing limitations in the performance of liquid metal ion sources. The ion beam group of Hughes Research Laboratory (HRL) has been largely responsible for the initial motivation for the project, and has expended considerable effort to identify appropriate materials for B emitters. The materials chemistry group of Los Alamos National Laboratory (LANL) has synthesized many of the alloy compositions selected during the latter stages of the project. The surface physics group at the Oregon Graduate Center (OGC) has been responsible for fundamental investigations of the alloy systems, such as studies of wetting, surface composition, alloy work functions,

source life, solubility of alloy, and emission properties. This effort is described below. Close collaboration between the parties has been maintained throughout the contractual period through a series of ion source workshops.

REFERENCES

1. Physics in Perspective, National Academy of Sciences, Washington, D.C., 1972.
2. Materials and Man's Needs, National Academy of Sciences, Washington, D.C., 1974.
3. R. L. Kubena, C. L. Anderson, R. L. Seliger, R. A. Jullens, E. H. Stevens, and I. Lagnado, J. Vac. Sci. Technol. 19 (1981) 916.
4. R. L. Seliger, J. W. Ward, V. Wang, and R. L. Kubena, Appl. Phys. Lett. 34 (1979) 310.
5. L. W. Swanson, Nucl. Instrum. Methods 218 (1983) 347.
6. H. Arimoto, A. Takamori, E. Miyauchi, and H. Hashimoto, Jp. J. Appl. Phys. 23 (1984) L 165.
7. T. Ishitani, K. Umemura, S. Hosoki, S. Takayama, and H. Tamura, J. Vac. Sci. Technol. A 2 (1984) 1365.
8. W. L. Brown and A. Wagner, Proc. Int'l Ion Engineering Congress--ISIAT '83 and IPAT '83, Kyoto (1983).
9. D. R. Kingham and A. E. Bell, 31st Int'l Field Emission Symposium, Paris (1984) 65.
10. G. Benassayag and P. Sudraud, 31st Int'l Field Emission Symposium, Paris (1984) 79.
11. G. I. Taylor, Proc. R. Soc. London 280 A (1964) 383.

12. D. R. Kingham and L. W. Swanson, 31st Int'l Field Emission Symposium, Paris (1984) 59.

13. D. R. Kingham, Surf. Sci. 116 (1982) 273.

14. S. Hardy and J. Fine, "Studies of Liquid Metal Surfaces Using Auger Spectroscopy," in Materials Processing in the Reduced Gravity Environment of Space, ed. Guy E. Rindone (Amsterdam: Elsevier, 1982), pp. 503-511.

15. S. Berglund and G. A. Somorjai, J. Chem. Phy. 59 (1973) 5537.

16. L. Goumiri and J. C. Joud, Acta. Metall. 30 (1982) 1397.

CHAPTER 2

THE IDEAL LIQUID METAL ION SOURCE

Successful development of a liquid metal ion (LMI) source depends upon the satisfactory confluence of several critical design considerations. A number of desirable properties of the alloy and substrate exist which cannot be fully and simultaneously satisfied in a given alloy/substrate combination. Usually a compromise of some sort must be made, based upon the most important emitter properties.

The first desirable property of the alloy is that it possess a low melting point, which minimizes reaction between alloy and substrate. High melting materials can be made compatible by formation of binary and ternary eutectic mixtures which lower the melting temperature. The optimum solution is to choose a low-melting compound containing the element of interest or a broad eutectic that is low-melting. A deep eutectic is less favorable because a slight digression from the eutectic composition, such as could occur during dissolution of the alloy by the substrate, begins precipitation of second phase material. A low-melting compound, by contrast, retains its liquid integrity during such digressions. On the other hand, deep eutectics frequently possess lower melting points than compounds, which minimizes reaction, so usually a compromise must be made between low melting points and liquid integrity.

A second desirable property of the alloy is that it possess low volatility at the melting point. Low volatility is necessary to conserve the liquid film supply and promote long life. Elemental boron, for example, cannot be used because it has a high vapor pressure at its melting point and would volatilize completely if operated at this temperature for any significant period of time. A general rule of thumb is that component partial pressures greater than 10^{-7} torr are unacceptable. Alloy combinations must be chosen that possess a low Gibbs free energy of formation in order for the mixture to have sufficient stablity to lower the activity, and, hence, the vapor pressure above the alloy. This is especially true in the case of As alloys. The best solution is to choose an alloy composition that is congruently vaporizing at the melting temperature, as preferential vaporization of a particular species would eventually alter the original composition of the eutectic and shorten the lifetime of the source.

Third, it is desirable for the alloy to possess a high relative bulk concentration of B or As at the melting point. This is so because, if field evaporation is assumed to be the mechanism of ion formation, the current of ion species i is linearly dependent upon the fractional bulk concentration of atom i at the time of emission [1]. Best yields of B^+ or As^+ are therefore obtained by choosing an alloy composition having the highest mole fraction of B or As compatible with low melting. In typical binary alloys of B or As with metals, enrichment of the surface with B or As is known to occur

due to surface segregation of the component possessing the lowest surface tension. In alloys of metals and nonmetals, this component is invariably the nonmetal. The enrichment factor can be as high as 10,000, as shown by Seah and Hondros [2]. This effect, however, does not increase the relative intensity of B or As in the ion beam because the emission characteristics reflect the bulk (not the surface) stoichiometry of the material.

Fourth, to produce a sufficient intensity of ion current, it is necessary for the alloy to possess a favorable combination of binding energy, ionization potential, and work function. In the simple Schottky "image hump" field evaporation model of ion formation, the activation barrier Q(F) for formation of a singly charged ion is given by

$$Q(F) = H + I - W - 3.8\ F^{1/2}$$

where H is the binding energy of the metal, I is its ionization potential (eV), W is the work function (eV), and F is the field in V/A [3]. The resultant current I_i of ion species i of charge n is

$$I_i = P_i c \exp\ (-Q_i(F)/kT)$$

where c is a constant, P_i is proportional to the bulk concentration of atomic species i, and T is the absolute temperature. It is easy to see that a slight lowering of the activation energy results in a dramatic increase in ion emission due to the exponential relationship between the variables.

Fifth, it is advantageous for the liquid alloy to possess a low surface free energy in order to experience good wetting of the

substrate. The governing relation is Young's equation, discussed ahead, which relates the degree of wetting with the combined influence of the solid-liquid, solid-vapor, and liquid-vapor surface tensions. Young's equation shows that the best wetting is experienced when the alloy has the lowest possible liquid surface energy. This is intuitively sensible, as liquids with high surface tensions tend to close in on themselves to form spherical drops (the figure of least area and energy) rather than spreading out evenly on a surface. Good wetting, defined as a contact angle less than 90 degrees, is necessary to facilitate liquid flow from the reservoir to the apex tip where emission occurs.

Sixth, it is important that alloy wetting occur without excessive attack of the substrate, i.e., the rate and extent of diffusion of alloy components into the substrate must be minimal. This is especially true for boron containing alloys, as B is known to readily diffuse into most refractory metals forming metal borides. Diffusion of alloy components into the substrate alters its electrical resistivity, leading to a situation where the circuit power must be continuously monitored to prevent radical changes in source temperature. It is also true that dissolution of the substrate into the alloy material changes the composition of the eutectic, which acts to increase the melting point of the liquid metal and shut the emitter off. To remelt the alloy, an increase in power is necessary, which also increases the rate of dissolution, resulting in a runaway condition which terminates with catastrophic breakdown of the

emitter. An apparent solution is to select the most inert substrate available, but this is usually incompatible with good wetting. In most contact systems, wetting is due to a lowering of the liquid-solid interfacial energy during chemical bond formation, so the liquid metal must interact with the substrate to some extent. Some level of chemical interaction is therefore necessary, but excessive reaction results in attack of the substrate material by the liquid film. It may be that the best solution is to have no substrate at all by using a consumable electrode with localized heating of the apex region. This possibility has not been addressed in this thesis, but is a subject for future research.

Seventh, it is advantageous for the source to possess favorable mechanical, electrical, and vacuum properties. The substrate material should be readily machinable into sharp needles and have sufficient mechanical strength to tolerate electric fields of the order of tenths of volts per angstrom. If the substrate is too brittle, as is the case for many fine glassy needles, it may not survive handling during wetting and assembly operations. The coefficient of thermal expansion of the substrate material and its ability to withstand temperatures of the order of 1000 K must be adequate to prevent misalignment during operation of the source in a focusing column. The substrate surface should be easy to clean (for consistent wetting) and the source should be able to function effectively in less than ultra-high vacuum conditions.

Finally, in addition to alloy and substrate properties, the source must possess favorable emission characteristics. For focused

beam and implantation applications, it is necessary for the source to possess a small virtual source size and high angular intensity. Other source emission characteristics which affect performance are the relative intensities of the various ion species, the energy spreads of the various ion species, and the angular current intensity distribution. The goal is to produce intense and stable emission of the appropriate ion in a long-lived and low noise source. This dissertation does not directly address properties of the focused beam; mass spectrometric data for B and As sources will be reported in future publications by the OGC group.

Table I summarizes the most desirable properties of a liquid metal ion source. In view of the rigorous and often conflicting requirements, it is remarkable that materials can be identified that satisfy many of these demands to a high degree.

TABLE I

PROPERTIES OF THE IDEAL LIQUID METAL ION SOURCE

What	Why
Low melting point (MP)	Minimizes reaction between alloy and substrate
Low volatility at MP	Conserves film supply and promotes long life
High relative bulk concentration of ion species	Ion emission of species i linearly dependent on bulk mole fraction of i
Favorable combination of binding energy, ionization potential, and work function	Activation energy of field evaporation process dependent on these variables
Low alloy surface free energy	Promotes wetting and spreading
Low solubility of alloy in substrate	Dissolution of alloy in substrate alters its resistivity, forcing changes in heater current
Low solubility of substrate in alloy	Dissolution of substrate into alloy alters the alloy composition and increases its MP
Favorable mechanical, electrical, and vacuum properties	Emitter must be electrically conductive, able to withstand V/A fields, possess low power consumption, and be able to function in less than UHV
Favorable emission characteristics	For focused beam applications, the source must possess a small virtual source size, high angular intensity, and small energy spreads for the various ion species.

REFERENCES

1. E. W. Muller and T. T. Tsong, Field-Ion Microscopy--Principles and Applications (Amsterdam: Elsevier, 1969).

2. M. P. Seah and E. D. Hondros, Proc. R. Soc. A, 335 (1973) 191.

3. Muller, pp. 56-62.

CHAPTER 3

THE THERMOCHEMISTRY OF WETTING

A. Surface Tension and the Surface Free Energy

Surface atoms reside in an environment markedly different from bulk atoms. Not only are they surrounded by fewer neighbors than bulk atoms, but there is also an anisotropic distribution of these neighbors. As a consequence, no net force exists on the bulk atom deep within the material, but the surface atom is attracted by the net inward pull of the dense bulk concentration. Work must therefore be expended to raise the particle to the surface. To extend the surface area, chemical bonds between surface atoms must be stretched, or more atoms must be raised, and the work performed against the atomic forces during this process is the origin of surface tension. The free energy residing in the surface is the work spent on moving particles from the bulk to the surface, or in stretching existing surface atoms. The tendency for liquid surfaces to contract and assume the smallest possible area is a consequence of surface tension.

Surface tension may be viewed from three complementary perspectives. In the first perspective, surface tension is defined as the force per unit length required to extend an elastic surface.

A case in point consists of a thin film of liquid supported on a rectangular framework containing one movable side (see Figure 3-1).

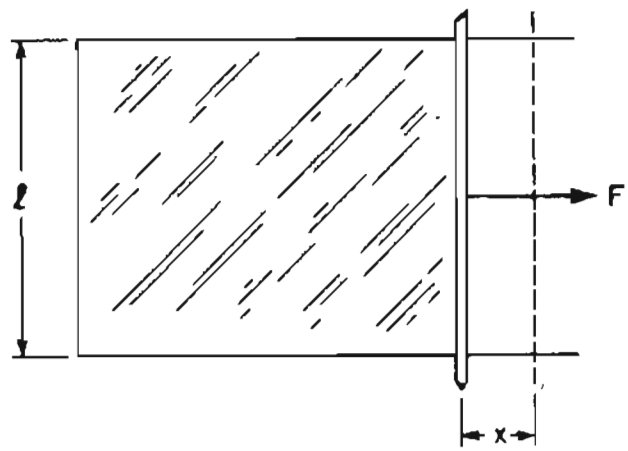

Figure 3-1. A rectangular framework supporting a liquid film with surface tension Θ.

If this side, of length l, is moved through a distance x so that new surface of area 2lx is created (the two sides of the film each contributing an additional area lx), the mechanical work required is $2lx\Theta$, where Θ is the surface tension. The surface tension may thus be considered as the force per unit length needed to pull the two sides of the surface out a distance x. If a force were no longer applied to the movable support, the liquid would return to its original dimensions. The surface tension is acting as a measure of cohesion, showing how much force is required to increase

intermolecular distances.

In the second perspective, the surface tension may be considered to be the energy per unit area needed to create more surface. By thermodynamic theory, the total reversible free energy of a surface at constant temperature and pressure is given by

$$W = GA$$

where G is the Gibbs free surface energy per unit area, and A is the surface area. Taking the differential of this expression, which has the effect of creating more surface, leads to

$$dW = d(GA)$$

and by the chain rule

$$dW = [d(GA)/dA]_{T,p}\, dA$$

$$= [G + A(dG/dA)_{T,p}]\, dA$$

The surface tension $\mathcal{G}$ is defined as the energy per unit area to create more surface

$$\mathcal{G} = (dW/dA)_{T,p} = G + A(dG/dA)_{T,p}$$

The first term of the expansion represents the energy/area necessary to create more surface by stretching the existing surface atoms. The second term is the energy/area necessary to create more surface by simple addition of more atoms. This term depends on atomic mobility and whether or not the new surface atoms are in a state of strain. It is nonzero for many cold worked solids at low temperatures because the new surface is due to unrelieved strain due caused by negligible diffusion rates. In the case of liquids, it is zero because liquid atoms are mobile and will be continuously transferred to the surface from the bulk and the number of atoms per unit surface area remains

constant. In this circumstance, no interatomic bonds are strained and the surface atoms maintain their relative displacements. There is thus no dependence of surface energy on area. Hence, only in the case of an unstrained surface does the surface tension equal the specific surface free energy.

The third perspective from which to view surface tension is in terms of chemical reactions. This viewpoint is especially important when speaking of the wettability of solids by liquid metals. It has been shown that an expenditure of energy is necessary to create new surface (e.g., paper does not spontaneously rip apart), and that the resulting surface atoms experience a net inward attraction not shared by bulk atoms. As a consequence, surface atoms possess a lower packing density (10^{15} atoms/cm^2) than bulk atoms

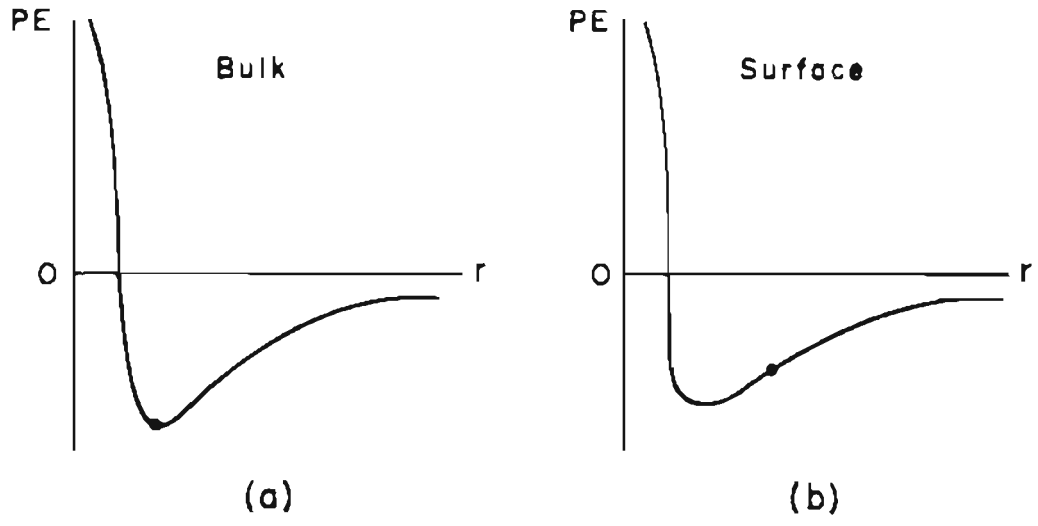

Figure 3-2. The potential energy (PE) diagram for an atom in the bulk and on the surface of the solid. In (a), an atom in the bulk is at the equilibrium spacing and feels no net force. In (b), the spacing between surface atoms is greater than the spacing between bulk atoms, resulting in a higher energy state and the generation of surface tension.

(10^{22} atoms/cm^3). Since surface atoms are farther apart than bulk atoms, they exist in a state of higher potential energy (see Figure 3-2).

The energy expended to create the surface thus resides in the broken surface chemical bonds. The importance for wetting phenomena is that wetting results from a lowering of the surface tension due to chemical reaction. If chemical reactions did not lower the system energy, they would not spontaneously occur.

B. Wetting, Spreading, and the Equations of Young and Dupre

For a liquid resting on a surface, one can determine the relationship between the different interfacial tensions from consideration of the balance of surface forces at the line of contact of the three phases (see Figure 3-3). The resulting expressions constitute the main thermodynamic equations of wetting theory.

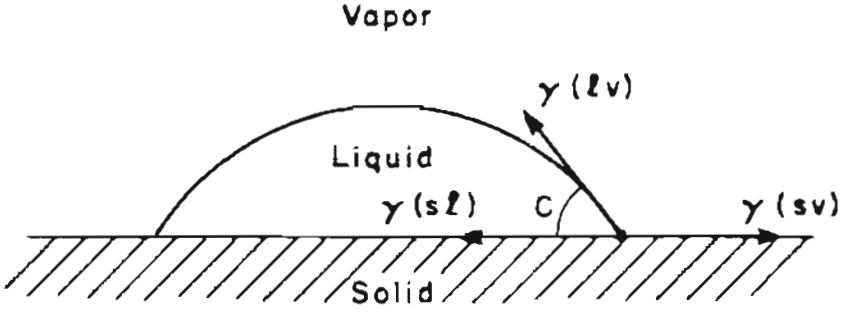

Figure 3-3. The equilibrium situation of a liquid drop on a solid surface used in the derivation of Young's equation.

Recalling that surface tension forces exert a tangential pressure along the surface, the balance of surface free energies along the interface results in Young's equation, first derived by T. Young in 1804 [1]:

$$\gamma(lv)\cos C + \gamma(sl) = \gamma(sv)$$

$$\cos C = [\gamma(sv) - \gamma(sl)]/\gamma(lv)$$

Here, $\gamma(lv)$ is the surface tension of the liquid-vapor interface, $\gamma(sl)$ that of the liquid-solid interface, $\gamma(sv)$ that of the solid-vapor interface, and C is the contact angle. The contact angle is defined as the angle between the solid surface and the tangent to the drop surface at the point of contact. For practical purposes, when the contact angle is greater than 90 degrees, the solid is said not to be wetted by the liquid. In this circumstance, drops of liquid have a tendency to move about on a surface and are not able to penetrate capillary pores. When the contact angle is near-zero, the liquid is said to wet the solid. It is easy to see from inspection of Young's equation that wetting improves as either $\gamma(sl)$ or $\gamma(lv)$ decreases. This frequently occurs during chemical reaction between the liquid and solid.

Young's equation has been criticized on a number of grounds, notably by Bikerman [2]. The major difficulty lies in the existence of the unbalanced vertical component of the liquid-vapor surface tension. A system in which an uncompensated force operates cannot be in equilibrium, but in the derivation of Young's equation, an equilibrium is presupposed in which only the three horizontal surface energy components participate. The dilemma has been resolved by

experimental evidence which suggests that small ridges appear in contact systems that are lifted by the vertical component. The vertical component is therefore balanced by the elastic stress induced upon the raised ridge. The effect is negligible for most ordinary metals and glasses, and most workers in the field assume the validity of the expression. Naidich [3] claims to have recently confirmed the Young relation experimentally.

A direct correlation exists between the wettability of solids by liquids and the energy of adhesion. Harkins and coworkers [4] defined the reversible work of adhesion between two phases as the energy necessary to separate a square centimeter of solid-liquid interface and re-form the solid-gas and liquid-gas interfaces. This is simply the energy necessary to pull the two phases apart, and corresponds to the difference in free energy between the states of Figure 3-4.

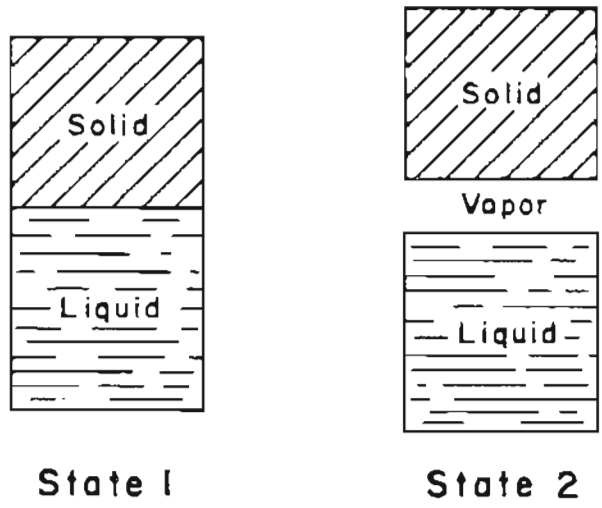

Figure 3-4. The two states used to define the work of adhesion as the difference in free energy required to eliminate the solid-liquid interface and reform the solid-gas and liquid-gas interfaces.

In terms of surface tension, the reversible work of adhesion is given by:

$$W(A) = \gamma(lv) + \gamma(sv) - \gamma(sl)$$

This is Dupre's equation. From this perspective, the work of adhesion is a convenient measure of the degree of chemical bonding between liquid and solid. Highly reactive systems result in increased wetting due to the greater degree of chemical bonding between solid and liquid. This may be seen directly by writing Dupre's equation in the form

$$\gamma(sl) = \gamma(sv) + \gamma(lv) - W(A)$$

It follows that the greater the adhesive energy W(A) between liquid and solid, the lower the surface tension $\gamma(sl)$. From Young's equation, this is precisely what is necessary to facilitate wetting. Energy released in the course of reaction between the liquid and solid can therefore be equated to the work of adhesion. In similar fashion, the work of cohesion W(C) may be defined as the reversible work required to separate liquid from liquid. Since $\gamma(sl)$ is now nonexistent,

$$W(C) = 2\,\gamma(lv)$$

Nonequilibrium conditions exist for which Young's equation does not describe the behavior of the contact system, since that equation was derived under supposed conditions of equilibrium. Two such conditions are those of complete wetting, when $\gamma(sv) > \gamma(sl) + \gamma(lv)$, and complete dewetting, when $\gamma(sl) > \gamma(sv) + \gamma(lv)$. In these cases, Young's equation is invalid because cos C becomes larger than unity, and equilibrium becomes impossible. It is therefore convenient to

introduce the spreading coefficient S to describe the wetting of a liquid on a solid. The spreading coefficient may be derived by consideration of a small virtual change in the surface free energy of the contact system. At constant T and P,

$$dG = [dG/dA(sv)]dA(sv) + [dG/dA(lv)]dA(lv) + [dG/dA(sl)]dA(sl)$$

but

$$-dA(sv) = dA(lv) = dA(sl)$$

and by the definition of surface tension,

$$[dG/dA(lv)] = \Theta(lv) \; ; \; [dG/dA(sv)] = \Theta(sv) \; ; \; [dG/dA(sl)] = \Theta(sl).$$

Substituting, and solving for $-[dG/dA(lv)]$ gives

$$-[dG/dA(lv)] = S = \Theta(sv) - \Theta(lv) - \Theta(sl).$$

The spreading coefficient S therefore represents the change in free energy when a liquid spreads over a solid surface. For decreases in free energy, such as occur for spontaneous reactions, S is positive. The system energy will be diminished by the action of spreading if the $\Theta(sv)$ exceeds the sum of $\Theta(lv)$ and $\Theta(sl)$. By utilizing the definitions of work of adhesion and cohesion, the spreading coefficient may be conveniently written as

$$S = W(A) - W(C).$$

From this viewpoint, the spreading coefficient provides a relative measure of cohesion and adhesion in the contact system. If the liquid has greater affinity for the solid than for itself, S is positive and spreading will readily occur. In general, this usually happens when a liquid of low surface tension is placed in contact with a solid of high surface tension.

C. The Gibbs Free Energy Function

Wetting has been shown to occur by operation of adhesive forces which lower the interfacial energy of the contact system. The thermodynamic parameter which provides the means to evaluate the feasibility of a given chemical reaction under specified conditions is the Gibbs free energy function. Any process in nature occurring at constant pressure is accompanied by a change in free energy, which is equal to the mechanical work exchanged during the process. The simplest interpretation of the free energy change is that reactions resulting in a loss of free energy are thermodynamically possible and are likely to proceed further toward completion as the change in free energy becomes increasingly negative in value. This interpretation follows from the definition of free energy. For the generalized reaction between a moles of A, etc., to form m moles of M, etc., written

$$aA + bB + \ldots = mM + nN + \ldots$$

the free energy change is related to the changes of enthalpy dH and entropy dS associated with the reaction by

$$dG = dH - TdS$$

where T is the absolute temperature. Hence, the Gibbs free energy function evaluates the feasibility of a given reaction by way of the difference between the enthalpy and entropy changes which occur during the reaction. When $dS = 0$, the enthalpy H is equivalent to the heat absorbed or evolved by the thermodynamic system during a process at constant pressure. Viewed in terms of reaction

probability, reactions that are exothermic are generally spontaneous and decrease the enthalpy, while those that are endothermic are generally nonspontaneous and increase the enthalpy. The entropy S measures the spontaneity of a given reaction with regard to randomness. By the second law of thermodynamics, there is a natural tendency for processes to proceed toward a state of greater disorder. Reactions that are spontaneous are associated with increasing dS, while those that are nonspontaneous are associated with decreasing dS. The Gibbs free energy change accounts only for the driving energy available and cannot predict the rate of a particular reaction limited by sluggish kinetics. It is often called the thermodynamic potential due to the similar role played by the seat of emf in an electrical circuit.

The Gibbs free energy change dG may be related to the equilibrium constant of the reaction by:

$$dG = -RT \ln K + RT \ln [a(M)a(N)/a(A)a(B)]$$

where K is the equilibrium constant and a(M), a(N), a(A), and a(B) are the activities of the various products and reactants at the given temperature T. By definition, the activity of a pure liquid, solid, or gas is equal to unity. When all of the reactants and products are in their pure standard states and the activities are unity, the change in the free energy is called the standard free energy change dG°. The isotherm then becomes

$$dG^{\circ} = -RT \ln K.$$

This direct relationship between the free energy change and the equilibrium constant is valid only when all of the activities are

unity; that is, all reactants and products are in their pure states. In cases involving solutions, the activity correction factor should be considered. However, since there is very little information available on the activities of substances in solution at high temperatures, it is generally necessary to assume that the activities of the individual components in liquid or solid solutions are equal to their mole fractions, and the activities of the components in gases are equal to their partial pressures.

D. Wetting in Equilibrium and Non-equilibrium Systems

The phenomena of wetting and adhesion have been studied since the early 14th century in low-temperature contact systems. The early studies addressed the wetting of various solid bodies by such common substances as water, mercury, and organic liquids. In contrast, studies of solid body wettability by molten alloys at high temperatures is a recent development possessing a number of unique features due to the high temperatures involved.

When a liquid is in contact with the surface of a solid body, the system may or may not be in thermodynamic equilibrium. Many contact systems at high temperature fall into the latter category due to the strong potential for interaction between liquid and solid at high temperatures. This is particularly true for high melting liquid metals.

For contact systems at equilibrium, the pressure, temperature, and chemical potential of each component are identical. When

equilibrium compositions of the contacting phases are brought together, the interface is characterized by a particular surface tension and the system remains at equilibrium. Any non-equilibrium effects due to surface segregation or kinetics are assumed to occur instantaneously and are therefore ignored. The interfacial energy $\theta(sl)$ is solely a function of the nature of the contacting phases and would decrease if their properties were made increasingly similar, the best wetting resulting when the phases are the same. This is because further reaction is prohibited at equilibrium, and $\theta(sl)$ can only change by changing the phases themselves. In such systems, the equilibrium equations of wetting are fully applicable, and the contact angle is given by Young's equation. Examples are contact systems with completely immiscible components.

For non-equilibrium systems, the pressure and temperature are usually identical, but the chemical potentials of the solid and liquid phases are not. Such a situation commonly occurs in binary isomorphous systems where the components are mutually soluble in all proportions and in all states. During contact, processes (e.g., diffusion, dissolution, and chemical reaction) occur which act to equalize the liquid and solid chemical potentials as the system approaches equilibrium. The change in component chemical potential has been found [5] to be directly proportional the corresponding change in surface tension, which in turn is related to the mechanism of reaction between liquid and solid. For systems where the solid phase is partially soluble in the liquid (but the reverse is not true), Aksay [6] has found that a minimum occurs in the graph of

surface tension vs time (see Figure 3-5). In contrast, for contact systems where a high-melting compound forms at the interface, the surface tension decreases to a particular value and remains constant. The formation of a compound at the interface is speculated to decrease the rate of component diffusion sufficiently to prohibit significant further reaction. Systems possessing non-equilibrium wetting obey the Young and Dupre equations only for very slow or quasi-static changes in contact angle.

E. Physical and Chemical Wetting

Wetting is often distinguished by the nature and intensity of chemical bond formation between solid and liquid. A formal correspondence exists between the terminology of wetting and surface adsorption. In the case of physical wetting, or physiwetting, the adhesive forces between solid and liquid are due to: (1) establishment of equilibrium chemical bonds, characterized by mutual saturation of free valences of the contacting surfaces; and, (2) Van der Waals, dispersive interactions. In physiwetting, the establishment of chemical bonding is not associated with rupture or partial dissociation of the interatomic bonds in each of the phases. The work of adhesion may therefore be written

$$W\ (eq) = W\ (sat) + W\ (vdv)$$

where W (sat) is the work of adhesion due to mutual saturation of free valences, and W (sat) is the work of adhesion due to establishment of Van der Waals bonding at the interface. The value

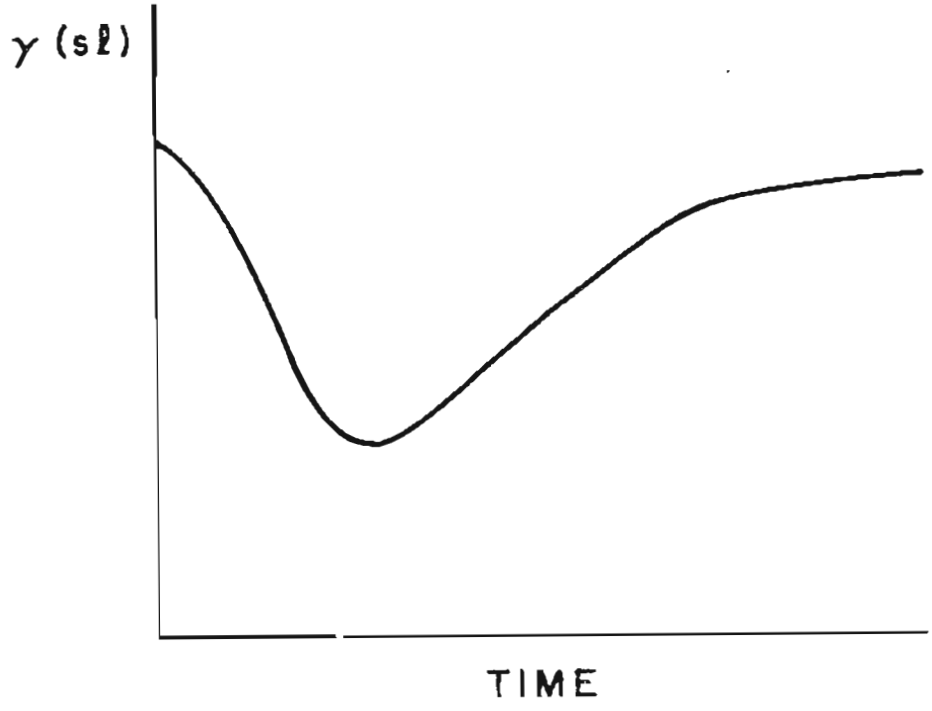

Figure 3-5. A graph of interfacial tension vs time for the case where the solid substrate is partially soluble in the liquid.

of W (sat) is usually small in systems where a large difference exists in the nature of the contacting phases, e.g., liquid metals and non-metallic crystals. In such cases the dispersion contribution is dominant, and can be readily estimated. The wetting is relatively insensitive of temperature, and typical bond energies are of the order of a few kcal/mole. Physically wetted systems are commonly found among phases with significant interatomic bonding and high surface energies.

In the case of chemical wetting, or chemiwetting, strong interactions between solid and liquid lead to significant adhesion and surface chemical reaction. Interphase atoms are bound by ionic or covalent bonding, with typical bond energies of 10-100 kcal/mole. The wetting is usually strongly temperature dependent, and is often manifested by the existence of a particular temperature (wetting threshold) where the contact angle begins to sharply decrease due to kinetics or reduction of an oxide layer. Substantial rupture and reformation of surface bonds occur during wetting. The high melting temperature liquid alloys and the substrates used in this study form examples of chemical wetting. Due to the chemical nature of the reaction mechanism, it is possible to estimate the energy of adhesion W (non-eq) from thermodynamical principles. For example, for the generalized reaction

$$mA + nB = p[A(m)B(n)]$$

describing the interaction between m moles of A and n moles of B to produce product AB, W (non-eq) is given by

$$W\ (\text{non-eq}) = dG = -RT \ln K + RT \ln [a(AB)^p / a(A)^m b(B)^n]$$

where a is the activity. Standard Gibbs free energies of formation as a function of temperature have been tabulated for many materials, and are readily available in the literature. The thermodynamic parameter of greatest use in predicting the degree of wettability appears to be dG(A) - dG(B), where dG(A) measures the affinity of the liquid for the solid, and dG(B) measures the affinity of the solid for itself. The best wetting occurs for low values of this parameter, which means that a strong tendency exists for breakdown of the solid and recombination with the liquid. This is discussed in more detail below.

F. Wettability of Solids by Liquid Metals: A Review of Current Understanding

1. Introduction

A considerable number of experiments has been performed to elucidate the phenomena of solid body wettability by high-temperature melts. The Soviet effort has been particularly extensive. The results are best summarized by Naidich [7], who divides the behavior into classes in accordance with the chemical nature of the wetted solid. Three classes are readily distinguished: (1) Ionic compounds, (2) Covalent compounds, and (3) Metals. Ionic and covalent compounds are solids with closed electronic configurations and saturated interatomic bonding. Wettability is usually possible only by rupture or partial dissociation of the near-surface bonding. In contrast, the wettability of a metalllic surface is relatively greater than

that of an ionic or covalent solid because wetting may occur without dissociating bonds within the metal.

Important perspectives are gained regarding liquid metal wettability through use of Auger electron spectroscopy. Since wetting depends critically on the near surface region of the interacting materials, only limited progress was made in the pre-1970 studies due to the limited availability of modern surface analytical techniques, although extensive measures were often taken to try to insure a high degree of purity and cleanliness for the materials used. Most of the existing information on wetting falls into this category. It will be shown below that wetting of liquid metal alloys to solid substrates is directly affected by the degree to which low-level impurities segregate to the alloy surface. Although significant bulk data have been obtained by standard metallographic and microprobe analyses, the question of what is occurring at the surface persists. Care in reading the early literature is therefore essential. Our review will focus on guiding principles rather than specific experiments.

2. The Wettability of Ionic Compounds by Liquid Metals

Considerable effort has been expended to understand the principles governing the wetting of ionic solids by metal melts. Metallic oxides (e.g., Al_2O_3, MgO, BeO, SiO_2, etc) have received the greatest attention. As a rule, metal oxides are poorly wetted by liquid metals, although there are important exceptions (Ti,

Zr, Mg, Al). The experimental facts (e.g., Figure 3-6) support the notion that: (1) oxide wettability increases with growing affinity of the liquid metal for oxygen; and, (2) a general inverse correlation exists between the thermodynamic stability of the metal oxide and its wettability by the liquid metal. The weaker the interatomic bonding between the metal and oxygen in the oxide, the greater the wetting of the oxide by the liquid metal.

These ideas are supported by structural and thermochemical considerations. The outermost surfaces of most high-melting oxides are formed by oxygen anions [8], which are large in comparison to the metal cations (see Figure 3-7). The reaction mechanism between a metal melt and a metal oxide is therefore controlled by a metallic interaction with the oxygen of the oxide, which may be written as follows:

$$LM + MO = M + LMO$$

where LM is the liquid metal, MO is the metal oxide, M is the metal cation of the metal oxide, and LMO is the liquid metal oxide formed during wetting. The change in Gibbs free energy for the reaction is

$$dG = dG(prod) - dG(react)$$

$$= dG(LMO) - dG(MO)$$

where dG(prod) is the free energy change associated with the oxidizing reaction of the liquid metal, and dG(react) is the free energy change associated with the metal forming the solid oxide (recall that there is no contribution to dG for elements). In other words, dG(prod) measures the thermochemical affinity of the liquid metal for oxygen, and dG(react) measures the thermochemical affinity

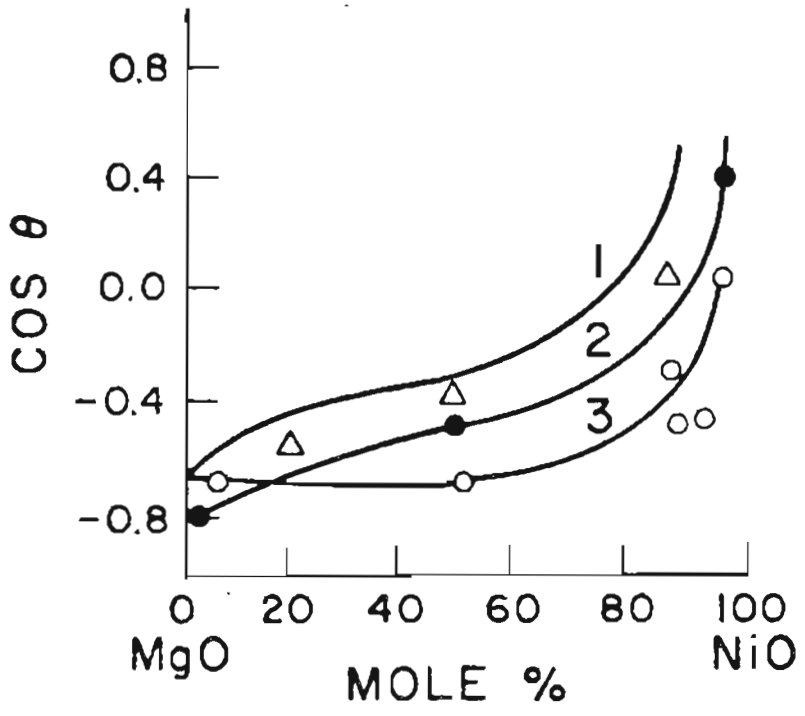

Figure 3-6. The wettability of solid solutions of MgO-NiO by 1-tin (1000 C), 2-copper (1200 C), and 3-silver (1100 C). Since dG (MgO) is less than dG (NiO), NiO is less stable than MgO and has lower contact angles.

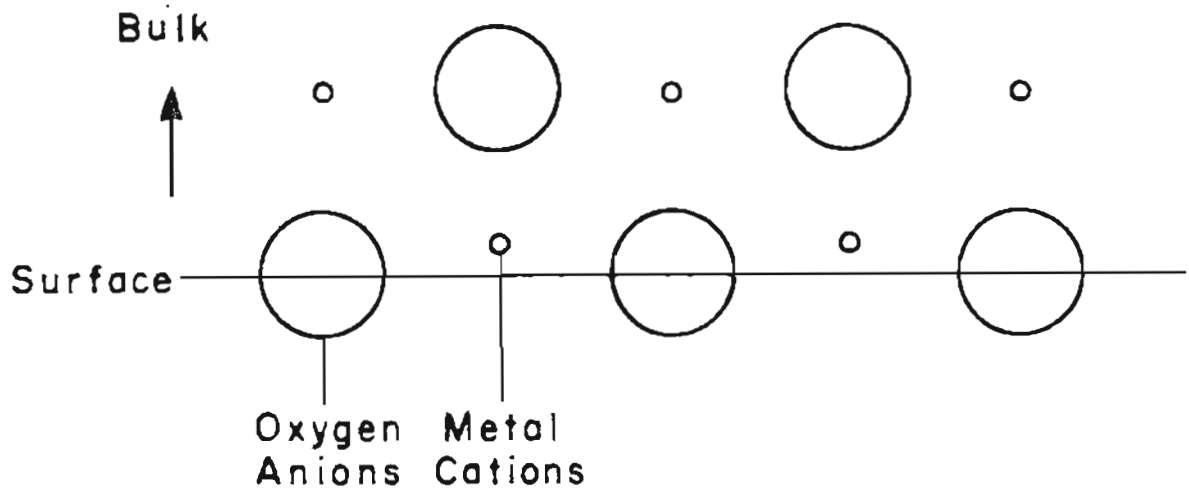

Figure 3-7. The surface structure of refractory oxides as proposed by Weyl [8].

of the solid oxide for oxygen. To facilitate wetting in nonequilibrium systems, it is necessary for intensive reaction to occur between the liquid metal and the solid oxide, which occurs when dG(prod) is as small as possible, and dG(react) is as large as possible. This simply says that dG measures the degree of solid oxide wettability by comparing the cohesive forces of the solid oxide with the adhesive forces between liquid metal and oxygen.

Naidich [9] provides data which compares the wettability of various oxides by liquid metals and the free energy of formation dG of the solid phase oxide and of the oxide formed by the liquid metals (see Figure 3-8). Fifty-three different contact systems are considered. Despite a good deal of scattering, there is a general tendency for wettability to decrease with decreasing values of dG. The fit may be subject to improvement by use of modern analytical equipment and improvements in experimental determinations of contact angle.

3. The Influence of Additives on Wettability

It was noted above that elements such as Ti and Zr represent notable exceptions to the rule that ionic solids are poorly wetted by liquid metals. In fact, a number of elements have been identified which, by themselves or by addition to an inactive metal, actively wet oxide materials. The property that each of the additives possess in common is a high affinity for oxygen. The discussion here will focus on Ti and O, which are sufficient to illustrate the principles

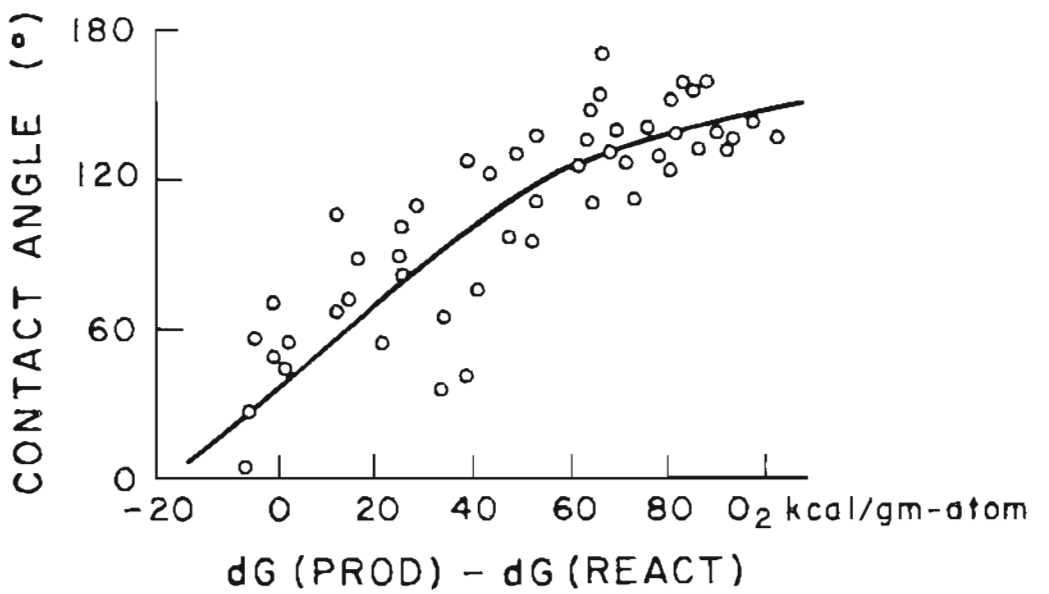

Figure 3-8. Correlation between the wettability of 53 oxides by liquid metals and the difference in free energy between the solid oxide dG(react) and the oxide formed by the liquid metal dG(prod). From Naidich [9].

involved.

To cite one example among many, for the case of wetting of Sn to SiO_2, addition of a small amount of Ti drastically lowers the contact angle [10]:

Ti content (atomic %)	0	1	2	3	4	6
Contact angle (^{o})	152	66	37	19	6	0

The sharp decrease in contact angle with small elemental concentrations of titanium is explained by the high reactivity of Ti to the predominantly oxide surface of the metal oxide substrate, and is a characteristic feature for additives that are interfacially active. The reaction mechanism involves surface segregation of the Ti to the liquid metal-solid oxide interface where an interlayer of TiO or Ti_2O_3 forms [11]. The accompanying reaction facilitates wetting.

A similar decrease in contact angle is found for small additions of oxygen to the liquid metal [12-13]. In this case, it is expected that neutral atoms of the liquid metal cannot be strongly bound at the interface due to repulsive forces between the electron cloud of the liquid metal and the negative ion of the oxide surface layer (see Figure 3-7). Interfacial bonding is possible, however, by the addition of a small amount of dissolved oxygen to the liquid metal. This occurs when atoms of the liquid metal shed valence electrons to atoms of dissolved oxygen (oxygen has high electron affinity). Wetting is thought to occur when the resulting positive ions are attracted to the oxygen anions of the solid oxide surface where they become ionically bonded. While direct experimental support for this

hypothesis is lacking, it appears to be possible to elicit similar improvements in wettability by substitution of other additives which are soluble in liquid metals and possess a high affinity for electrons [14-16]. The role of oxygen is apparently not specific.

4. The Wettability of Covalent Solids by Liquid Metals

Covalent high-melting solids such as nitrides, borides, and carbides are characterized by low Gibbs free energies of formation and are quite stable. Due to the high interatomic strength and closed electronic configurations of these materials, the equilibrium contribution W (eq) to the work of adhesion is negligible, and wettability is possible only by intensive interaction between atoms of the solid and the liquid metal. Due to its importance in liquid metal ion source applications, the discussion here will focus on the properties of carbide and graphite wettability. We mention only that, since the thermodynamic stability of these materials generally increases in the order carbides, borides, and nitrides, then wettability by liquid metals is expected to decrease in the same order.

For good wetting of graphite, the liquid metal must enter into reaction with carbon by forming carbides, dissolving carbon, or diffusing into carbon. The role of physical forces is minimal. The specific mechanism of interaction appears to depend upon the properties of the liquid metal [17]. Different bonds can be established because C has four valence electrons and can be either a

donor or acceptor of electrons. Ionic bonds are favored if the liquid metal is predominantly electropositive, i.e., a metal from the alkali or alkaline earth families. In these cases, a carbide interlayer is often formed. Metallic bonds are favored if the liquid metal is a transition metal with unfilled d-shell orbitals. Here, the C atom donates electrons to the d-band of the liquid metal to arrive at a satisfactory electronic configuration. The carbon is therefore positively ionized. Using electron transfer data, Franzevich [18] has determined the charge of dissolved carbon in transition metals:

Transition metal	Ti	Ta	W	Fe	Co	Ni
Value of C charge	+4.0	+2.8	+0.6	+3.8	+2.6	+1.8

The general trend is for C to donate sufficient electrons to complete a filled or half-filled shell. Covalent bonds are favored if the liquid metal possesses outer p electrons, such as occur for elements on the right side of the periodic table. Stable carbides often result from the interaction. The highest adhesive energies result from metallic bonding, i.e., liquid transition metals display the greatest wettability of covalently bonded solids.

An extensive collection of empirical data on the wettability of graphite by liquid metals exists, particularly in the Russian literature. Naidich [19] provides a useful summary of this literature, classified by subgroups of the periodic table. The lowest degree of graphite wettability is displayed by metals of the IV-B, V-B, and VI-B subgroups (see Figure 3-9). These metals are practically inert to graphite. They do not form stable carbides, and

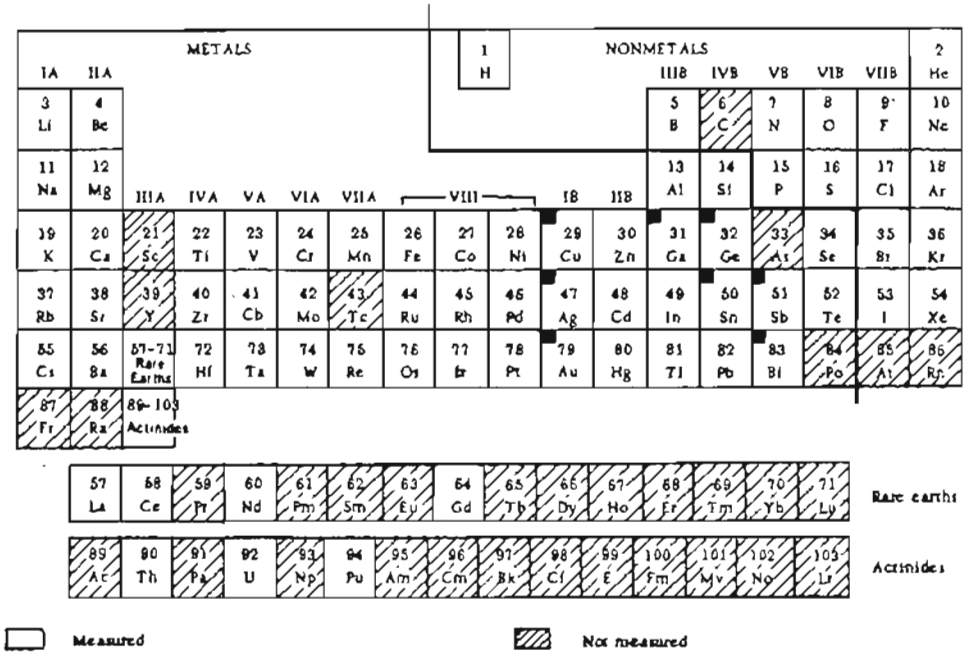

Figure 3-9. The wettability of graphite by liquid metals of the IV-B, V-B, and VI-B groups. Elements labeled by ■ have been shown to be practically inert to graphite. Details are given in [9]. Experimental surface tension values have been reported for liquid elements denoted by □.

dissolve only small amounts of C (0.001-0.1 atomic %) up to the boiling point of the liquid. Typical bond energies are low, of the order of 0.5-1.0 kcal/mole. The highest degree of graphite wettability is displayed by the transition metals, as discussed above (see Figure 3-10). Liquid transition metals react strongly with graphite, either in pure form or as additives to other elements. Typical adhesive energies are near 20-30 kcal/mole, and wetting occurs by carbide formation, chemical interaction, or dissolution of the graphite in the melt. The adhesion activity is related to the extent to which the metallic d-band is empty. As a whole, the energies of adhesion decrease from Ti to Ni, corresponding to an increase in the filling of the metallic d-band. For example in the case of adhesion to graphite:

Metal	Ti	Fe	Ni
W (erg/cm^2)	3920	3340	2985
θ (deg)	0	37	45

Intermediate in graphite wettability are elements forming covalent bonds with carbon. The elements which have been studied in this class are Si, Ge, Al, and B. In pure form, these materials wet graphite with adhesive energies of the order of 10 kcal/mole. The adhesion is good, but is on the whole lower than that of transition metals. An interesting observation relevant to the boride materials studied in this report is that a small amount of B added to metals appears to increase the wettability to graphite. This is seen in the case of Cu [20-21]. Pure copper by itself is inert to graphite, forming a contact angle of 140 degrees; however, when 5% B is added

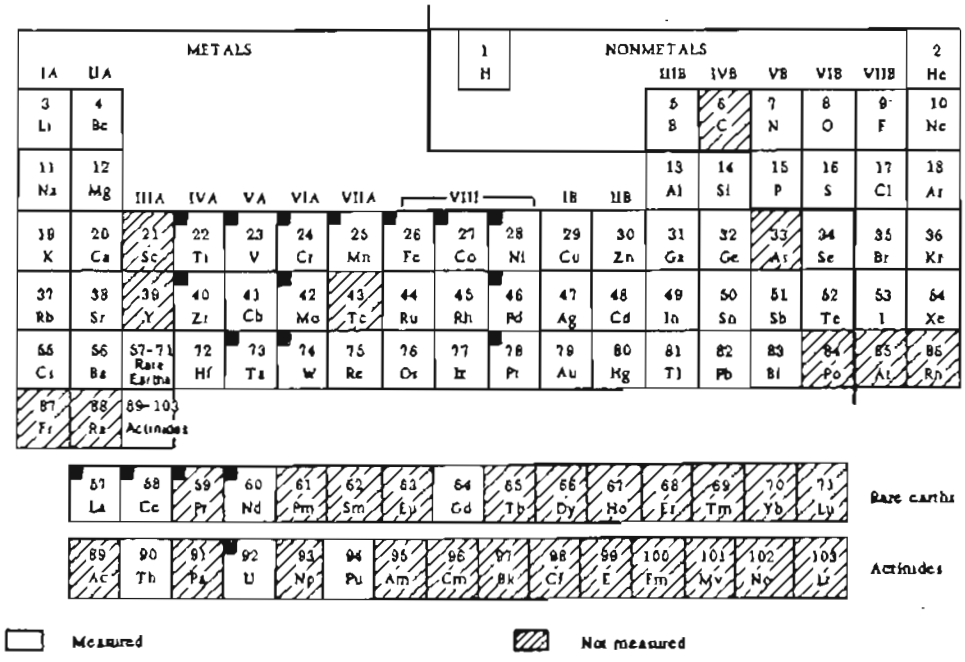

Figure 3-10. The wettability of graphite by liquid transition metals. Elements labeled by ■ have been shown to react strongly with graphite. Details are given in [9]. Experimental surface tension values have been reported for liquid elements denoted by □.

to it, the contact angle dramatically decreases to 36 degrees. Apparently, the boron segregates to the interlayer to form boron carbides. Based upon this information and the excellent wetting displayed by transition elements on graphite, one expects that borides of transition metal elements are likely to strongly react with carbon and wet with small contact angles.

5. The Wettability of Metals with Liquid Metals

The high degree of reactivity of metals is well known, and therefore metal-metal contact angles are expected to be small. Our studies have confirmed this for the case of B and As-containing liquid metal alloys on metals. The same general laws governing wettability in contact systems of liquid metals and covalent and ionic solids are also applicable in liquid metal-solid metal systems. That is, wettability depends upon the solubility of the liquid metal in the solid, and the ability of the system to form interfacial compounds. These assertions have been verified in studies by Hildebrand [22] and Tamman and coworkers [23]. Nonwetting systems are found in cases where there is neither interaction nor solubility.

Two interesting studies uncovered during this work provide guiding principles governing the selection of materials for best wetting. Gorjunov [24], who investigated the dependence of wetting on phase diagram appearance, found that wettability increases as the phase diagram changes from one with simple immiscibility to one with

eutectics, compounds, and solubility, as expected by the chemical reaction theory of wetting. Similarly, studies by Bailey and coworkers cited by Taylor [25] show that wettability in solid metal-liquid metal systems increases as the difference in fusion temperature between the metals decreases. This simply means that wetting is better in systems where the metals are alike, due to the greater degree of mutual solubility and diffusion in such systems.

In most studies of wettability, implicit faith is placed in the purity and integrity of the materials used. Numerous situations in the literature exist where initial reports of poor wetting have later been found to occur because of an unreduced oxide layer at the surface of the solid [26]. Heat treating, chemical reaction, and ion etching have been commonly employed to clean wetting surfaces, but in the absence of Auger electron spectroscopy and other surface sensitive probes, the assumption of surface cleanliness is dubious at best. The importance of using in situ surface analytical techniques in the study of contact systems is the subject of the next chapter.

REFERENCES

1. T. Young, Trans. R. Soc. 94 (1805) 65.
2. J. J. Bikerman, Physical Surfaces (New York: Academic Press, 1970).
3. Ju. V. Naidich, Kontaktnie Javlenia v Metallicheskih Rasplavah, Nakova Dumka, Kiev, 1972.
4. W. D. Harkins, Z. Phys. Chem. 139 (1928) 647; The Physical Chemistry of Surface Films (New York: Reinhold, 1952).
5. A. A. Zhukhovitsky, V. A. Grigorjan, and E. Mihalik, DAN USSR 155 (1964) 392.
6. J. A. Aksay, C. E. Hoge, and J. A. Pask, J. Phys. Chem. 78 (1974) 1178.
7. Ju. V. Naidich, Prog. Sur. Membrane Sci. 14 (1981) 353.
8. W. A. Weyl, Ceram. Age 60 (1952) 28.
9. Naidich, Prog. Sur. Membrane Sci. 14 (1981) 385.
10. Ibid., p. 388.
11. Ju. V. Naidich, V. S. Juravlev, and V. G. Chuprina, Poroshkovaja Metallurgia 11 (1973).
12. K. Momma and H. Suto, J. Japan. Inst. Metals 24 (1960) 374.
13. Naidich, Prog. Sur. Membrane Sci., pp. 391-393.
14. G. A. Holden and W. D. Kingery, J. Phys. Chem. 59 (1956) 557.
15. D. A. Bradhurst and A. S. Buchanan, J. Phys. Chem. 63 (1959) 1486.

16. D. A. Bradhurst and A. S. Buchanan, Austr. J. Chem. 14 (1961) 409.

17. Naidich, Prog. Sur. Membrane Sci., pp. 409-445.

18. I. N. Franzevich and I. I. Kovensky, DAN Ukranian 8 (1961).

19. Naidich, Prog. Sur. Membrane Sci., pp. 414-428.

20. Ju. V. Naidich and G. A. Kolesnickenko, Uzaimodeystvie Metallicheskih Rasplavov s Poverhnostju Almaza e Graphita, Nakova Dumka, Kiev, 1968.

21. Naidich, Prog. Sur. Membrane Sci., p. 421.

22. I. Hildebrandt, T. Hognaas, and H. Taylor, J. Am. Chem. Soc. 45 (1923) 2828.

23. G. Tamman and F. Arnstz, Z. Anorg. Chem. 192 (1930) 43.

24. Ju. V. Gorjunov, Uspeki Chimii 33 (1964) 9.

25. J. W. Taylor, J. Nucl. Energy 2 (1955) 15.

26. M. E. Schrader, J. Coll. Interface Sci. 100 (1984) 372.

CHAPTER 4

EXPERIMENTAL PROCEDURE

A. Vacuum Requirements, Wetting Procedure, and Temperature Measurements

There appear to be few fundamental limitations preventing the study of low vapor pressure liquid surfaces under conditions of ultra-high vacuum. Indeed, the experimental arrangement of most standard commercial vacuum systems is ideally suited for such studies. The majority of work here was carried out in an ULTEK TNB-X 250 l/s ultra-high vacuum system, containing a Physical Electronics CMA Model 10-155 Auger Electron Spectrometer. This system has a base pressure of 1 X 10^{-10} torr. Conditions of ultrahigh vacuum were maintained throughout the early experiments to minimize contamination which could substantially affect the chemical and electronic properties of the surface being investigated. Later work showed pressures less than the 10^{-6} torr range to have little effect upon the liquid surfaces and this requirement was relaxed. Nonetheless, no experiment was begun at pressures greater than 1 X 10^{-7} torr.

The sample support mechanism is shown in Figure 4-1. This mechanism allowed an unusual perspective of the alloy surface to be appreciated due to the adjustable electrical contacts on each side of the solid substrate. A temperature gradient could be generated

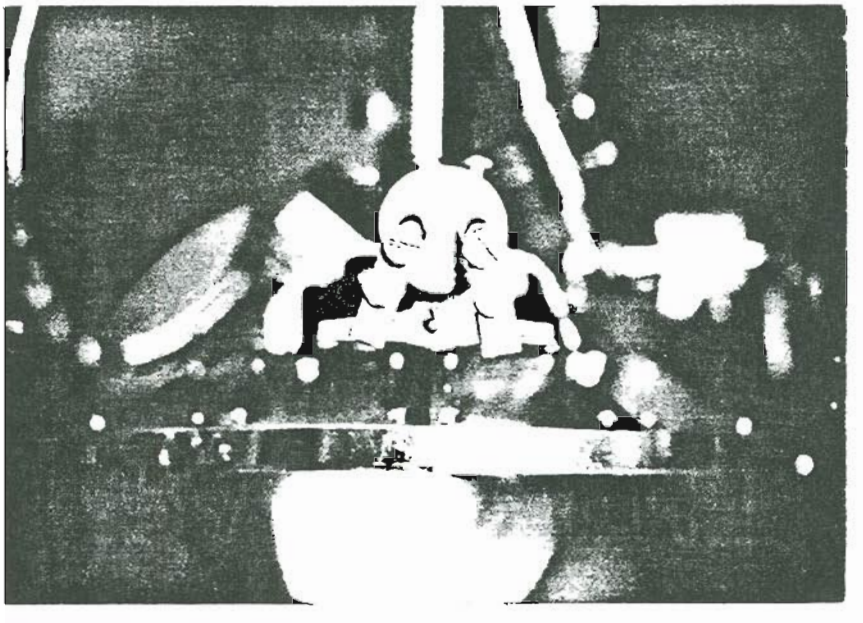

Figure 4-1. Specimen support mechanism with alloy and substrate installed. The view is through the front window port of the ultra-high vacuum chamber at OGC.

across the ribbon which enabled observation of the alloy under liquid and solid conditions simultaneously. This proved to be advantageous in many experiments, but in general was burdensome due to the difficulty in achieving uniform heating of the substrate. A typical wetting experiment utilizing a solid fragment of alloy began by mounting the substrate in a horizontal plane inside the vacuum chamber. A small amount of solid alloy was then placed atop the substrate and the system was evacuated. Contact between alloy and substrate was maintained by gravity and no adhesive was used. The substrate was then heated resistively by a D.C. power supply until alloy melting and wetting was observed. If wetting occurred with a small contact angle, it was necessary to vent the chamber and remount the sample in a vertical plane in order to face the Auger beam. If the contact angle was poor, analysis of the resulting droplet could proceed without re-evacuation. A vertically positioned Auger analyzer would have allowed faster turnaround times by making sample remounting unnecessary. Powdered alloys were usually applied to a vertically oriented substrate in the form of a slurry with acetone to facilitate adhesion. The acetone completely volatilized at low temperatures with no effect on the alloy composition or subsequent wetting. Analysis was possible at any time after evacuation.

Temperatures were measured by means of a single wavelength (0.65 micron) micro optical pyrometer manufactured by Pyrometer Instrument Co, Inc, Bergenfield NJ, USA. Knowledge of the substrate emissivity as a function of temperature allowed an absolute temperature calibration to be formulated by comparison of alloy and substrate

brightnesses (see Figure 4-2). Eutectic melting temperatures were determined by direct observation during heating. An overall morphological change in appearance of the alloy, accompanied by a sudden change in reflectivity of the surface could be easily observed in both optical and scanning electron microscopes. The melting temperature of off-eutectic compositions is more difficult to determine, as a sequence of melting events is observed rather than a definite transition from solid to liquid. In such cases, the temperature at which liquifaction is first observed through a low-power optical microscope is defined as the melting point. Small amounts of low-level inpurities in the alloys appeared to have little effect on the measured melting points, and we believe our melting temperatures to be accurate to 5 degrees for eutectics and 20 degrees for off-eutectics. The alloy surfaces were found to be effectively cleaned of adsorbed gases by annealing and no sputtering was necessary.

B. Auger electron spectroscopy

A number of surface sensitive analytical techniques have been employed in this study of liquid metal alloys. The most useful has been Auger electron spectroscopy, which provides information concerning the chemical identity of surfaces. A vast literature exists on the topic of Auger analysis [1]; however, it is useful to provide a brief description of the technique with special reference to the study of liquid surfaces.

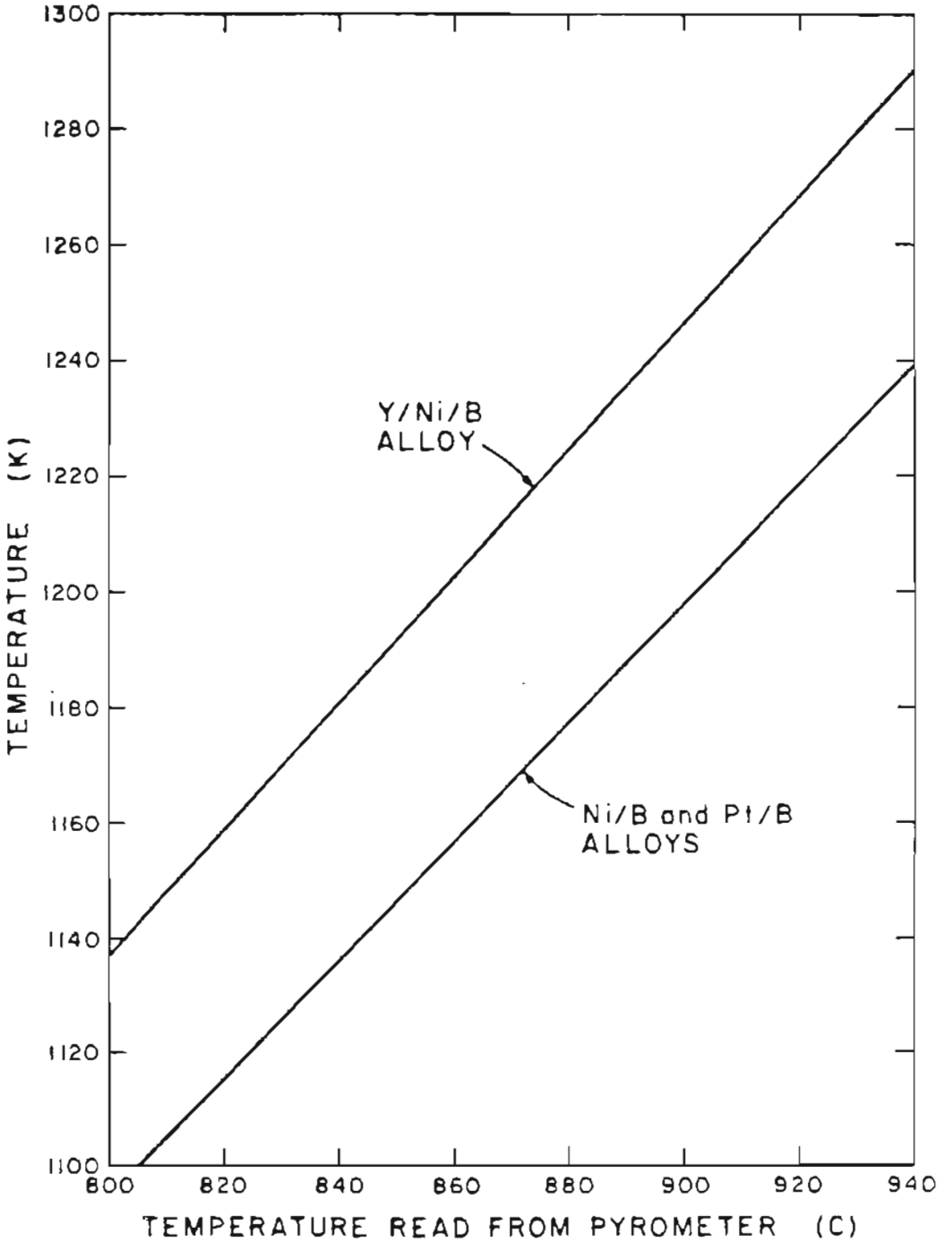

Figure 4-2. Low temperature calibration scale for prewetted HRL alloy combinations. The calibration for Pd/Ni/B could not be measured directly and was assumed to be identical to the calibration for Ni/B and Pt/B alloys.

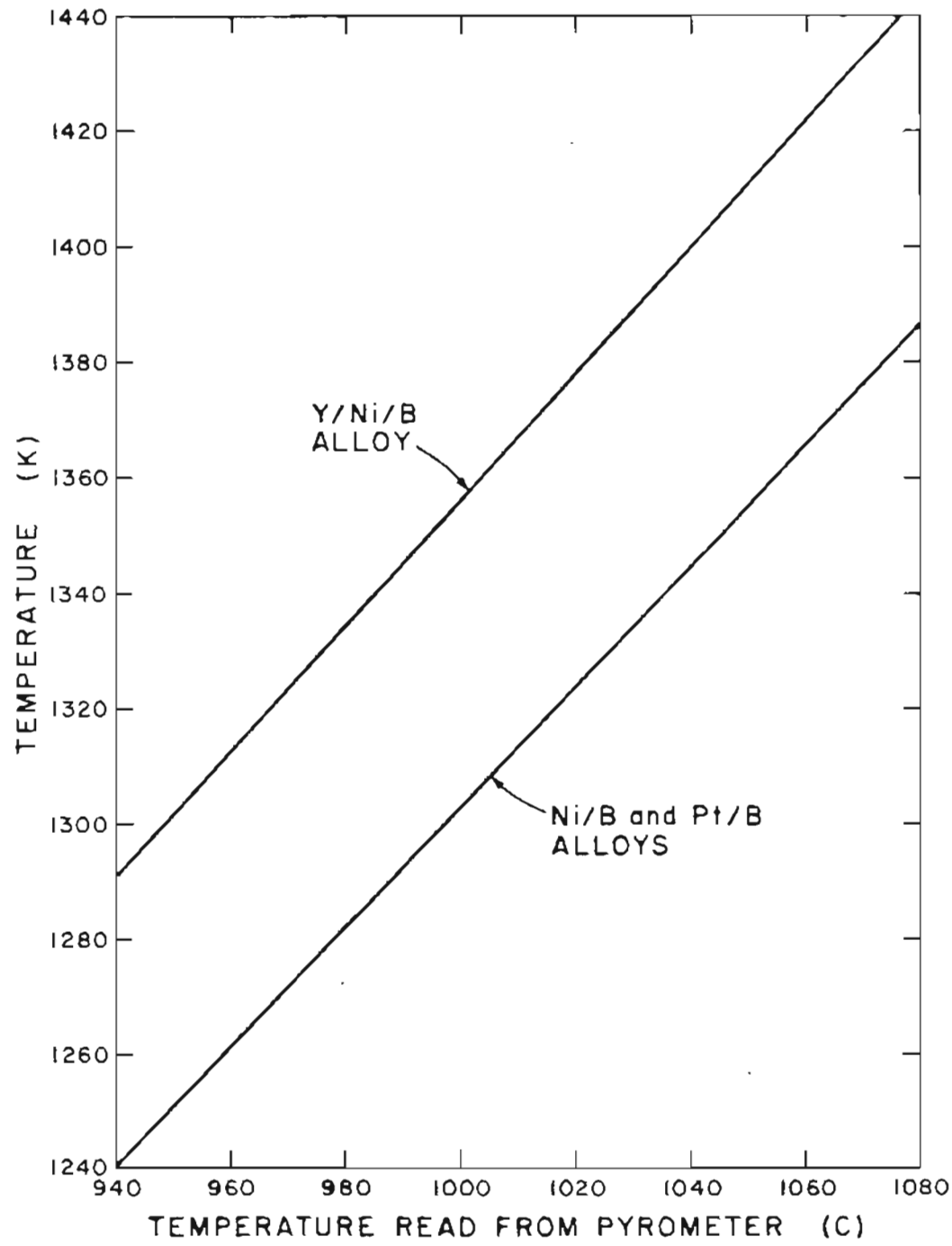

Figure 4-3. High temperature calibration scale for prewetted HRL alloy combinations.

1. The Auger emission process

Auger electron spectroscopy characterizes the elemental composition of a surface by measurement of the energy of electrons originating from a 3-state transition within the surface atoms of the material. When a core level (say, K) of a surface atom is ionized by an incoming electron beam of a few kV in energy, the vacancy may be filled by electronic transition from one of the higher energy states of the atom (say, L_2). The energy difference between these two states is used to ionize a second (Auger) electron from yet a third state (say, L_3). The atom is left doubly ionized, and the Auger electron will have a kinetic energy characteristic of the parent atom (see Figure 4-3).

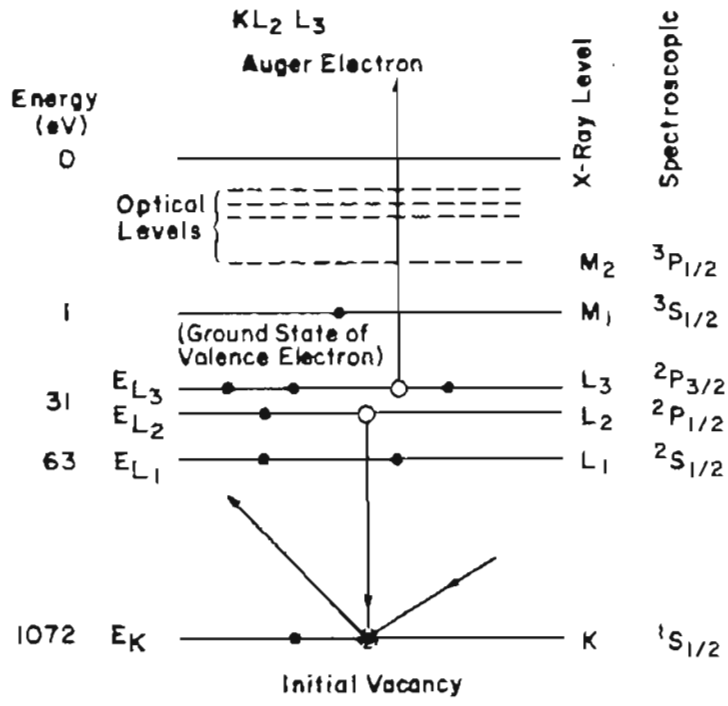

Figure 4-3. The Auger emission process for a Na atom. The particular transition illustrated is designated KL_2L_3.

The ejected electrons give rise to peaks in the secondary electron spectrum of the material which can be used to unambiguously identify the composition of the surface. Primary beam energies of 3-10 keV are used because the ionization cross-section for most elements is a maximum when

$$E_p/E_i = 3.0\text{-}5.0$$

where E_p is the primary beam energy, and E_i is the ionization energy of the involved core level.

2. The surface sensitivity of Auger spectroscopy

The surface sensitivity of the Auger technique arises from the limited mean free path of electrons with kinetic energy in the range 20-2000 eV. Only for transitions which occur within a few angstroms of the surface is the electronic mean free path sufficient [2] to allow ejection of Auger electrons without loss of energy and removal from the Auger signal. Due to the large background of secondary electrons on which the Auger peaks are superimposed, the Auger electrons are often detected by electronic differentiation of the secondary electron distribution function N(E). The resulting Auger spectrum is the function dN(E)/dE. The peak-to-peak magnitude of the characteristic Auger peaks in a differentiated spectrum, when corrections are allowed for the relative ionization cross-sections of the elements, is directly related to the elemental concentration of the surface atoms that produced the Auger electrons. Quantitative accuracy for routine analysis is of the order of 10-20%.

In addition to deexcitation by the Auger process, relaxation of the electron energy levels may also occur by X-ray fluorescence. In X-ray spectroscopy, when the vacant core level is filled by an electron from a higher atomic state, the energy is emitted as a characteristic photon of energy hf = E(upper) - E(lower). In a typical experiment where the surface is excited by an electron beam, both processes are occuring at the same time. For detection of elements of low atomic number, however, Auger spectroscopy is superior to X-ray fluorescence spectroscopy. This is because the ratio of Auger to X-ray yield favors the Auger process for elements of Z < 33 (see Figure 4-4). At larger Z, the X-ray fluorescence yield begins to slowly increase at the expense of the Auger process. Since the Auger transition probabilities are large for light elements, surface impurities in concentrations as small as 1% of a monolayer (10^{13} atoms/cm^2) may be detected.

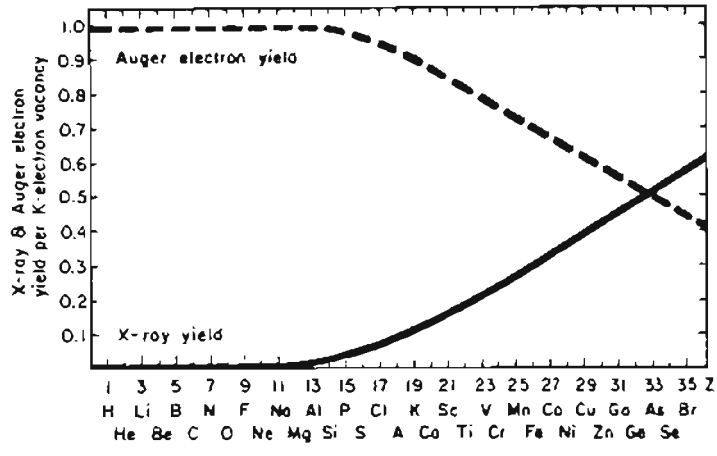

Figure 4-4. Auger and X-ray yields for K-shell vacancies vs atomic number. From G. A. Somorjai, Principles of Surface Chemistry (Englewood Cliffs, Prentice-Hall, 1972).

3. The energy of Auger electrons

The kinetic energy of Auger electrons is given by the difference in binding energies of the electron levels involved. For example, for a KL_2L_3 Auger transition:

$$E(\text{Auger e-}) = E_K(Z) - E_{L2}(Z) - E'_{L3}(Z) - \Phi$$

where $E_K(Z) - E_{L2}(Z)$ represents the difference in binding energy of the K and L_2 levels, $E'_{L3}(Z)$ is the ionization energy of the singly ionized surface atom, and Φ is the work function. The energy level of the singly ionized atom is used because the difference in energy between the K and L_2 levels is given to an atom which has already lost an electron during the initial core level excitation. This energy is greater than the ionization energy of the L_3 level in a neutral atom because of the increased nuclear charge seen by the electrons in a singly ionized atom. To facilitate theoretical calculations, the approximation is often made that:

$$E'_{L3}(Z) \sim E_{L3}(Z + 1)$$

meaning that the energy of the L'_3 (ionized) level is nearly identical to the L_3 (neutral) level with one more proton in the nucleus.

4. Quantitative analysis of Auger spectra

Two routinely used, semiquantitative methods exist which provide an approximate determination of the Auger elemental composition of surfaces. A calculation from first principles has not yet been attained due to inadequate understanding of backscattering factors

and matrix effects.

The first method determines the surface composition by comparison to external standards. Auger spectra from the unknown specimen are compared with those from a standard of known concentration. The concentration of element a in the test specimen $N_a(t)$ can be related to that in the standard $N_a(s)$ by:

$$N_a(t)/N_a(s) =$$

$$[I_a(t)/I_a(s)][l(s)/l(t)][(1+R_b(s))/(1+R_b(t))]$$

where I_a is the emitted Auger current produced by a particular Auger transition in element a, l is mean free path of the Auger electron, and R is the backscattering factor [3]. When the test sample and standard are similar, the last two factors of this relation are of order unity, and determination of the relative concentrations reduces to a measurement of the relative Auger currents.

A less accurate but commonly used method for quantitative analysis of Auger spectra employs elemental sensitivity factors calculated by Palmberg et al. [4]. The elemental sensitivity factor is a measure of the relative probability for a given Auger transition to occur. The atomic surface concentration of element x can be expressed as [5]:

$$C_x = (I_x/S_x)/\Sigma(I_a/S_a)$$

where S_a is the relative sensitivity of element a. The method is only semi-quantitative because the matrix-independent sensitivity factors neglect the variation in mean free path and backscattering factor with material. The surface elemental compositions calculated

from Auger spectra in this dissertation have been determined using this method, using a 5 kV excitation energy and 2 eV p-p modulation voltage. In the case of Pt/B alloys, overlapping Pt and B Auger peaks occur near 179 eV, which creates problems for quantitative analysis because both B and Pt contribute to the spectral feature. In order to deconvolve the contributions, the ratio of the 1967 eV and 179 eV Auger peak heights of elemental Pt were calculated and compared to the same ratio for the Pt/B alloy. This procedure allows an estimate to be made of the relative contribution of each element.

5. Chemical Effects in Auger Spectra

In addition to the determination of surface elemental composition, Auger spectroscopy can be used to analyze the electronic environment of surface atoms as indicated by the chemical shifts of the characteristic Auger peaks [6]. This is because the different chemical states of elements are due to a shift in the binding energies of inner-shell electrons upon the change of valency. A change in the environment of an atom in the surface region may produce the following changes in the Auger electron spectra: (1) shifts in the energy at which the various Auger lines occur; (2) changes in the relative intensities of the the Auger lines in different groups; (3) changes in the shape of a group of Auger lines. It has been possible to determine the existence of compound formation in the liquid metal alloys by analysis of Auger chemical effects. These effects will be detailed below.

C. Other Surface Analytical Techniques

A number of additional surface analytical techniques have been utilized to study the liquid alloys. Studies of the vaporization rate of the various alloy components has been carried out by using a line-of-sight Ultek Model 200 quadrupole mass spectrometer (QMS). The QMS allowed direct measurement of the evaporation rate of volatile mass species as a function of temperature. A dedicated Hitachi RMU-7 mass spectrometer, specifically designed to accommodate analysis of liquid metal ion sources, was used to characterize the emission properties of the liquid alloys. The setup is shown in Figure 4-5. This instrument is capable of a resolution of 600 at m/e = 500 and, when combined with a focusing filter lens retarding energy analyzer, can provide information on the charge states, energy spreads, and relative amounts of the field evaporated species.

A JEOL Model JSM-35 scanning electron microscope (SEM) has been used to study surface morphology under different conditions of time and temperature. Energy dispersive X-ray analysis (EDX) has provided information concerning the alloy bulk composition. Work function measurements have been recorded by a field emission retarding potential (FERP) technique [7] which possesses the unique property of measuring the absolute work function of the alloy surfaces. Work function values are accurate to 0.05 eV, and have been measured on the cleanest available alloy surfaces.

An X-ray photoelectron spectrometer (XPS or ESCA) manufactured by Leybold-Heraeus has been used to aid in the identification of

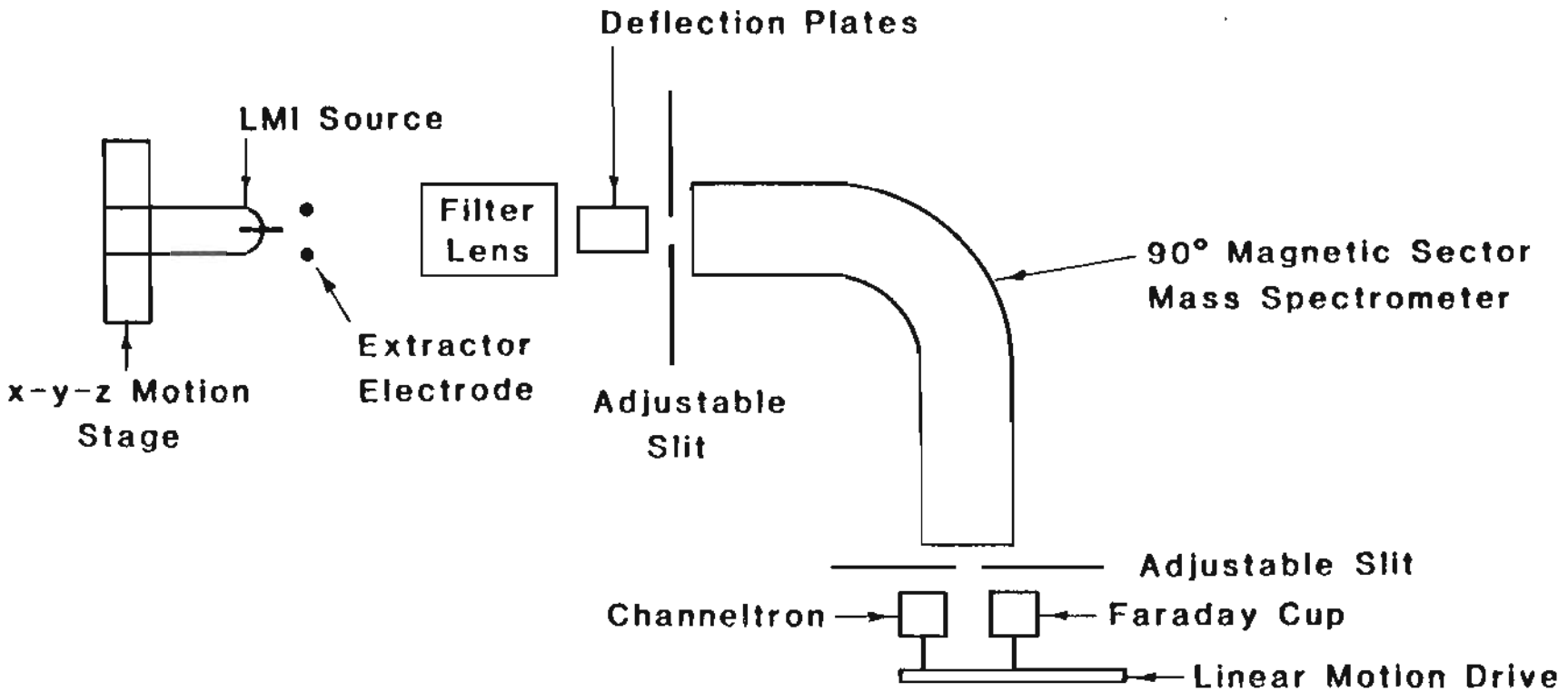

Figure 4-5. Block diagram of the RMU-7 single focusing mass spectrometer/energy analyzer system at OGC.

chemical compound formation in the liquid alloys. Scanning Auger spectroscopy (SAM) has provided high-resolution compositional information of second-phase material in the alloys. A schematic diagram of the analysis system used at OGC showing the primary analysis instruments used to characterize the liquid surface is given in Figure 4-6.

SAM and ESCA measurements were carried out at the Center for Research in Surface Science and Submicron Analysis (CRISS) at Montana State University. This facility is a National Science Foundation regional center for surface studies, and possesses a high-resolution scanning Auger microprobe (Physical Electronics, Model 595) capable of simultaneous SEM and Auger analysis of surfaces. After adding a special sample mounting stage to allow sample heating, a detailed investigation of the solid-to-liquid phase transition of the liquid alloys was possible. The resulting data has provided valuable insight into the alloy interfacial phenomena. ESCA was used primarily to identify compound formation in the alloys, but in general the results were disappointing on the small samples we studied due to the limited spatial resolution of existing instruments and the near-identical binding energies of boron-containing compounds. Information concerning the chemical environment of surface species was more readily obtained by analysis of chemical effects in Auger spectra. This situation was unusual in that ESCA is usually the instrument of choice in the identification of chemical bonding on surfaces. Our results point out the need for further study and compilation of Auger chemical effects.

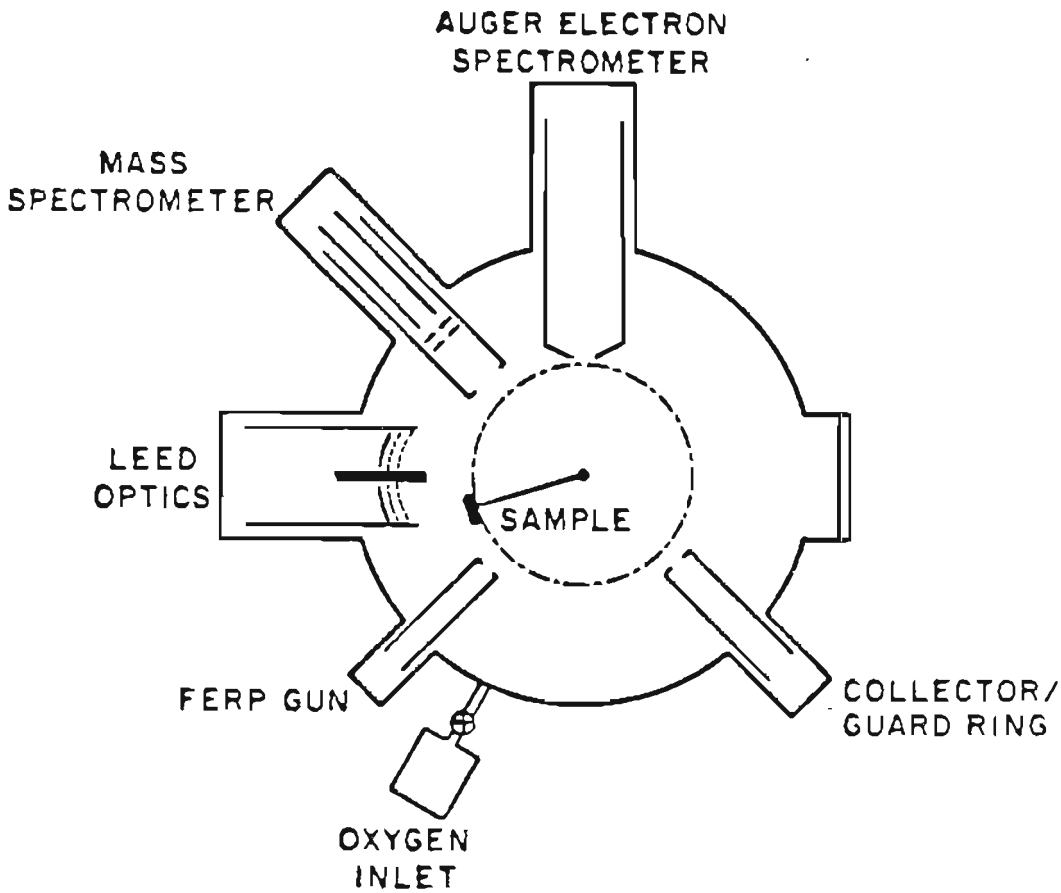

Figure 4-6. Schematic diagram of the surface analysis system at OGC.

REFERENCES

1. D. T. Hawkins, Auger Electron Spectroscopy: A Bibliography 1925-1975 (New York: IFI/Plenum, 1977).

2. A. W. Czanderna, ed., Methods of Surface Analysis, Vol. 1 (Amsterdam: Elsevier, 1975), p. 164.

3. Ibid., p. 181.

4. P. W. Palmberg, G. E. Riach, R. E. Weber, and N. C. MacDonald, Handbook of Auger Electron Spectroscopy, Physical Electronics Industries, Inc., Edina, 1972.

5. Ibid., p. 9.

6. T. W. Haas, J. T. Grant, and G. J. Dooley III, J. Appl. Phys. 14 (1972) 1853.

7. R. W. Strayer, W. Mackie, and L. W. Swanson, Surf. Sci. 34 (1973) 225.

CHAPTER 5

SURFACE STUDIES OF PREWETTED HRL ALLOY COMBINATIONS

A. Introduction

The initial goal of the OGC effort was to determine the critical properties of the alloy and substrate that provide reasons for improper source operation and guidance for successful source development. The outcome of these measurements has allowed not only a determination of the appropriate alloy/substrate combinations and source performance, but also a clearer understanding of the alloy and substrate properties and further insight into the mechanism of LMI source operation.

Attempts by the HRL group to develop a liquid metal ion source of B were carried out during the years 1977-83. The results were largely unsuccessful. It was found that boron eutectics corrosively attacked the refractory metal substrates (e.g., W) employed in previous designs using low-melting liquid metals [1]. Efforts to decrease the rate of attack by using alternative metal substrates and by formation of an an interfacial layer to prevent penetration resulted in source lifetimes of no more than 20 hours. Carbon, in the form of polycrystalline graphite, was investigated as a substrate material from 1979-83, and found to have limited success when

combined with an appropriate wetting agent. An empirically derived procedure generated during this period to facilitate best results was found to be highly irreproducible, and resulted in a classification scheme that ranked systems into graded classes of wetting according to the degree to which the procedure was carried out correctly (see Figure 5-1).

The poorest wetting resulted when no wetting agent was applied, i.e., wetting of pure alloy to virgin carbon. In these cases, a poorly-wetted droplet of alloy formed with a contact angle > 90 degrees. The best wetting case appeared to arise from the following operations, although the results were difficult to reproduce:

a. The center of one side of the graphite substrate is coated with a slurry of red boron powder in acetone to a thickness of about 0.005 inches.

b. The graphite is then flash heated to a temperature of T = 2400 C, after which the heat is immediately removed. This temperature is greater than the melting point of the boron.

c. A powdered sample of eutectic is mechanically mixed with excess boron powder (1 - 3% of alloy by weight) and applied as a slurry with acetone to the graphite.

d. The graphite is then heated to temperatures near T = 1400 C and held at this point while the alloy melts and flows.

Steps a. and b. of this procedure were coined "boronization," and step c. was called "boron fluxing." Contact systems displaying excellent wetting properties as a result of this procedure were termed "ideally boronized." Studying the photos of Figure 5-1, it is

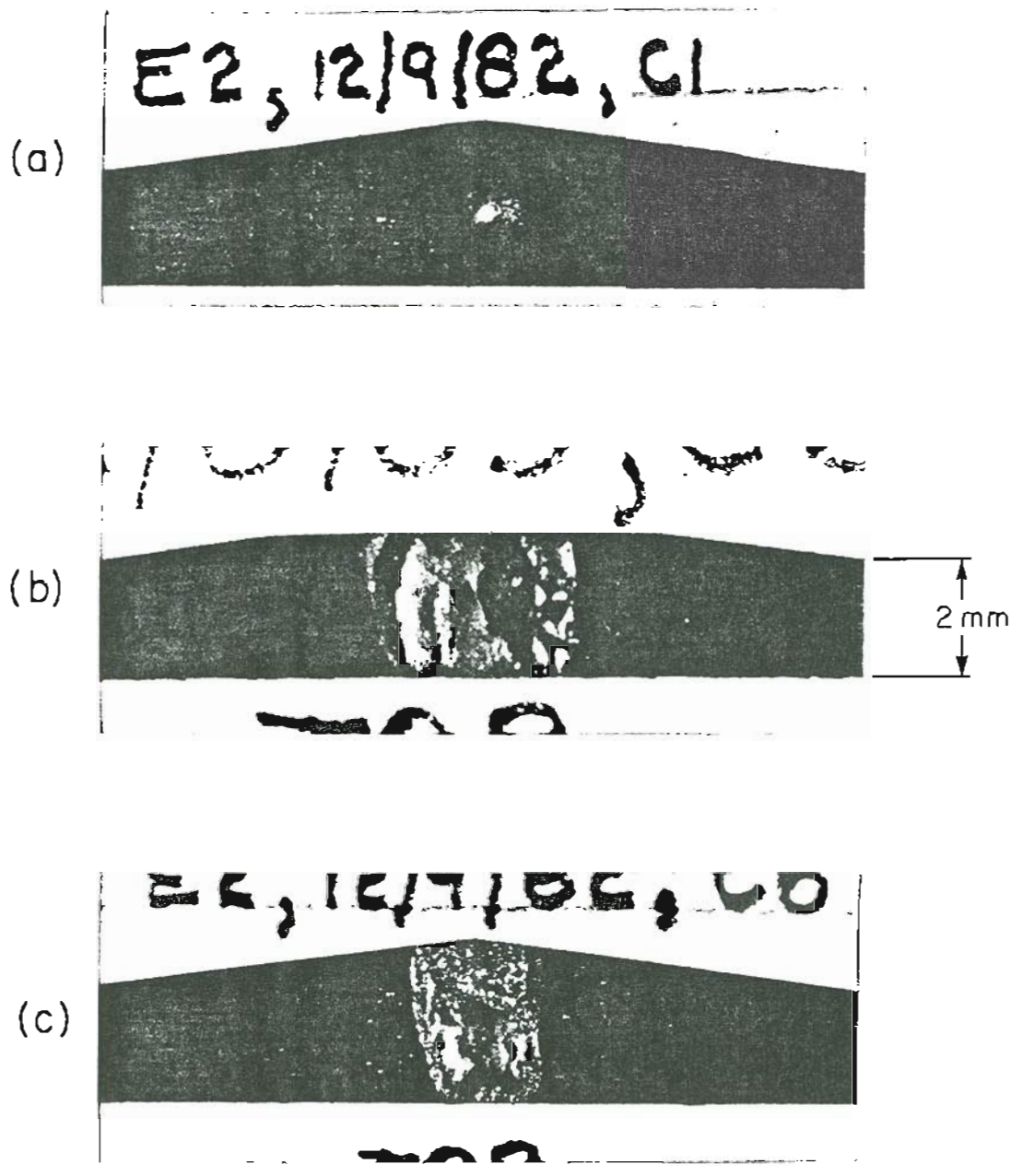

Figure 5-1. The varying degrees of wetting success found in the early work at Hughes Research Laboratory. (a) Nickel boride alloy on virgin graphite; (b) Boron-fluxed nickel boride alloy on virgin graphite; (c) Nickel boride alloy on "ideally" boronized graphite.

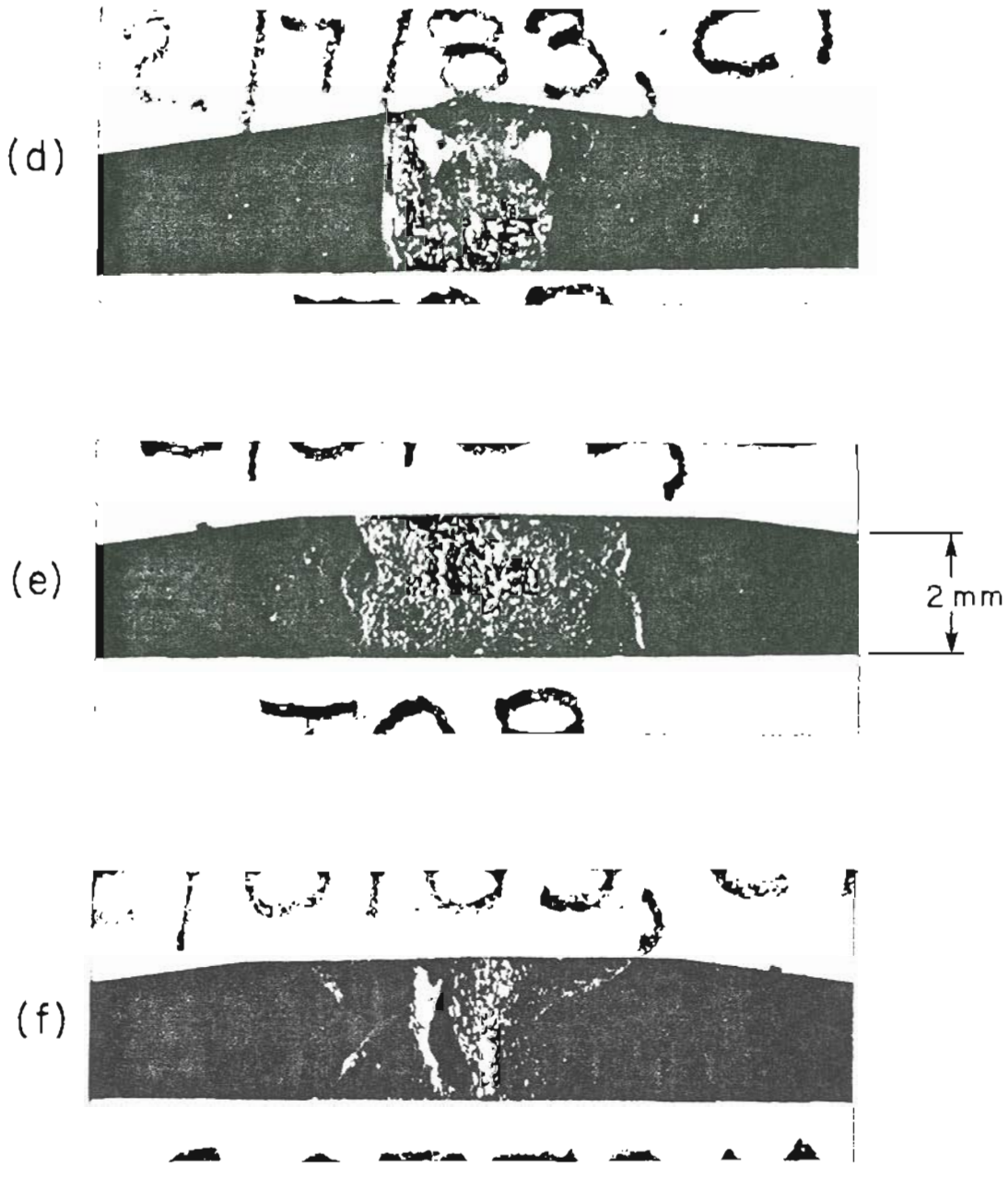

Figure 5-1 (continued). (d) Boron-fluxed nickel boride alloy on "lightly" boronized graphite; (e) Boron-fluxed nickel boride alloy on "ideally" boronized graphite; (f) Bottom, nonboronized side of (e).

apparent that wetting and flow may occur over regions of the graphite that have not been subject to boronization, as the alloy is observed to wet the nonboronized, backside of the substrate.

In view of the limited success of the early Hughes work, a major effort was undertaken by the OGC group to establish the role of excess boron and boronization on the wetting behavior and contact angle of prewetted alloy combinations. The systems selected were logical first choices in that each alloy contained at least one low-melting eutectic. The alloys were prewetted by HRL and supplied to the OGC group as a sintered mass of alloy on a flat ribbon of graphite. Each system varied with respect to boronization pretreatment, boron fluxing, and temperatures reached during the boronization and wetting process. The Y/Ni/B eutectic on Re was also studied during this period to discover the mechanism of failure and supply reasons for the limited lifetimes observed during preliminary work by the Hughes group. In retrospect, the lack of controls in the early work resulted in considerable labor on our part to sort out the relevant parameters from the irrelevant.

B. Studies of the Y/Ni/B on Re system

We begin with surface investigations of the Y/Ni/B on Re contact system. Two samples of identically prepared $Y_{62}Ni_{23}B_{15}$ eutectic above a Re substrate were studied. The melting point of the alloy was determined to be T = 1102 K by the experimental procedure described above. The solid-to-liquid phase transition appeared to be

abrupt and complete when viewed through the optical microscope, signifying that the alloy was close to a system eutectic.

A reproducible phase separation occurred in the alloy after a few hours of heating at temperatures slightly above the melting point, forming separate B-rich and B-poor regions that were easily discerned with the naked eye. Close observation showed both regions to have resolidified, and further heating of the alloy at temperatures significantly above the original melting point was necessary to remelt the surface. This is seen in Figure 5-2, which shows the status of the alloy surface after 70 hours of heating at a temperature slightly above the initial melting temperature. A temperature of 1146 K was needed to remelt the non B-rich phase, and 1192 K was necessary to melt the B-rich phase. Notice that the alloy has yet to fully wet the substrate, and that C and O signals persist in the surface. This indicates that carbide and oxide phases have formed, as surface CO could not exist at this elevated temperature.

Dissolution of Re is indicated as the cause of this unusual melting behavior and phase separation. Re is present in large concentrations throughout the alloy, and possesses a melting point of T = 3453 K which will raise the melting point of the solvent alloy. Lateral diffusion of Ni may additionally contribute to the phase separation, as the B-rich region appears to be depleted of Ni following long-term heating. Further, the concentration of Ni in this phase rises steadily with temperature, reaches a maximum prior to melting, then nearly vanishes.

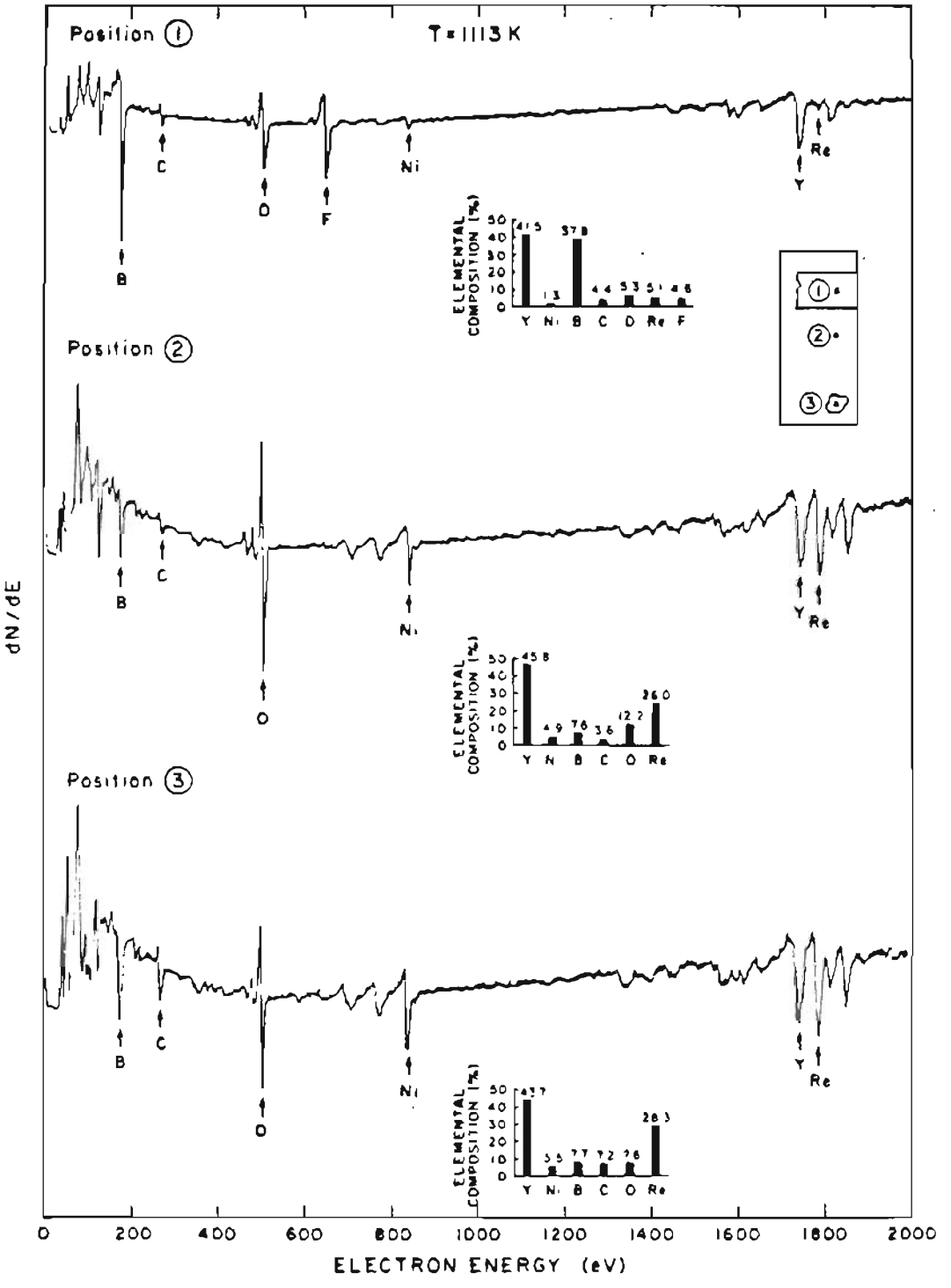

Figure 5-2. Auger surface elemental composition for the $Y_{62}Ni_{23}B_{15}$ alloy surface after long-term heating at 1113 K. Discernible B-rich (position 1) and B-poor (positions 2 and 3) regions are evident. High concentrations of Re are also evident.

A high-resolution scanning Auger study of the alloy surface at room temperature after 500 A sputter cleaning is displayed in Figure 5-3. Previous to this, the contact system had been heated to temperatures as high as T = 1350 K to insure complete liquifaction of the surface. Several different regions are found, which are identified by areas of different contrast. The points investigated suggest the precipitation of second-phase material during cooling. Four relatively pure binary phases are found: Y-Ni, Y-Re, Y-O, and Y-B. In view of the oxygen affinity of the components, formation of an yttrium oxide is not surprising because Y_2O_3 is by far the most energetically favorable oxide. Further, one might expect Y to form a stable phase with B, because Y is a group IIIB metal with valence +3 which forms highly stable borides similar to those of La, another group IIIB metal. By comparison, nickel and rhenium borides are less stable. Point 2 of Figure 5-3 shows that Y and B are strongly correlated.

Work function studies on the alloy surface after initial melting and resolidification yielded an average value of 3.5 eV. Interestingly, after exposure to the system vacuum for several days, the work function changed very little, in spite of the fact that both visual and compositional surface changes had occurred. The carbon and oxygen contamination were substantially greater, and the alloy assumed a powdery white appearance which could be restored to metallic luster by heating. Apparently, the compounds formed by contamination (e.g., yttrium oxides) have work functions in the 3.5 eV range.

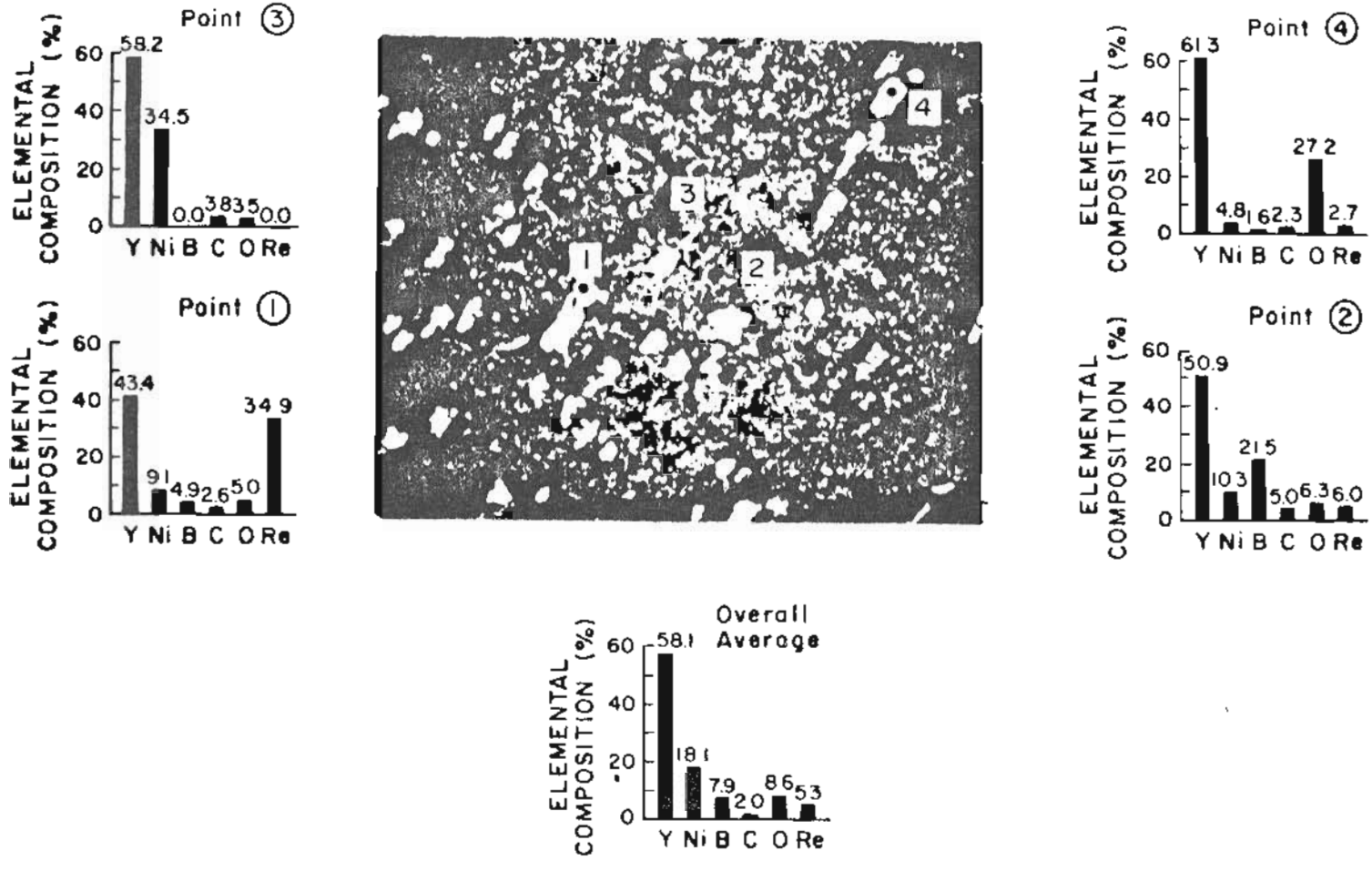

Figure 5-3. Auger surface elemental composition of four distinct phases on the Y/Ni/B surface. A total of 500 A of the surface layer was removed by Ar^+ sputtering before these measurements.

The wetting properties of this contact system are excellent. Wetting was determined visually and by observation of uniform brightness over the ribbon as the alloy temperature is raised. Prior to wetting, the alloy appeared brighter than the Re due to the difference in emissivity between the materials. Wetting was found to occur at T = 1200 K, a temperature nearly 100 degrees above the initial melting point of the alloy and a few degrees higher than the melting temperature of the B-rich separated phase. The alloy flowed over both sides of the Re ribbon and the coverage appeared to be complete. In spite of this, however, there remained regions where Re was detectable by Auger analysis.

That the existence of Re in the alloy is the key factor relevant to successful use of this contact system as a source of B ions may be demonstrated by analysis of phase diagrams for the component binaries. A search of the literature has failed to uncover a phase diagram for the Y/Ni/B ternary; however, diagrams for the binary systems are readily available and are reproduced in Figure 5-4. The ternary system may be formed by combining the three diagrams into the sides of a base triangle. Detailed interpretation of the resultant diagram is difficult, and the conclusions are only qualitative. The procedure is to fold the three binaries to form an angle normal to the base triangle, and then roughly determine where the liquidus and solidus are located by connecting the solid and liquid regions of each binary. An isothermal cut is then taken through the temperature of interest, and the result projected onto the base triangle to give a pictorial view of the alloy at a given temperature. This is

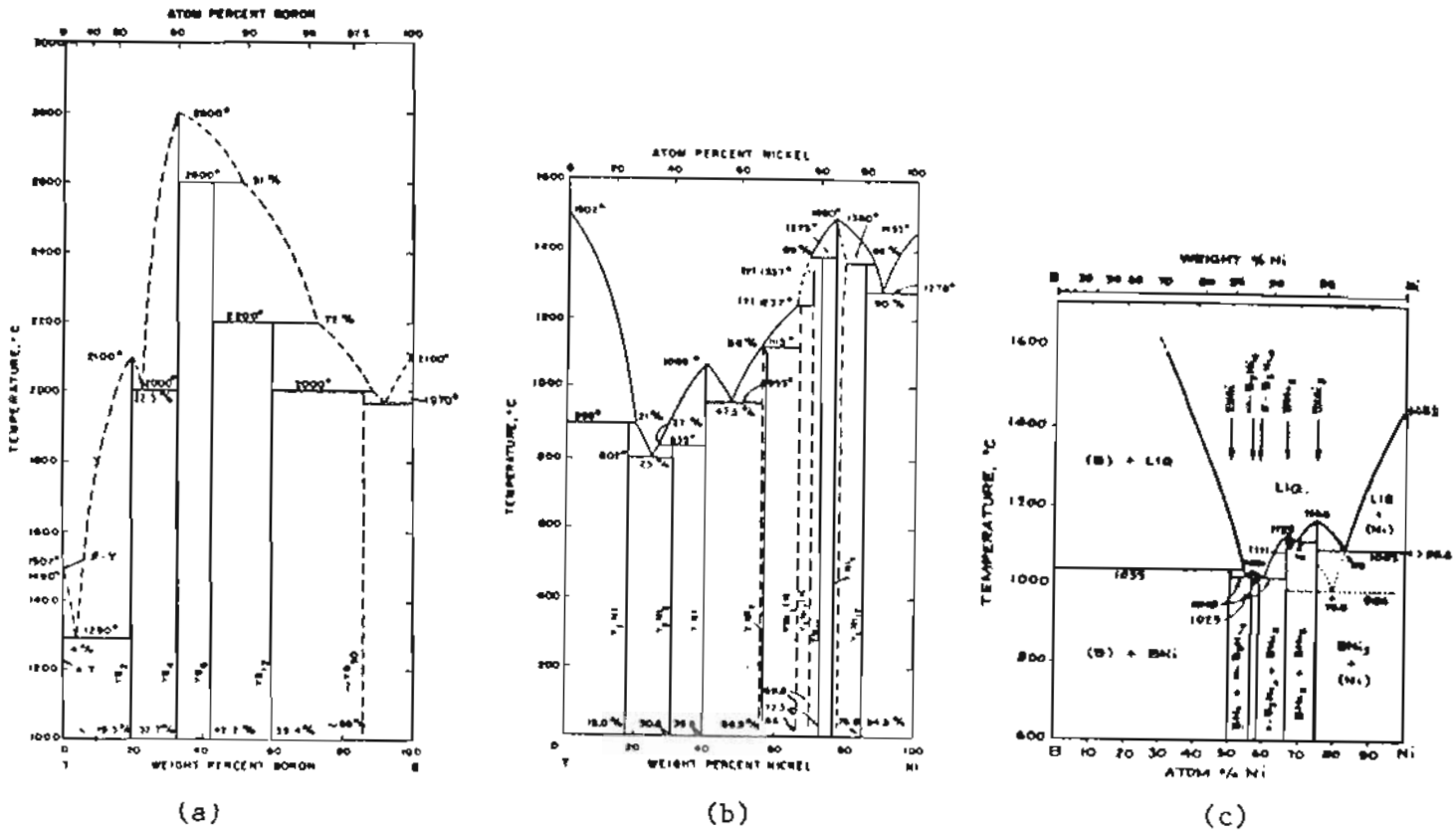

Figure 5-4. Phase diagrams of the Y-B, Y-Ni, and Ni-B binary systems. Sources: (a) and (b): K. A. Gschneider, Rare Earth Alloys: A Critical Review of the Alloy Systems of the Rare Earth, Scandium, and Yttrium Metals (D. Van Nostrand, Princeton, 1961); (c): W. G. Moffatt, The Handbook of Binary Phase Diagrams (General Electric, 1978).

accomplished for the Y/Ni/B system in Figures 5-5 and 5-6 for two temperatures. A temperature of 1270 K was chosen for the isothermal cut in Figure 5-5 because it is observed that the lowest binary eutectic of the alloy occurs on the Ni-Y section of the diagram at 1075 K with a Ni concentration of 25 a/o. The Ni/(Ni + Y) atom ratio of our alloy is 27% with an experimental melting point of 1102 K, meaning that the alloy is near this eutectic on the Y-Ni binary diagram.

It is found that the alloy can melt and retain its liquid state only over a very small range of compositions. At melting, the temperature and composition of the alloy are correctly matched to put the alloy in a liquid region of the ternary triangle. Over a period of time, however, the increase of Re and/or diffusion of Ni changes the alloy composition and drives the material into a solid region of the phase diagram. The result is that the alloy solidifies. Further increases in temperature act to widen the zone of liquifaction and enable the alloy to remelt, but as shown in Figure 5-6, the temperature would have to be nearly 1500 for the alloy to remain liquid over a workable range of compositions. But then the rate of Re solubility will also increase causing solidification to recur. The dissolution of Re therefore acts to raise the melting temperature of the alloy and prohibit further ion emission due to a solidified Taylor cone.

Additional support for this view of alloy operation was found through study of the emission characteristics of a wetted LMI source of Y/Ni/B on Re. Relative amounts of the various elements in the ion

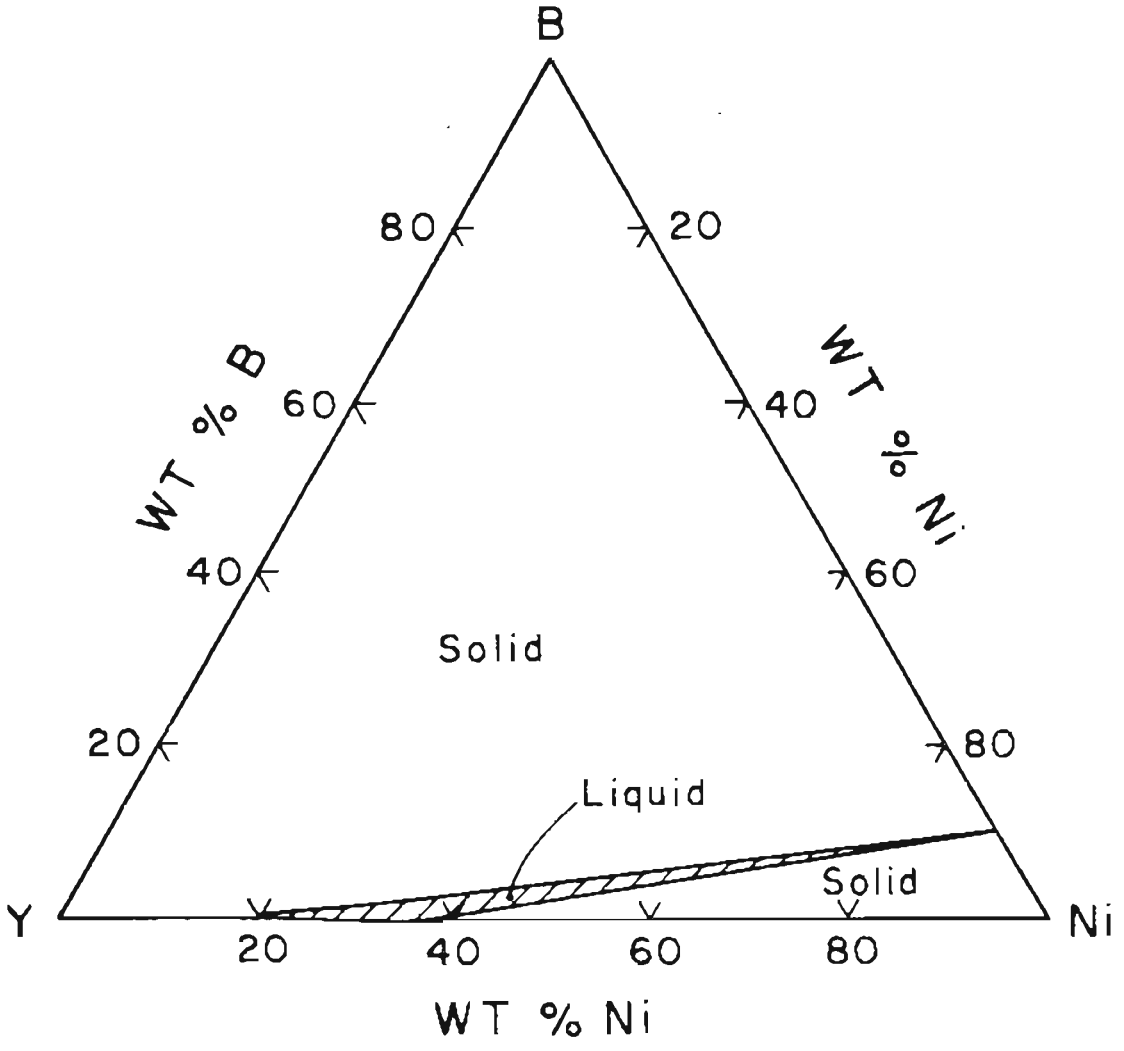

Figure 5-5. Isothermal section (at T = 1275 K) of the Y-Ni-B phase diagram projected onto the base triangle.

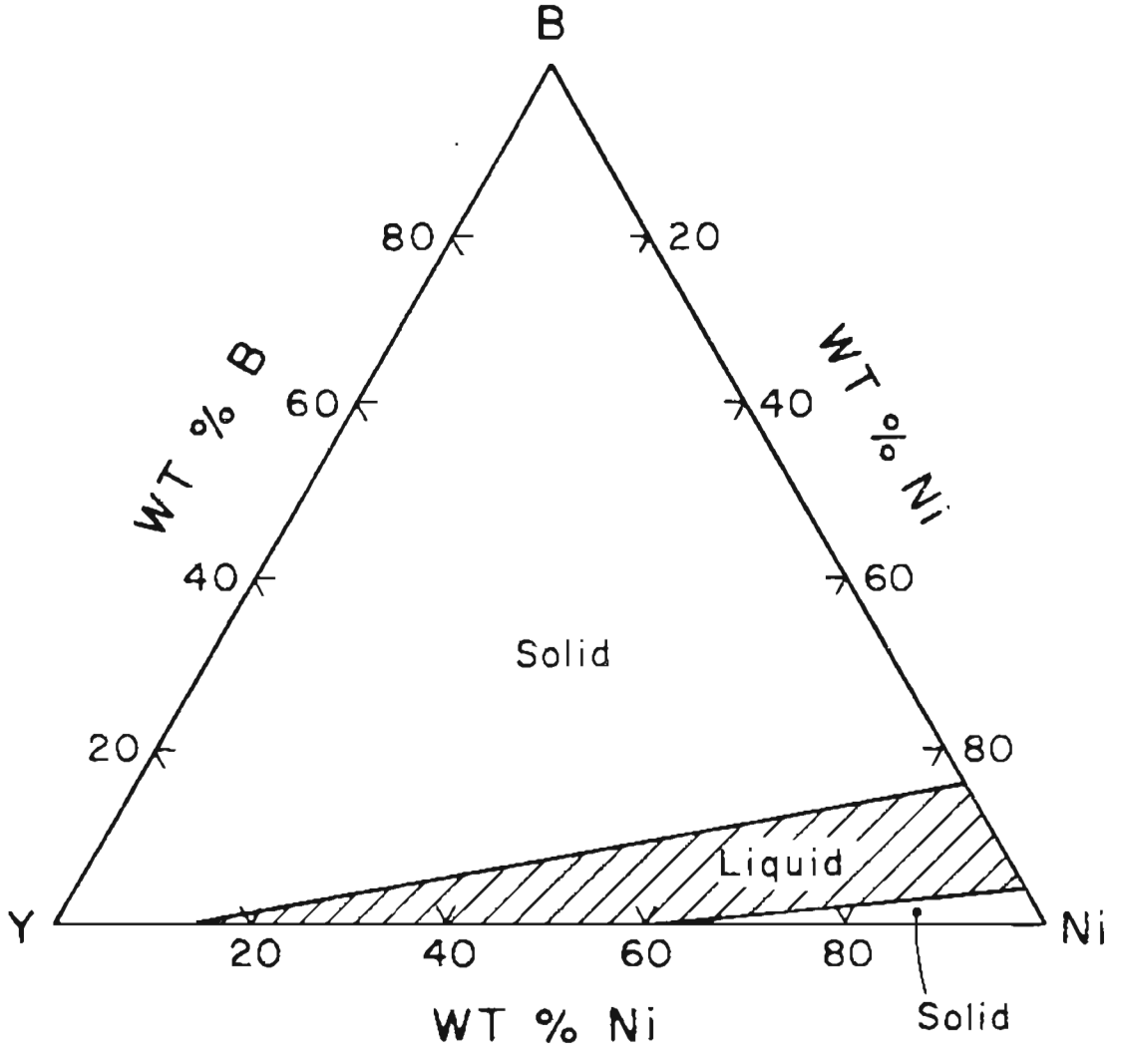

Figure 5-6. Isothermal section (at T = 1475 K) of the Y-Ni-B phase diagram projected onto the base triangle.

beam at 10 microamps of total current and alloy temperature T = 1280 K are shown in Table II.

TABLE II

RELATIVE AMOUNTS OF VARIOUS ELEMENTS IN THE ION BEAM OF THE $Y_{62}Ni_{23}B_{15}$ ALLOY AT 10 MICROAMPS TOTAL CURRENT AND 1280 K

Mass	Relative Abundance*
B^+	0.0023
B_2^+	5.2×10^{-5}
Ni^+	0.36
Ni^{++}	0.036
Ni_2^{++}	0.037
Ni_3^+; Y_2^+	0.010
Ni_4^+	0.0059
Y^+	0.19
Y^{++}	1.00
Y^{+++}	0.35
Y_3^+	0.0017
YNi^{++}	0.16
YNi^+	0.16

*Based on peak areas and uncorrected for variation of system sensitivity with mass.

The alloy source was stable in the temperature range 1160 to 1280 K. With decreasing temperature, the current shut off at T = 1114 K, in good agreement with the experimental melting point of 1102 K. The total amounts of the various components in the bulk, surface, and ion phases are shown in Table III. During operation, the emitter displayed considerable variation in surface phase composition and showed increased surface Re concentration with operating time. The ion beam shows a disappointingly small amount of B in the beam.

TABLE III

COMPARISON OF Y, NI, B COMPOSITIONS IN THE BULK, SURFACE AND EMITTED PHASES OF THE $Y_{62}NI_{23}B_{15}$ LMI SOURCE

Phase	Elemental Ratios
Bulk	$Y_{62}Ni_{23}B_{15}$
Surface (1280 K)	$Y_{46}Ni_{26}B_4Re_{23}$
Ion Beam (1280 K)	$Y_{71.9}Ni_{28}B_{.1}$

The Y/Ni/B on Re emitter displayed stable operation for 22 hours at T = 1260 K. At temperatures slightly greater than the melting point of the alloy, the emitter was unstable due to increases in melting temperature with operating time. This corresponds with the observed separation into B-rich and B-poor phases noted above. Furthermore, observations during and after operation indicated an increasing presence of a second solid phase atop the liquid film. After the source failed, scanning electron examination of the emitter structure showed evidence of multiphases, displayed in Figures 5-7 to 5-9. X-ray microprobe analysis revealed a significant amount of Re in the alloy film. In addition to losing a significant amount of reservoir material, the thickness of the film on the emitter increased by roughly 10 microns, i.e., the emitter radius changed from 12 to 25 microns after operation. The film color was also found to change from silver-grey to black during operation. Upon removal from the mass spectrometer, the alloy surface formed a white powder. Since B does not oxidize to a white powder at room temperature, it is likely that the white powder is Y_2O_3.

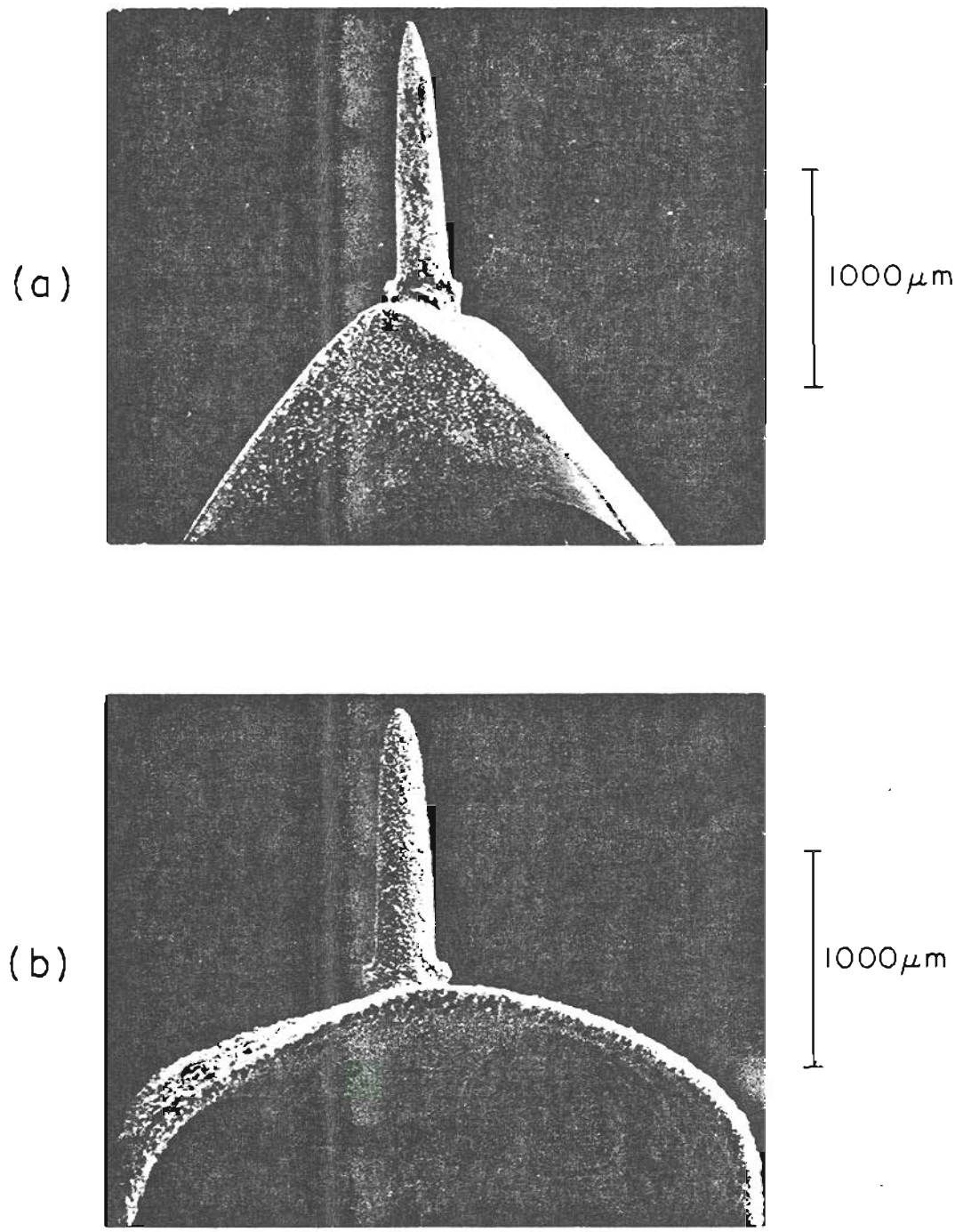

Figure 5-7. SEM micrographs of the Y/Ni/B on Re LMI source before (a) and after (b) 22 hours of operation at 1260 K.

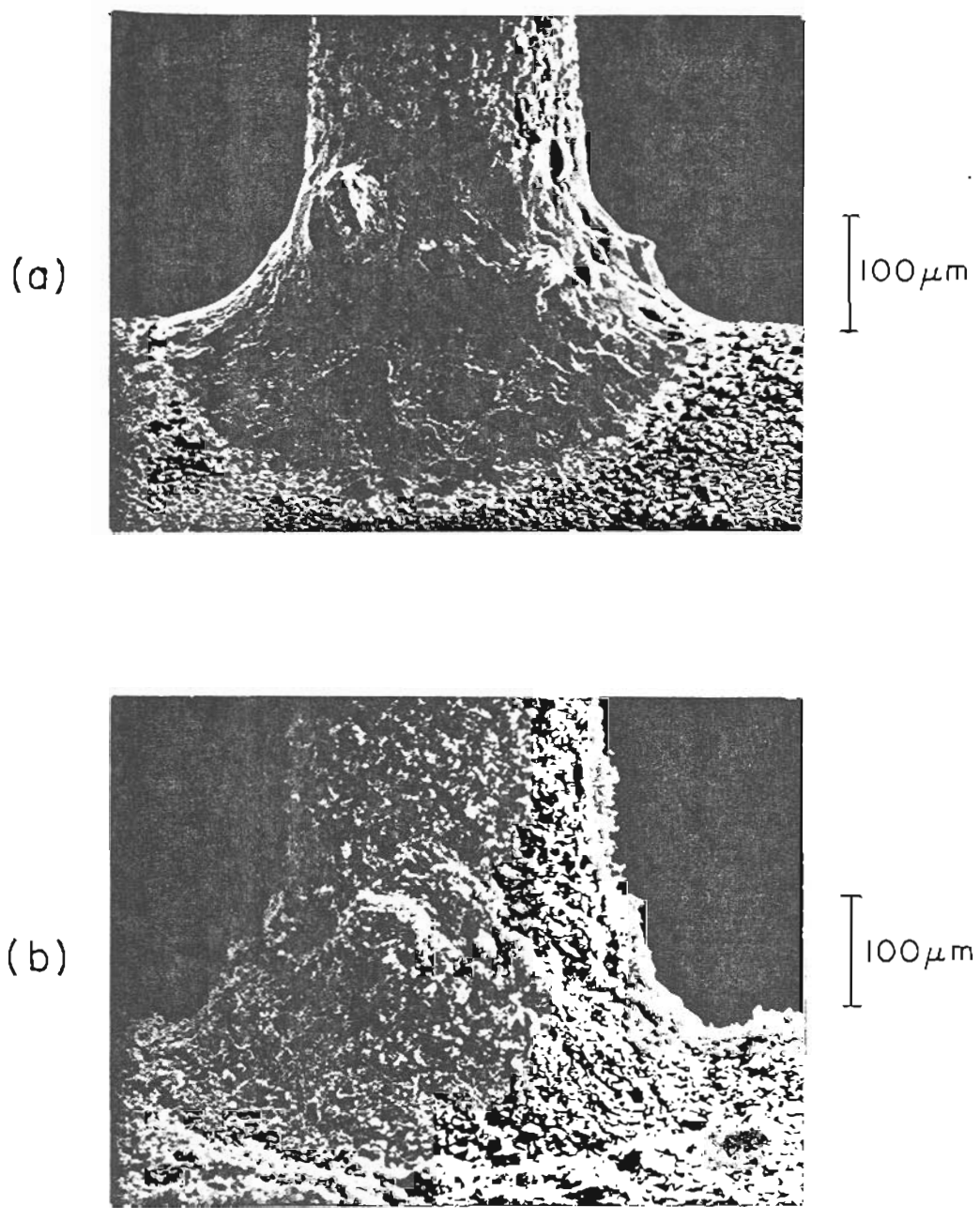

Figure 5-8. SEM micrographs of the emitter shank of the Y/Ni/B on Re LMI source before (a) and after (b) 22 hours of operation at 1260 K.

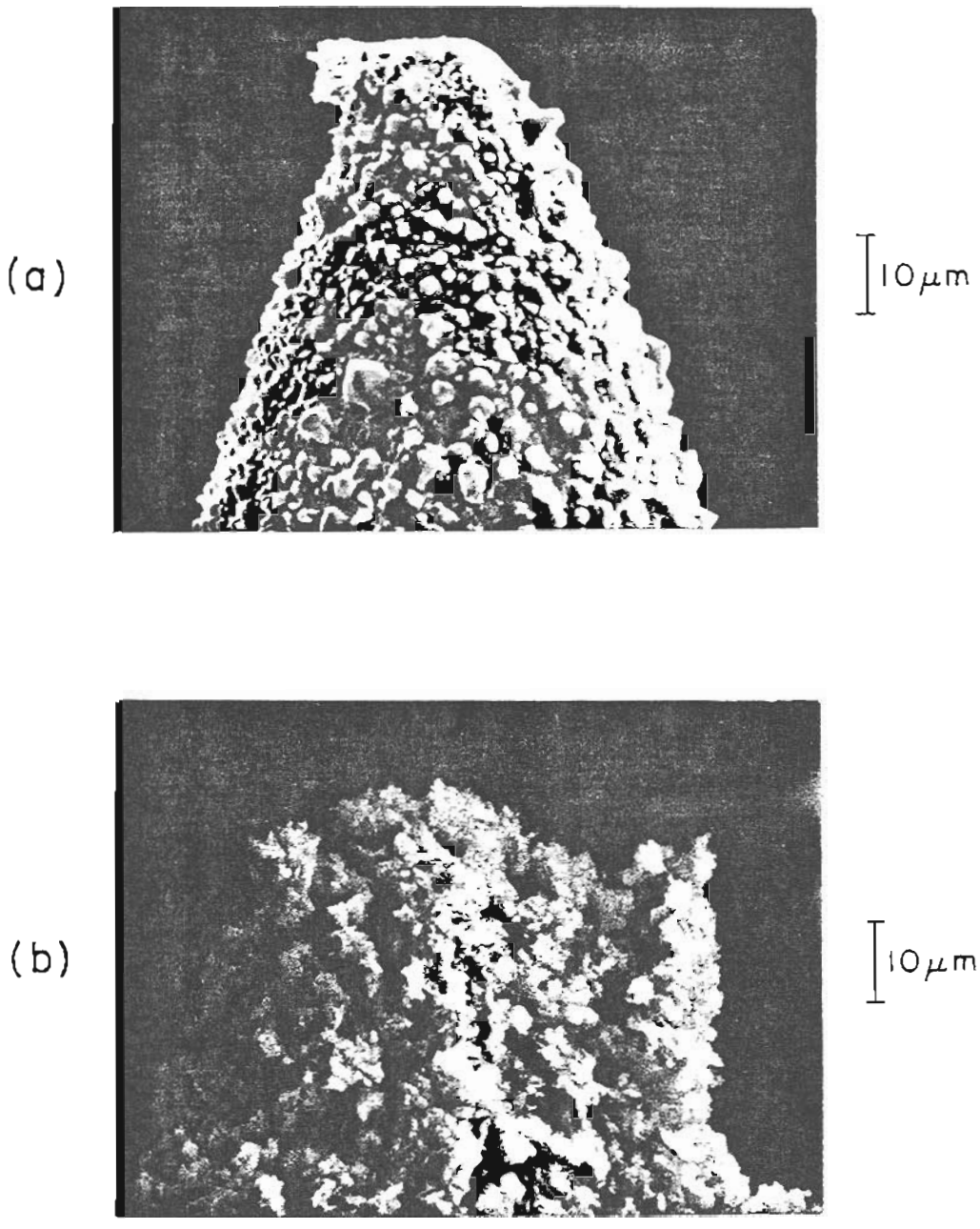

Figure 5-9. SEM micrographs of the emitter tip of the Y/Ni/B on Re LMI source before (a) and after (b) 22 hours of operation at 1260 K.

The relative abundance of the ion species in the emission versus total current and temperature are shown in Figures 5-10 and 5-11. Table IV shows the relative abundance of component elements in the beam vs temperature at 10 microamps total current.

TABLE IV

RELATIVE ABUNDANCE OF $Y_{62}NI_{23}B_{15}$ IN THE ION BEAM VS TEMPERATURE AT 10 MICROAMPS CURRENT

Relative Amount	Temperature (K)
$Y_{29}Ni_{30.8}B_{.16}$	1260
$Y_{66}Ni_{33.8}B_{.19}$	1310
$Y_{67.5}Ni_{32.1}B_{.43}$	1385

In spite of the significant concentration of Re observed in the alloy surface, none was found in the ion beam. This absence is most likely due to formation of solid phases in the alloy surface that prevent emission. Further, although the B abundance in the beam was found to increase with temperature, its level from the outset was much lower than the approximately 5 - 15% abundance measured at the surface. Like Re, the lack of B is believed to be due to precipitation of solid Y-B and Re-B phases at the source operation temperature. Increasing the temperature acts to drive the reaction toward the liquid phase, e.g., YB(s) = Y(l) + B(l), and accounts for the increased B signal with temperature. Unfortunately, increases in temperature also increase the rate of Re dissolution in the alloy which raises the melting temperature of the liquid film by formation of high-melting rhenium boride phases.

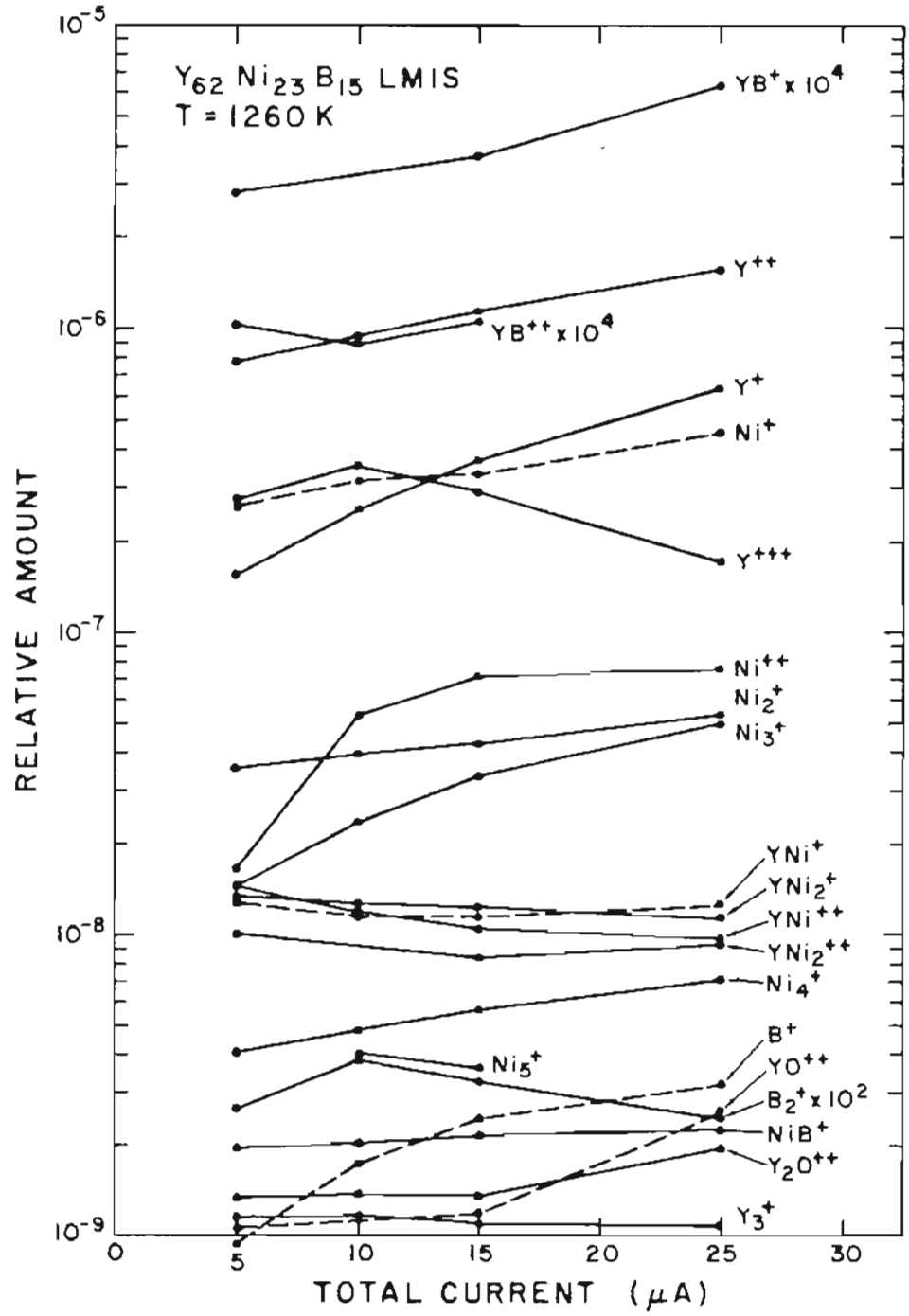

Figure 5-10. Relative amount of various species in the ion beam of the Y/Ni/B on Re LMI source vs beam current.

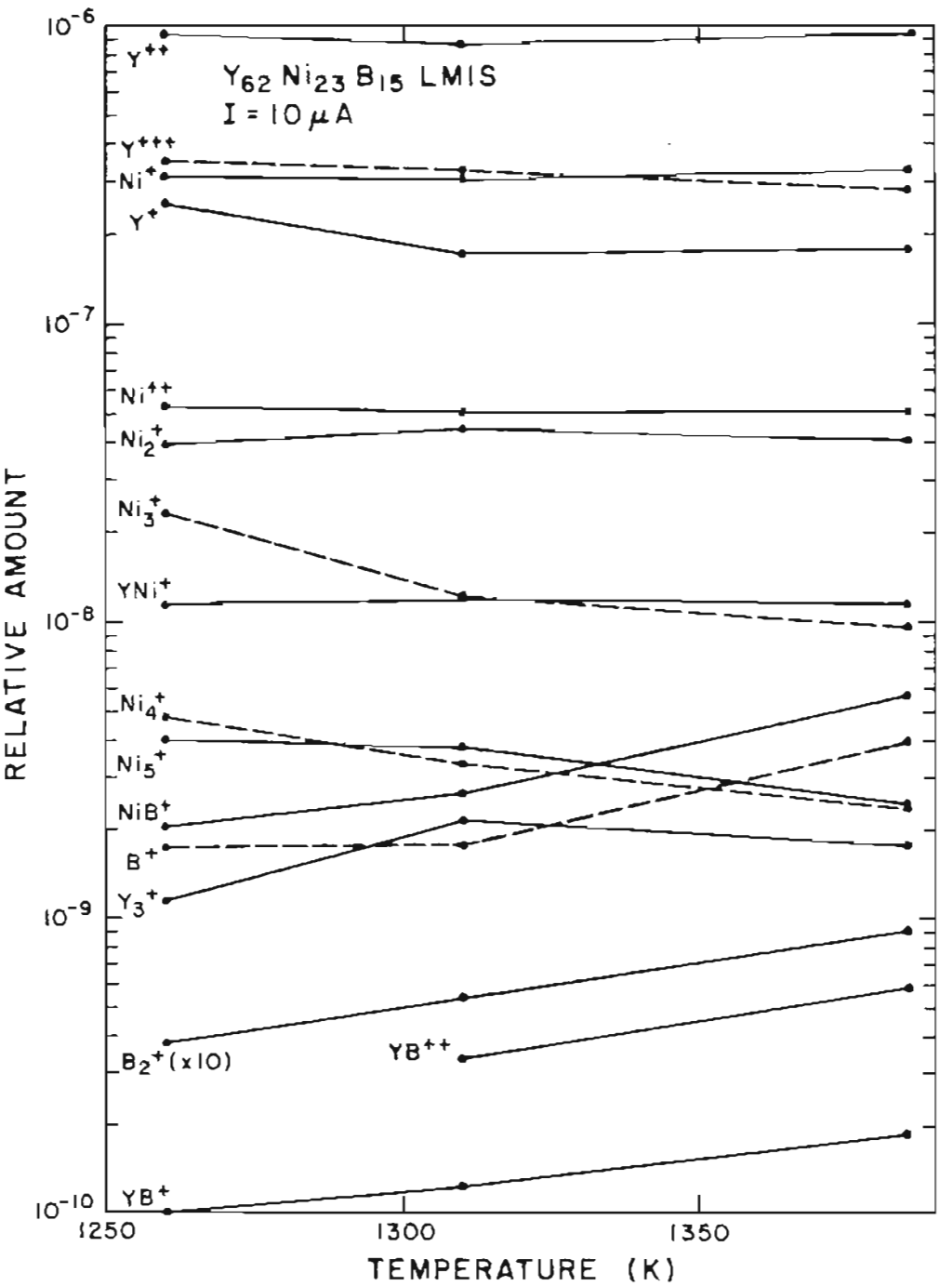

Figure 5-11. Relative amount of various species in the ion beam of the Y/Ni/B on Re LMI source vs emitter temperature.

C. Studies of the Ni/B on C System

A number of samples of $Ni_{45}B_{55}$ on C were studied. The controls which varied from sample-to-sample and served as the basis for research were boronization, boronization temperature, and boron fluxing. It was later found that these experimental controls were not controls at all, but contained a number of elements that were inherently irreproducible. Only after considerable experimental effort was it possible to isolate the sources of irreproducibility and determine the actual parameters that influenced wettability.

The melting point of the Ni/B binary was determined to be T = 1292 K by observation of well-wetted contact systems. In these systems, the melting was relatively sudden, supporting the conclusion that the alloy composition was near the eutectic of the binary. Other systems, however, were poorly wetted and consisted of localized droplets of alloy atop the substrate. The discussion here considers each of these subcategories in turn, with a view to exposing the important differences in wetting behavior between the systems.

1. Studies of Well-wetted Ni/B Contact Systems

Contact systems in this subcategory were well-wetted to begin with and remained so with heating, usually spreading over the pure graphite substrate by distances of the order of millimeters with increasing temperature. Surface contamination was minimal, and consisted of small amounts of nitrogen and carbon which persisted after cleanup. Unmelted boron originating from the boron fluxing

pretreatment was often observed in the alloy. An example is given in Figures 5-12 to 5-13, which show a sample of boronized and fluxed alloy in its "as received" condition at room temperature and at a temperature of about 25 degrees below the melting point of the alloy. The view is of the reverse side of the ribbon. During the wetting process, the alloy had wet and flowed to the nonboronized backside of the graphite ribbon. In Figure 5-13 early evidence of melting is observed. Sharp structural edges are beginning to soften and the alloy has moved outward over the substrate by nearly 10 microns. We define the melting point of the alloy as T_m = 1292 K, even though there is evidence of melting at T = 1267 K, because the most dramatic change of phase occurs at T_m. Compositionally, the light areas consist of equal concentrations of B and Ni, and the dark areas are pure B corresponding to the excess boron added to the alloy. The leading edge of the moving alloy front appears to be B-rich, which may indicate the formation of boron carbide at the interface. Chemical wetting processes require the formation of such an interfacial compound to promote good wetting.

The composition, melting point, and phase behavior of the alloy allow an approximate determination to be made of the melt stoichiometry and position on the binary phase diagram. Since the melting point of the alloy was determined to be 1292 K (1019 C) on material with nearly equal atomic fractions of B and Ni, the alloy is close to the eutectic of the binary system, shown in Figure 5-14. Given this information, a reasonable estimate of the phase behavior with temperature may be formulated. At point A of Figure 5-14, for

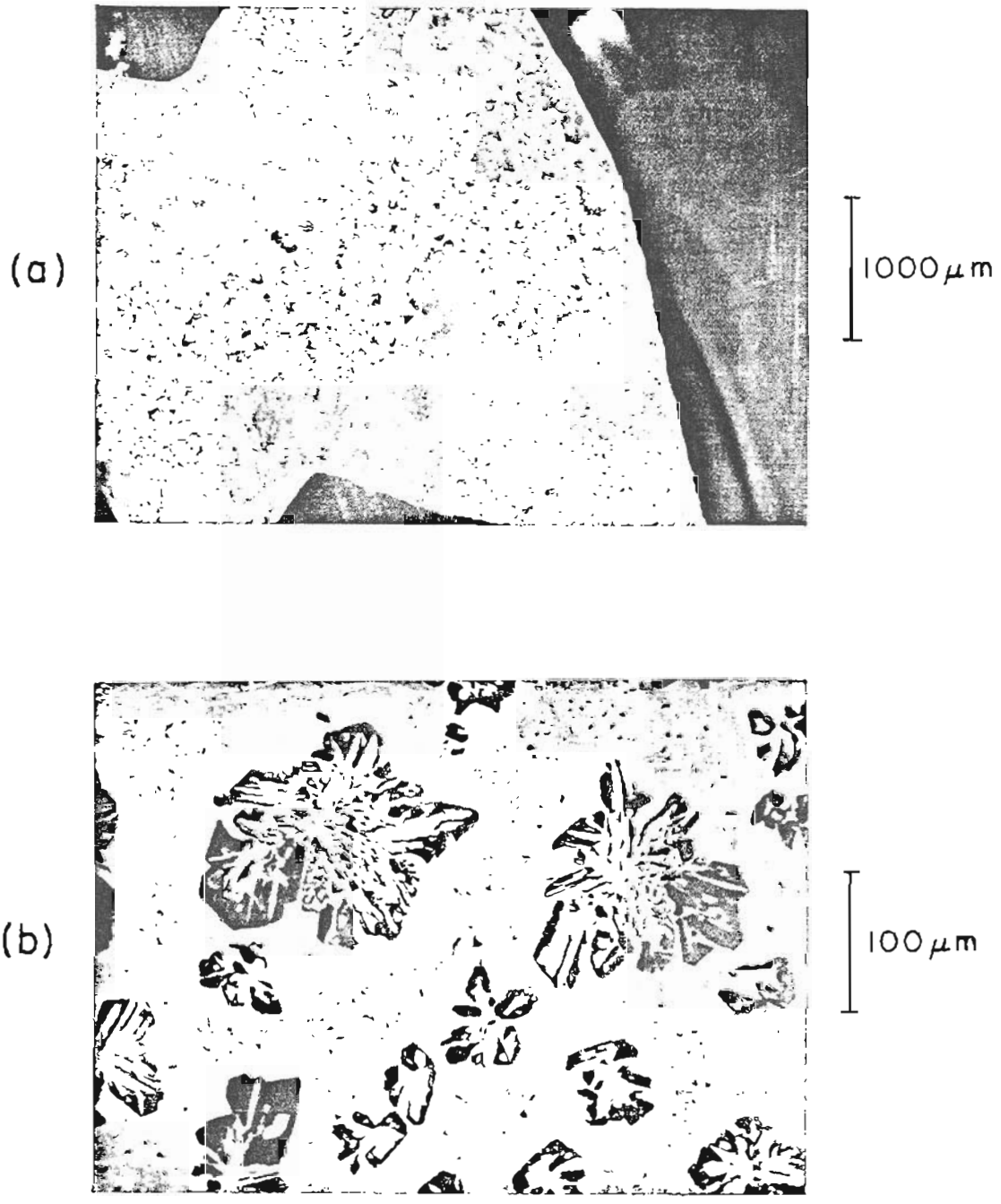

Figure 5-12. SEM micrographs of the Ni/B on C alloy (HRL: E-3; D-3) in its "as received" condition. (a) Overall view of the wetting; (b) Crystalline precipitates within the alloy.

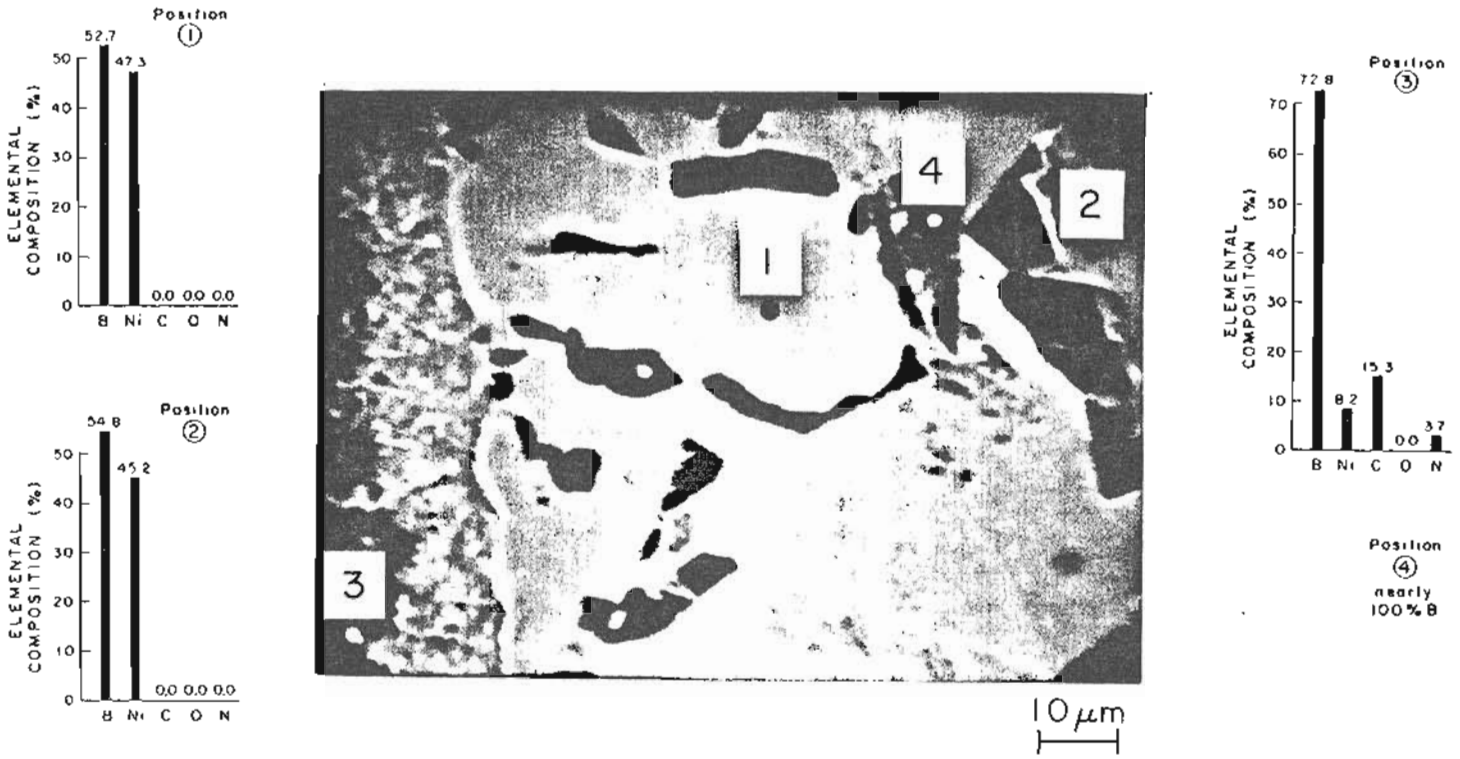

Figure 5-13. The Ni/B on C alloy surface (HRL: E-3; D-3) immediately prior to melting at T = 1267 K = T_m - 25°.

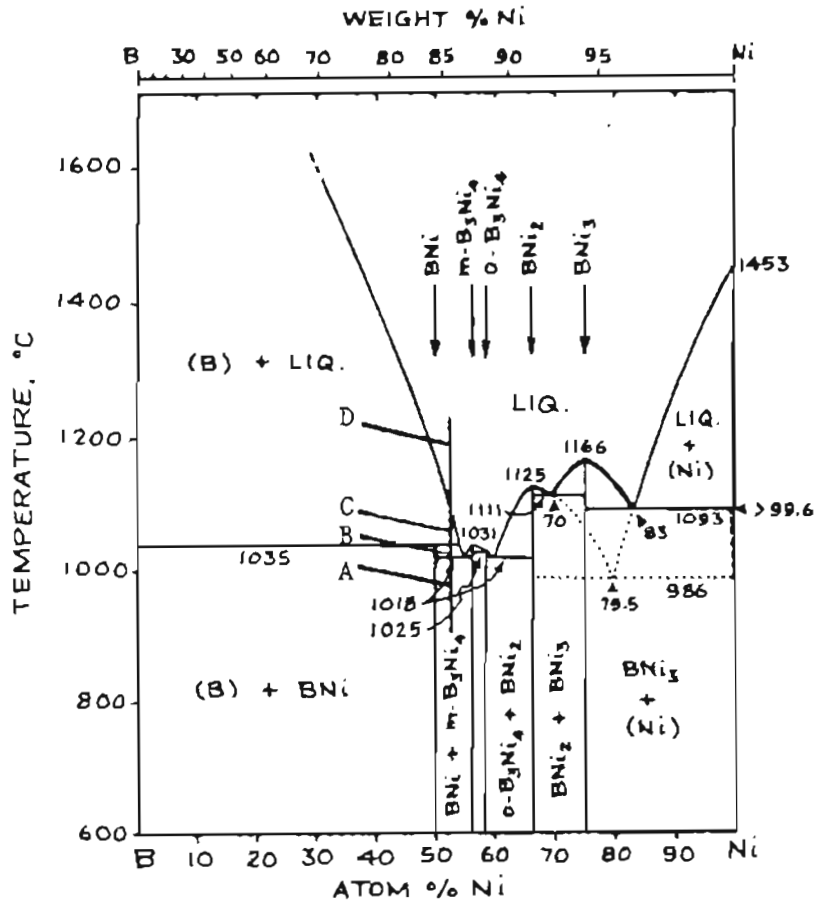

Figure 5-14. The phase diagram of the Ni-B system, with a likely phase progression indicated.

example, the composition of the alloy before melting will be about 60% BNi and 40% m-B_3Ni_4. During heating to point B, liquid alloy of the eutectic composition will begin to form. Further temperature increases to C results in a mixture composed of 5% solid B and 95% liquid BNi, becoming more B-rich until the temperature reaches 1100 C. The resulting liquid stoichiometry at high temperatures will be about 100% NiB, the composition derived experimentally for the liquid alloy. It is likely that the addition of extra boron has caused the slight shift toward the B side of the eutectic.

Detailed elucidation of the fully melted surface proved difficult due to the rapidly changing surface morphology above the melting point. Even with the high speed capabilities of the scanning Auger microprobe, the liquid film changed too quickly to adequately analyze localized positions on the surface. A motion picture system would be necessary to fully characterize the reaction sequence at melting. Valuable information was obtained, however, by setting the instrumentation to its fastest possible analysis rate compatible with sufficient statistics. Figure 5-15 is a typical view of the melted, well-wetted film, displaying an area-average composition of the surface framed in the SEM photo and three specific analysis positions. The compositional distributions reflect the speed of liquid motion during the analysis and are best interpreted as area-averaged compositions determined from regions of order 10 microns about each position. The melted surface consists of nearly equal concentrations of Ni and B, with no evidence of surface contamination. The original alloy/substrate boundary has moved out

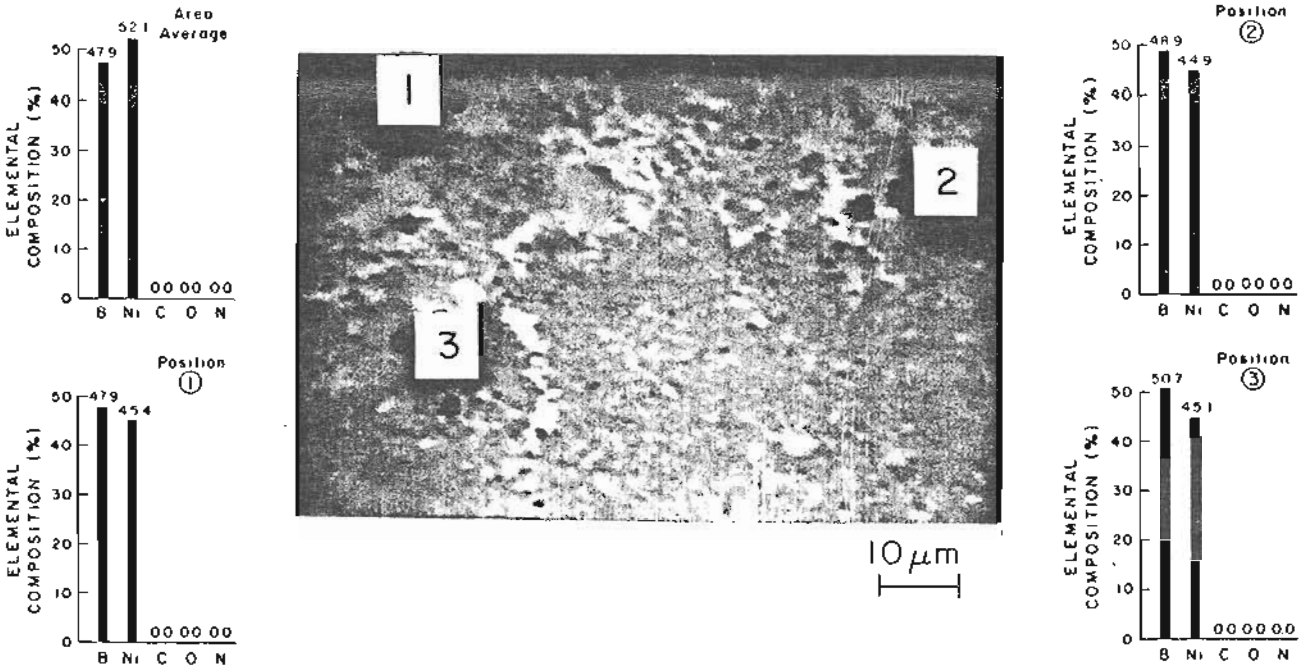

Figure 5-15. The Ni/B on C alloy surface at the melting point (1292 K). The view is the same as in Figure 5-13. The alloy/substrate boundary has moved out about 30 microns to the left of the photo field of view.

over the substrate by nearly 30 microns at the time of this data. Uneven electrical contacts in the support mechanism allowed an unusual view of the alloy to be observed in Figure 5-16. The lower side of view (a) of this figure shows that the bottom half (the side just discussed) of the alloy is fully melted while the upper side is not, and contains dark solid structures that Auger mapping later determined were pure, unmelted boron originating from the fluxing operation.

The behavior of the resolidified surface after cooling to room temperature reflected the expected precipitation of solid B and Ni phases predicted from the phase diagram (see Figure 5-17). The cooled surface was formed by rapid quenching as the temperature was lowered quickly enough to inhibit the approach to equilibrium. The appearance of additional dark structures correspond to precipitated boron.

Graphite dissolution was found to occur in Ni/B contact systems at temperatures greater than 100 degrees above the alloy melting point. During a high temperature experiment designed to investigate the rate of alloy volatilization, the alloy vapor pressure was examined by quadrupole mass spectrometry at T = 1400 K for nearly 20 minutes to determine if significant rates of thermal evaporation were occurring. No volatile species were found at this temperature. Previous to this treatment, no C was found in the alloy surface. Afterward, however, regions could be found in the surface with irreversible carbon concentrations ranging from 5 - 30%. To determine the nature of interdiffusion at the interface of the alloy

(a)

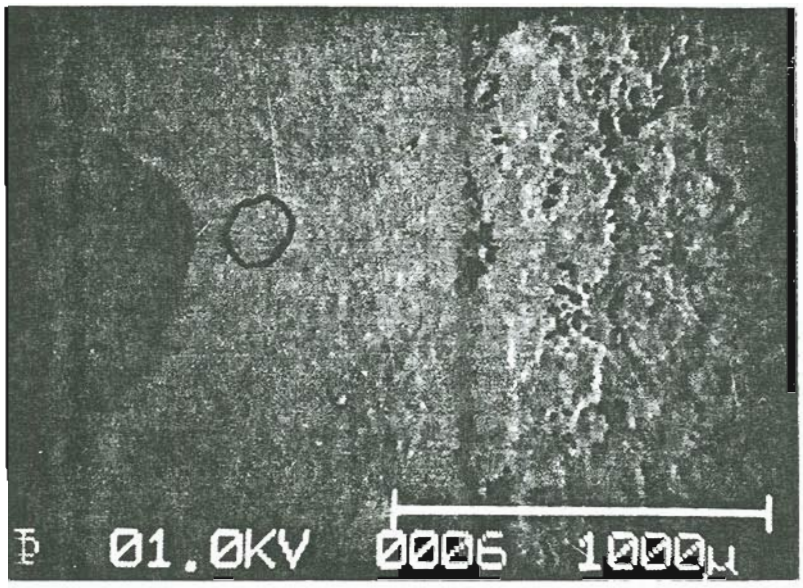

(b)

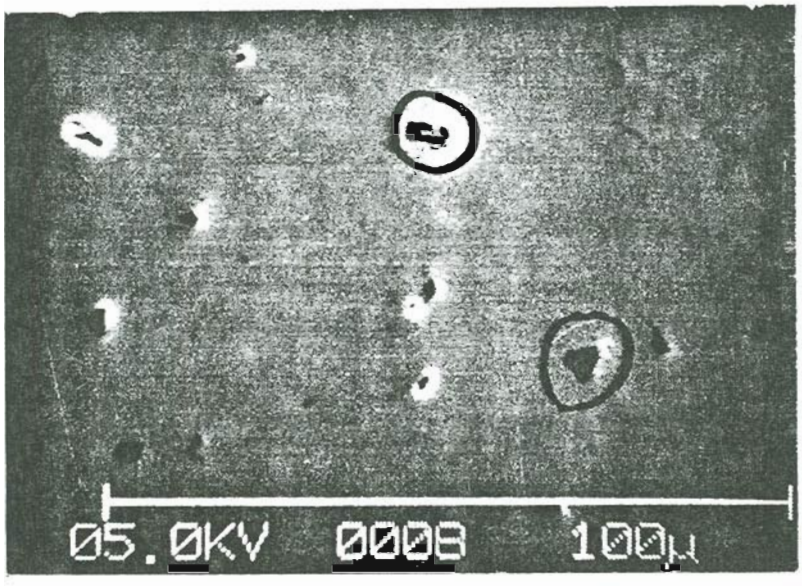

Figure 5-16. Views of the Ni/B on C alloy at the melting point. (a) Low magnification view of the central alloy region, showing that the lower portion of alloy is melted, while the upper region is solid; (b) High magnification view of dark precipitates within the alloy.

(a)

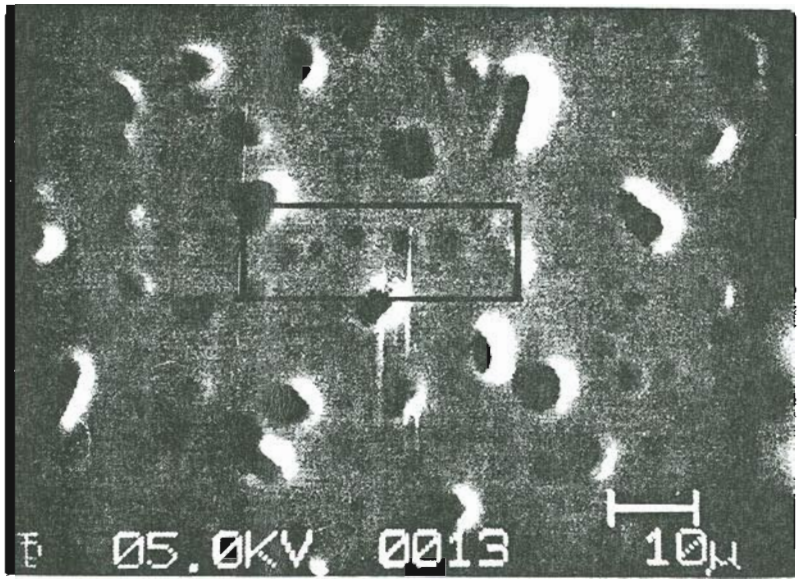

(b)

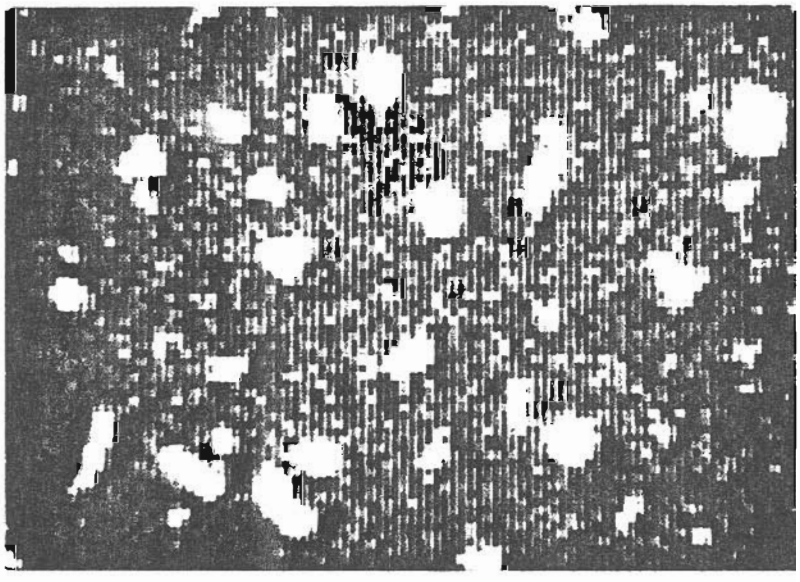

Figure 5-17. Views of the Ni/B on C alloy after resolidification. The temperature is 1267 K. (a) Representative view of the surface, showing second phase precipitation; (b) An enhanced B Auger map of (a).

and substrate, the Ni/B on C system was fractured and mounted in such a way to permit a cross-sectional examination of the interface. A SEM photo of the fractured cross-section is shown in Figure 5-18. The interface is unexpectedly sharp and covered with a 10 micron layer of alloy material. Area-averaged and point-by-point Auger studies revealed no dissolution of alloy components into the graphite. This is a remarkable result, given the high degree of porosity of the graphite. Studies to be discussed later, however, show that dissolution of alloy may occur during long-term heating at high temperatures.

The work function of the nickel boride alloy was determined by the FERP method to be 5.1 eV and is reported in Table V, where values for the platinum boride alloy are also recorded. Within the accuracy of the measurement (0.05 eV), little change is noticed relative to heat treatment. Comparison to values tabulated for the pure components is difficult, since work function values depend on numerous parameters whose effects are not well understood.

TABLE V

ALLOY WORK FUNCTIONS

Treatment	Work Function (eV)*	
	$Ni_{55}B_{45}$	$Pt_{72}B_{28}$
Heat to T_m - 50, cool to 300 K	5.05	4.81
Heat to T_m, cool to 300 K	5.09	4.83
Heat to T_m + 50, cool to 300 K	5.12	4.83

*For the pure elements: Ni: 4.7 (211) - 5.9 (111) OGC
B: 4.5; Pt: 5.0; C: 4.7
(Fomenko tabulation)

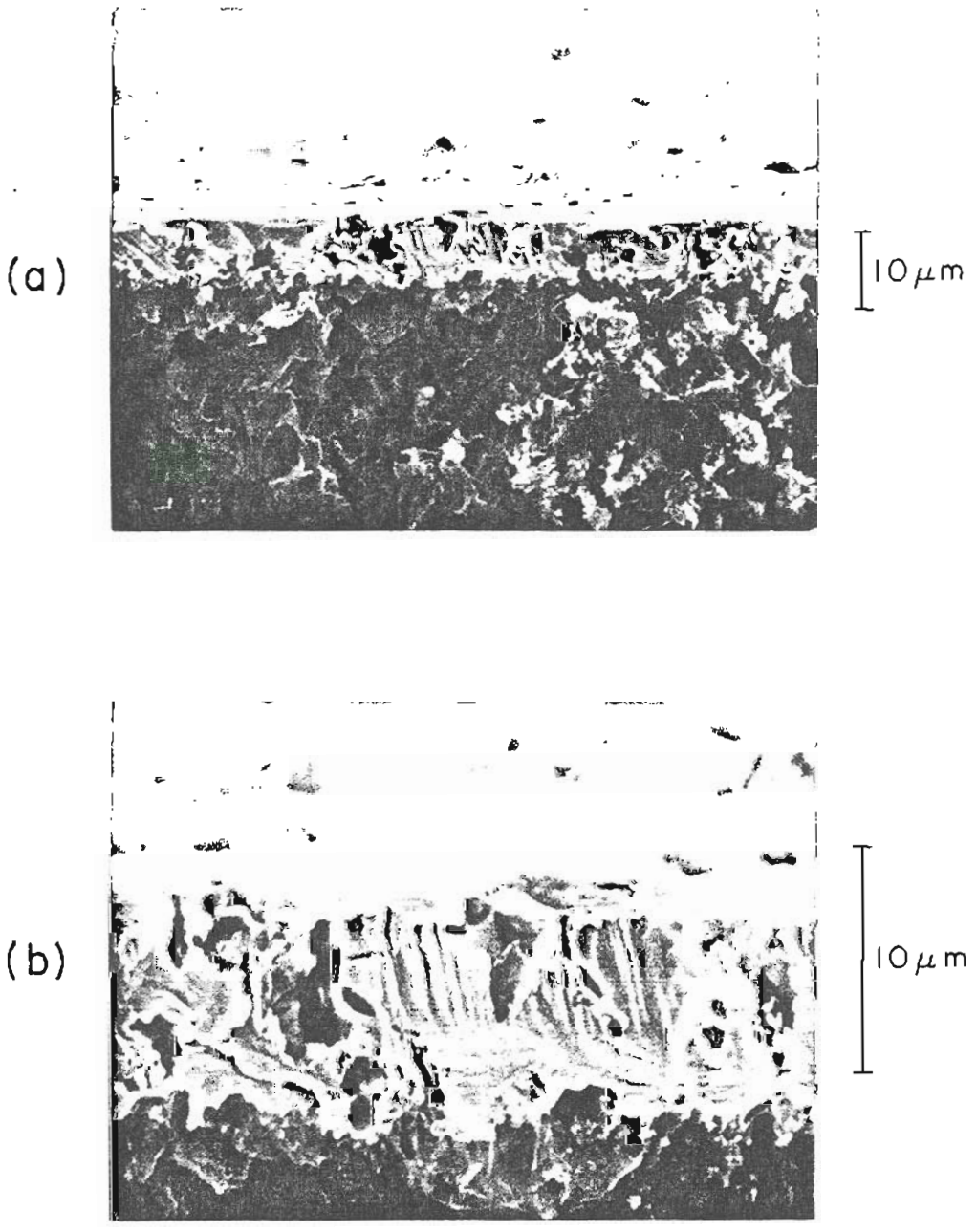

Figure 5-18. Cross-sectional views of the Ni/B on C alloy after fracture. Given the porosity of the graphite, the alloy/substrate interface is remarkably sharp, with no evidence of interpenetration.

2. The poorly-wetted Ni/B on C Contact System

The degree of initial wetting of poorly-wetted Ni/B contact systems was highly variable. Examples existed containing large central droplets of alloy and regions with wetting characteristics ranging from poor to fair. Liquid flow was possible only by high-temperature treatment and even then, asymmetrical melting and flow properties were the rule rather than the exception. Figure 5-19 shows a typical example of a partially-wetted alloy in its "as received" condition. This alloy had previously been treated with 3% additional boron and "light" boronization pretreatment of the graphite substrate. The wetting consists of localized droplets of alloy atop the substrate. Figure 5-20 is an Auger point analysis of the clean molten surface at a temperature of T = 1345 K = T_m + 50°. High percentages of C and N are observed, particularly on the stationary right-hand side of the alloy. The left-hand side, containing significantly less C and N, has begun to spread past the boronized region and onto the virgin carbon substrate. The C signal is not due to adsorbed CO, since all oxygen has been thermally desorbed by heating. Electron micrographs of the surface after 50 hours of heating at 1355 K are shown in Figure 5-21. In this figure, the alloy has spread significantly over the virgin substrate on the right side of the ribbon. On the left side, containing large concentrations of C and N, the alloy has remained stationary. Similar behavior has been found to occur in a number of contact systems possessing poor wettability. Instances exist where only one

(a)

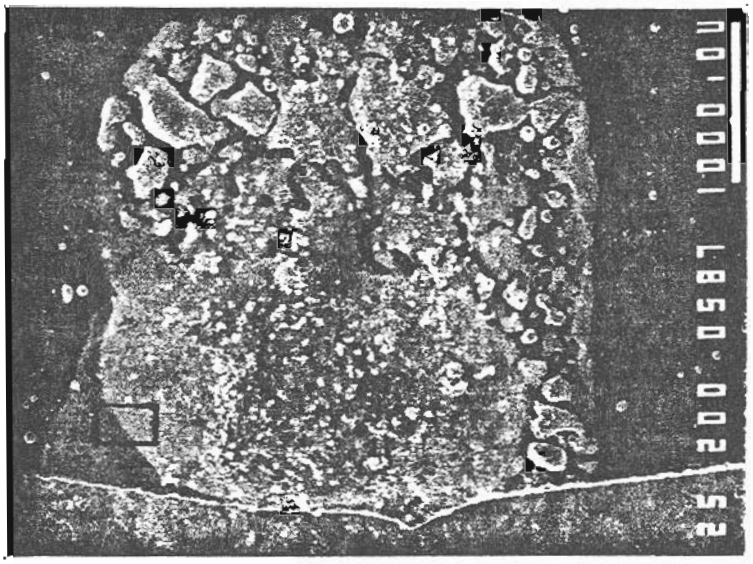

(b)

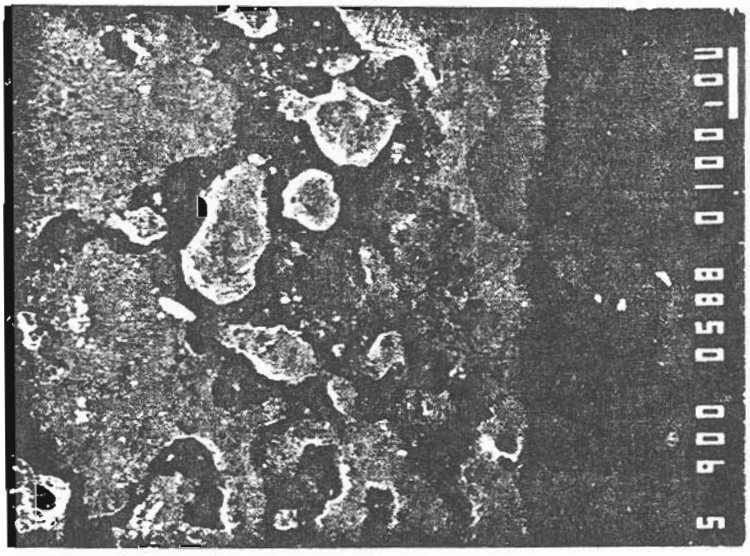

Figure 5-19. SEM micrographs of the Ni/B on C alloy (HRL: E-9; #1) in its "as received" condition at 300 K. (a) Overall view of the wetting; (b) View of the boxed region of (a).

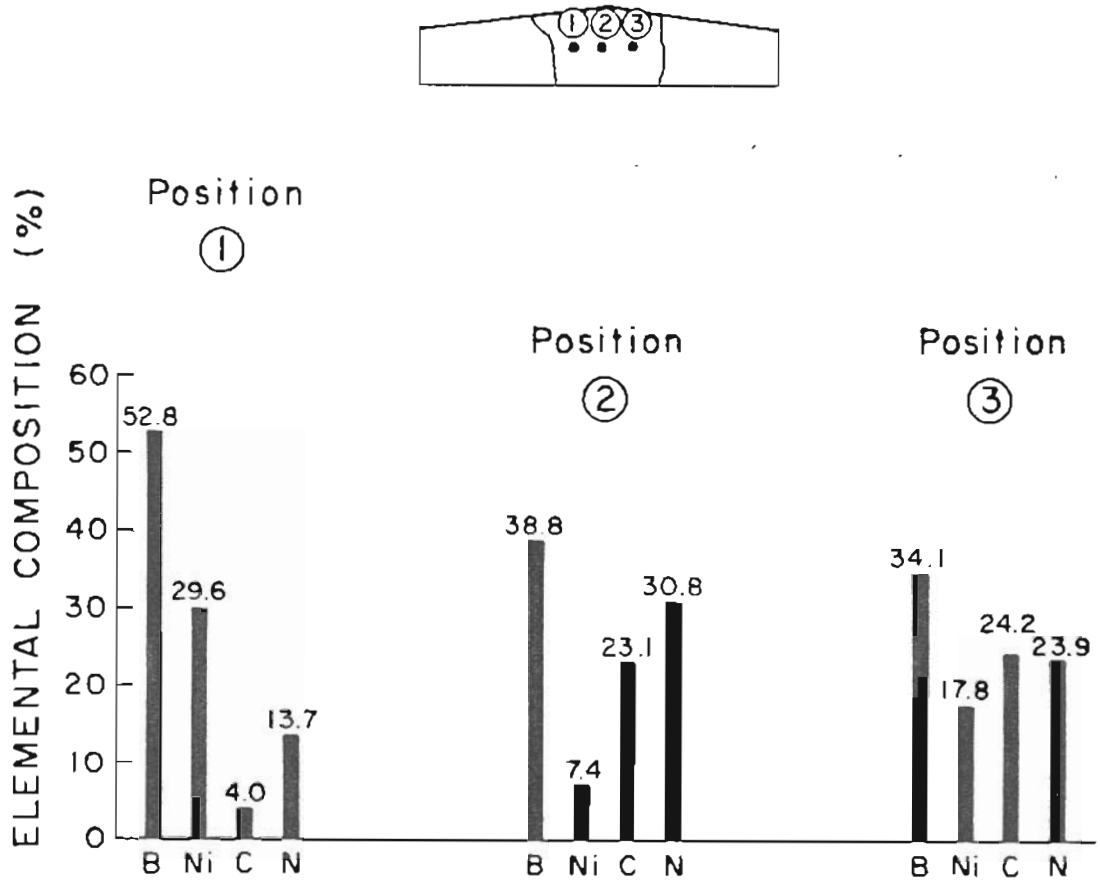

Figure 5-20. Auger surface elemental composition vs position for the Ni/B on C (HRL: E-9; #1) alloy at T = 1345 K = T_m + 50°. High percentages of C and N are notable on the middle to right side of the alloy that has not flowed during heating.

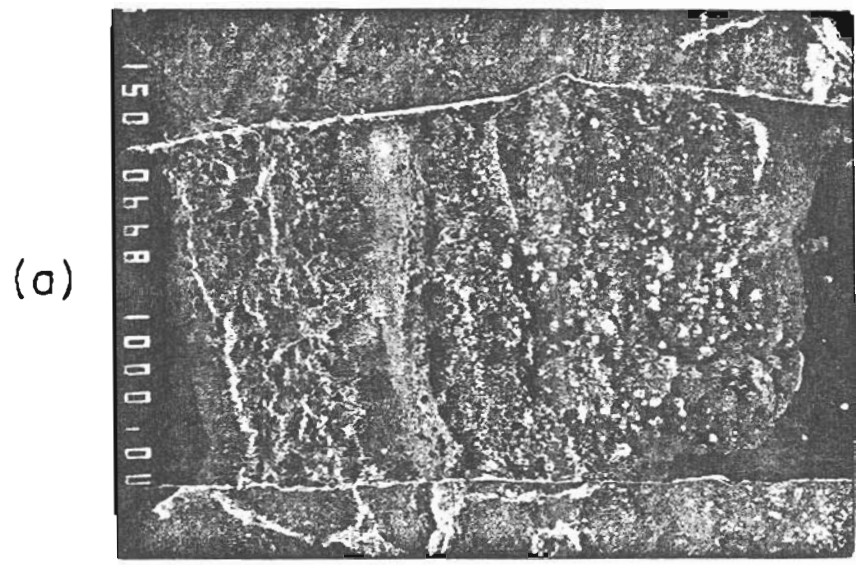

Figure 5-21. Views of the Ni/B on C alloy (HRL: E-9; #1) at 300 K after long-term heating above the melting point. (a) Overall view of the alloy surface. The left half of the alloy has spread over the substrate by a few millimeters while the right half has remained stationary; (b) Precipitated crystal structure within the central region of the alloy.

boundary is observed to advance while the other does not. The possibility of temperature gradients across the alloy surface due to unequal electrical contacts in the support structure was subsequently ruled out because cases of asymmetrical flow were found in samples where careful temperature measurements showed uniformity within 5^{o} across the ribbon. The cause of this asymmetrical flow is discussed in section 4 below.

3. Carbide and Nitride Auger Chemical Effects

A number of Auger chemical effects were found to be associated with the high concentrations of C and N characteristic of non-spreading boundaries in the alloys. These chemical effects provide a direct and unambiguous determination of compound formation in the alloys and explains the lack of liquid flow during presence of these elements. The chemical effects are catalogued in this section.

Reference to Figure 5-22 shows that the B(KLL) = 179 eV Auger peak is strongly influenced in spectra taken on portions of the alloy surface where strong signals of N and C were present. The chemical shift of the B peak is evident by the dramatic shape change in the peak and by the 9 eV downward shift in energy of the peak. Comparison to a pure standard Auger spectrum of boron nitride displayed in Figure 5-23 verifies that the chemical shift found in the liquid surfaces is due to the presence of BN in the alloy. The presence of BN in the alloy surface is not unexpected because boron nitride possesses a Gibbs free energy of -34.6 kcal/mole near the

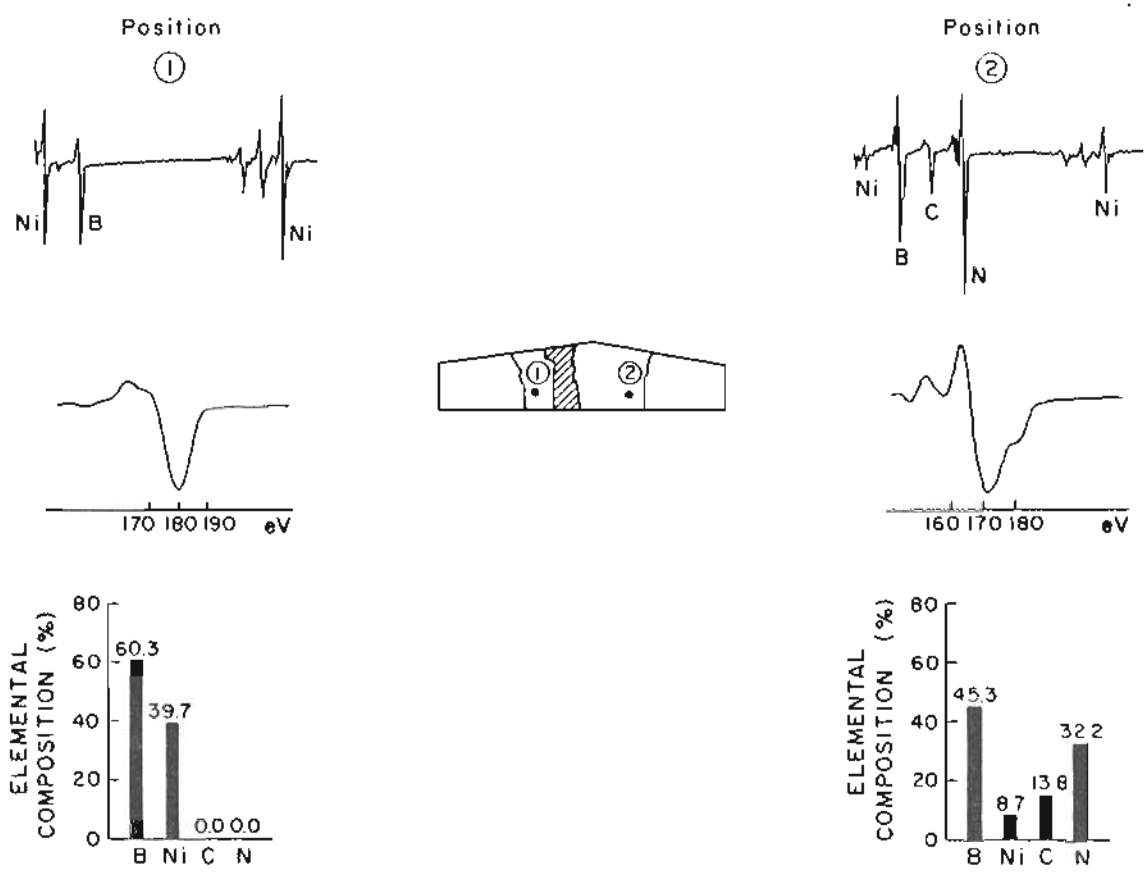

Figure 5-22. Auger chemical shift of the B(KLL) = 179 eV spectral line due to formation of BN. (Left) Normal B peak. (Right) Chemically shifted B peak. For each position: (Top) Full Auger spectrum; (Middle) Magnified B peak; (Bottom) Surface elemental composition.

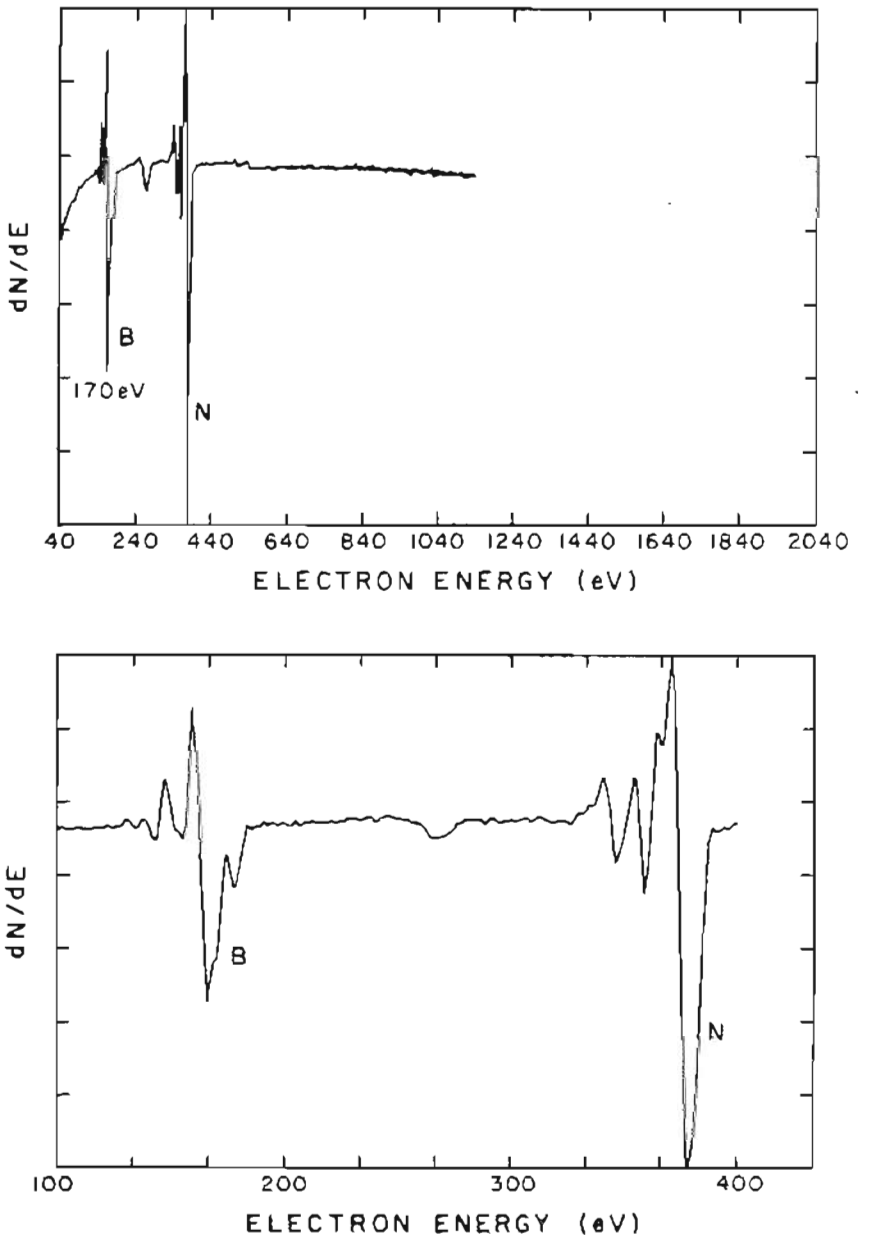

Figure 5-23. Boron nitride standard Auger spectrum. Note the distinctive peak shape and -9 eV chemical shift of the B peak (from D. Jones, Materials Analysis Laboratory, Tektronix, Inc.).

melting point of the nickel boride eutectic (see Table VI). It is therefore thermodynamically able to form. The structure and properties of BN are given in Figure 5-24. Its lattice is isomorphic with graphite.

TABLE VI

GIBBS FREE ENERGIES OF FORMATION OF COMPOUNDS CONTAINING ALLOY COMPONENTS

Compound	dG_f(kcal/mole)	
	1200 K	300 K
Boron carbide (B_4C) [a]	-8.6	-9.2
Boron nitride (BN) [a]	-34.6	-53.7
Nickel carbide (Ni_3C) [b]	+6.1	+7.6

[a] Source: JANAF Thermochemical Tables, 2nd Edition, U.S. Dept. of Commerce, National Bureau of Standards, 1970.
[b] Source: G. V. Samsonov, Properties Index 20.2, Plenum Handbook of High Temperature Materials, 1964.

Boron carbide was also found to exist in the alloy surfaces, as determined by comparison of standard Auger spectra of boron carbide with similar spectra of the alloy. Boron carbide was suspected to form in the alloys because of the nonvanishing C signal that was repeatedly observed to accompany the N concentrations in the alloys. Two different samples of boron carbide were studied and found to have similar effects on the Auger spectra.

The first boron carbide specimen was supplied by HRL, and was in the form of a flat ribbon of zone refined material a few mils in thickness and about 10 mm X 5 mm in area. Figure 5-25 contains two

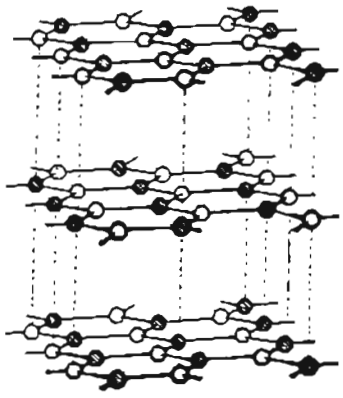

Properties:

Color: White, transparent to light; material contaminated with carbon is gray.

Feel: Greasy, similar to talc.

Particle size: Varies from submicroscopic amorphous to flakes up to 20 microns in diameter.

Sublimation temperature: 3,000 C at 760 mm.

Melting point: Above 3,000 C under pressure with nitrogen.

Equilibrium dissociation pressure: 158 mm at 2,045 C.

Thermal conductivity: Very low for the powder because of its low bulk density.

Specific heat equations:

B: $Cp = 1.54 + 4.40 \times 10^{-3} T.$

N_2: $Cp = 6.50 + 1.00 \times 10^{-3} T.$

BN: $Cp = 3.22 + 8.00 \times 10^{-3} T.$

$2\ BN = 2B + N_2$: $\Delta Cp = 3.14 - 6.20\ T.$

(The above equations are not highly accurate and hold only for temperatures below 1,173 C.)

$\Delta H_{298.1}^{\circ} = -31,530$ calories.

$\Delta F_{298.1}^{\circ} = -27,690$ calories.

Figure 5-24. The structure and selected properties of boron nitride.

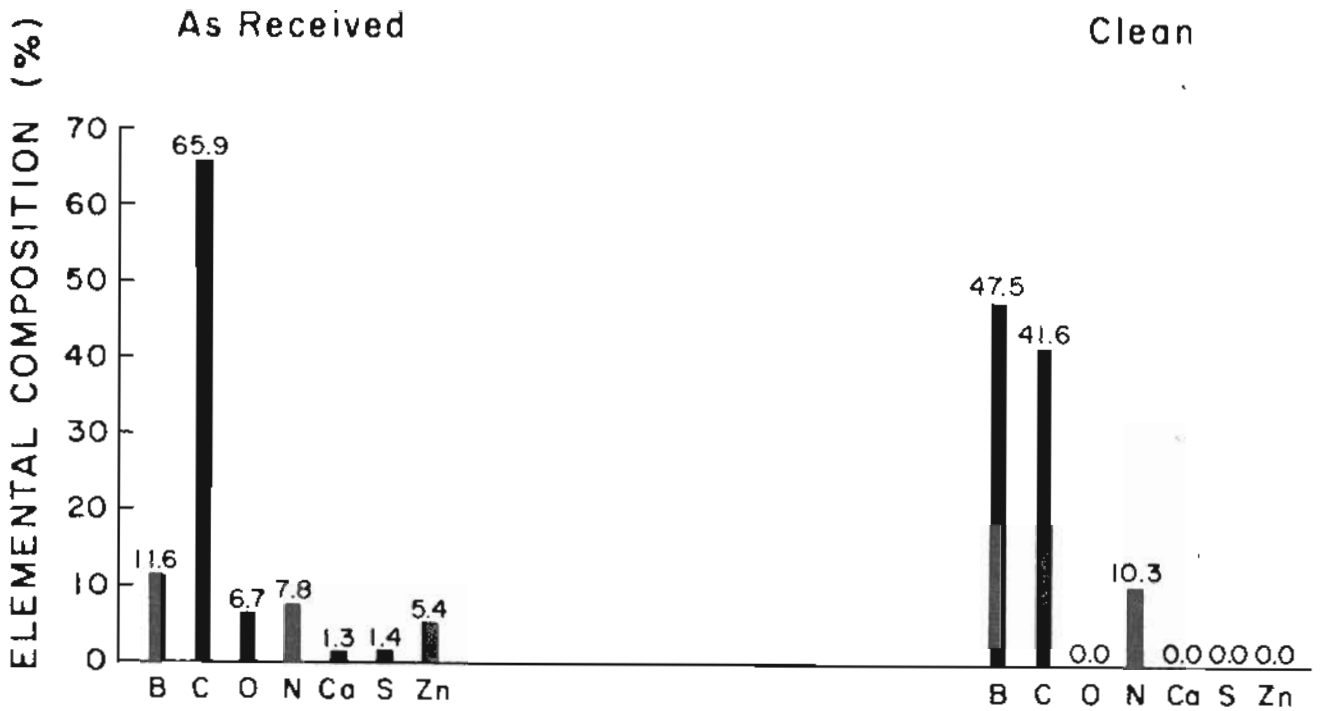

Figure 5-25. Average Auger surface elemental composition for boron carbide (B_4C). The compositions for three positions atop the "as received" and clean surface have been averaged. The surface was cleaned by heating to 1880 K. Nitrogen remains even at this high temperature.

bar graphs representing the average Auger surface elemental composition of three positions on the surface of the "as received" and clean boron carbide. The clean spectrum was taken at room temperature after heating the specimen to 1880 K. Two observations are pertinent. First, nitrogen persists on the surface in significant concentrations even at high temperature. It therefore probably exists as BN, as elemental nitrogen would have volatilized at lower temperature. However, no evidence of the BN chemical shift is found in the spectrum. This is probably due to competition of chemical effects. Boron nitride causes a shape change and energy shift in the B peak while boron carbide causes changes in the carbon peak but none in the B peak. The surface is predominantly boron carbide and the B_4C chemical effect wins. Second, notice that the elemental compositions of thermally cleaned boron carbide do not correspond to stoichiometric B_4C. This is of minimal importance for our concerns here because sample- and instrument-dependent effects and complications inherent in the Auger process which affect the calculation of elemental percentages can be sidestepped by defining the sample of boron carbide measured as the standard to which other spectra can be compared. Details of the chemical shift are provided in Figure 5-26. There is a shape change in the C(KLL) = 272 eV peak but no change in the energy of either B or C peaks. The shape change takes the form of a small oscillation on the low energy side of the C peak. Such an oscillation has been often observed in Auger studies of carbides [2], and originates from chemical bonding of B to C in the compound.

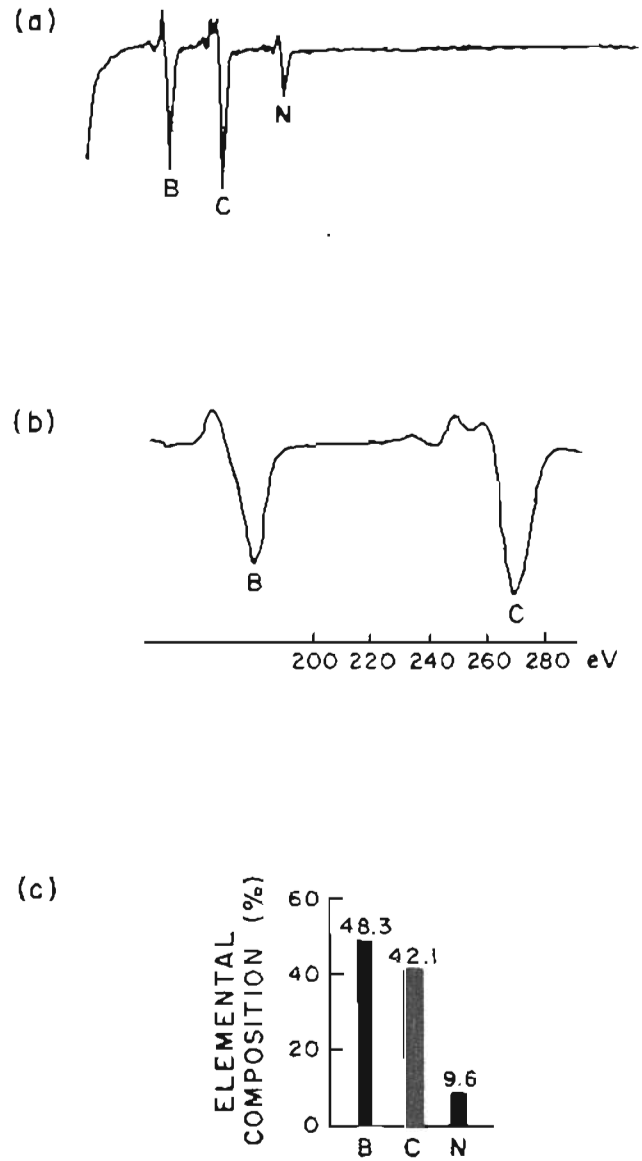

Figure 5-26. Boron carbide standard Auger spectrum. Chemical bonding of B to C is evidenced by the small oscillation on the low energy side of the C(KLL) = 179 eV peak. There is no change in the energy of either peak. (a) Full spectrum of B_4C at 300 K after heating to 1880 K; (b) A blowup of the B-C spectral region; (c) Surface elemental composition calculated from (a).

The second boron carbide specimen consisted of a surface layer of chemically vapor deposited boron carbide supplied by LANL. The layer was investigated by Auger spectroscopy prior to wetting, and the spectrum between 160 eV and 300 eV is shown in Figure 5-27 at a temperature near the melting point of the nickel boride eutectic. The Auger chemical shift is identical to that found for the sample of zone-refined material described above, consisting of a shape change of the C peak. No energy shifts were discovered in either peak. This is in contrast to the results of Hanke and coworkers [3], who find no shape change for boron carbide. The composition of the CVD layer is cleaner than the zone-refined material, which contained a nonvanishing component of N. Nonetheless, the composition of the surface is far from stoichiometric, and consists of more C than B.

Identification of confirmed chemical effects in the spectrum of liquid metal alloys provides a distinctive fingerprint by which to positively affirm the presence of high-melting carbides and nitrides in the alloys. The verification of BN and B_4C formation in the alloy has important bearing on the issue of alloy spreading, as the high melting compounds will render the parts of the alloy surface where they predominate unmelted and incapable of liquid flow. The result is a solid surface which will not spread. The presence of high-melting carbides and nitrides is the primary reason why the N- and C-rich sides of eutectic alloys do not flow upon heating. This is seen further in the example below.

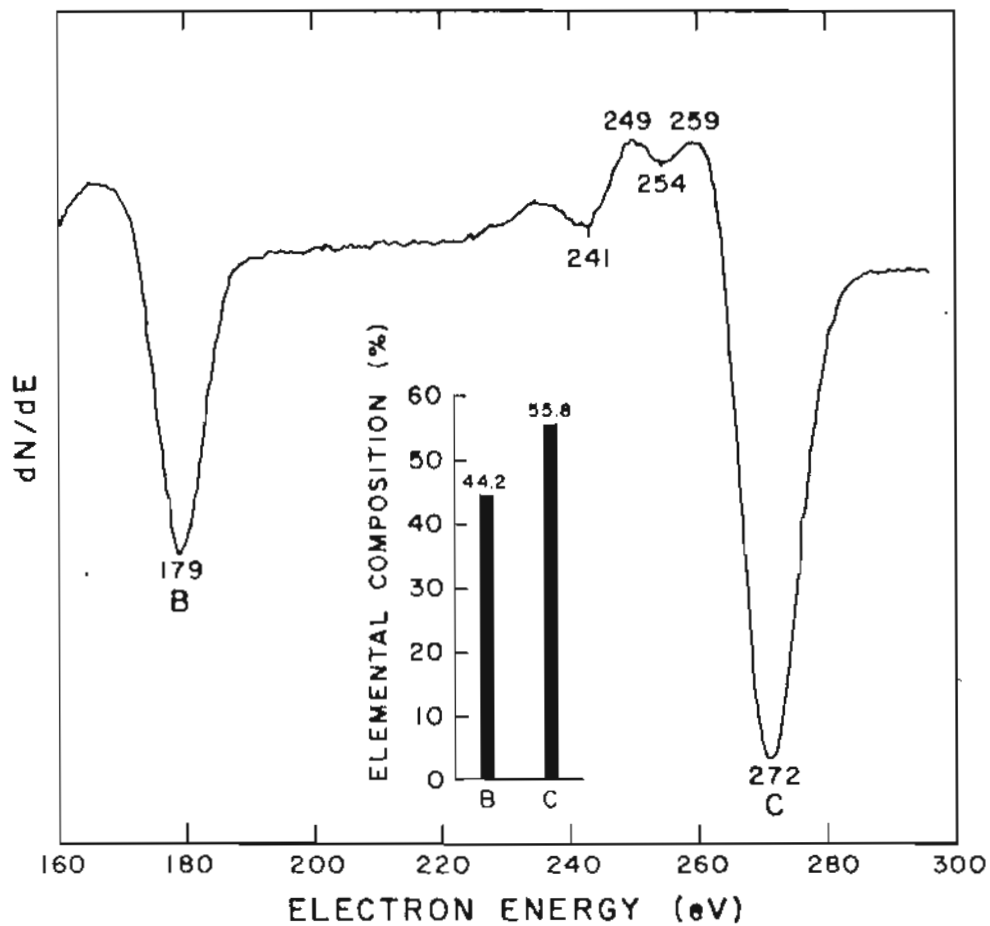

Figure 5-27. Auger spectrum of CVD B_4C (LANL: "M") atop amorphous graphite between 160 and 300 eV. The chemical shift consists of a shape change of the C (272 eV) peak, but no change in energy of either B (179 eV) or C peaks. The inset is the surface elemental composition given by this spectrum.

4. Effects of High-melting Carbides and Nitrides on Spreading and Flow

Having characterized a method to identify high-melting carbides and nitrides, it is now possible to explain the asymmetrical flow behavior found in the prewetted liquid metal alloys. Figure 5-28 provides a photograph of a representative, poorly-wetted Ni/B specimen in its "as received" condition at room temperature. This contact system had been boronized but no additional B was added to the alloy. Auger point analysis of two positions atop the central droplet of alloy show large concentrations of C and N. At positions outside the central droplet, no remnant of the boronization process can be found. The sampled positions consist entirely of C, in spite of the fact that a definite topological boundary can be seen visually separating the ends of the ribbon from the middle. There was no boron anywhere on the surface except on the alloy droplet. This was found to be the rule rather than the exception for prewetted contact systems which had undergone boronization preprocessing.

As the temperature was increased to the melting point, a liquid alloy front appeared to the right of the central droplet and was observed to slowly move outward with time. The advance of liquid appeared to proceed from the underside of the droplet rather than by melting of the droplet sidewall. An attempt to illustrate the situation is shown in Figure 5-29. Auger analysis of the moving front shows that it consisted entirely of B and Ni. In contrast, the droplet remained intact and stationary. Although all O (and hence

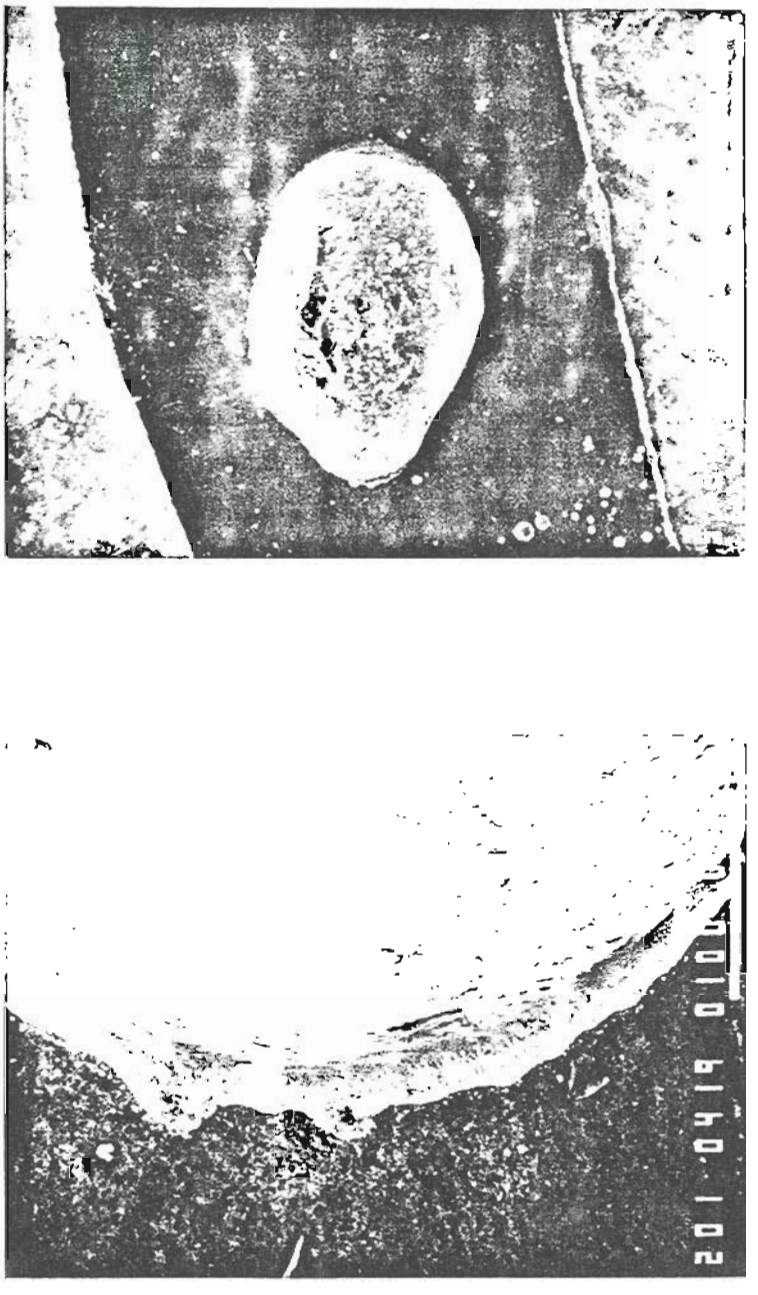

Figure 5-28. SEM micrographs of the poorly-wetted Ni/B on C alloy (HRL: E-4; B-4) in its "as received" condition at 300 K. (a) Overall view; (b) High magnification view of the left alloy/substrate boundary.

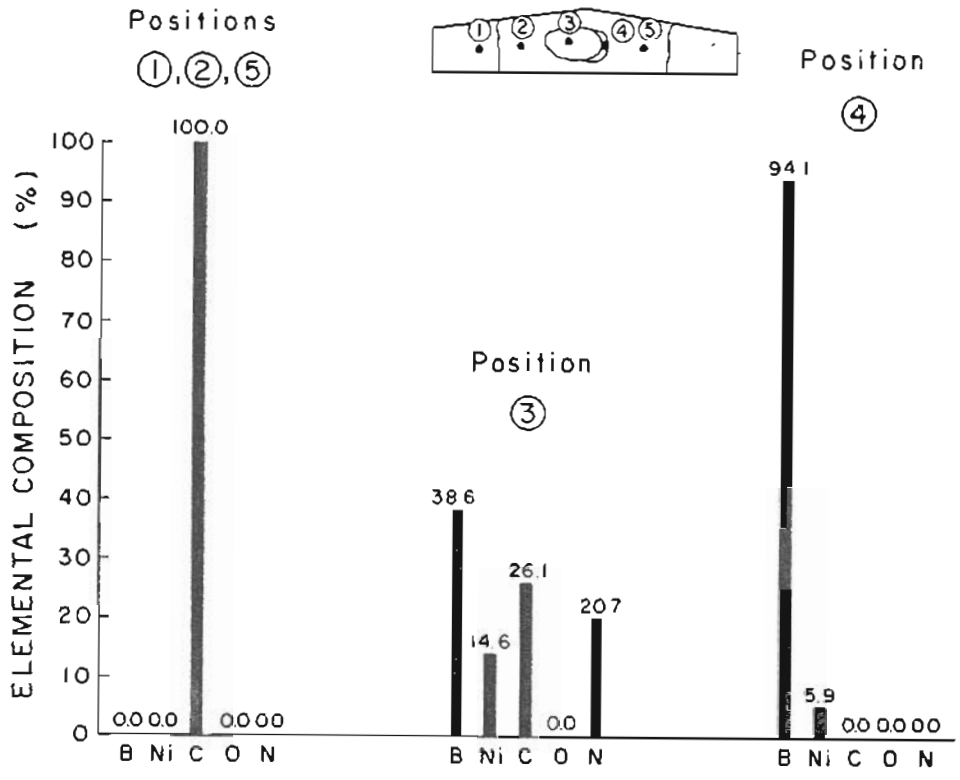

Figure 5-29. Auger surface elemental composition vs position for the poorly-wetted Ni/B on C alloy at T = 1292 K = T_m. A liquid alloy front has appeared to the right of the central droplet.

CO) had volatilized through heating, significant quantities of N and C persisted. The Ni/B-rich liquid front advanced over a pure carbon substrate which contained no trace of B or boronization preprocessing. This is further support that pure Ni/B alloy wets virgin carbon.

The boron peak of most spectra taken on the alloy droplet surface showed the characteristic chemical shifts due to formation of BN and B_4C in the droplet surface. A time sequence describing the advance of the liquid alloy as it expanded over the substrate is shown in Figures 5-30 to 5-31. After 3.0 hours at the melting point, the liquid alloy had expanded outward to the right by distances of the order of millimeters, leaving behind the original solid droplet. No motion to the left of the droplet was found. The composition of the expanding front remained entirely B and Ni, with no trace of C. This was found to be the case in all studied alloys, i.e., where newly-wetted alloy existed, there was little or no trace of the underlying graphite in the alloy either by way of incomplete wetting or dissolution. Alloy samples containing freshly-wetted regions of near-zero contact angles invariably consisted of alloy components only and little or no C and N. Note that C and N persist in large concentrations, however, in the stationary droplet.

It was frequently possible to crack the nitride shell of the original droplet with temperature cycling. As depicted in Figure 5-31, for example, the poorly-wetted droplet described above split open at its right side as the temperature was raised to 20 degrees above the melting point, resulting in a rush of alloy out onto the

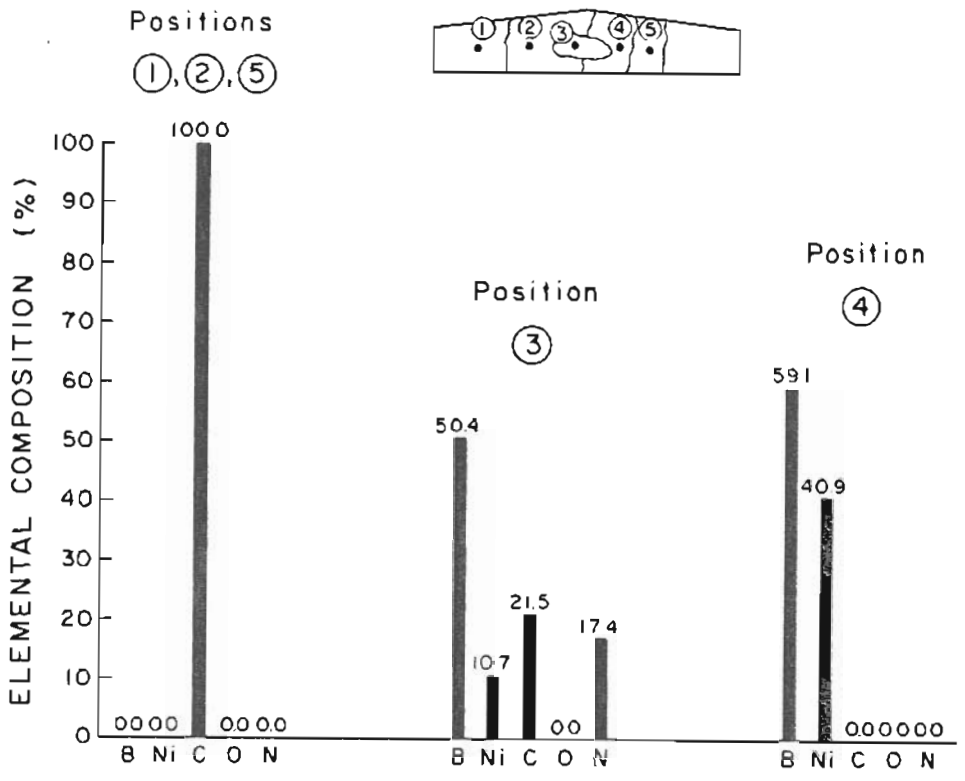

Figure 5-30. Auger surface elemental composition vs position for the poorly-wetted Ni/B on C alloy at T_m. This measurement was taken 3 hours after the first appearance of the alloy front.

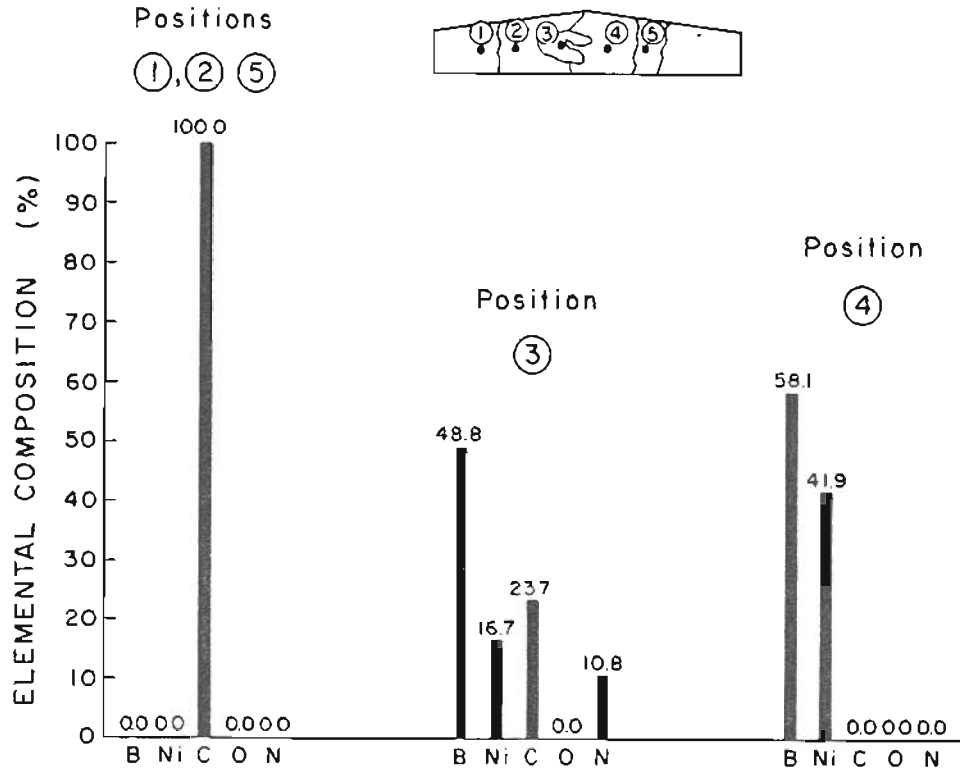

Figure 5-31. Auger surface elemental composition vs position for the poorly-wetted Ni/B on C alloy at T = 1315 K = T_g + 20°. The central droplet has "cracked" during the increase in temperature, resulting in a sudden release of alloy onto the ribbon.

previously wetted area to the right side of the ribbon. An Auger analysis of the usual areas showed little change compositionally. The droplet shell which remained was mostly C and N and the well-wetted region contained only B and Ni. Scanning electron micrographs of the resulting wetted surface after cooldown are shown in Figure 5-32.

D. Studies of the Pt/B on C contact system

Two samples of $Pt_{72}B_{28}$ eutectic alloy were studied in detail at OGC and CRISS. Both specimens contained localized regions of poor- and well-wetted alloy and had been subject to boronization pretreatment and boron fluxing of the alloy. Asymmetrical flow characteristics were found to occur in both samples, and the alloys possessed large amounts of surface C and N that did not vanish upon high-temperature treatment. The melting point of the Pt/B eutectic was experimentally determined to be T_m = 1196 K by observation of the best wetted sample at a surface composition of B = 70% and Pt = 30%. The melting of this sample was found to be sudden and complete, supporting the conclusion that the alloy composition was close to the eutectic of the binary mixture. The other Pt/B sample was found to have a melting point significantly higher as a result of larger concentrations of C and N. Even then, only a few droplets were observed to melt.

The first specimen of prewetted Pt/B eutectic (HRL:E3,12/9/82,C1) was studied using the fixed-beam Auger system at OGC. In an

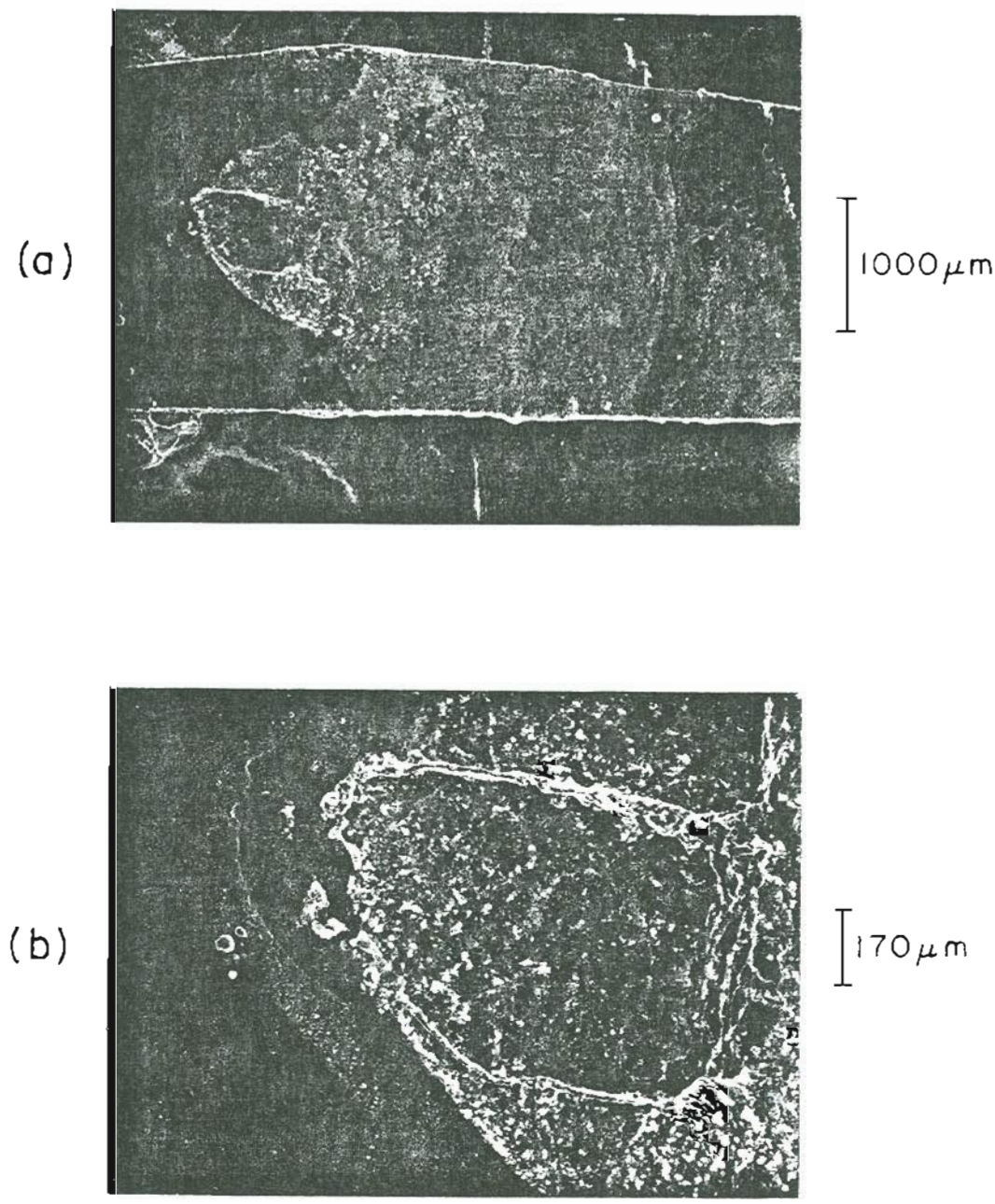

Figure 5-32. Views of the Ni/B on C alloy of Figure 5-28 after heating and wetting. The left side has not wet, but the right side has. (a) Overall view of the wetted graphite; (b) A magnified view of the position once occupied by the poorly-wetted droplet.

experiment to monitor the long-term heating behavior of this alloy, the left-hand alloy/substrate boundary was found to move outward by millimeters over the pure graphite substrate. The right-hand side remained stationary. Composition vs position measurements taken after the motion are shown in Figure 5-33. Positions atop the moving front are composed chiefly of B and Pt, while positions at the stationary center and right side of the alloy showed heavy concentrations of C and N. Unfortunately, evidence of boron nitride chemical shifts cannot be assured in Pt/B alloys due to interference of overlapping peaks near 179 eV. However, the inhibiting role of C and N on wetting is again observed.

Comparison of the melting behavior and composition of the alloy to the binary phase diagram of Pt-B showed that the alloy was nearest the second lowest, B-rich eutectic, which is located at a composition of B = 43% and Pt = 57% and a transition temperature of 1213 K. This is discussed further later. Substantial surface segregation of B is indicated. Unusual wetting and viscosity characteristics were observed during heating of the alloy. The molten Pt/B alloy appeared initially to be much less viscous than the Y/Ni/B and Ni/B systems. With rising temperature, a dark area developed within a section of previously well-wetted alloy that appeared to be uncovered graphite. Indeed, subsequent Auger analysis of this region showed a large percentage of graphite. Further increases in temperature caused the alloy to return to its former state having no uncovered areas and the behavior was not reproducible. The work function of this sample was determined to be 4.8 eV and showed little change following cycles of

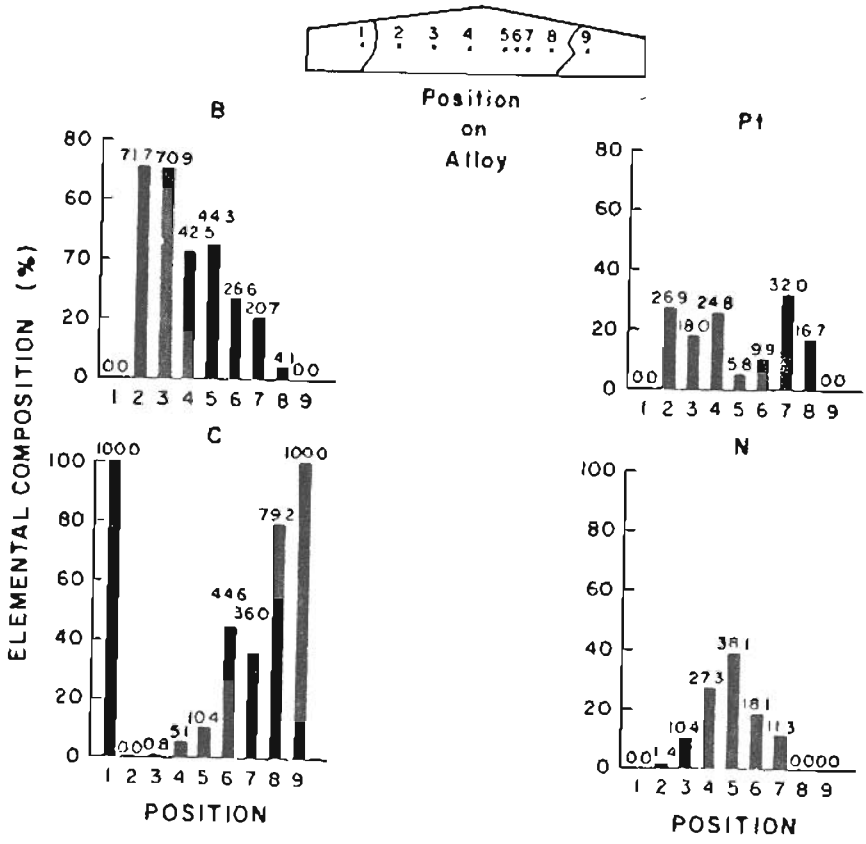

Figure 5-33. Auger surface elemental composition vs position for the Pt/B on C alloy at 1282 K at the end of long-term heating. The O signal was less than 3% at all positions and is not recorded.

heating. The results are summarized in Table V.

The second specimen of prewetted Pt/B on C alloy (HRL:E3,12/8/82,C2) was studied in the high-resolution scanning Auger microprobe at CRISS. A high-magnification SEM view of the "as received" alloy photographed by this instrument is shown in Figure 5-34. Areas of mixed wetting are evident. A blowup of one such area is shown in Figure 5-35, which shows the condition of a typical location at the alloy/substrate boundary. An attempt to analyze the composition within the round, light structures within the photo at room temperature detected only C. An area-averaged composition taken over a large area near the center of the alloy region revealed mostly C and O, with small amounts of Pt, B, and N. It is interesting that C is so dominant in the poorly-wetted droplets of Pt/B, whereas in the case of the Ni/B surface, Ni and B signals could still be detected through the C coverage. The same measurements were repeated after heating to T = 1147 K = T_m - 50°, where T_m is the melting point determined on the first sample of Pt/B. The large droplet of poorly-wetted alloy remained unchanged at nearly 100% C while the region near the center of the alloy began to show B and Pt signals emerging from decreasing C and O concentrations. Sputtering 25 A of the circled area of Figure 5-35 had little effect. Rather than attempt additional sputter cleaning, we decided to further heat the sample.

When increasing the temperature to T = T_m, no evidence of melting was discerned. The temperature had to be raised to T = 1290 K before changes indicative of melting occurred. The dynamics of

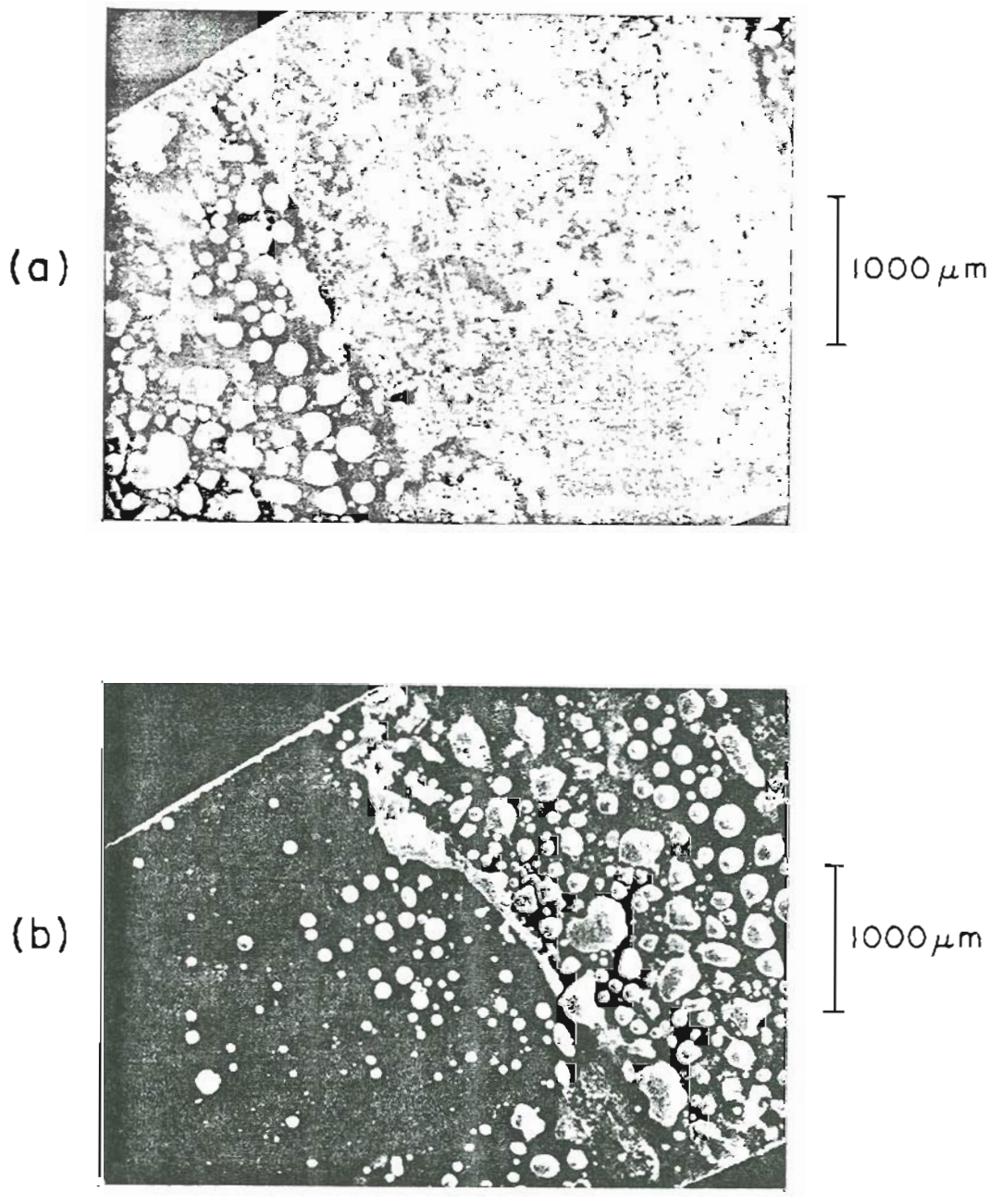

Figure 5-34. Views of the Pt/B on C alloy (HRL: E-2; D-2) in its "as received" condition at 300 K. (a) View of the central alloy region, showing poor wetting; (b) View of the alloy/substrate boundary.

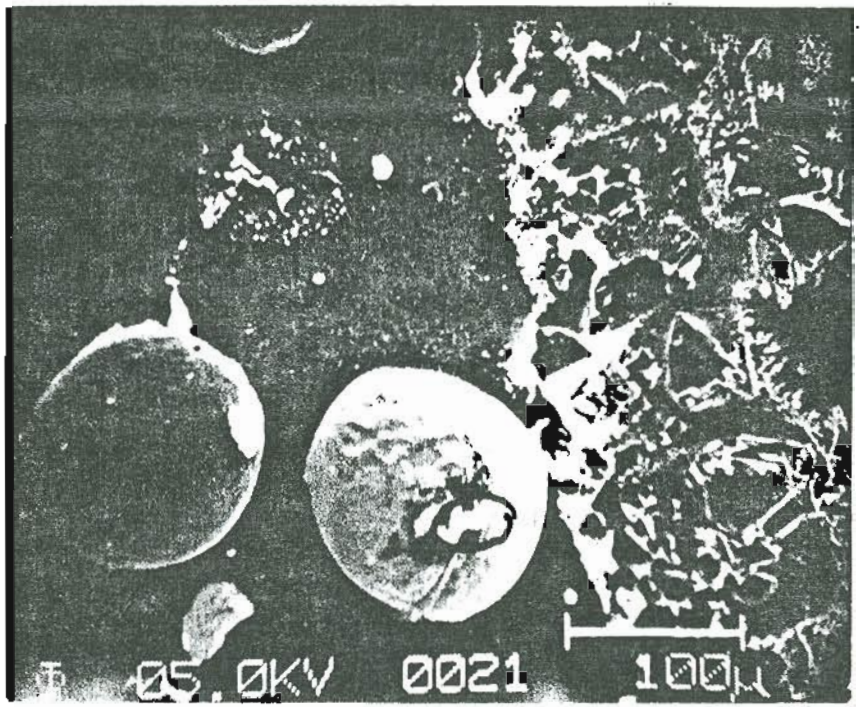

Figure 5-35. View of the "as received" Pt/B on C alloy (HRL: E-2; D-2) surface at 300 K. The photo records a region at the alloy/substrate boundary.

melting were significantly different from the first Pt/B sample, and nearly 0.5 hour was required for a majority of the surface to melt. The alloy appearance at this time is shown in Figure 5-36. A shrinking of the large droplets and subsequent deposit of molten material at the boundary is clearly discerned in this photograph. Auger analysis of the features showed that the alloy surface is composed of a mixture of Pt/B with a ratio of about 1.8 and that all C had disappeared from the poorly-wetted droplets. It was not clear at this time where the C had gone, since it was unlikely to have volatilized. Nevertheless, the disappearance of C and the wetting of the substrate appeared to be connected. This phenomenon will be discussed further later. After about 25 minutes at elevated temperatures, the alloy/substrate boundary shown had moved out over the substrate by 3-4 mm. This movement was also found in the first sample of Pt/B on C. Little change was found in the appearance of the surface during resolidification, which is in contrast to the Ni/B alloy, where B precipitation occurred throughout the alloy upon cooling. Only a few precipitates were observed when cooling the Pt/B alloy. This is probably because the Pt/B alloy has less B to begin with. Few of the large precipitates of B present in the "as received" Ni/B surface were similarly discerned in the "as received" Pt/B surface. More significant is the wetting behavior of the resolidified surface. The surface remained well-wetted during cooling below the melting point and the spherical droplets found initially did not recur. This proved to be the case for all contact systems studied. Once the surface is wetted, it does not dewet.

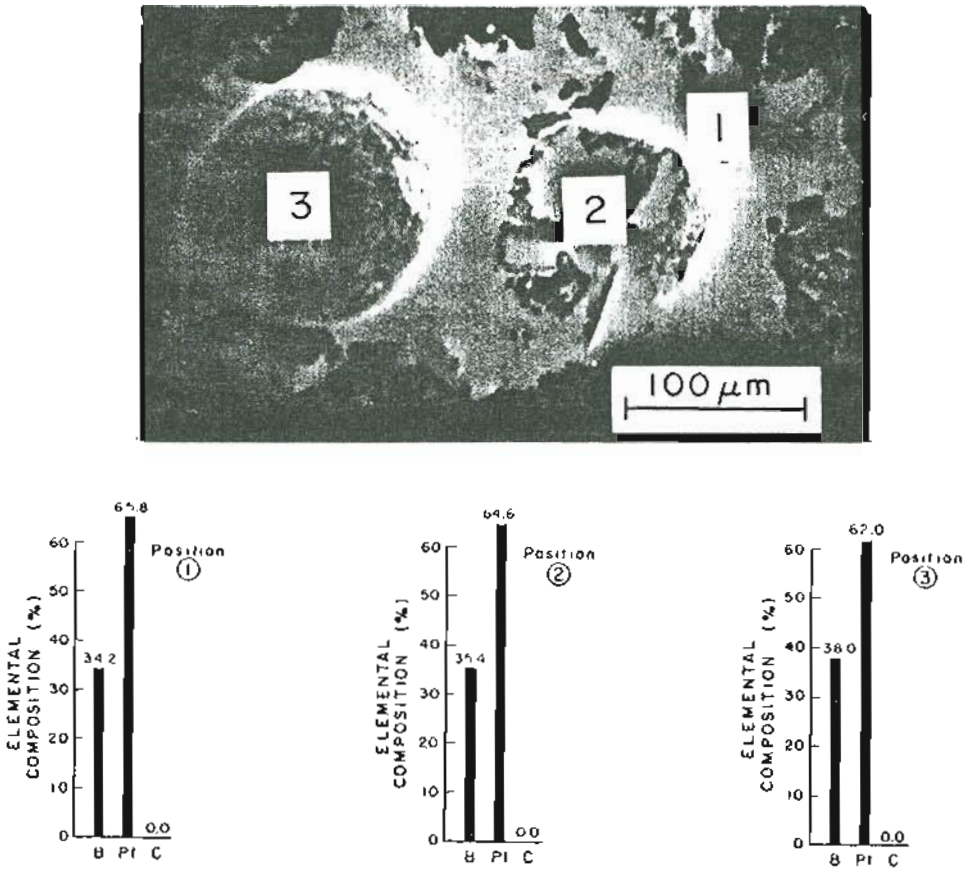

Figure 5-36. The beginning of melting of the Pt/B on C alloy at 1290 K.

An explanation of these observations similar to the Ni/B results can be developed from the binary phase diagram for the Pt-B system shown in Figure 5-37. Based upon the compositional and melting behavior, it appears that the surface of the alloy proceeds through the sequence of phase changes lying to the B-rich side of the eutectic. Imagine such an alloy in the solid state, depicted by point A in Fig. 5-37. Its composition at this point is a solid solution of 14% alpha-B and 86% Pt_2B. Heating to point B forms a liquid eutectic composition and a solid solution composed of alpha-B and Pt_3B_2. Further heating (point C) continues this sequence with solid alpha-B surrounded by a liquid solution with a composition near Pt_3B_2. A final heating to point D results in a fully molten solution of 45% B and 55% Pt. This succession of reactions is in qualitative agreement with our observations which show the ratio of Pt to B near 1.5-2.0 and the sequence of phases observed experimentally.

An experiment designed to disclose the degree of interdiffusion of B into the substrate resulted in conclusions similar to those for the Ni/B system. Auger and SEM analyses of fractured cross-sections of the Pt/B alloy showed little or no solubility of B into graphite. The converse was also investigated, by way of a long-term heating experiment. After return from CRISS, Auger reexamination of the alloy is shown in Figure 5-38. Carbon and oxygen are seen in all sampled locations, a circumstance which is not unexpected after system evacuation and before heating. Also not unusual is the high C signal at the right side of the alloy where wetting is poor and

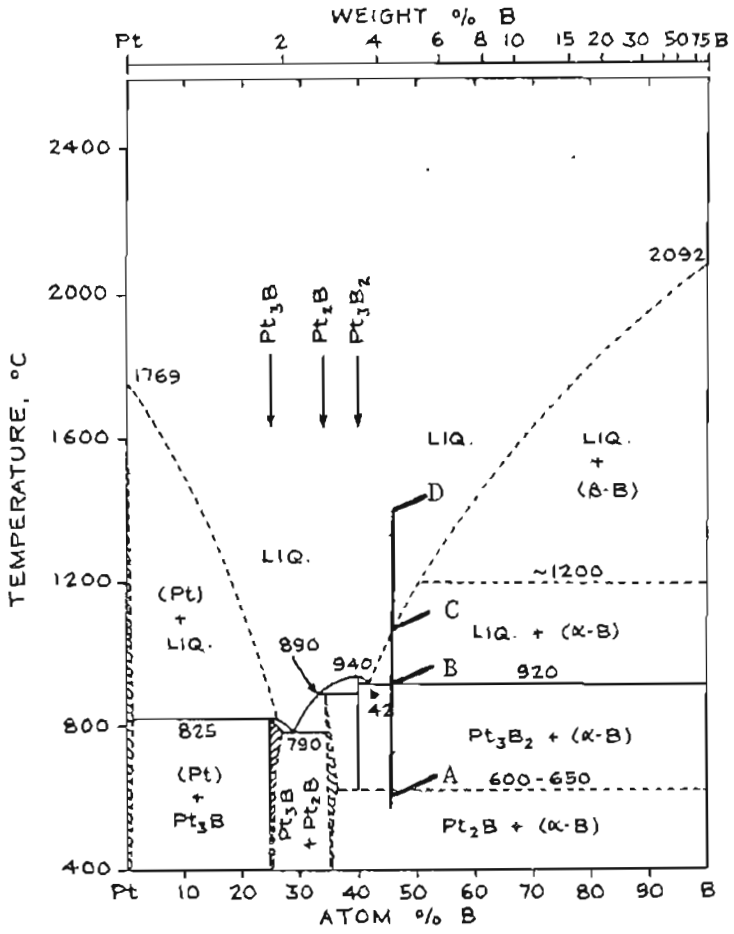

Figure 5-37. The phase diagram of the Pt-B system, with a likely phase progression indicated.

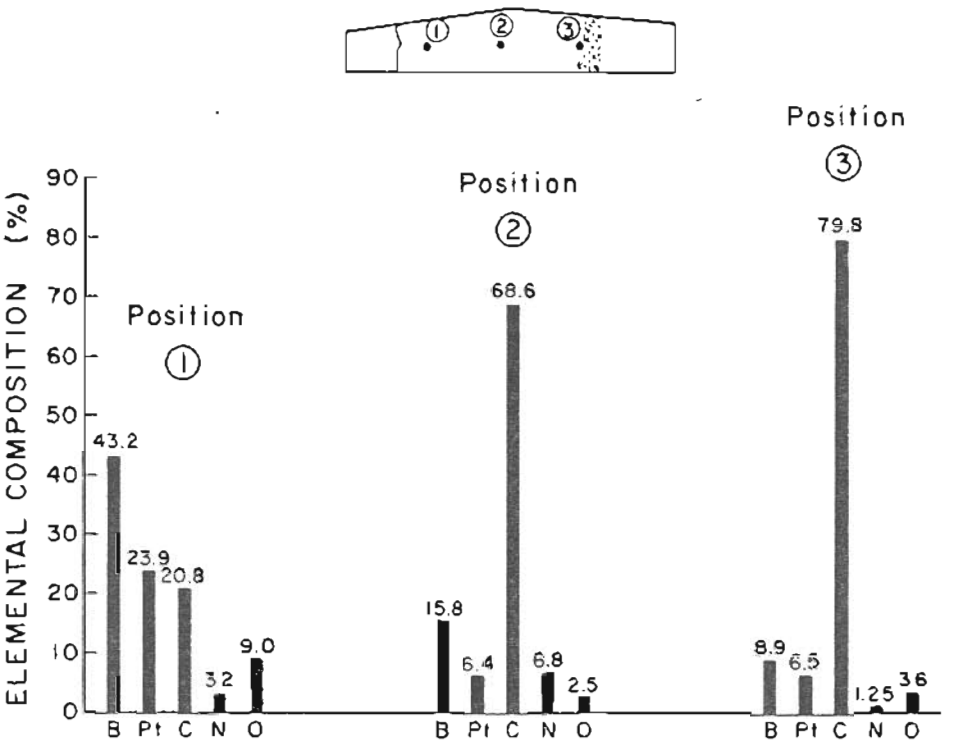

Figure 5-38. Auger surface elemental composition vs position for the Pt/B on C alloy following readmission into the vacuum chamber. The temperature is 300 K.

droplets of alloy predominate. Figure 5-39, which displays composition vs position after heating to above the melting point, shows that C has vanished from the well-wetted left side, but is still present in the center and at the right of the alloy. At this time, the Auger beam was adjusted to monitor a single, fixed point within the well-wetted region while the temperature was kept constant at T = 1292 K, about 100 degrees above the observed melting point of the alloy. No carbon was observed to appear during 100 hours of this treatment. The only elements present were B, Pt, and a small amount of N. This lends support to the notion that little alloy-substrate interaction is taking place at the temperatures tested. At higher temperatures, however, it is expected that B will dissolve C. It is also known that Pt and Pd dissolve considerable quantities of C [4].

E. Study of the Pd/Ni/B on C Contact System

Two samples of $Pd_{40}Ni_{20}B_{20}$ on C were examined in the high-resolution Auger system at CRISS. The initial wetting properties of this contact system were much the same as in the Pt/B system. One sample of Pd/Ni/B was poorly-wetted, while the second possessed regions of wetting ranging from good to poor. The poorly-wetted sample could not be made to flow at all, even at temperatures as high as 1600 K. The sample containing mixtures of droplets and well-wetted areas was observed to flow, but only reluctantly and at elevated temperatures. The reason, as expected, was the high concentration of carbides and nitrides found in the

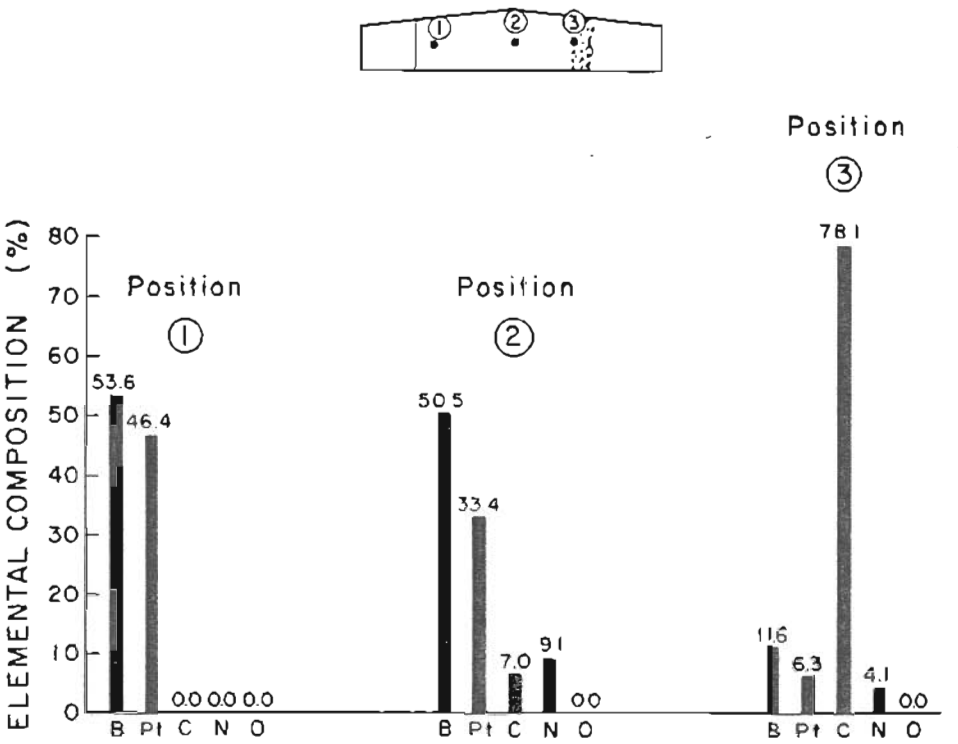

Figure 5-39. Auger surface elemental composition vs position for the Pt/B on C alloy at the beginning of long-term heating. The temperature is 1292 K = T_m + 50°. Position 1 is identical to position 1 in Figure 5-38, while positions 2 and 3 are close to, but not identical with, positions 2 and 3 of the previous figure.

alloys, which inhibited flow due to the high melting points of these compounds. The results are detailed below.

A scanning electron micrograph of the poorly-wetted Pd/Ni/B system in its "as received" condition at T = 300 K is shown in Figure 5-40. The substrate had received boronization pretreatment, but no additional boron fluxing was added to the alloy material. Wetting consists of localized droplets of alloy on the ribbon, which was determined to be solely graphite. No evidence of prior boronization was found. This is seen in Figure 5-41, which shows the Auger surface elemental composition atop, below, and far to one side of droplet 1 in Figure 5-40. There is no B anywhere on the surface except within the alloy droplets. Analysis of other droplets at temperatures ranging from T = 300 K to 1300 K showed typical concentrations of 50% C, 25% N, and 10-20% B. Pd and Ni were not found in this temperature interval.

Only after increasing the temperature to T = 1450 K did Pd and Ni begin to appear in the Auger spectra. Traces of Fe and S were also frequently seen. A typical droplet composition at this temperature is given in Figure 5-42. Having been unable to cause the droplets to melt at temperatures as high as T = 1600 K, it was decided to suspend further attempts at heating and analyze the composition of other droplets. The temperature was subsequently lowered to 1100 K and held constant in order to prevent readsorption of background gases. Auger elemental compositions of other droplets are reported in Figures 5-43 to 5-44. Clearly evident are high amounts of surface C and N, even after the high heating described above. Chemical shifts

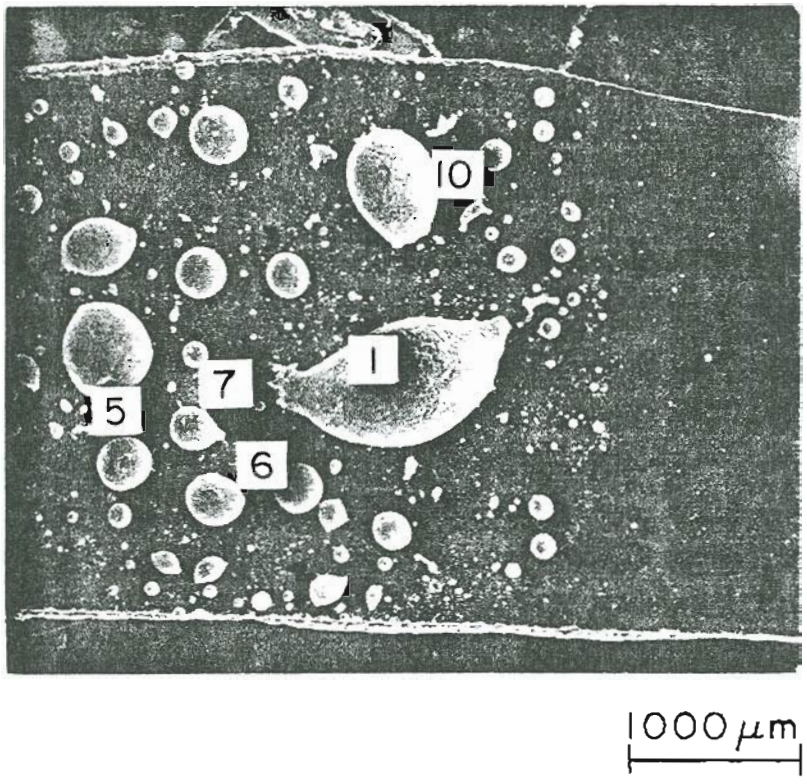

Figure 5-40. The poorly-wetted $Pd_{40}Ni_{40}B_{20}$ on C alloy in its "as received" condition at 300 K. The numbers refer to analysis positions to be discussed ahead.

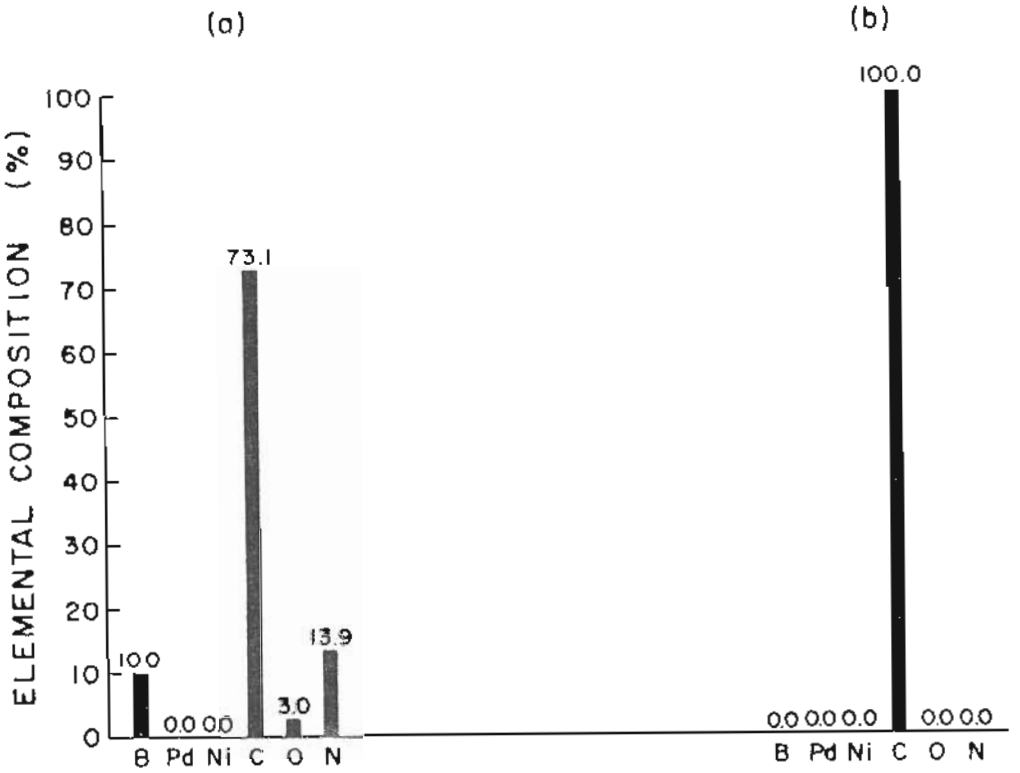

Figure 5-41. Area-averaged Auger surface elemental composition of the (a) Large droplet 1 of Figure 5-40; (b) Region directly below droplet 1 and the region far to one side of the central alloy region.

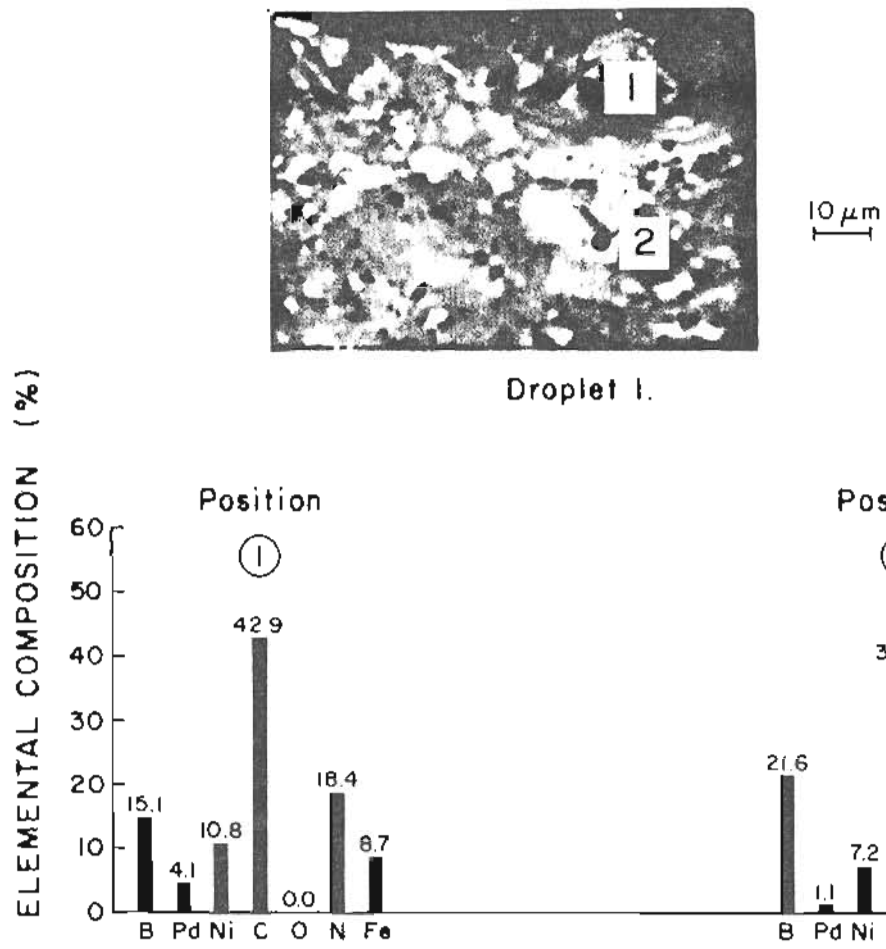

Figure 5-42. Area-averaged Auger surface elemental composition of 2 positions on droplet 1 of Figure 5-40. The temperature is 1450 K.

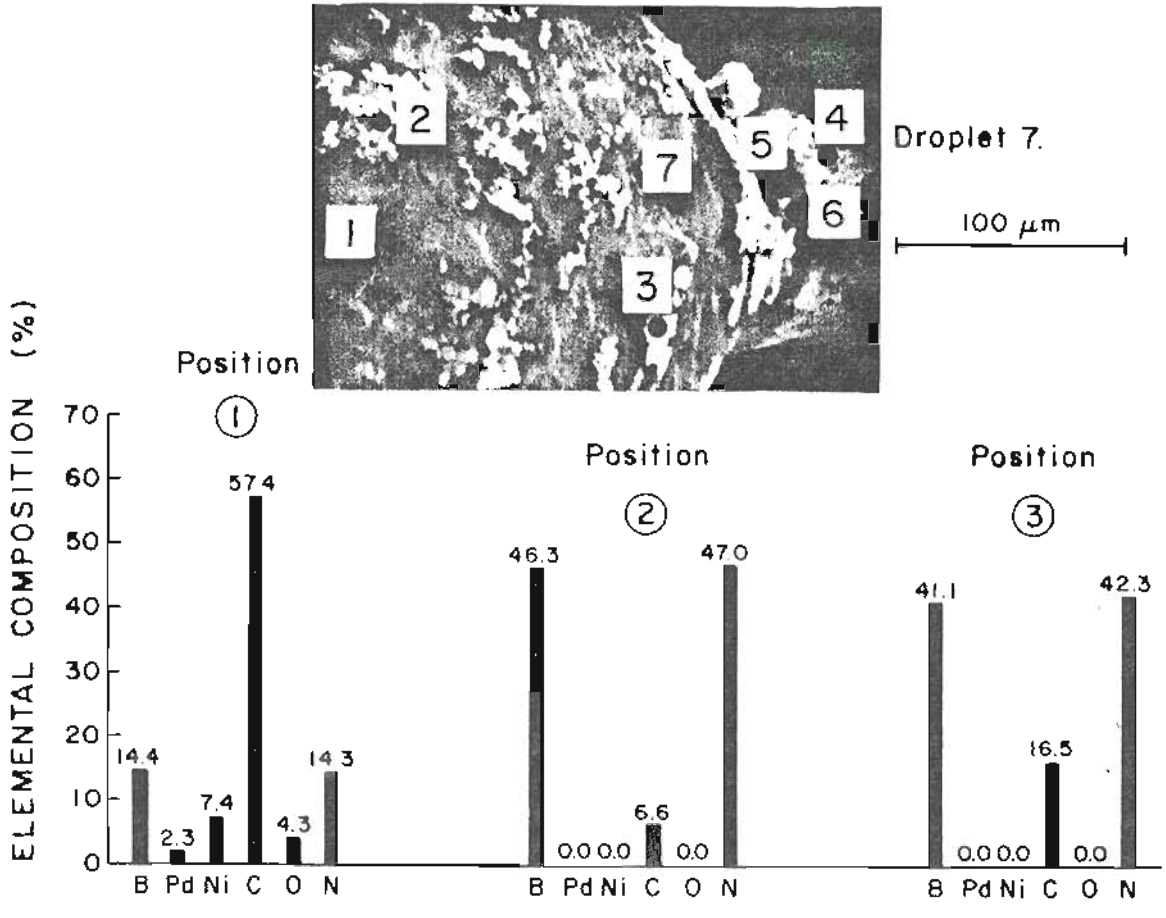

Figure 5-43. Area-averaged Auger surface elemental composition of 3 positions of droplet 7 of Figure 5-40, shown above at high magnification.

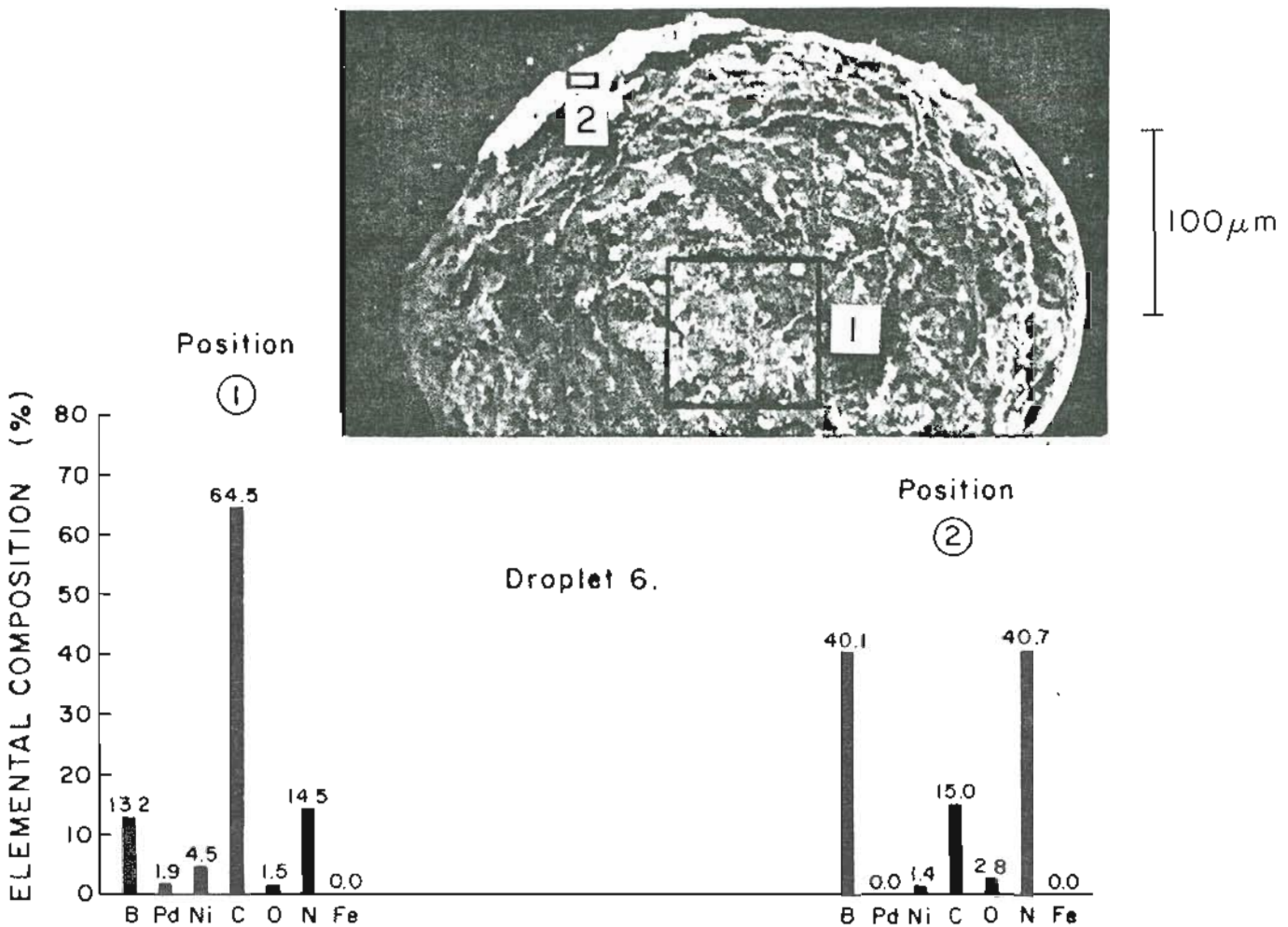

Figure 5-44. Area-averaged Auger surface elemental composition of droplet 6 of Figure 5-40, shown above at high magnification. The temperature is 1100 K.

indicative of boron nitride formation appeared in nearly every spectrum, and the ratio of B to N was nearly 1 to 1. This was particularly notable in droplets containing high secondary yield, shell-like structures, such as position 2 of Figure 5-43 which appears to be composed of nearly 80% pure BN.

An interesting edge-on view of this surface showing the variety of contact angles is shown in Figure 5-45. If the droplets had contained pure alloy with no evidence of C and BN impurities, the surface tension and adhesive energy of the contact system could be determined by knowledge of the alloy density and measurement of the contact angle [5]. Unfortunately, the alloy is far from pure. Nevertheless, the photos are instructive in light of the unusual perspective offered and the hysteresis of contact angle.

A scanning electron micrograph of the partially-wetted Pd/Ni/B on C alloy containing a mixture of good and bad wetting is shown in Figure 5-46 in its "as received" condition at 300 K. This contact system had been subjected to boronization pretreatment of the graphite and extra boron was mixed with the alloy. The left side of the ribbon consists of poorly-wetted alloy droplets, while the right side shows good wetting. The compositionally of the "as received" surface is reported in Figures 5-47 to 5-48. The expected high concentrations of C are present throughout the surface, in addition to significant amounts of B and N in nearly a 1 to 1 ratio.

Heating this alloy specimen to 1300 K showed little change in surface composition. Not until the temperature was increased to 1440

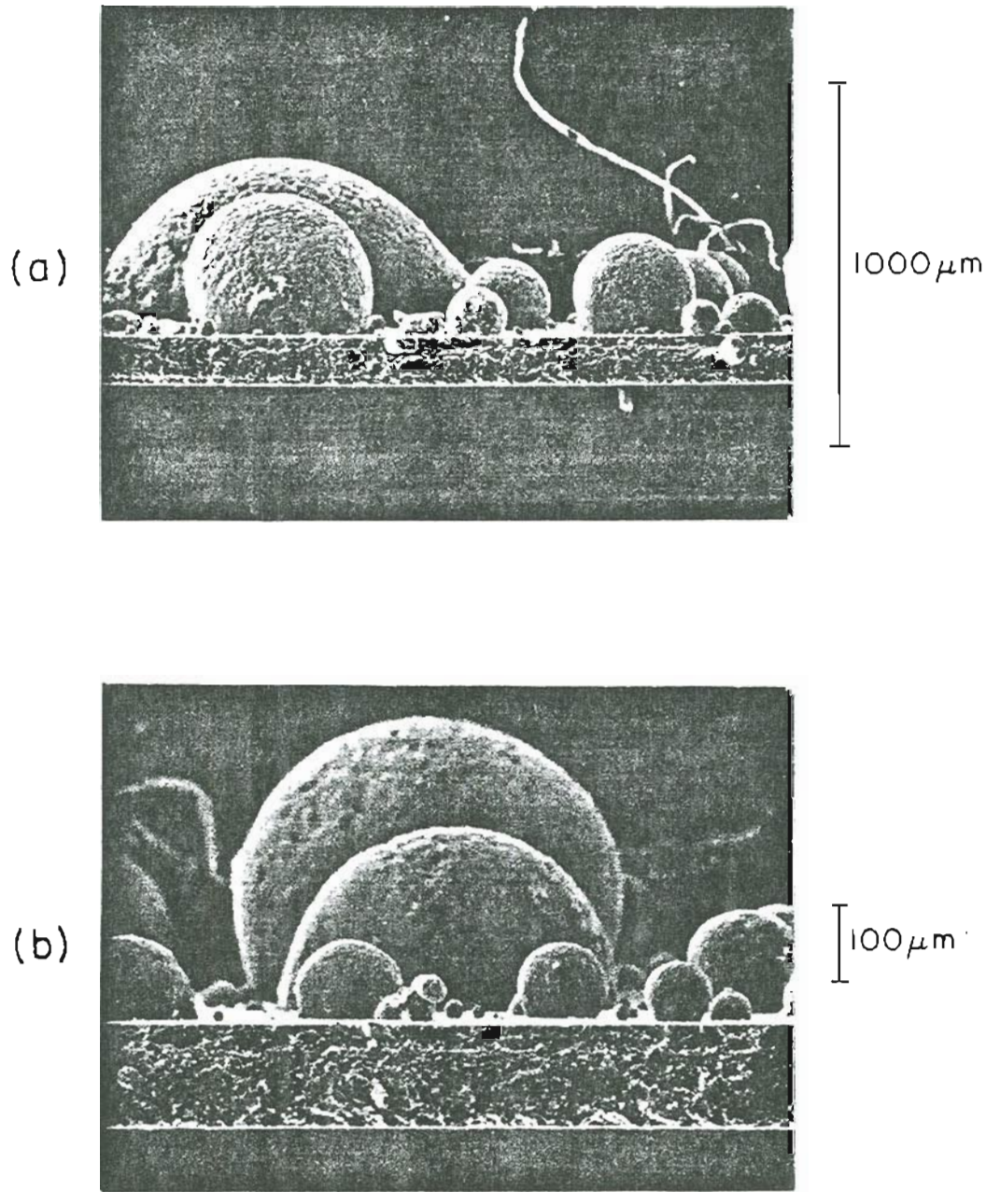

Figure 5-45. Side views of the poorly-wetted droplets of Pd/Ni/B that are shown from above in Figure 5-40.

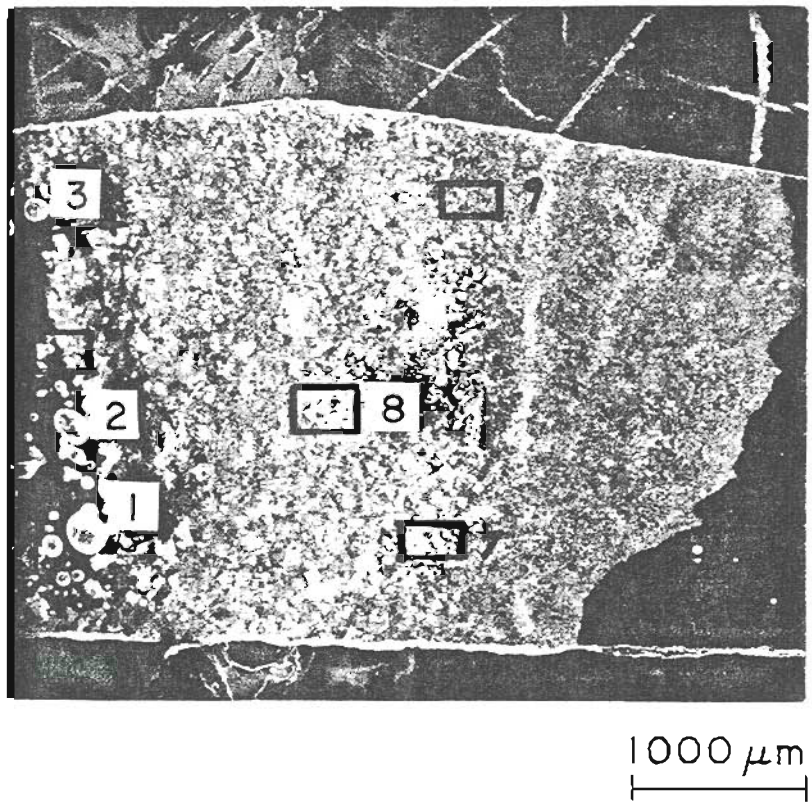

Figure 5-46. The Pd/Ni/B on C alloy (HRL: E-6; B-6) in its "as received" condition at 300 K. The numbers refer to analysis positions to be discussed ahead.

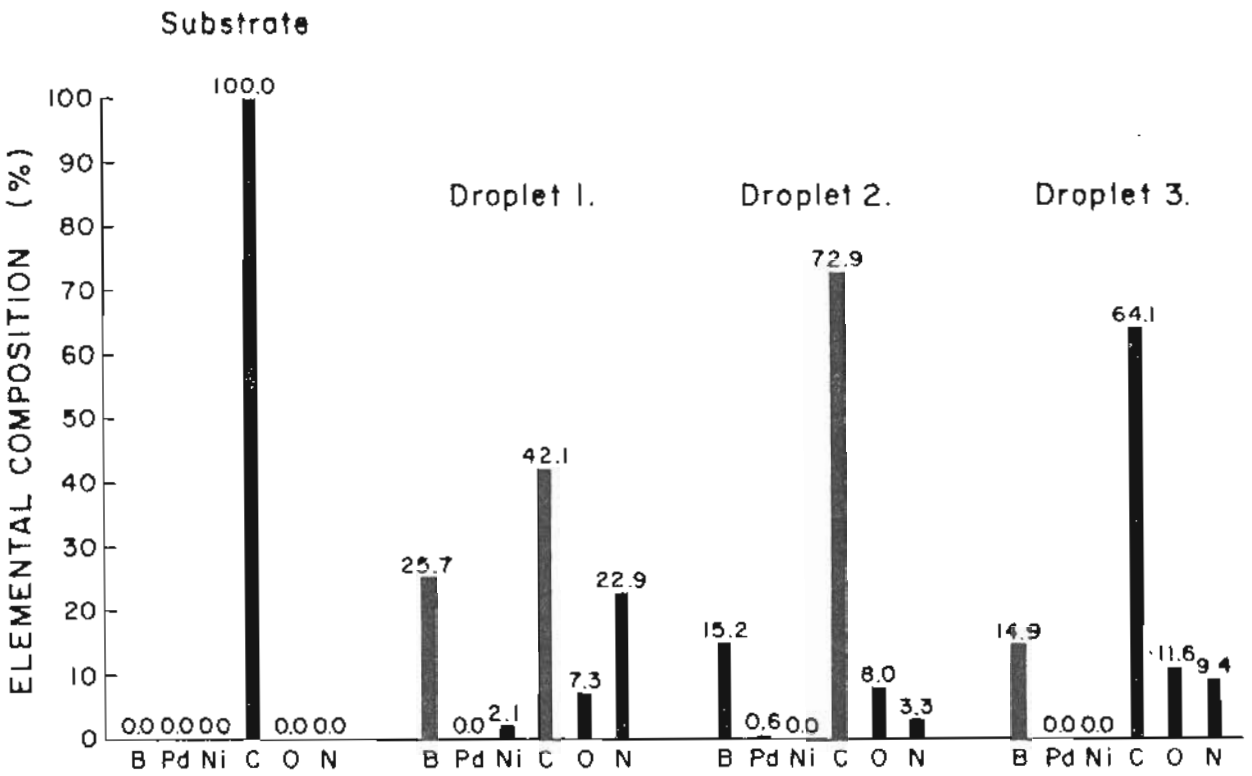

Figure 5-47. Area-averaged Auger surface elemental composition of the "as received" Pd/Ni/B on C alloy at 300 K. Positions monitored are: far to the left of the alloy region and droplets 1-3 from Figure 5-46.

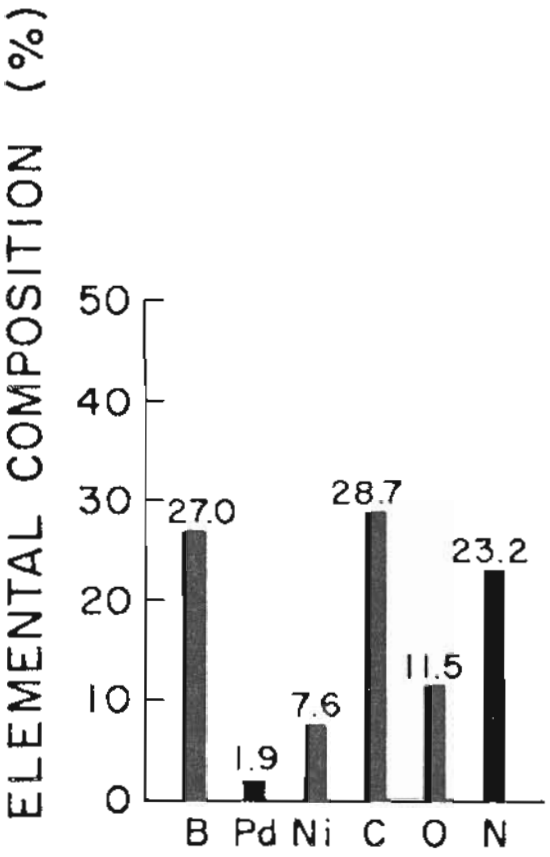

Figure 5-48. Area-averaged Auger surface elemental composition of the "as received" Pd/Ni/B on C alloy at 300 K within the boxed area 8 of Figure 5-46.

K did liquid flow occur. This is shown in Figures 5-49 to 5-50. The sharp line separating alloy and substrate at low temperatures can no longer be discerned due to the outward motion of alloy. Oxygen has vanished, so all adsorbed CO has been removed by heating. Although C has decreased, it is still present at most positions monitored. Positions 3, 6, and 7 are most interesting in Figure 5-49. Position 3 appears to be nearly 96% pure BN; heating has had little effect on the B and N signals, while CO has been desorbed. Positions 6 and 7, formerly 100% C, have been covered by liquid alloy and exhibit primarily the alloy components Pd, Ni, and B. Figure 5-51 shows the Auger composition of an unusual morphology which developed in the surface. Positions 1 and 2 of that figure appear to be well-wetted, but also contain a small amount of C. It is likely that the C signal originates from low-level alloy impurities and substrate dissolution at the high temperature used during the analysis.

Increasing the temperature to 1520 K caused a dramatic sequence of droplet decomposition which is recorded in Figures 5-52 to 5-53. Figure 5-52 shows the beginning of melting, with three positions within the scene monitored. Position 1 corresponds with the efflux of liquid alloy from the droplet, and is composed of alloy components plus a small amount of C and N. This region appears to be well-wetted, so C appears to originate from low-level impurities and substrate interaction at these elevated temperatures. Position 2 is the remnant of a shell of BN that encased the droplet at lower temperatures. High temperatures have fractured this shell and subsequently released pure liquid alloy materials.

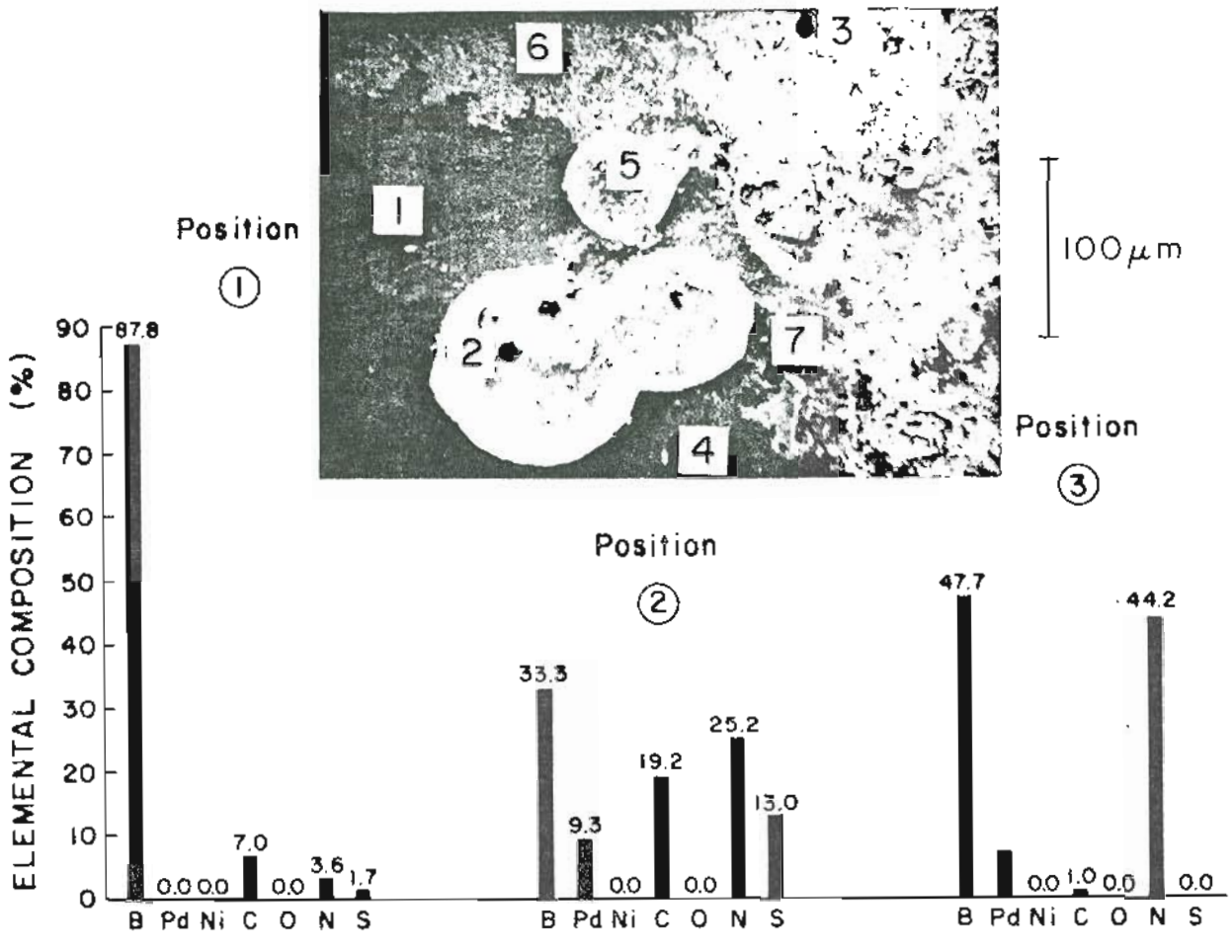

Figure 5-49. Auger surface elemental composition of 7 positions at the alloy/substrate boundary at 1440 K.

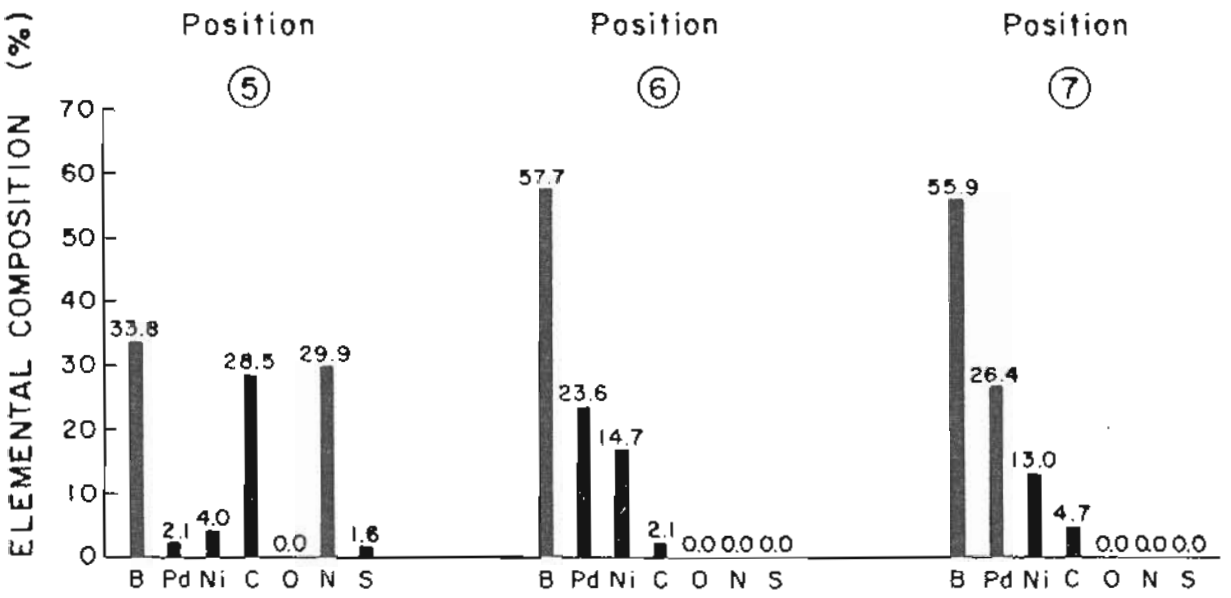

Figure 5-49 (continued). Auger surface elemental compositions of positions 5-7. Position 4 was 100% C.

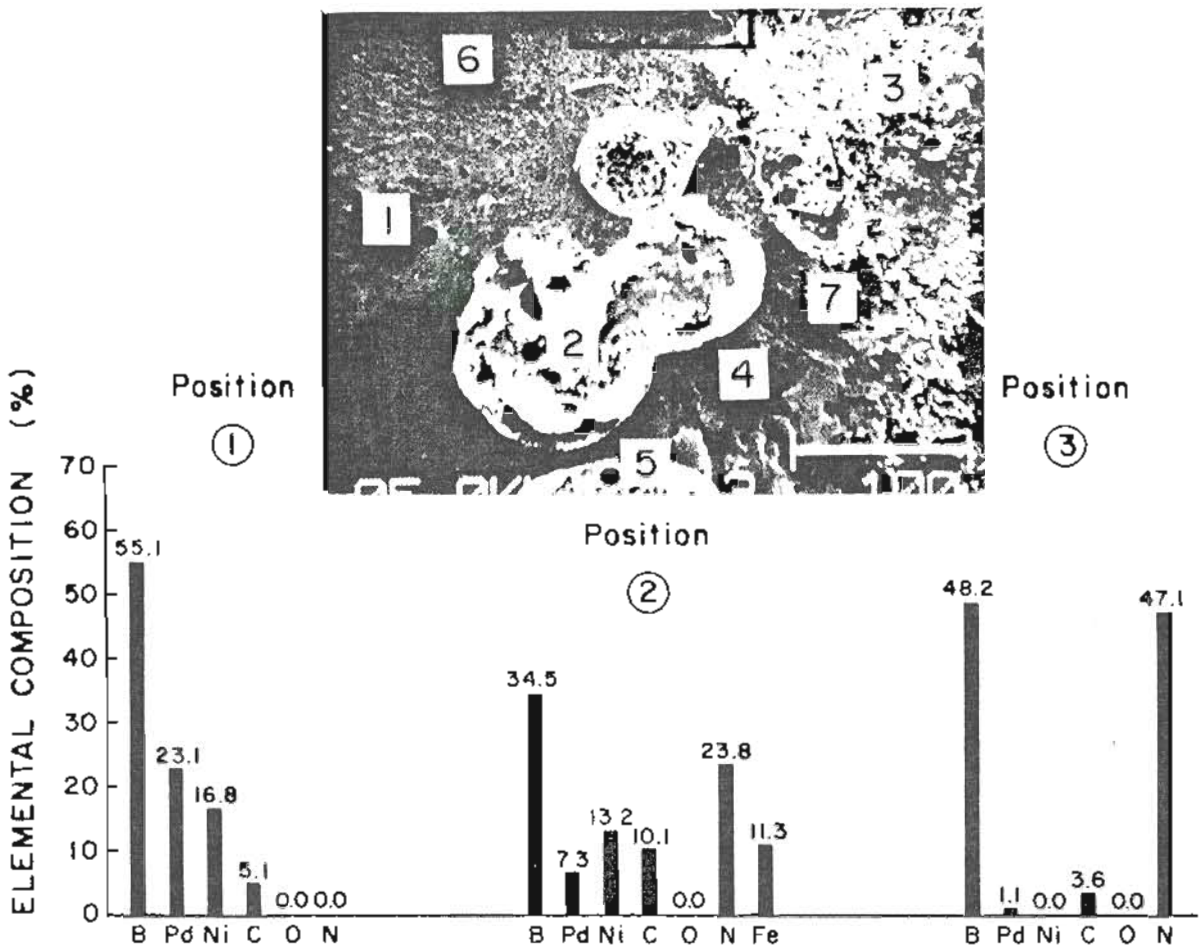

Figure 5-50. Auger surface elemental composition of the same structures as shown in Figure 5-49, but after 1 hour at 1440 K.

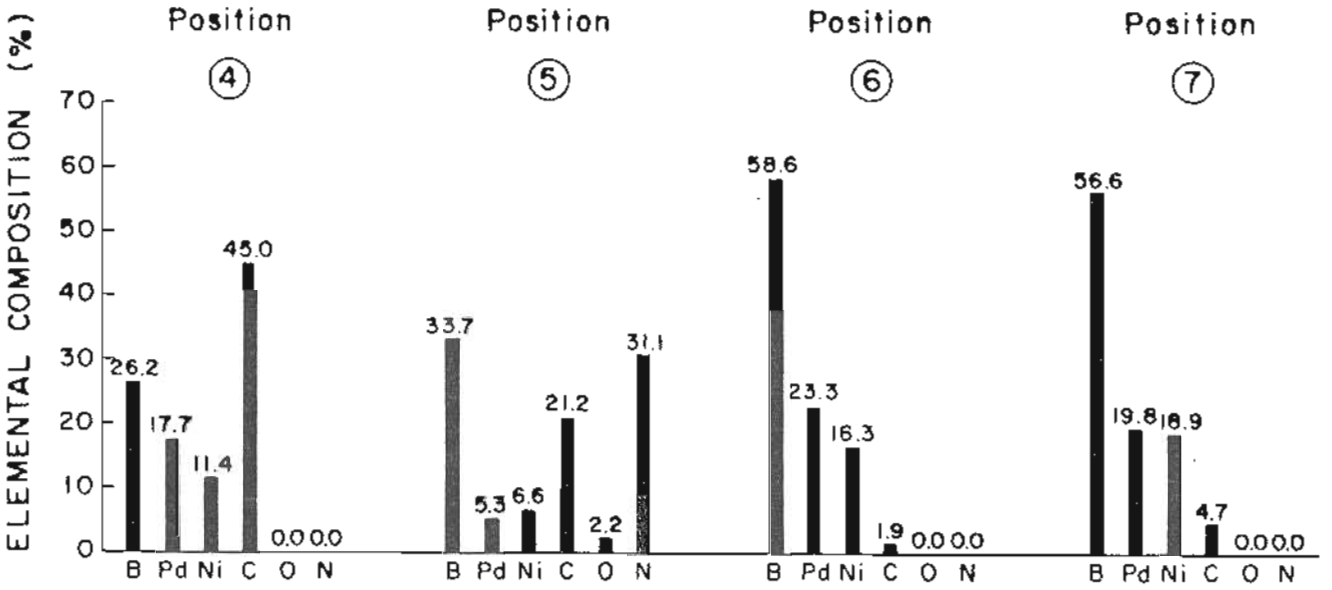

Figure 5-50 (continued). Auger surface elemental composition of positions 4-7 after 1 hour at 1440 K.

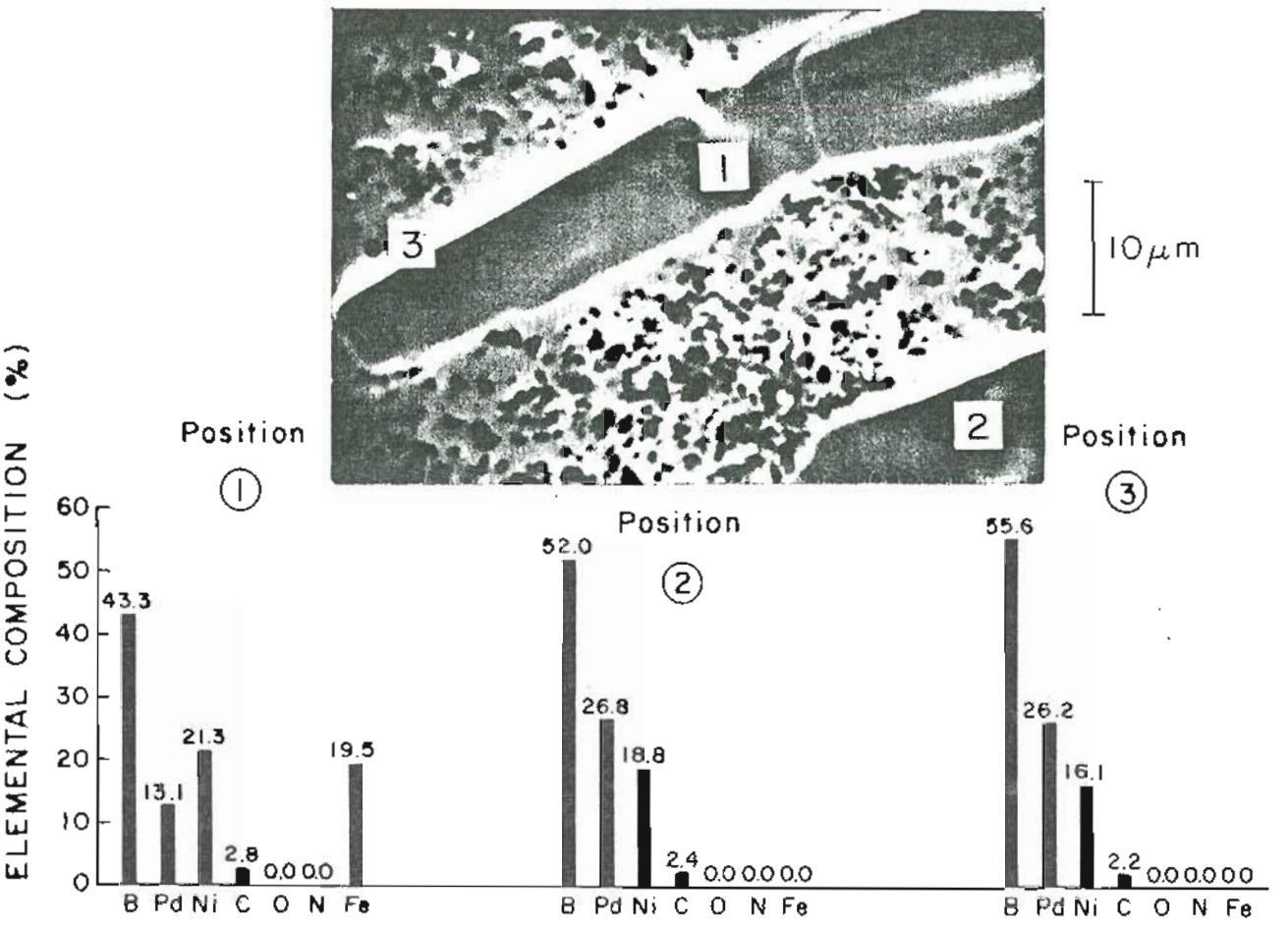

Figure 5-51. Auger surface elemental composition of unusual morphology within the boxed area of Figure 5-50. The temperature is 1440 K.

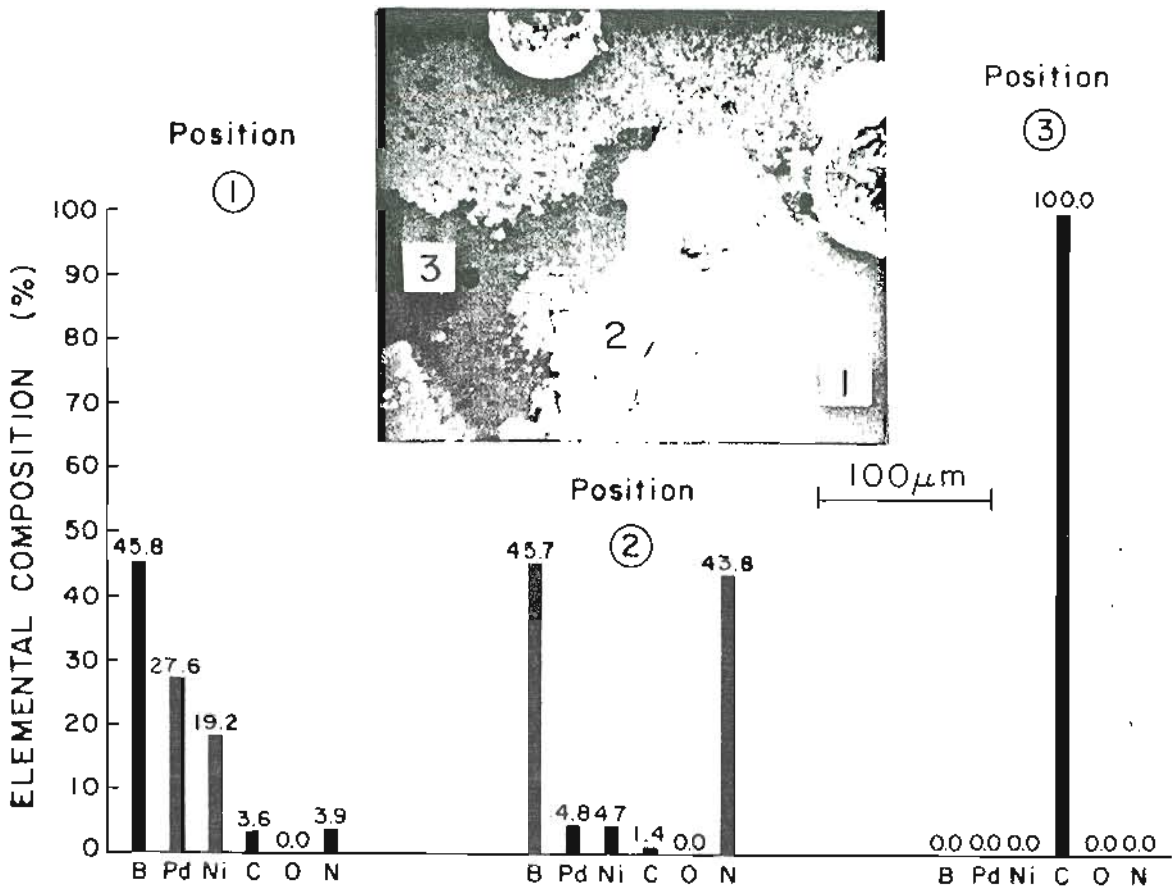

Figure 5-52. Area-averaged Auger surface elemental composition of 3 positions at the alloy/substrate boundary at 1520 K. A droplet has started to decompose.

The view 30 minutes later is shown in Figure 5-53. The liquid alloy of the original droplet has wet and spread over a large area, and structures similar to those in Figure 5-51 have formed near position 1. The analysis of these structures reveal that they are composed entirely of alloy components and merely reflect an unusual perspective of the liquid alloy frozen in time.

No attempt to determine work functions, rates of volatility, or melting temperatures of the Pd/Ni/B system were undertaken due to the extreme contamination of the alloy surfaces.

F. Conclusions

Studies of prewetted HRL contact systems have provided valuable insight into the mechanisms preventing wetting and spreading of liquid metal alloys, but the early work suffered from lack of adequate experimental controls during preprocessing. It was therefore difficult to assess the value of boronization pretreatment and boron fluxing.

The Y/Ni/B on Re system has a work function of 3.5 eV, the lowest of the three contact systems measured. It also has the lowest experimental melting point of 1102 K. Wetting of the Re substrate is excellent, and no alloy components were observed to volatilize at temperatures up to 1300 K. The system suffers, however, from a high degree of substrate/alloy solubility that causes significant amounts of Re to dissolve into the alloy. Since Re has a melting point of nearly 3500 K, the result is an increase in the melting point of the

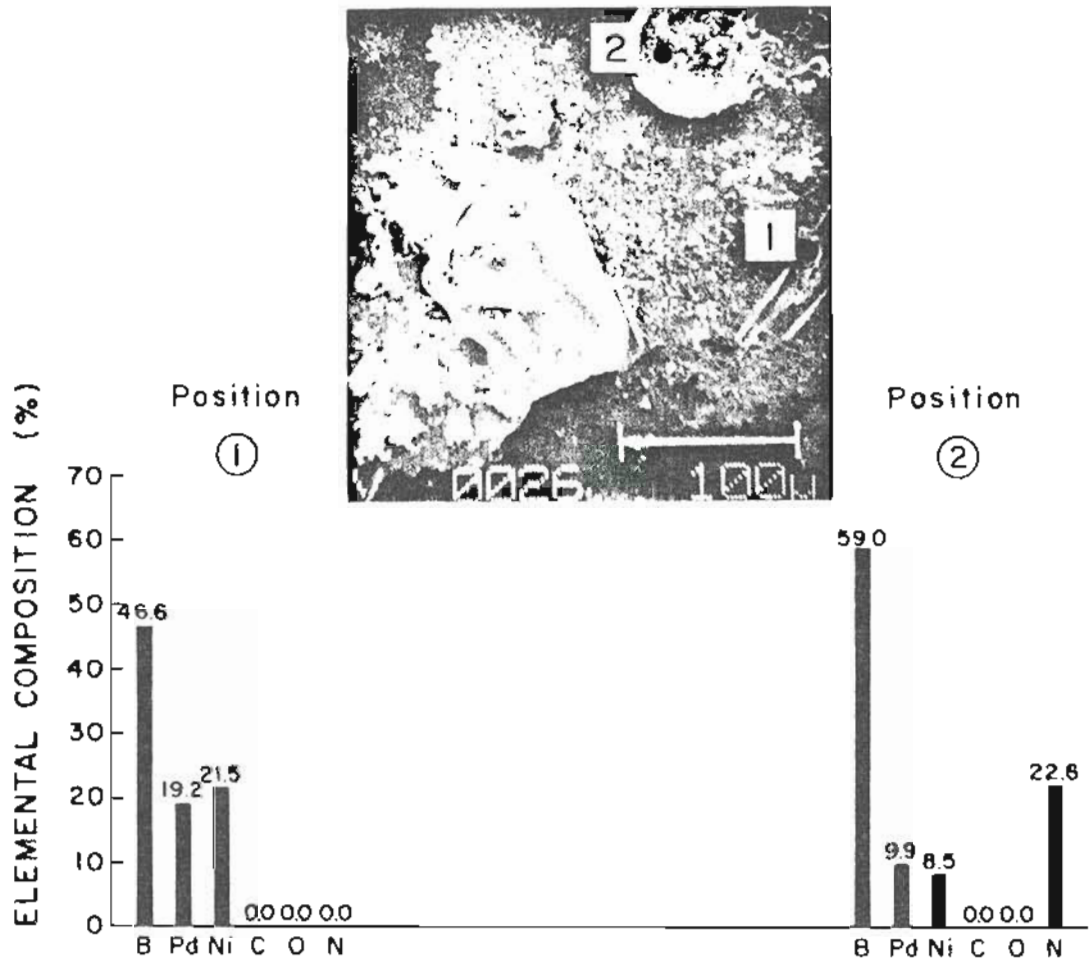

Figure 5-53. The same view as in Figure 5-52, but 30 minutes later. The temperature remains at 1520 K.

alloy solution. Consequently, the once liquid metal alloy source suffers a liquid-to-solid phase transition and ion emission is curtailed as the Taylor cone solidifies. Further, the absence of Re in the ion beam is most likely due to formation of rhenium boride phases in the alloy. Yttrium also appears to form yttrium boride compounds with the result that little B^+ is found in the ion beam. A final problem is the high oxygen affinity of Y which prevents effective cleaning of the alloy and causes development of oxide phases in the alloy. The surface percentage of B near the melting point was found to be about 40%, lowering to 20% as Re dissolved in the alloy.

The Ni/B on C system has a work function of 5.1 eV, the highest of the three contact systems measured. It also has the highest melting point of 1292 K. Wettability of the carbon substrate appears to be excellent when the alloy surface is rid of high-melting carbides and nitrides. Much of the surface, however, remains solid at useful temperatures, since BN and most carbides have melting points far in excess of the pure alloy eutectic. Noticeable carbon dissolution appears in the alloy at temperatures greater than 100 degrees above the alloy melting temperature. No volatilized alloy components were observed in mass spectrometric vaporization studies at temperatures up to 1400 K. The solubility of the alloy in the substrate remains to be further inveatigated. The surface percent of B at the melting point was normally the highest among the four alloy systems, averaging about 60%.

The Pt/B on C contact system has properties intermediate between those of Ni/B and Y/Ni/B. Its work function is 4.8 eV, and it has a melting point of 1196 K. Similar remarks can be made with respect to wettability on carbon substrates that were made for the Ni/B system. No observable dissolution of C occurred in well-wetted alloys at temperatures up to 100 degrees above the alloy melting point. The alloy does not appear to be soluble in the substrate at the low temperatures tested. Boron surface coverages averaged near 50% for well-wetted alloys near the melting point.

The Pd/Ni/B on C contact system wet the substrate with great difficulty due to the large amounts of BN and C contamination on the surface. One specimen could not be made to flow even at elevated temperatures, and the other sample flowed with great reluctance. Once wetting and spreading did occur, however, the wetted alloy was found to consist of pure alloy components with little or no C and N and excellent wetting properties. This was the case for all alloys studied. Work functions, solubility rates, and volatility could not be measured adequately due to the large contamination present.

In summary, early work on prewetted HRL specimens showed that the Ni/B and Pt/B contact systems offered promising candidates for sources of B^+, provided that the alloys could be fabricated from pure alloy components and the LMI source was operated near the melting temperature. The Y/Ni/B on Re system suffers from poor choice of substrate and a high affinity of Y to O. It is difficult to assess the Pd/Ni/B on C system due to the high contamination of the specimens. We suspect that it will possess properties similar to

those of Ni/B and Pt/B, but it is difficult to form conclusions without further studies on purer samples. A summary of results on prewetted contact systems is included in the Appendix.

A plausible correlation between the presence of high-melting nitrides and carbides and lack of wetting has been established. Both boron nitride and boron carbide have been positively identified in the alloy surfaces. Such substances have high melting points which render the alloy surface incapable of liquid flow. BN melts at 3273 K and B_4C melts at 2573 K.

It was difficult to determine at this early stage whether boron nitride or boron carbide was more effective in suppressing wetting, as it was rare to find cases of poorly-wetted alloy containing BN but not B_4C. Most poorly-wetted droplets of alloy contained an abundance of both which made it hard to isolate the effects on wetting. A related question is where the nitride and carbide phases originate. To probe this source, an experiment was designed to attempt to manufacture BN through N_2 exposure. That direct nitration of boron can form BN is reported by Samsonov [6], who describes experiments which show that direct nitration of amorphous boron in a stream of nitrogen can yield a product composed of 94.3% BN at a temperature of 1600 C. Increasing the temperature to 2000 C increases the yield to 99.5%. One of the initially poorly-wetted Ni/B on C alloys which later wetted by high temperature cycling was exposed to 50 L of nitrogen gas (10^{-6} torr for 50 sec) at temperatures ranging from T_m to $T_m + 150^o$ = 1170 C. No BN was subsequently detected in the freshly-wetted Ni/B region. The same

experiment was run with O_2 exposure, the goal of which was to react oxygen with nitrogen and thus deplete the surface of nitrogen. No decrease of N was detected at the exposures and temperatures tried. These results were positive rather than negative, as they indicated that BN will not be formed during LMI source operations under poor vacuum conditions. It will be shown later that carbide and nitride phases are formed during the initial wetting process when C and N segregate to the surface.

REFERENCES

1. Private Communication, Hughes Research Laboratory.

2. J. T. Grant and T. W. Haas, Phys. Lett. 33 A (1970) 386.

3. G. Hanke and K. Muller, J. Vac. Sci. Tech. A 2 (1984) 964.

4. Yu. V. Naidich, Russian J. Phys. Chem. 42 (1954) 1023.

5. M. Humenik and W. D. Kingery, J. Amer. Cer. Soc. 37 (1954) 18.

6. G. V. Samsonov, et al., Boron: It's Compounds and Alloys (U.S. Department of Commerce, July 1962), p. 186.

CHAPTER 6

WETTING AND SURFACE STUDIES OF LIQUID METAL ALLOYS OF BORON

A. The Controversy Surrounding Boronization

The initial work was not able to establish any useful connection between boronization preprocessing, boron fluxing, and wettability due to the confusing and uncontrolled set of procedures established by the HRL studies. The group of specimens which underwent the ideal procedure appeared to display significantly better wetting than the others, but having observed numerous instances of non-nitrogen and non-carbon containing alloys that wet a non-boron containing substrate, we began to suspect that boronization had little if any positive effect. Further, an elementary calculation to determine the boron volatility as a function of temperature shows that nearly 20 microns/second of boron is volatilizing from the surface at 2700 K, a typical temperature allowed by the HRL group during the boronization process. This rapid vaporization occurs because boron has a vapor pressure of 3×10^{-1} torr at this temperature. It was therefore likely that much of the boron used in the pretreatment was vaporized from the ribbon during high heating. In this event, the boron that was originally used to promote wetting was subsequently removed from the surface, resulting in an unnecessary processing procedure.

Auger and ESCA studies of graphite ribbons which had undergone boronization pretreatment showed little or no boron. This was especially true for ribbons containing prewetted alloy, such as those detailed above. Not a single example existed which contained boron near the center of the prewetted part of the graphite ribbon. To enable study of the boronization process without interference from the wetted alloy, analysis was made of two ribbons which had undergone boronization without any added alloy.

The first ribbon studied (HRL:E2,12/8/82,C1) was described by HRL as a good example of a lightly boronized graphite ribbon containing a few patches of heavy boronization (see Figure 6-1). ESCA and Auger studies of this specimen showed no sign of B at all, either on the as-introduced surface or after Ar^+ sputtering. ESCA analysis showed only C and O before sputtering, and only C and Ar were observed after sputtering. The detectability limit for B, deduced from the noise in the region where the B peak was expected, was about 0.8% relative to C, and no B was detected at this level. In addition, the C peak observed for this sample was virtually identical to that of pure graphite. Auger analysis of various portions of this ribbon gave identical results. What then are the darker appearing areas near the center of this specimen? The answer is that the areas are carbon, in an altered, highly crystalline form. This is seen in Figure 6-2, which shows SEM photographs of the the areas of the ribbon thought to represent regions of "light" and "heavy" boronization.

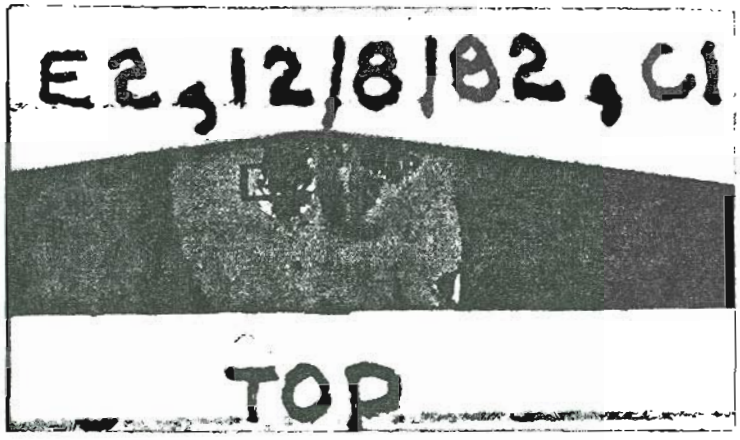

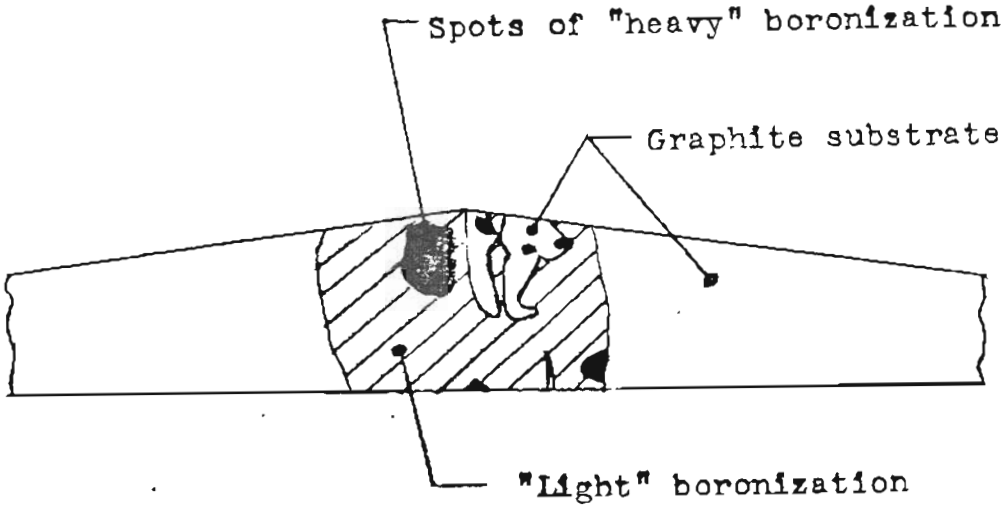

Figure 6-1. A sample of graphite "boronized" by Hughes Research Laboratory. Areas denoted by "heavy" boronization are actually crystalline forms of carbon.

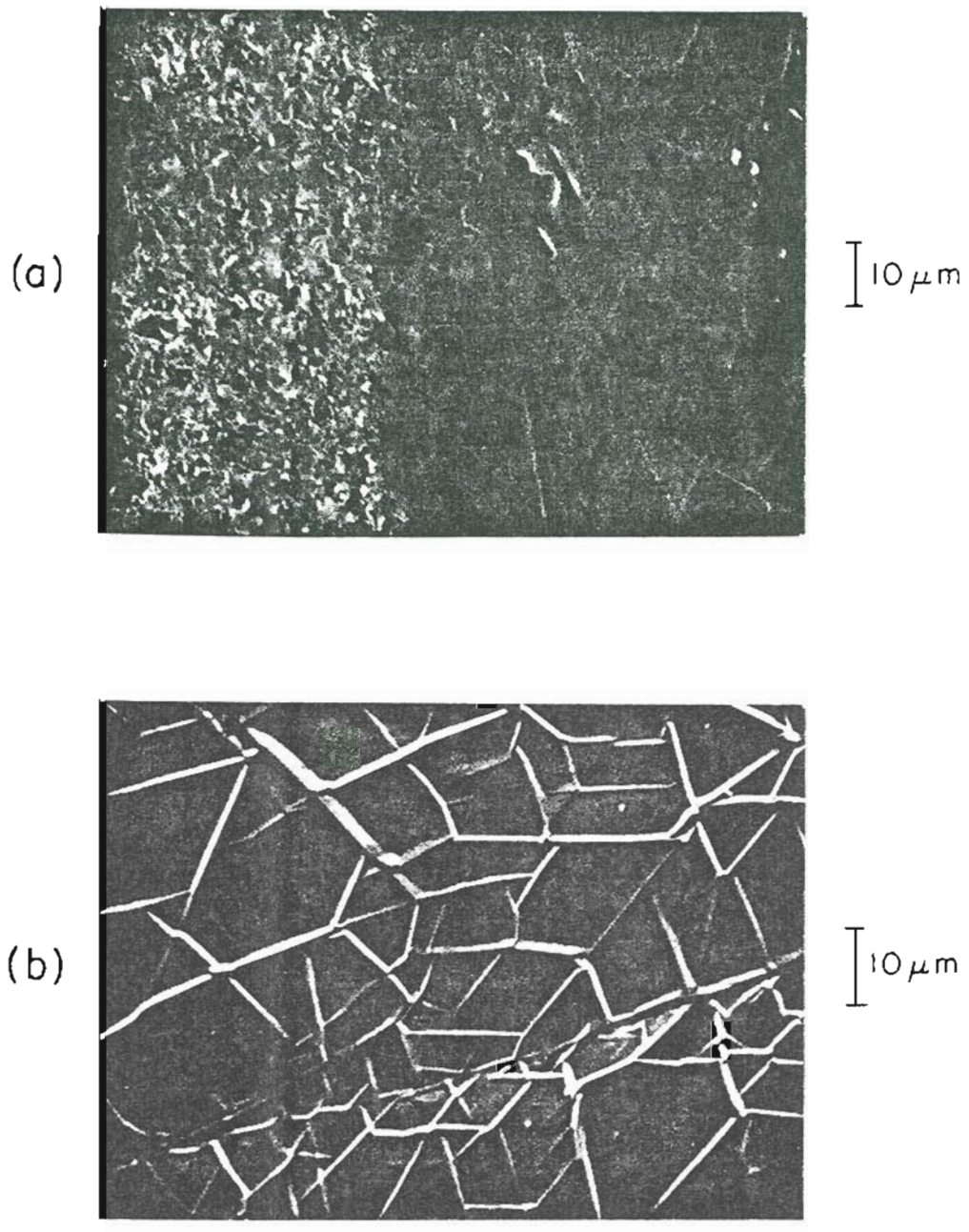

Figure 6-2. SEM micrographs of "boronized" graphite. The view is of the boxed area of Figure 6-1. (a) View of the boundary between "light" (left) and "heavy" (right) boronization regions. Auger and ESCA analyses detected only carbon within the pictured field; (b) A magnified view of the crystallinity within the "heavy" boronized region.

The process whereby amorphous carbon is converted to artificial or synthetic graphite by heat treatment is called graphitization, and is described as follows [1]. As the calcination temperature (1000-1300 C) of the filler component of amorphous graphite is reached, the slow formation of crystalline graphite begins. The reaction hastens at temperatures from 1500-2000 C during which time the graphite outgasses and undergoes a slight (0.2-0.6%) volume expansion. At 2600 C, crystalline growth predominates. The mechanism appears to involve displacement and rearrangement of groups of planes to achieve three-dimensional ordering, supplemented by movement of single C atoms and rings to fill vacancies in existing crystallites. Chemical bond rearrangement, condensation, and carbide decomposition do not appear to contribute significantly to the ordering. The presence of O_2 and CO_2 in the residual gas background enhances the process. Based upon the evidence above, it is likely that the high-temperature treatment used during boronization has resulted in graphitization of the carbon. The presence of B and/or poor vacuum may act as a catalyst for the process.

The second ribbon (HRL:2/8/83,C5) studied was described as a "nearly perfect" example of an ideally boronized ribbon. ESCA analysis of this specimen revealed a C/B ratio of about 1/5 after 30 minutes of Ar^+ sputtering. Since it is expected that the analyzed area of the specimen included both the boronized region and part of the graphite substrate (the analyzed region was approximately 1 mm x 1.5 mm for these ESCA studies), this fraction must be viewed as a

rough guide only. Additionally, since the C(1s) binding energies of B_4C and the graphite standard were nearly identical, one could not determine if the surface was B_4C or graphite by ESCA.

This specimen was also fractured and mounted laterally to permit high-resolution Auger examination of the interfacial cross-section. Auger line scans of B and C were performed along three lines intersecting the interface. The results were very similar, and only the measurement along line 1 is reported in Figure 6-3. It is observed that the interface is quite sharp, with both B and C signals rising sharply as the interface is crossed (the zero of the distance scale is at the top of the SEM photo). It is difficult to say whether or not boron carbide has formed at this interface. Because of this uncertainty, and due to the uncontrolled nature of the flash heating step of the boronization process, it is difficult to draw further conclusions for this sample, and the results are reported primarily because this particular ribbon comprised the only case where a B remnant of the boronization process was found in the original group of samples preconditioned by HRL. At least a dozen such samples were studied in the course of our experiments.

To underscore the case for the rapid volatilization of B from a graphite ribbon, an experiment was performed using Auger spectroscopy to determine when boron begins to evaporate from such a surface. Figure 6-4 shows SEM micrographs of a graphite ribbon painted with a thin layer of B-powder and acetone. The ribbon was subsequently introduced into the vacuum environment and heated while monitoring a fixed position of the surface with the Auger spectrometer. The

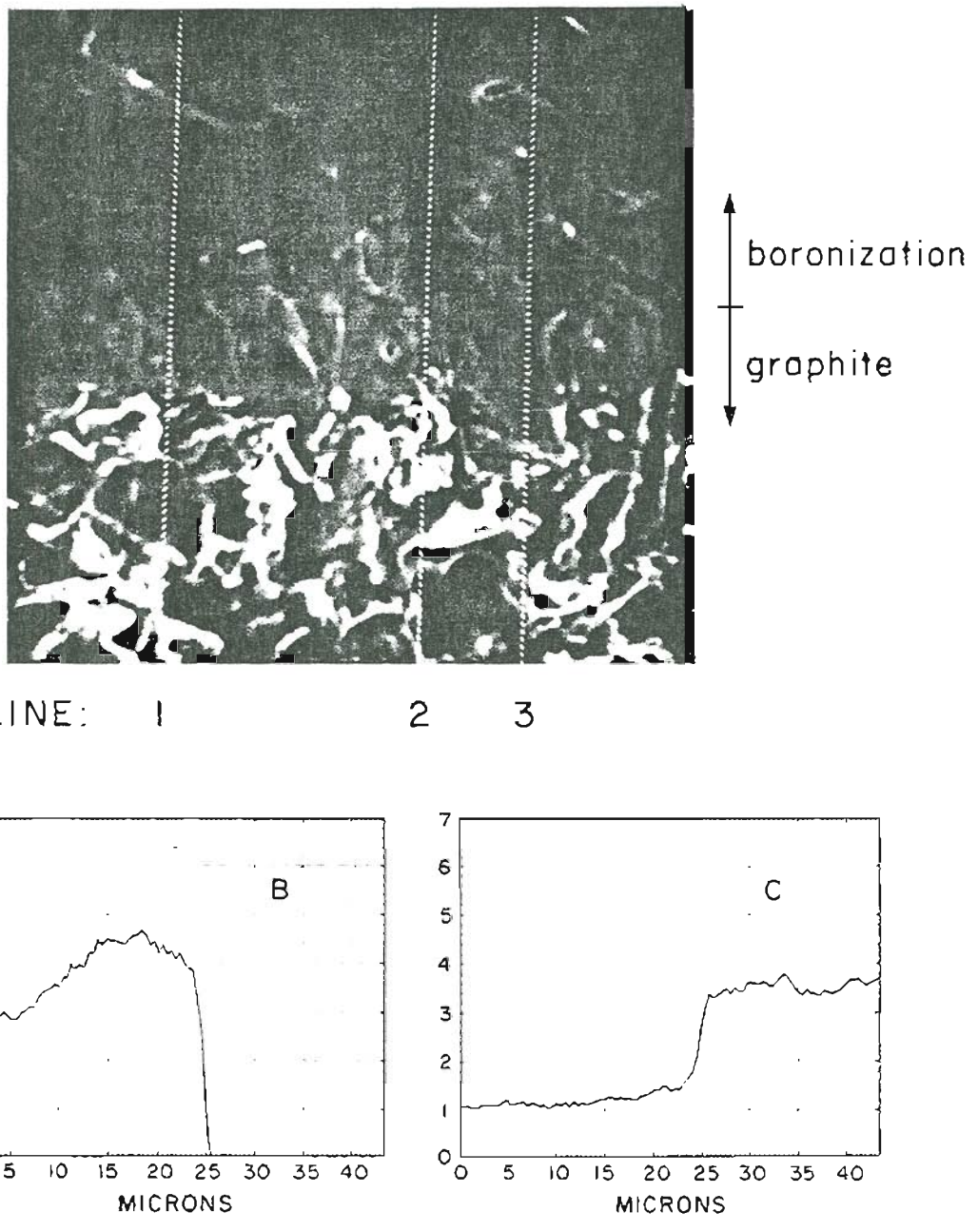

Figure 6-3. Auger line scans over the boronization/graphite interface. The ribbon has been fractured and mounted to probe the cross-section. (Top) View of the cross-section, with the location of the line scans indicated; (Bottom) Auger line scans of B and C. The results are for line 1.

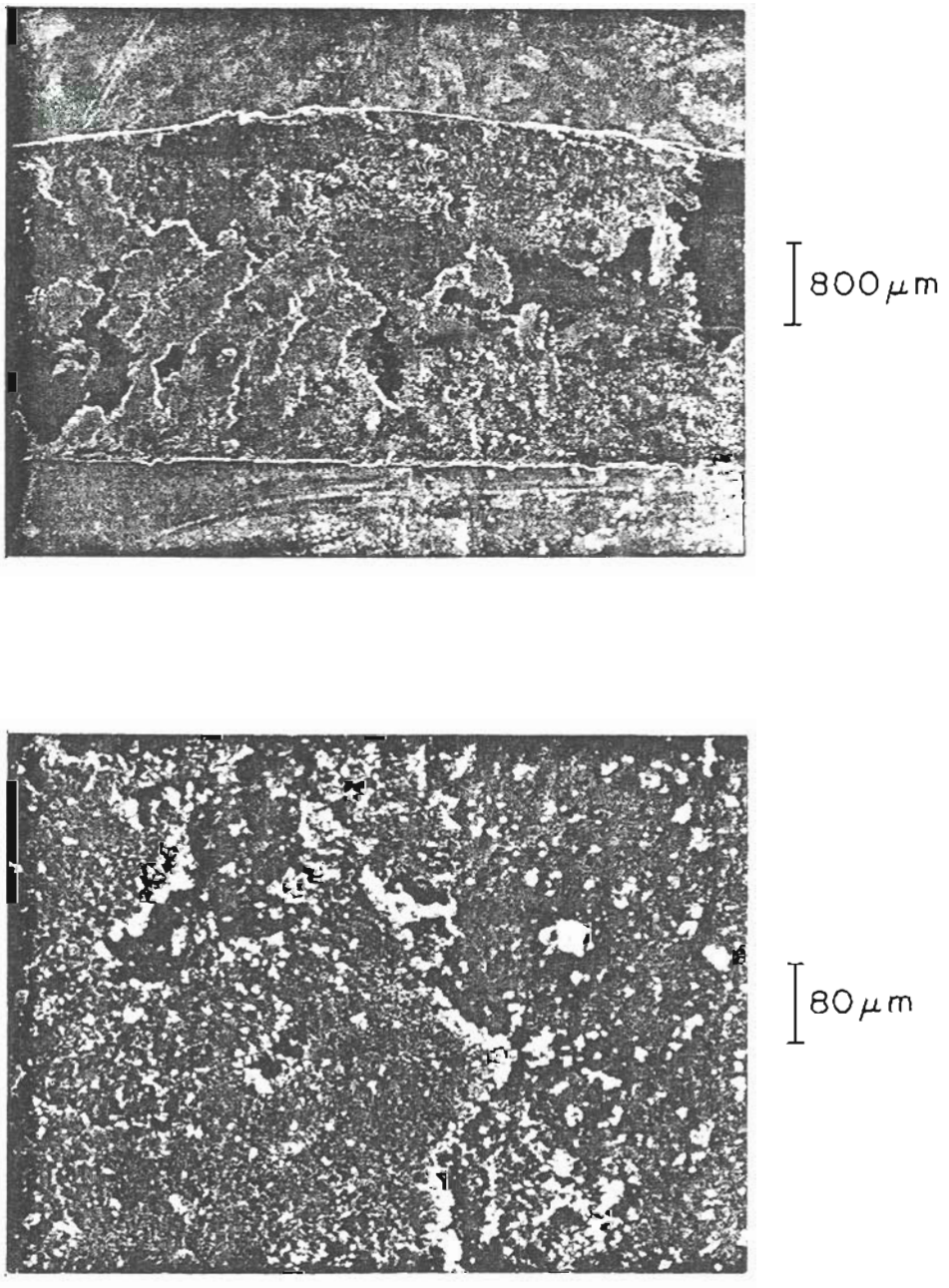

Figure 6-4. A graphite ribbon covered with a slurry of B-powder and acetone before heating.

results are shown in Figure 6-5. The significant conclusion is that nearly all boron has volatilized at temperatures near 2000 K (1727 C). Figure 6-6 analyzes other points of the surface after heating. There is little B anywhere on the ribbon.

It may be argued that the results are invalid because the surface was not flash heated. Calculation of surface evaporation rates, however, show that volatility is extremely sensitive to temperature. Doubling the temperature from 1500-3000 K changes the volatility rate by 10 orders of magnitude. At 2673 K (2400 C), the temperature typically used in the HRL process, about 5 microns of B are evaporating per second. This is demonstrated in Figure 6-7, which is a semi-logarithmic plot of temperature vs microns/second of B leaving the surface. It is clear that hesitation of even one second at high temperature results in rapid depletion of B from the surface.

An unexpected corollary found during the experiment is shown in Figure 6-5. In the temperature range from 1600-1800 K, the chemical shift indicative of boron carbide appeared. This is important because it provides further information about the process of B_4C formation. Examples to be discussed below show that boron carbide may be formed near the expanding front of a wetted alloy, and within the interior of the alloy if certain conditions are satisfied. Here, boron carbide is found to form at the interface of a boron-carbon layer after a few minutes at about 1600 K. From the thermochemical theory of wetting, such an interfacial compound is not unexpected, as boron carbide has a favorable Gibbs free energy of formation in the indicated temperature range. It is likely that temperatures of 1600

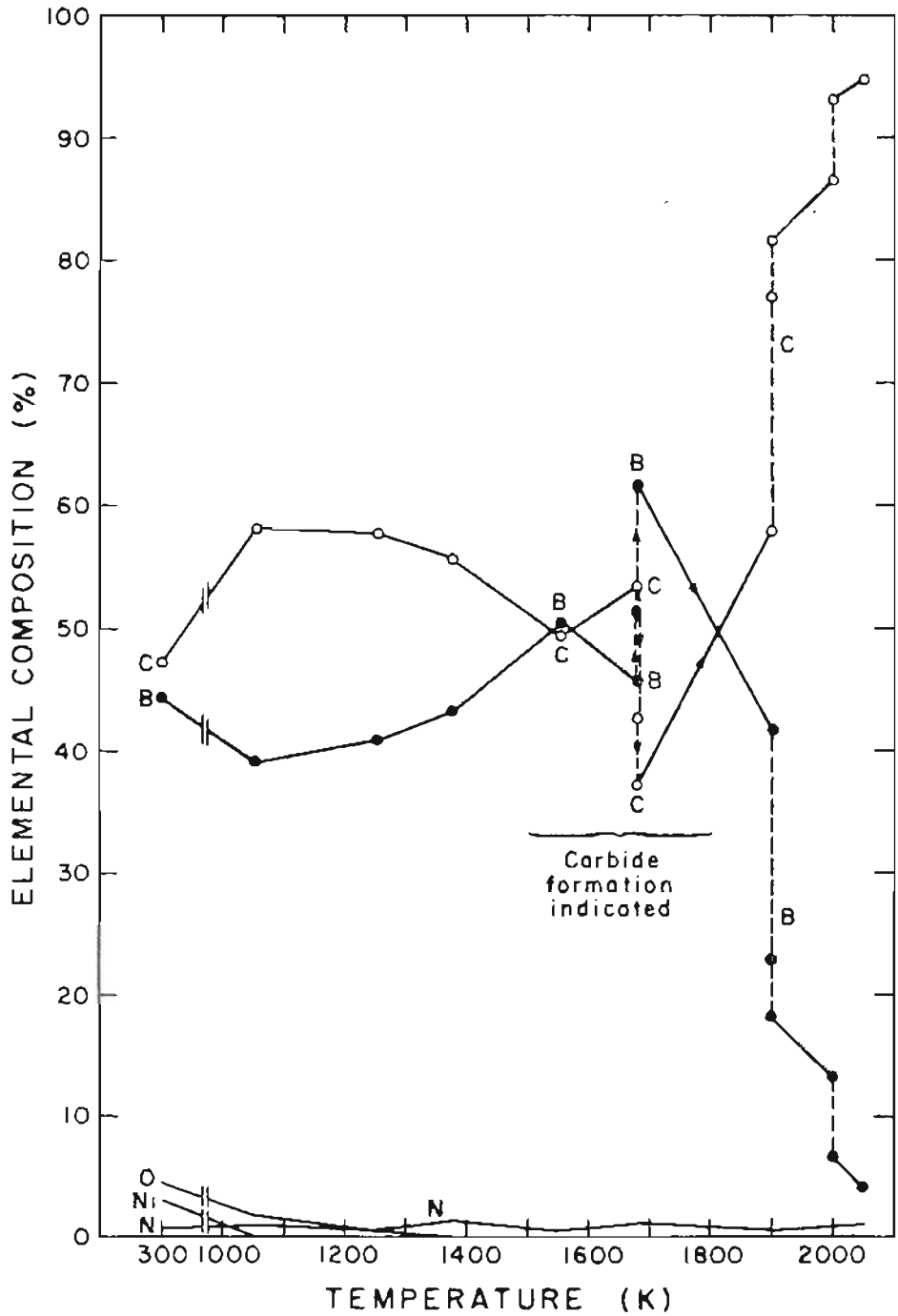

Figure 6-5. Auger surface elemental composition vs temperature for the slurry of B-powder and acetone on graphite. Note that the B signal is near zero at T = 2052 K (1777 C). The dashed lines indicate that successive Auger spectra were taken at a fixed temperature, the rate of volatilization being so rapid. The time between points is about 10 minutes.

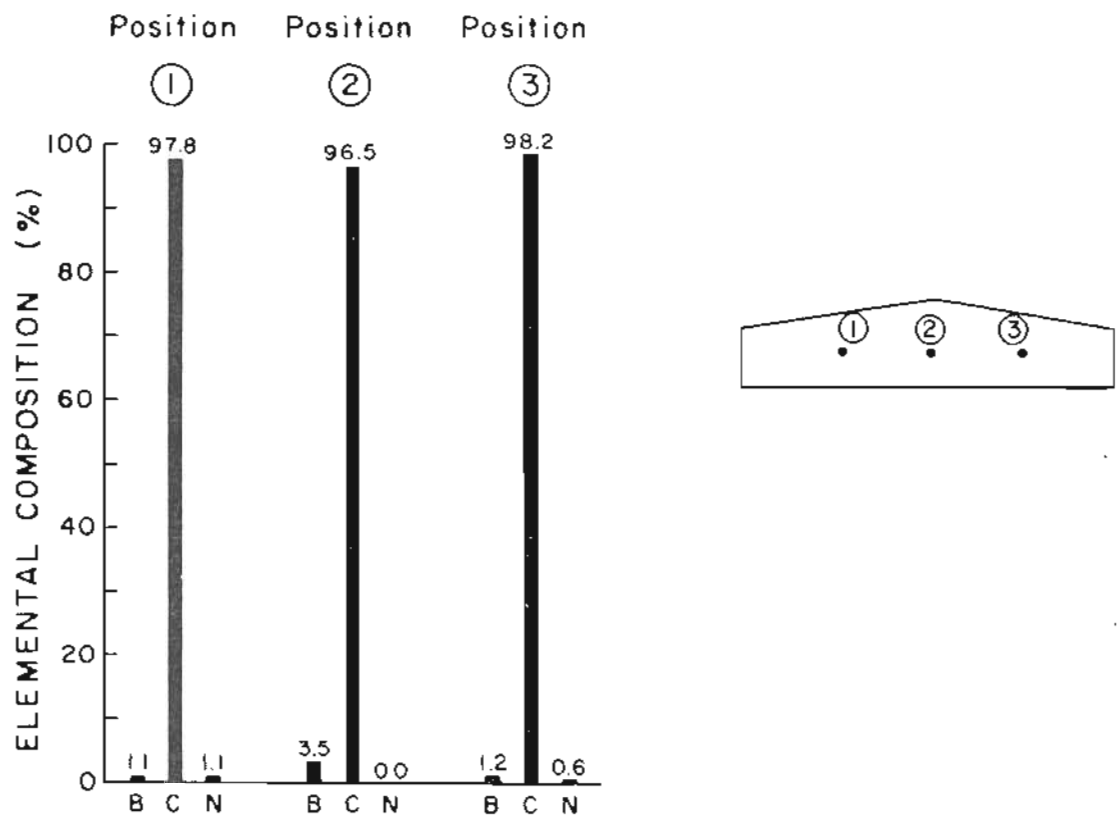

Figure 6-6. Auger surface elemental composition vs position for the "boronized" graphite after heating. There is little B anywhere on the surface.

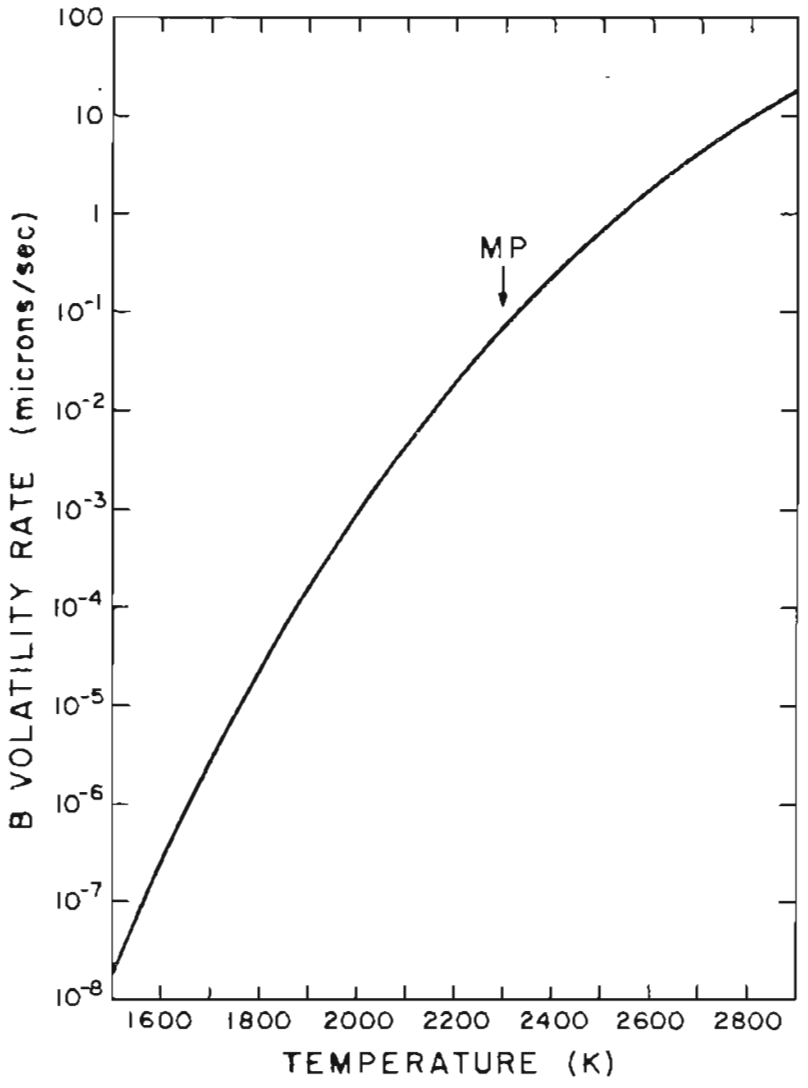

Figure 6-7. Theoretical B volatility vs temperature. Notice the strong dependence between the two: a doubling of temperature from 1500-3000 K causes the evaporation rate to increase by 10 orders of magnitude. Calculated from formulas in S. Dushman and J. Lafferty, Scientific Foundations of Vacuum Technology, 2nd ed. (New York, Wiley, 1962), p. 18.

K are necessary to flash away the free B and reveal the underlying boron carbide interlayer.

In conclusion, experiments to elicit the role of boronization in prewetted specimens showed that all B had volatilized from the graphite surface at temperatures well below those attained during flash heating of the ribbons. Boron carbide was revealed just prior to volatilization. SEM analysis of boronized specimens of graphite showed substantial crystal formation in areas thought to be regions of "heavy" boronization. It is evident that a C phase transition had occurred, whereby the substrate had been graphitized by the high temperature flash employed in the process. It is possible that the resulting surface aids in wetting B-containing liquid metal alloys to C, and in part explains the success obtained by the HRL process.

B. Studies of Wetting in Contact Systems Containing Ni/B Alloys

Despite the mass of evidence showing the absence of boron on prewetted specimens, the controversy over boronization preprocessing remained an issue throughout our studies, in part because of the dramatic improvements in wetting when something involving boron was added to the contact systems. Testimony to this fact was given by the number of well-wetted systems that underwent some sort of boron processing. In light of the lack of reproducibility of the HRL process and the limited information gained by studying specimens which had been prewetted, the OGC group assumed responsibility for performing fundamental wetting experiments on a number of

alloy/substrate combinations. Results of these investigations are detailed below.

1. Wetting Studies of Ni/B (OGC) to C (virgin)

A 20 g specimen of Ni/B eutectic alloy was synthesized at OGC by the arc melting technique. A similar sample was prepared by the LANL group. Details of the OGC procedure follow. Stoichiometric amounts of B powder and Ni metal were weighed and mixed mechanically. The mixture was placed in a graphite crucible with a molybdenum lid and enclosed in a second graphite crucible. The entire unit was then placed in a sintering furnace that was backfilled with 25" of He and the alloy was sintered for 1.0 hour at 1000 C. The furnace heating elements were also graphite and a quartz evaporation shield to detect evaporation losses during sintering was added to the furnace. No losses were observed. The sintered specimen was next introduced into the arc melter which was successively purged with pure Ar gas, a 1-to-1 Ar-He mixture, and pure He. The arc melter was then backfilled with a 1-to-1 mixture of Ar-He to a pressure of 20", and the tungsten stinger was applied to the sintered mixture and worked continously through the alloy for complete mixing.

Emission and Auger spectroscopic analysis of the resultant alloy revealed that the OGC material was quite pure but slightly Ni-rich, containing a bulk composition of Ni = 63.7% and B = 36.3%. By comparison, the lowest eutectics of the Ni/B system have Ni concentrations at about 55% and 60%. Table VII summarizes the

emission spectrographic characterization of the alloy. The major impurities and C = 0.10%, N = 0.01%, and O = 0.005%, although there are traces of other contaminants traceable to conditions existent in

TABLE VII

EMISSION SPECTROSCOPIC ANALYSIS OF THE $Ni_{55}B_{45}$ ALLOY MANUFACTURED AT OGC

Element	Relative Abundance (w%)
Ni	90.5
B	> 10.0
C	0.019
O	0.0011
N	0.003
W	0.1-1.0
Mo	0.01-0.1
Fe	0.01-0.1
Ti	0.01-0.1
Cu	0.001-0.01
Mg	0.001-0.01
Al	0.001-0.01
Si	0.001-0.01

the arc melter. Note that the percentages just quoted are atomic percentages, while the numbers in Table VII are weight percentages.

The average Auger analysis of three positions on the surface of the OGC material in its "as received" condition is shown in Figure 6-8. The impurities mentioned above are present, in addition to Cs, Ca, and S which were not tested for in the emission analysis. The Cs originates from an unrelated previous use of the vacuum chamber and is desorbed from the chamber walls during bakeout. Similar measurements after Ar^+ sputtering of the surface are displayed in

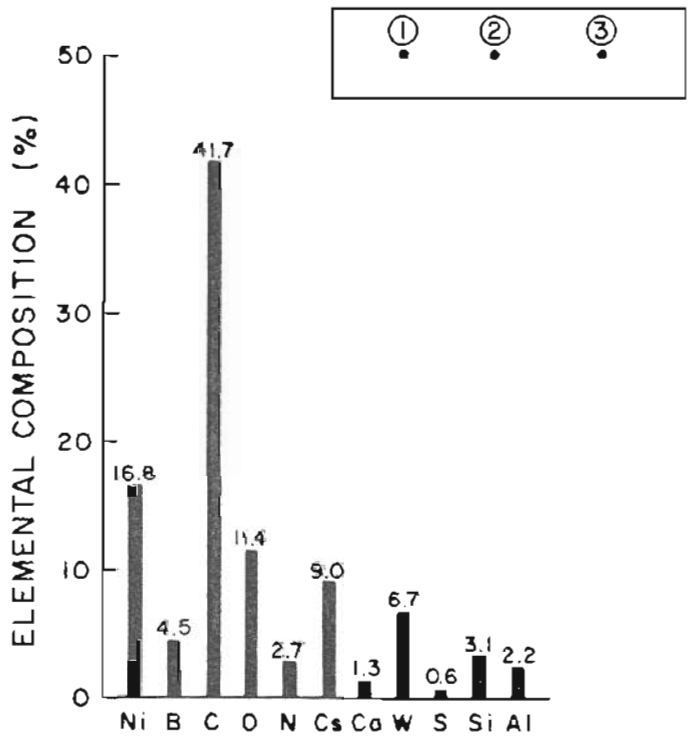

Figure 6-8. Average Auger surface elemental composition of three positions atop the "as received" Ni/B alloy manufactured at OGC. The temperature is 300 K.

Figure 6-9. The primary contaminant of the clean surface is C. Scanning electron micrographs of a thin slab of the OGC alloy are given in Figure 6-10.

Wetting of Ni/B (OGC) to C (virgin) by the method detailed above proved to be unsuccessful. In this experiment, a flat slab (5 mm X 5 mils) of alloy cut from the interior of the arc melted boule was laid atop a ribbon of virgin polycrystalline graphite (from Union 76 Corporation) and heated slowly until melting was observed at 1305 K, which is 10 degrees above the lowest eutectic of the Ni/B system. This procedure was followed because it was straightforward and allowed comparison with HRL wetting experiments, which were performed in similar fashion. The wetting sequence is diagrammed in Figure 6-11. At melting, the left side of the alloy slab was observed to retreat into the alloy with the contact angle becoming less favorable as the movement proceeded. Increasing the temperature further, the right side of the alloy slab behaved similarly, resulting in a poorly-wetted droplet of alloy with a near-180 degree contact angle. Simultaneous with this was the development of two characteristic regions of the alloy droplet which were observed in many cases of alloy wetting. The side of the droplet nearest the graphite was found to be about 50 degrees brighter than the top side of the droplet and to be identical in brightness temperature to the graphite substrate.

In the procedure followed by HRL, the temperature of the contact system was usually raised to around 1700 K to facilitate wetting, and frequently much higher for poorly-wetted samples. To investigate

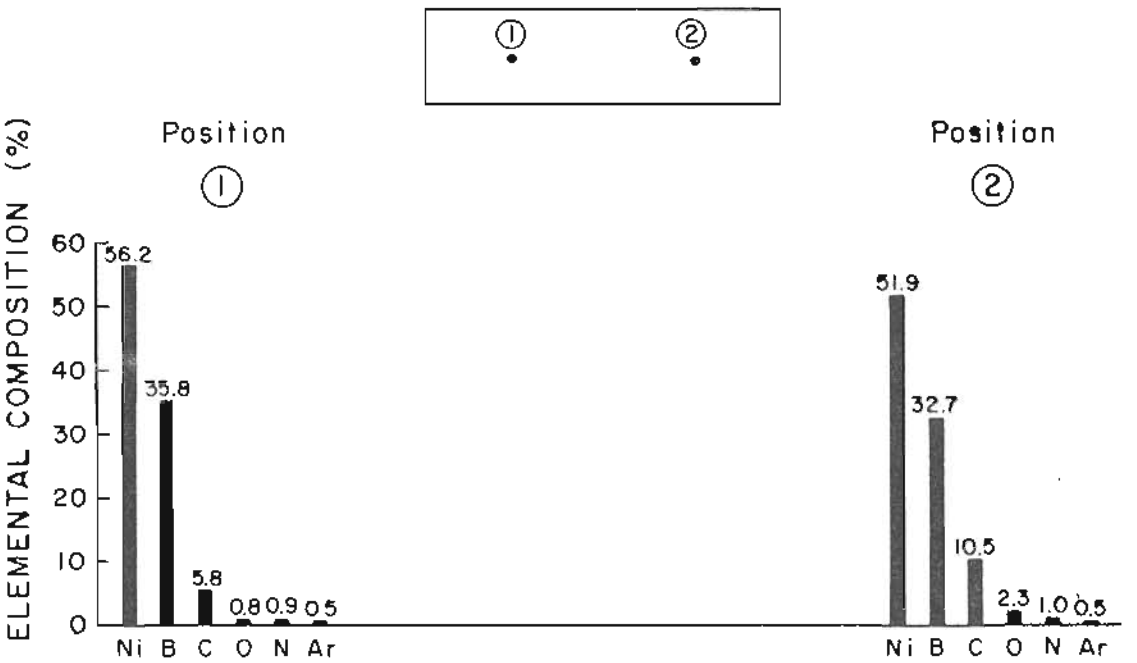

Figure 6-9. Auger surface elemental composition of the Ni/B alloy manufactured at OGC after Ar^+ sputter cleaning.

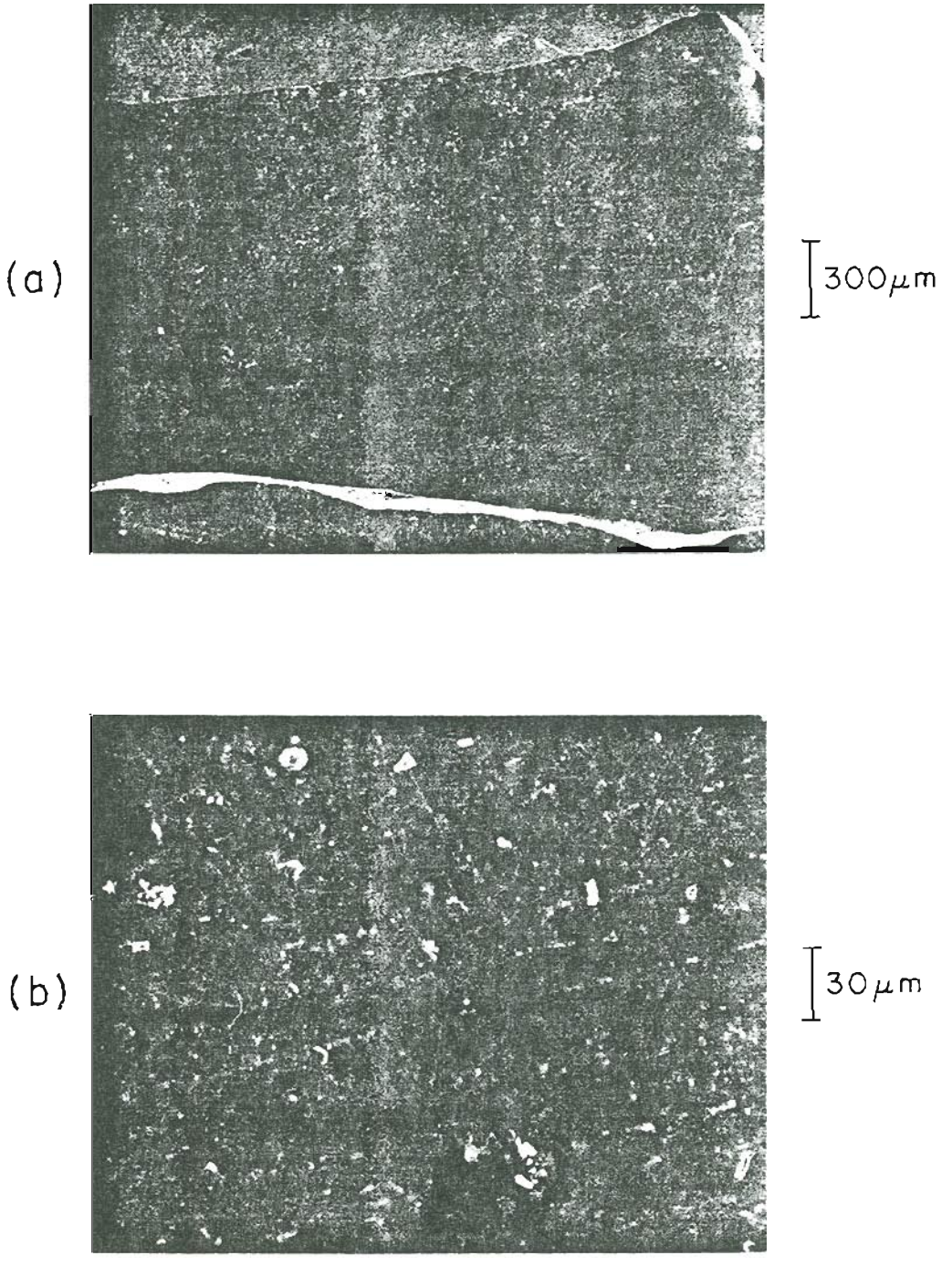

Figure 6-10. SEM micrographs of a thin slice of the Ni/B alloy manufactured at OGC. (a) Overall view; (b) A magnified view of the central region of (a).

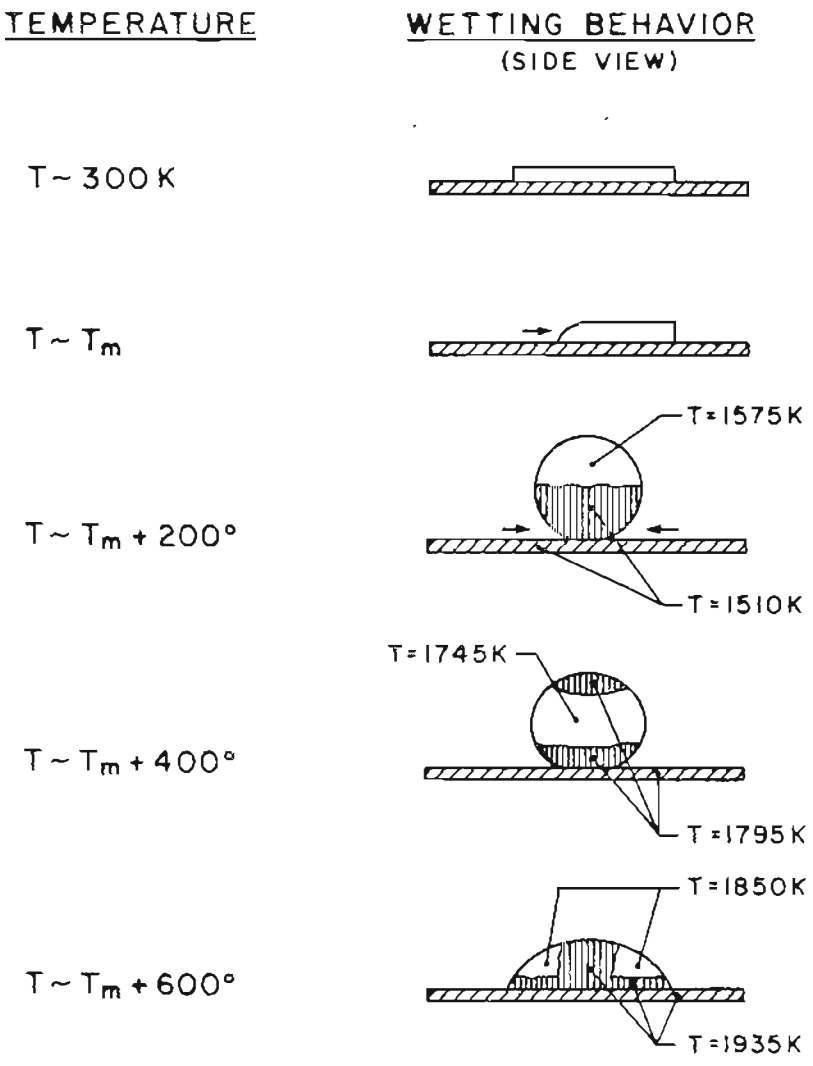

Figure 6-11. Wetting behavior va temperature for wetting of Ni/B (OGC) on C (virgin). The melting point T_m of the alloy was determined to be 1305 K. The temperatures shown are of apparent pyrometer brightness, corrected assuming the emissivity of C.

this regime, and to see if wetting would occur with increasing temperature, we decided to systematically raise the temperature rather than remain at a fixed temperature for an extended period. The lower two drawings in Figure 6-11 detail the observed behavior. With rising temperature, the top limb of the droplet began to develop a bright region which grew toward and eventually met the expanding bright region at the bottom of the droplet. The contact angle began to decrease with time as the alloy started to reluctantly wet the substrate.

Top and side views of the wetting behavior after high heating are shown in Figure 6-12. The graphite ribbon had fractured after 20 minutes at 1900 K due to thermal expansion in the support structure and the experiment was therefore terminated. Photos (a)-(b) show that the alloy has begun to flow over the substrate by distances the order of millimeters, displaying behavior similar to that observed in studies of prewetted specimens where poorly-wetted droplets were found to fracture with heat treatment and flow over virgin material. In the newly wetted region, the wetting behavior is excellent, and the contact angle is near-zero.

Auger analysis of the droplet and wetting front after reinsertion into the vacuum system revealed that the top of the droplet was nearly 100% C. The wetting front was difficult to analyze with the fixed-beam system because the position where the incident beam struck the target could not be discerned precisely, but it appeared to consist mostly of C with small but non-zero concentrations of B, Ni, and N. Such high concentrations of C are not unexpected at elevated

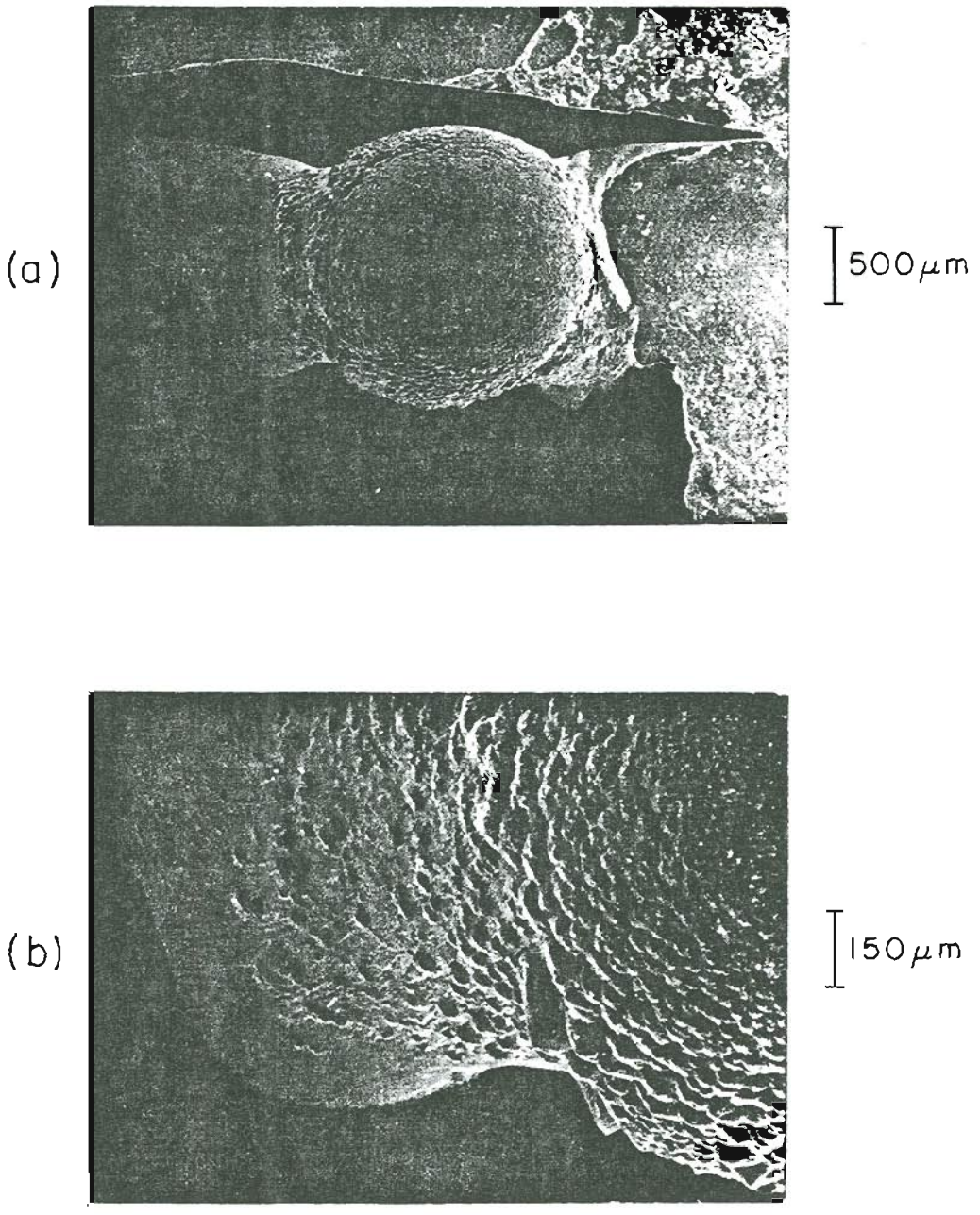

Figure 6-12. The wetting behavior of Ni/B (OGC) on C (virgin) after high heating. (a) Top view; (b) A magnified view of the lower left of the droplet in (a).

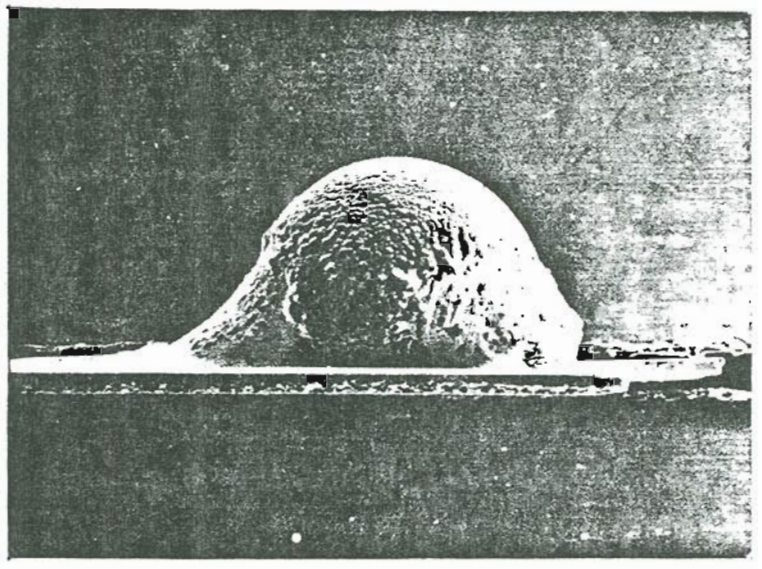

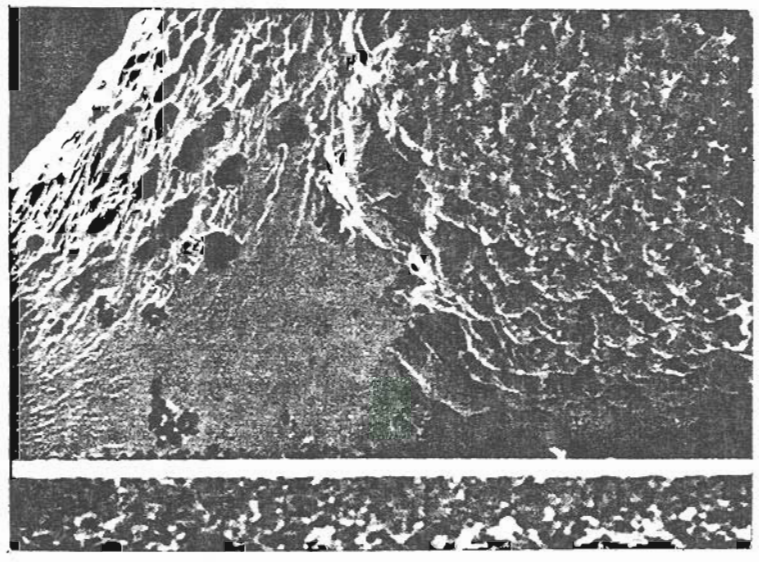

Figure 6-12 (continued). Cross-sectional views of the wetting of Ni/B (OGC) on C (virgin). (c) Scene corresponding to the view observed through the UHV chamber window; (d) The lower-left side of the droplet in (c).

temperatures, as previous work has shown that substrate dissolution in the alloy occurs at temperatures greater than 100 degrees above the alloy melting point for Ni/B alloys.

Volatilization of C from the graphite is also significant at such temperatures, as evidenced by the presence of a dark residue on the Macor^{R} support structure behind the ribbon that was not present before the high heating. These observations are important in explaining the high concentrations of C found in samples from HRL that underwent a similar wetting history. Utilizing high temperatures during wetting promotes dissolution of graphite into the alloy and results in the very thing that previous work has found to impede wetting. Of final note is the shape of the Auger C peak in spectra taken of the droplet surface. This shape is that of elemental carbon and no indication of carbide chemical effects were found. The alloy surface is therefore covered with a thick layer of carbon which originates from the substrate at high temperatures. Later, we will see that carbon also originates from low-level impurities in the alloy which surface segregate when the alloy is first melted.

A second, identical experiment with Ni/B (OGC) and C (virgin) was performed for reproducibility and to gather further data. An alloy specimen of irregular shape was used rather than the flat specimen used in the first trial. The wetting behavior was quite similar to the first experiment. At the melting point, the alloy initially began to collapse onto the substrate as though it was going to wet, but then quickly closed into itself and formed a poorly-wetted

droplet of material. Simultaneously, the lower half of the droplet developed a similar area possessing the same brightness as the graphite, a brightness temperature about 60 degrees hotter than the top (darker) portion of the droplet. Photos of the alloy while molten and after cooling to room temperature are shown in Figure 6-13. Unfortunately, the discrimination in brightness is poorly resolved in the reproduction. The boundary between bright and dark portions of the droplet appeared to move upward slightly as the temperature of the droplet was increased. The darker upper half was determined to be molten due to the characteristic flash of light emitted as the temperature of the droplet was lowered through the melting point. Additionally, this part of the droplet oscillated when the vacuum chamber was repeatedly struck.

No such behavior was found for the bottom part of the droplet. It therefore appeared that the molten material in the upper hemisphere of the droplet was contained in a solidified cup of material formed in the lower part of the alloy.

Scanning electron micrographs of the contact system after cooling are shown in Figure 6-14. Photos (a)-(c) show evidence of the expected crystal growth with irregular patches of (lighter) impurity and dark unidentified features. Photo (f) is a blowup of the recrystallized structure atop the droplet, corresponding to growth of BNi_2 crystallites away from material of eutectic composition which remains in the crevasses. The contact angle and the boundary

(a)

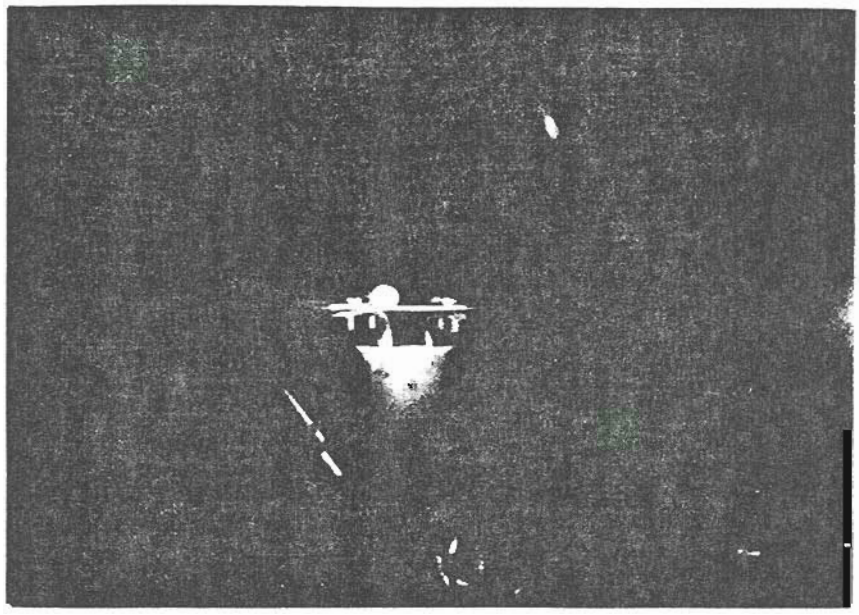

(b)

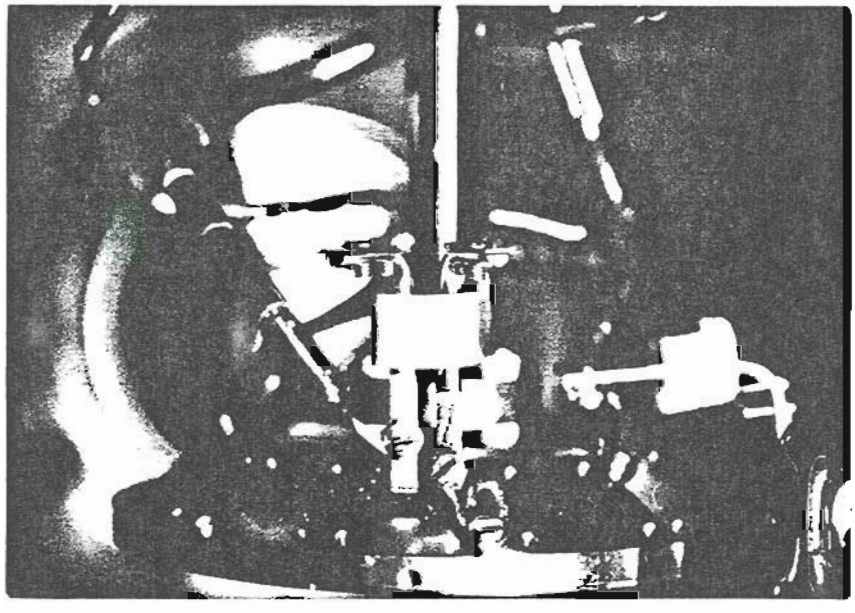

Figure 6-13. Photographs illustrating the wetting characteristics of Ni/B (OGC) on C (virgin). (a) View immediately after alloy melting. A bright/dark division of the droplet is present that cannot be seen in the reproduction; (b) The view after cooldown.

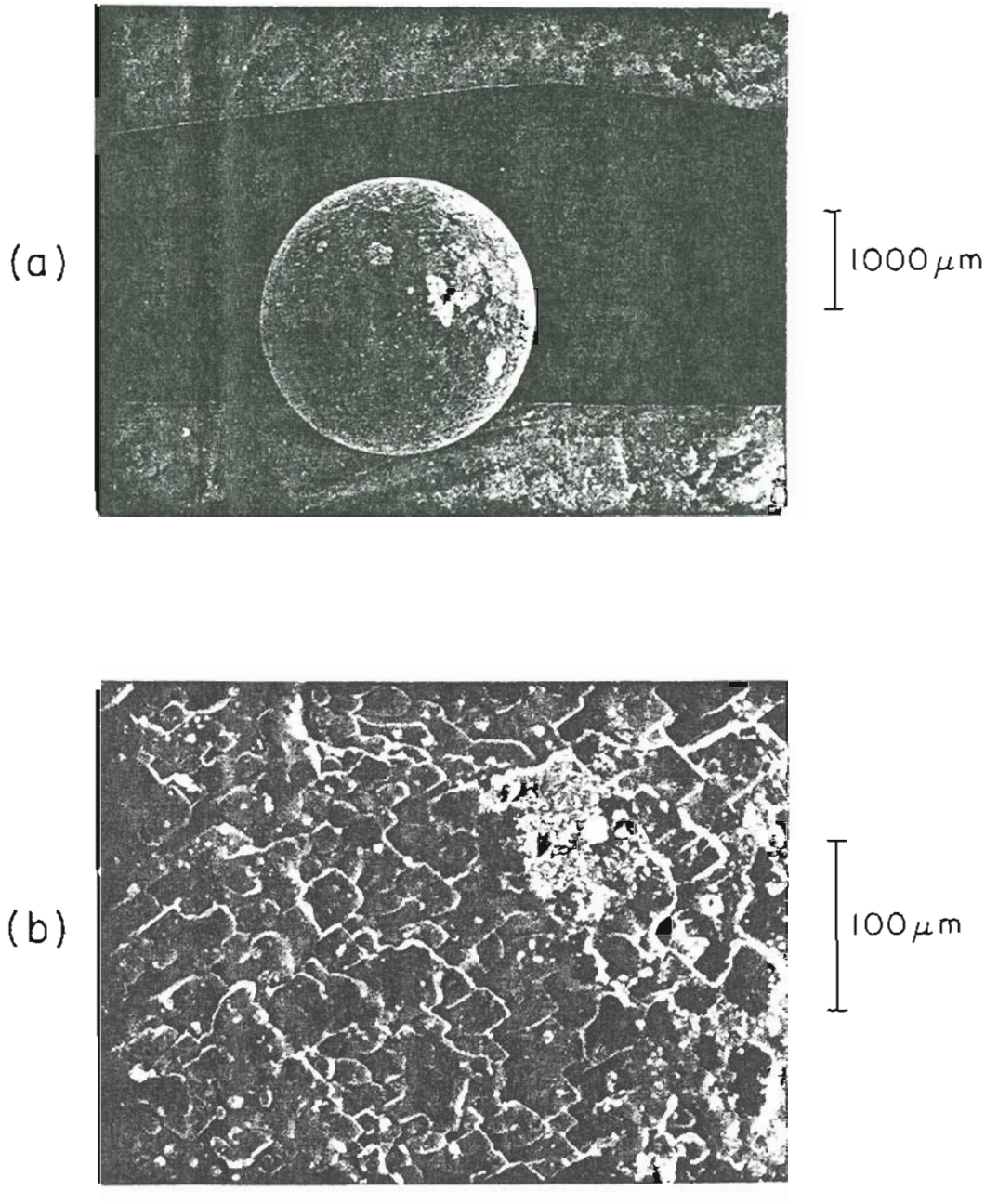

Figure 6-14. The wetting behavior of Ni/B (OGC) on C (virgin). (a) Top view; (b) Near the center of the droplet.

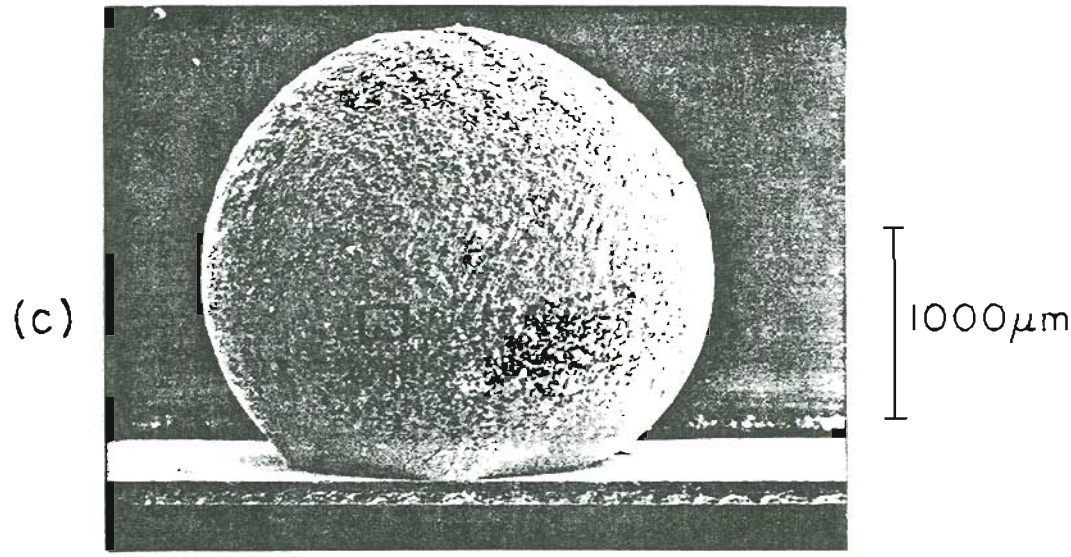

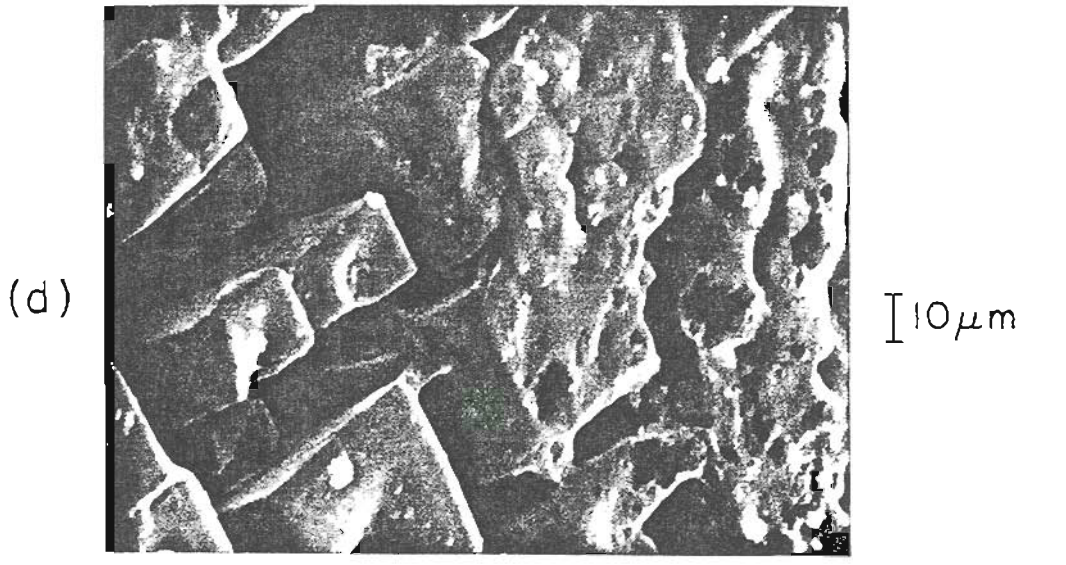

Figure 6-14 (continued). (c) Side view of the droplet showing the contact angle; (d) Magnified view of the microstructure after solidification. Crystal growth is evident.

separating bright and dark molten regions are visible in photo (d), while a blowup of the boundary is shown in photo (e). The lower half of the droplet appeared to have the higher concentration of dark, irregular features which later analysis proved to be carbon.

2. Wetting Studies of Ni/B (LANL) to C (virgin)

Here, Ni/B (LANL: #273-7C; Ni=.53, B=.47) alloy synthesized by the LANL group was wetted to virgin carbon. The wetting procedure was identical to that above, with the exception that the alloy was not heat stressed. Rather, the temperature was increased until melting occurred and then held rigorously constant at fifty degrees above the melting point for nearly two days. A mounting arrangement that enabled Auger analysis during heating was also employed. The wetting characteristics were very similar to those described above for OGC alloys, and are shown in Figure 6-15. At melting, the irregular alloy specimen of Ni/B began to collapse toward the substrate but then subsequently pulled back into itself and formed a poorly-wetted droplet. Simultaneously, the bright and dark regions were formed within the molten droplet.

Figure 6-16 details the variation of contact angle with time at an alloy temperature of fifty degrees above the melting point. After two hours, the contact angle decreased from nearly 180 degrees to 90 degrees as spreading proceeded over the virgin substrate. After 36 hours, the contact angle was about 30 degrees. The location of the bright/dark boundary on the droplet surface also changed during this

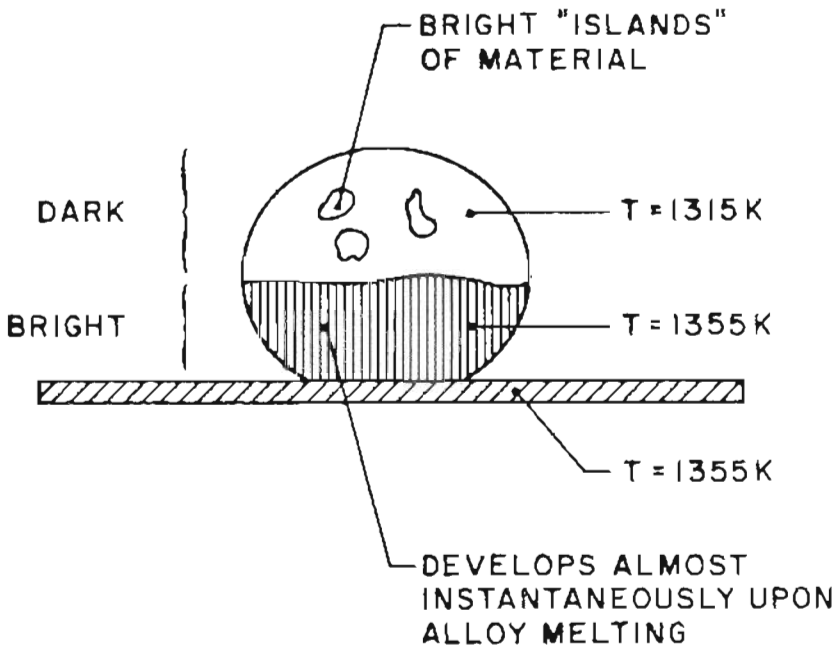

Figure 6-15. Wetting characteristics of Ni/B (LANL: #273-7C; Ni=.53, B=.47) on C (virgin) immediately after melting. The temperatures shown are of apparent pyrometer brightness, corrected assuming the emissivity of C.

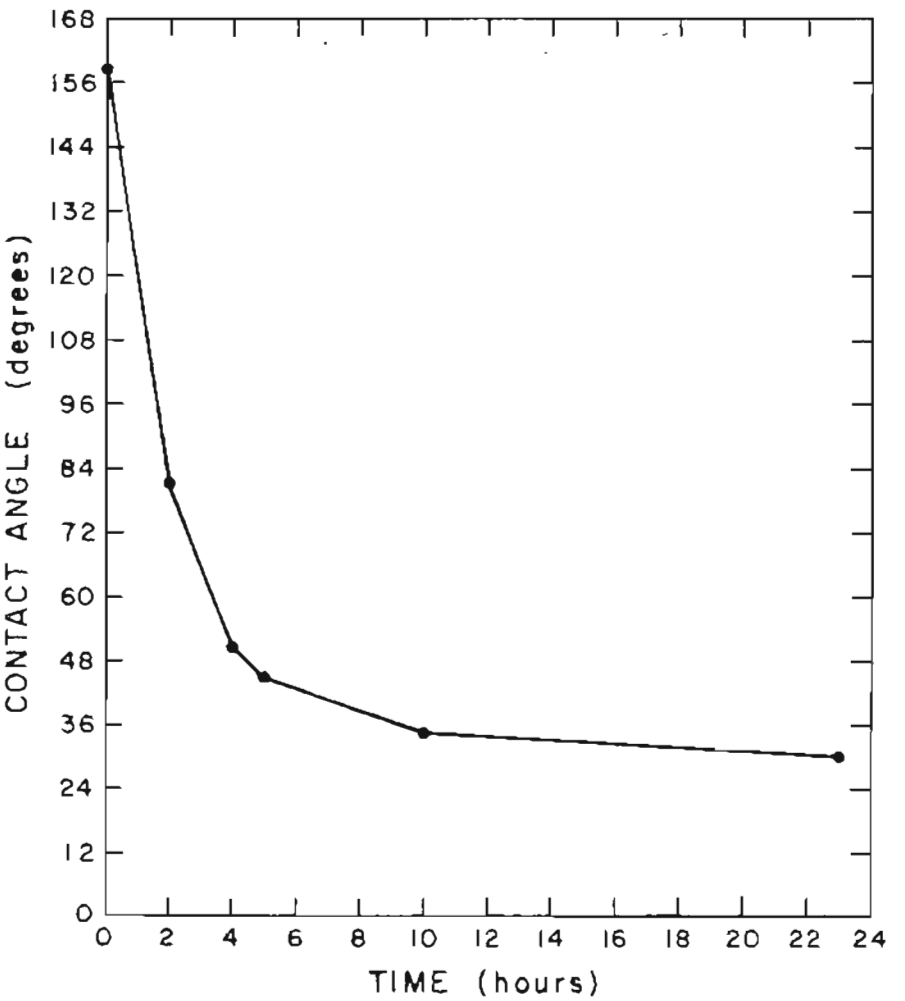

Figure 6-16. Contact angle vs time for the wetting of Ni/B (LANL: #273-7C; Ni=.53, B=.47) on C (virgin).

period. As the contact angle decreased, the bright lower half of the droplet decreased in size when viewed from the side, and became localized at the contact system interface. SEM examinations of the alloy after 36 hours of operation show that the alloy has expanded distances the order of millimeters over the front side of the substrate, and the leading edge of the flow has a contact angle of near-zero.

Following removal of the specimen from the vacuum system, it was found that a portion of alloy had flowed through the graphite substrate and wet the backside of the ribbon. This is shown in Figure 6-17. Subsequent studies revealed that the alloy had not flowed through a favorably disposed series of pores in the graphite, but rather had chemically attacked the graphite. This fact has significance for wetting, for a metallic alloy cannot chemically react with material that it first cannot wet. Thus, again it is found that the Ni/B eutectic wets virgin carbon under a certain set of conditions. Auger characterization of the backside flow and cross-section of this unusual specimen follow.

Auger analysis of the backside wetting showed that the rim of the flow contained boron carbide, while the interior contained pure alloy components that were Ni-rich. Once again, wetting and contaminant-free alloy appear to be connected. This is demonstrated in Figures 6-18 to 6-19, which show the Auger composition of two positions near the alloy/substrate boundary after the specimen had been reintroduced into the vacuum system. Position 1 at the alloy boundary appears to be a complex ternary of B, Ni, and C, perhaps

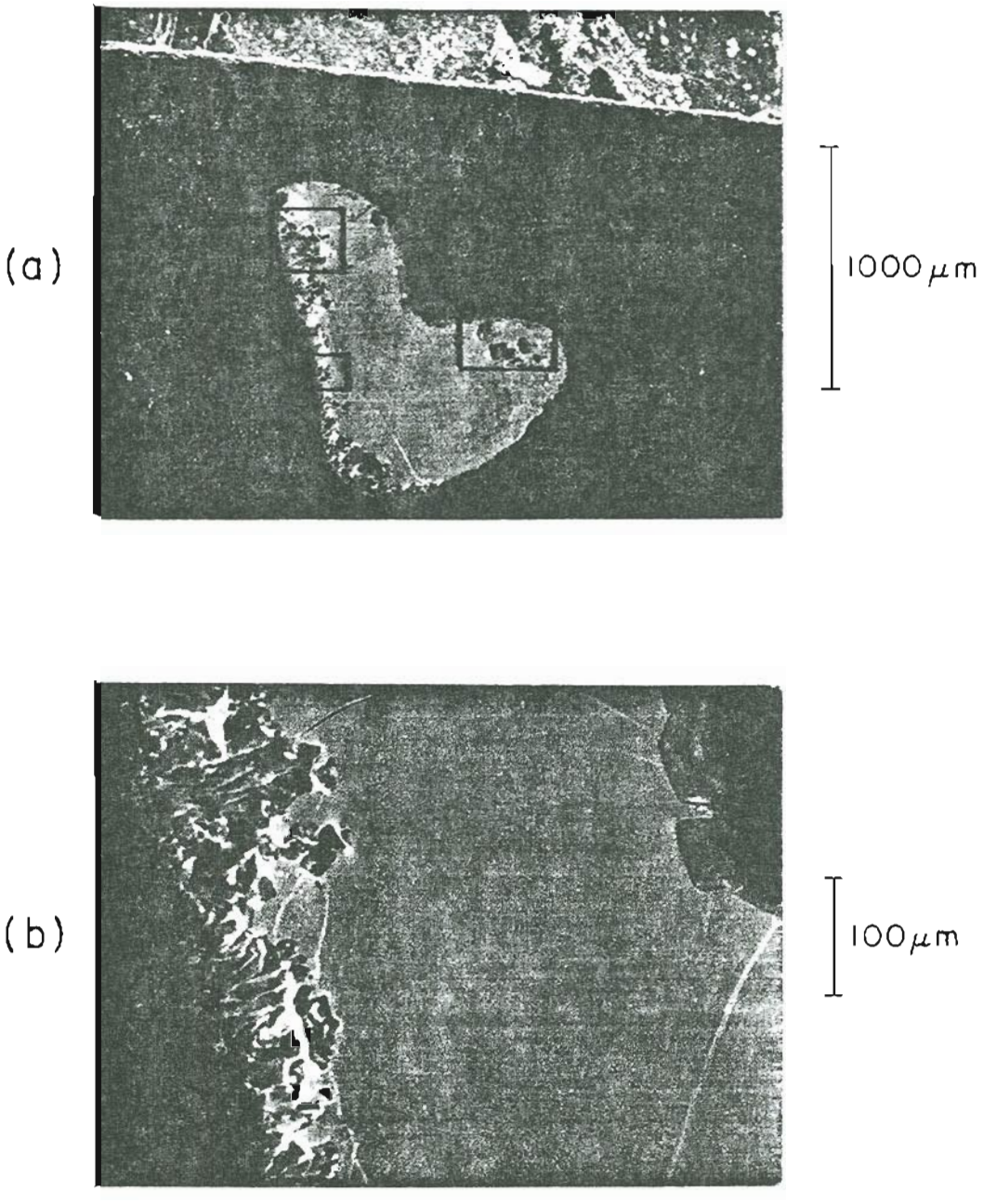

Figure 6-17. Wetting of the backside of the Ni/B (LANL) on C (virgin) caused by flow through the ribbon. The contact angle is near-zero. Second phase material has formed at the leading edge of the flow.

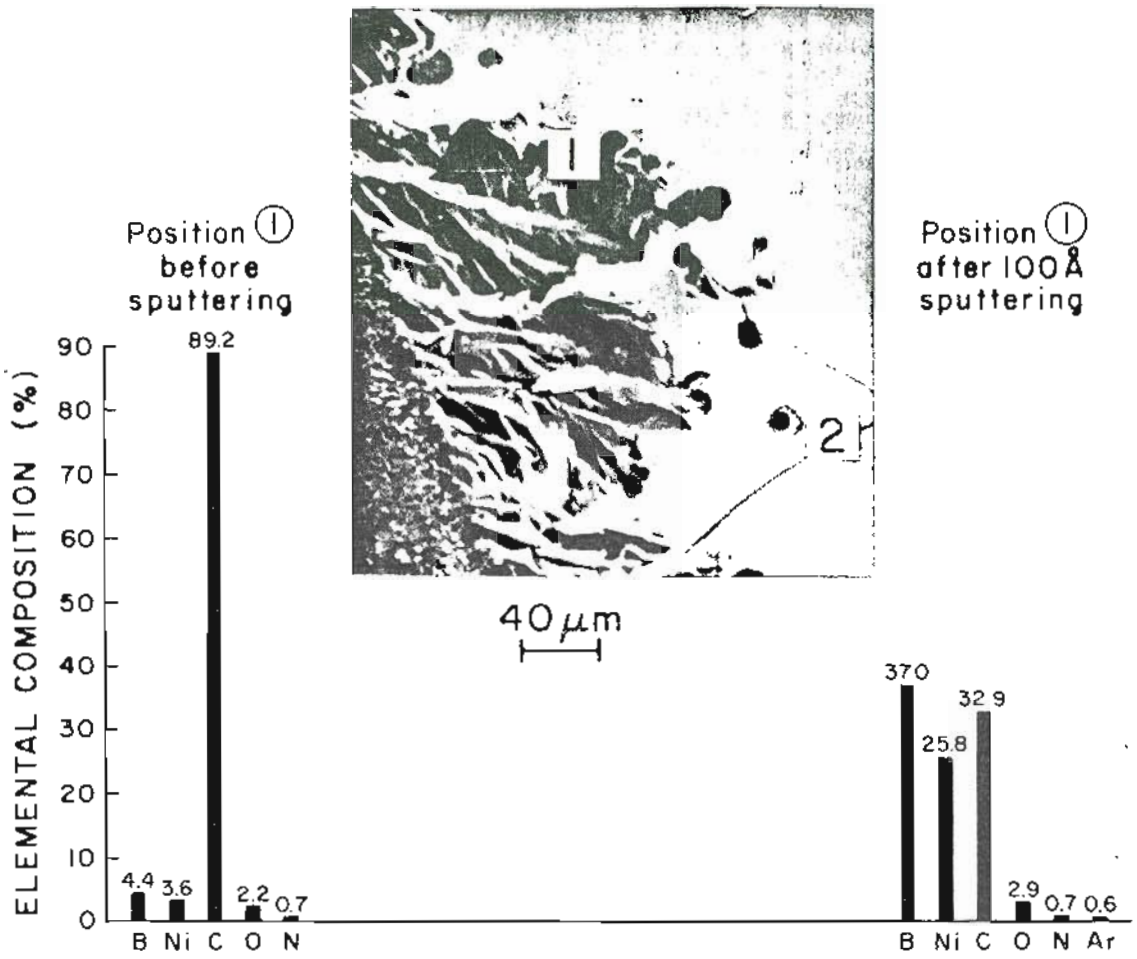

Figure 6-18. Auger surface elemental composition before and after sputtering the Ni/B (LANL) alloy that has penetrated the C ribbon and wetted the backside. The view shown is within the upper left-hand boxed area of Figure 6-17, at the alloy/substrate boundary.

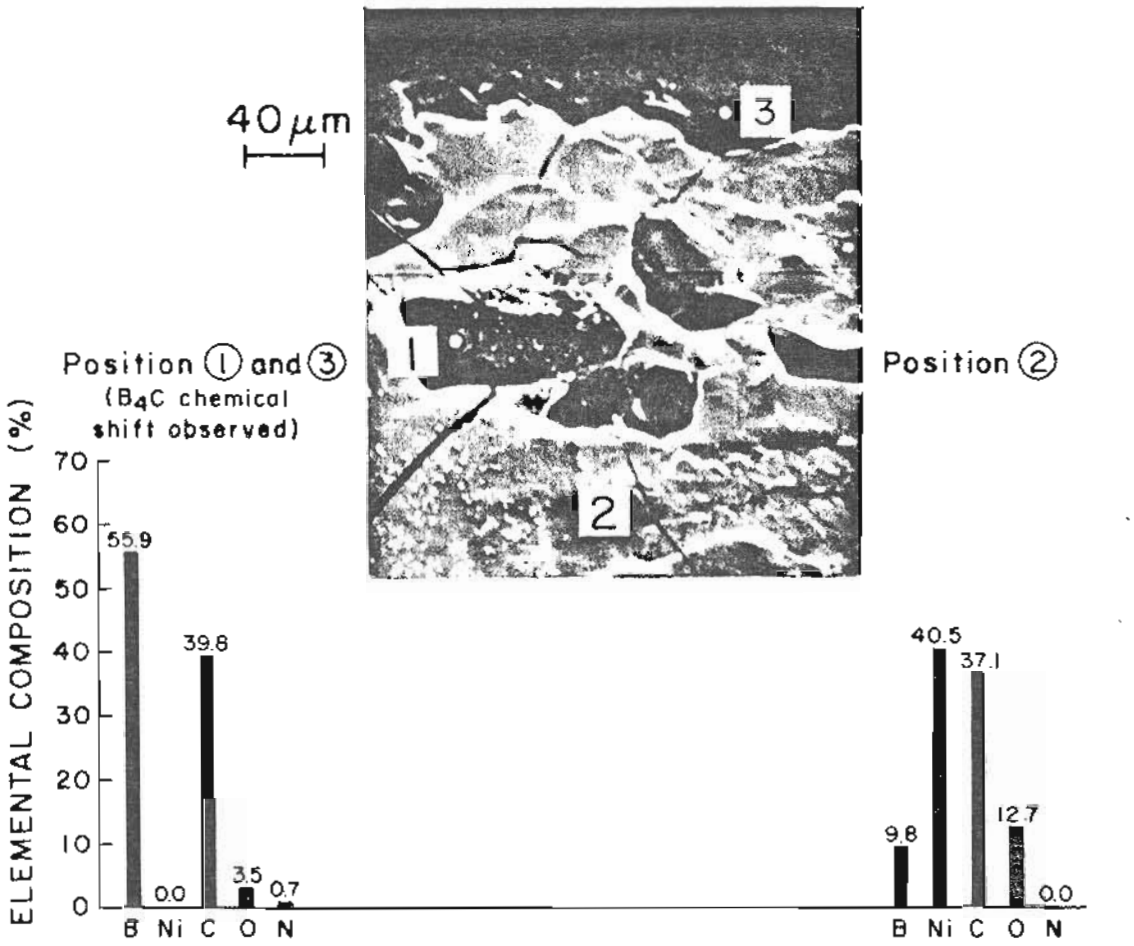

Figure 6-19. Auger surface elemental composition vs position for the Ni/B (LANL) alloy that has penetrated through the C ribbon and wetted the backside. The view shown is within the right-hand boxed area of Figure 6-17, near the alloy/substrate boundary. The surface has not yet been sputtered.

formed as the alloy moved out over the graphite. Although the characteristic shape change of the C peak due to the presence of boron carbide could not be definitively established at this position, it is likely that boron carbide has been formed. This is reinforced in Figure 6-19, which shows that analysis of other points near the alloy/substrate boundary are nearly 100% boron carbide. NiC possesses unfavorable energetics and is not expected to form.

In contrast, Auger analysis of several positions in the interior of the backside alloy show that the interior consists of pure alloy components that are Ni-rich relative to the LANL stoichiometry. The best explanation of this behavior consistent with other data is that the alloy is being robbed of B during formation of B_4C. This is supported by analysis of a cross-section of the alloy, discussed below. Initially, we thought that the Ni-rich interior partially explained why the B-fluxing step in the HRL wetting procedure appeared to facilitate wetting. The reasoning went as follows. If substantial amounts of boron carbide or a complex ternary of Ni, B, and C form at the alloy/substrate boundary, then the B that originally made up the eutectic has to be depleted in the process. This results in an elevated melting point for the alloy as the alloy climbs the Ni-rich liquidus of the binary phase diagram for Ni/B. The result is that liquid flow ceases. However, if extra B is added to the alloy, it could act to offset the lost B and conserve the alloy composition. We have since ruled out this possibility after the discovery of surface segregation in the alloys, although the mechanism could be operative for alloys where significant carbide

formation occurs.

A hypothesis that formation of boron carbide does support is the decrease in contact angle with time observed for this alloy. There are only two possibilities to explain this time dependence consistent with present understanding of wetting: either something is forming at the interface or something is being depleted from the interface. Either reaction acts to decrease the liquid-solid surface tension and promote wetting. Evidence cited above showed that boron carbide is formed at the surface of a heated ribbon of boronized graphite, and here we find it at the wetting front at significantly lower temperatures. This indicates that boron carbide can be formed at temperatures near the melting point of the alloy, but sluggish kinetics slow down the reaction. This behavior was suggested earlier for prewetted alloys which initially consisted of poorly-wetted droplets which later were found to melt and spread with heat treatment. The disappearance of large amounts of surface carbon from the droplets may be explained by the formation of boron carbide at the interface. This will be elaborated further in a later section.

Further evidence of boron carbide formation in this contact system is seen in Figure 6-20, which provides a perspective of the massive extent of the alloy attack. The alloy has dissolved a large portion of graphite, and the interior of the central alloy droplet is laced with second phase material. This is in contrast to the vast majority of other alloy droplets we have sectioned, whose interiors appear to be relatively free of such material. Auger surface elemental compositions at several positions within the cross section

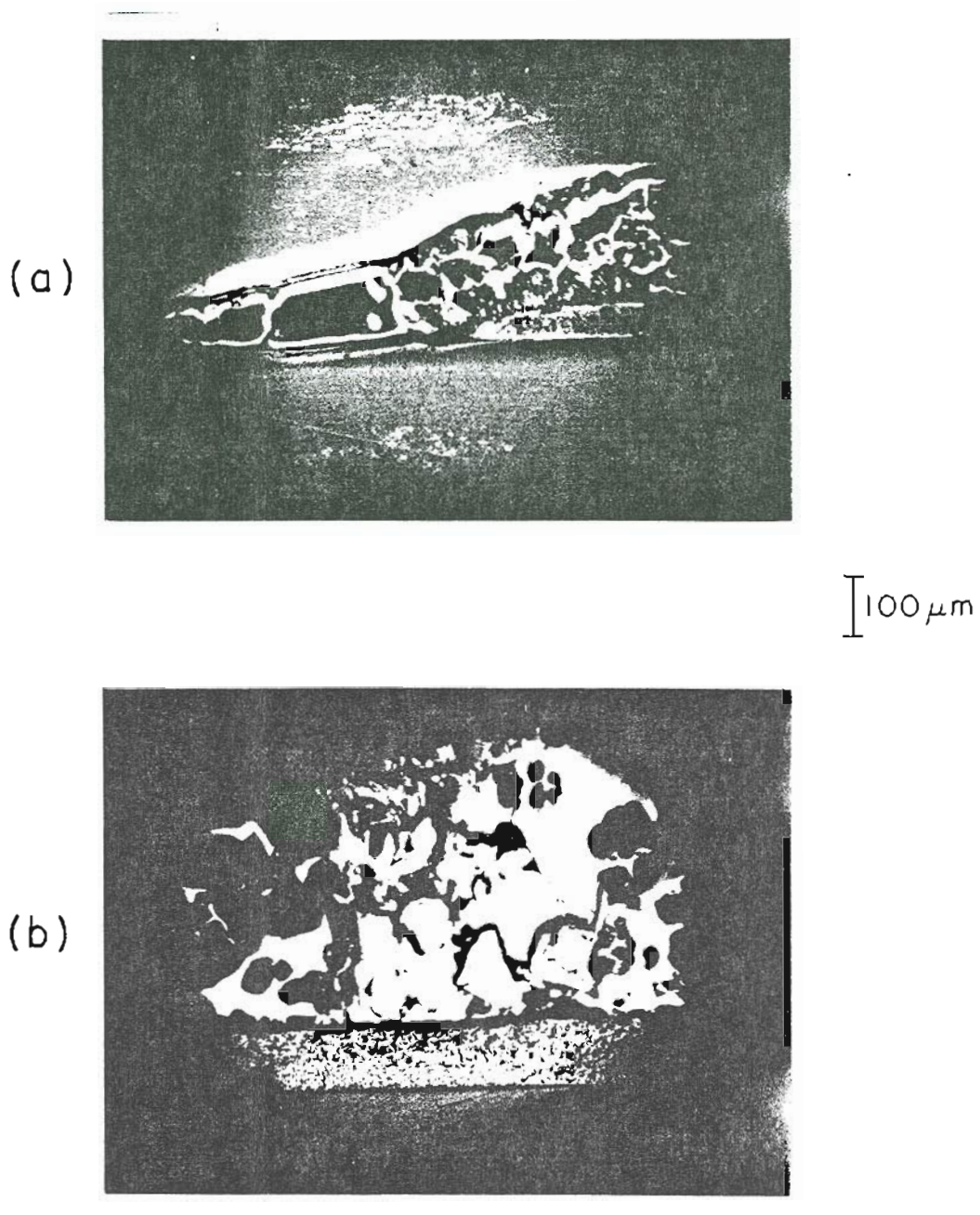

Figure 6-20. Light micrographs of the cross-section of the Ni/B (LANL) on C alloy that passed through the ribbon. (a) View showing the continuum of alloy through the ribbon; (b) View of the alloy/substrate interface beneath the central droplet of alloy.

are shown in Figure 6-21. The photo of Figure 6-21 is deceptive in that little of the graphite ribbon remains, a result due, not to alloy attack, but to uneven grinding during removal of the ribbon from the plastic mold used during sectioning. The second phase material (positions 3 and 5) appears to be B_4C; curiously, however, the carbide Auger chemical shift we have routinely observed in other spectra was absent here. Position 2 within the alloy material is Ni-rich, while a second position (position 6) is near stoichiometry. Positions 1 and 4 in the graphite substrate show significant concentrations of Ni. Previous studies of graphite cross sections also indicated that Ni (rather than B) is the alloy component that diffuses into the substrate, although to nowhere near the extent found here.

Hence, this specimen depicts the metallurgical situation of a liquid metal contact system containing boron and carbon after excessive reaction between the substrate and the alloy. When the carbon activity in the alloy is excessive, the reaction is characterized by significant carbide formation within the bulk of the material. In studies of previous specimens, evidence of carbide formation has been indicated, but only on the surface of the alloy droplets. The interior of most droplets are characteristically free of impurities. The results here are best viewed in terms of what happens to boron-containing alloys during excessive reaction with the substrate. During such severe attack, boron carbide is able to form within the alloy interior.

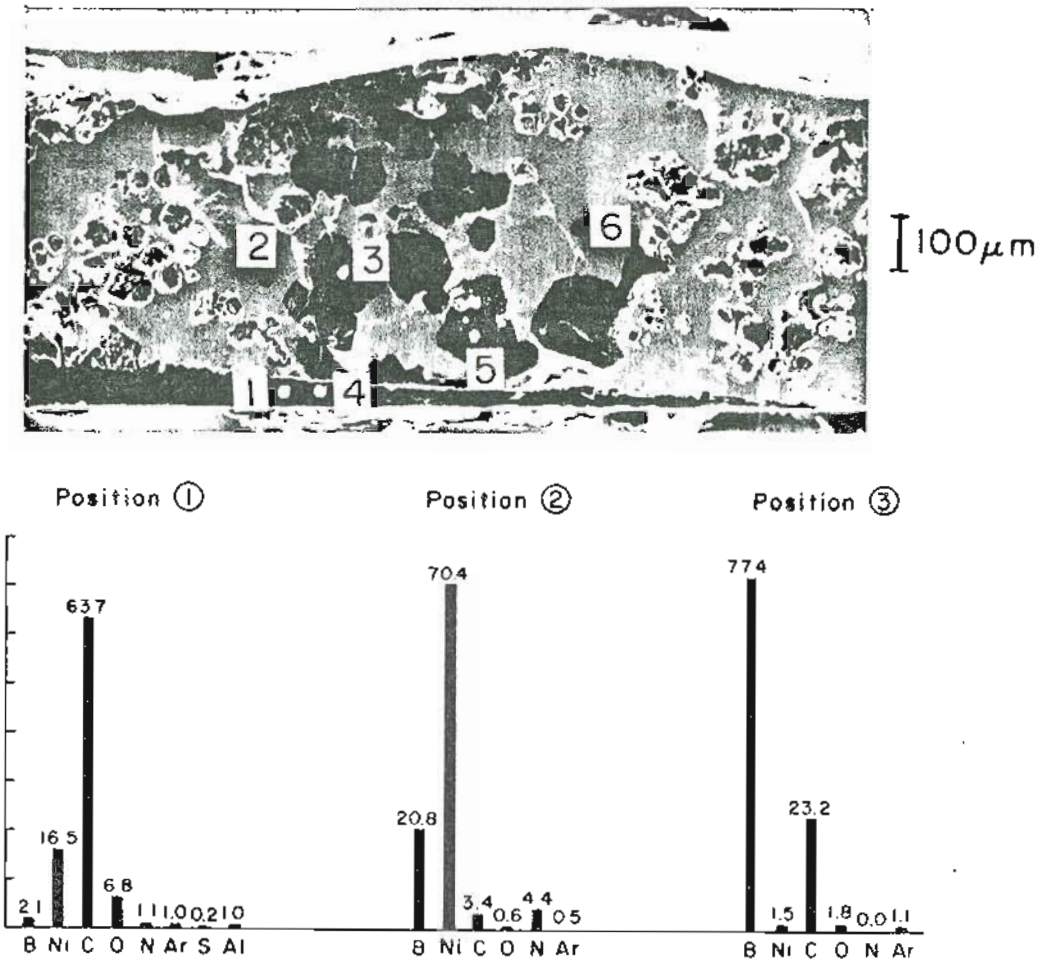

Figure 6-21. Auger surface elemental composition for 6 positions within the cross-section of the Ni/B (LANL: #273-7C; Ni=.53, B=.47) on C that has penetrated the graphite. The surface has been cleaned by Ar^+ sputtering.

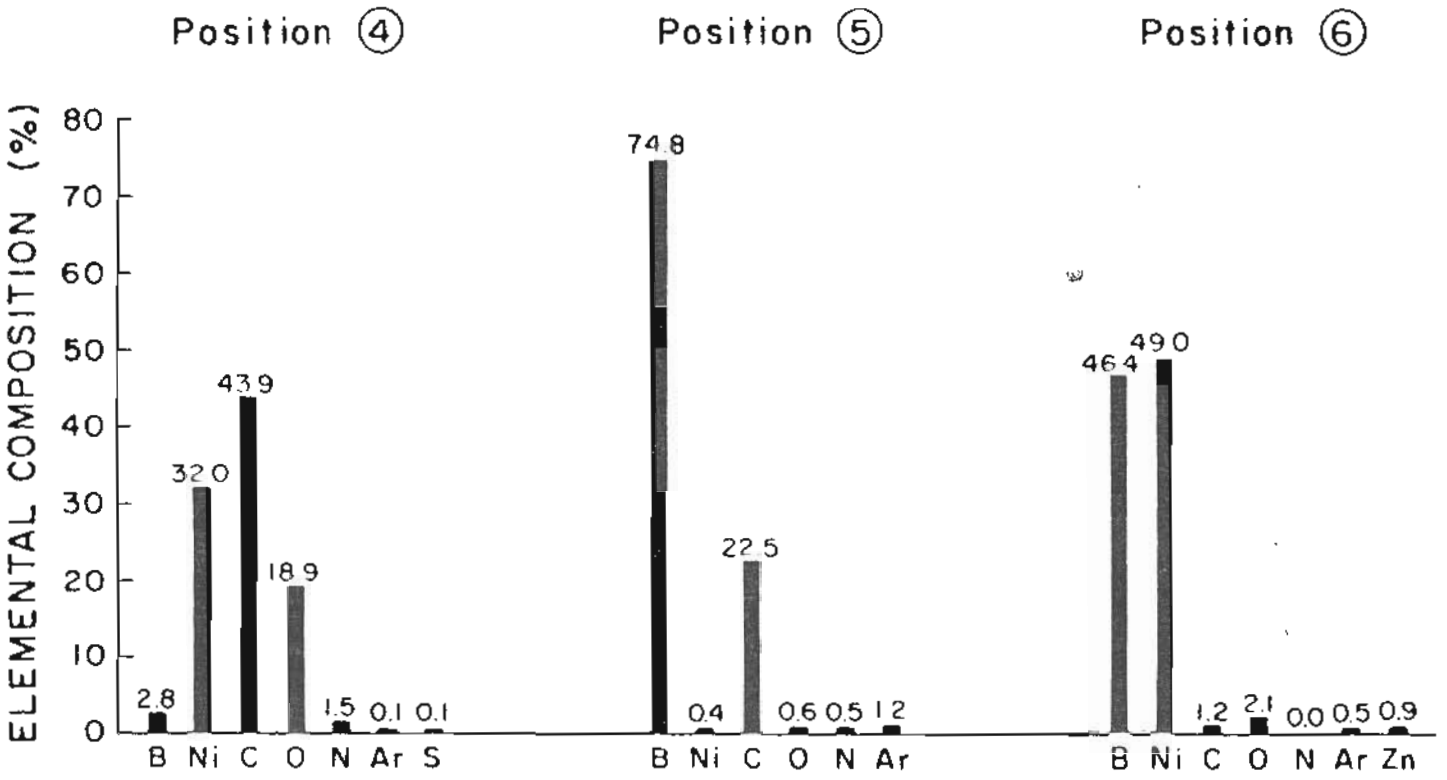

Figure 6-21 (continued). Positions 3-6 of the Ni/B on C cross-section.

3. The Influence of Carbon Ruboff

An extensive effort was mounted to isolate the source of the high surface concentrations of C and N in the molten alloys. One early hypothesis advanced by the OGC group to explain the large concentrations in the molten alloys centered upon the properties of the graphite supplied by the Union 76 Corporation. Although later work failed to support this theory, its effects were observed periodically throughout this work and are of sufficient importance to discuss here.

Carbon ruboff refers to the idea that the surface of the graphite consists of loosely bonded grains which may be mechanically separated from the surface in the process of alloy wetting. Technical information supplied by the manufacturer [2] indicates that the graphite utilized as substrates in our wetting experiments has been "specially processed (carbon impregnated) to virtually eliminate particle 'ruboff'. . .the process does not affect machined tolerances but does fill the pores and coat exposed surfaces with a film of carbon material." In terms of wetting behavior, a liquid alloy with strong affinity for the substrate would act to pick up carbon particles during liquification and form the heavy layer of C detected on the surface of poorly-wetted droplets. The issue reduces to a question of the relative importance of cohesive and adhesive forces in the contact system. If the adhesive forces between the molten alloy and the graphite are greater than the cohesive forces between

the particles of graphite, then ruboff may occur. The result is a molten droplet covered with carbon and a suppression of wetting.

Experiments to be described below have shown that the hypothesis of carbon ruboff is largely unnecessary. The most prominent experimental observation it is unable to explain is the existence of excellent wetting of impurity-free alloy. Recall from previous discussion that numerous cases exist where the carbon shell on poorly-wetted droplets may be fractured, resulting in the effusion of pure alloy material out onto the virgin carbon substrate with subsequent excellent wetting. The pertinent question is: Why does not this material also suffer carbon ruboff and result in poor wetting? The postulate of carbon ruboff cannot respond to this criticism, as it predicts that carbon particles should be removed from the substrate in every instance of contact between alloy and substrate. As will be shown later, the dilemma is resolved by the surface segregation model of alloy behavior, which views the source of the surface carbon to be segregated impurities inherent to the alloy.

An instance where carbon ruboff appeared to be real occurred during an experiment designed to investigate the possibility of wetting to a second graphite substrate which was inserted into the upper hemisphere of a poorly-wetted droplet of alloy. The goal was to determine if wetting would occur by penetration, and to investigate the response of the droplet to lateral forces. It was found that the surface tension forces governing the shape of the droplet were quite remarkable. The droplet would yield to lateral

forces exerted by the second graphite ribbon, and a strong thrust by a pointed end of the graphite was necessary to penetrate the surface tension shell. Upon so doing, the adhesive forces between the second graphite ribbon and the interior of the alloy were excellent, and the alloy could have been pulled away from the original substrate. After leaving the system in this configuration for a few minutes, however, a material with brightness temperature identical to that of the graphite was found along the line of penetration and persisted after the second ribbon was pulled out of the molten alloy. This observation confirms the existence of carbon dissolution and possible ruboff in the alloy systems at high temperature.

C. Studies of Wetting in Contact Systems Containing Pt/B Alloy

1. Studies of Prewetted Pt/B on Re

The focus of investigation regarding Pt/B alloys centered upon critical assessment of the extent of reaction between the alloy and metallic substrates such as rhenium. Rhenium is an excellent choice of substrate material in contact systems containing boron due to its demonstrated ability to resist attack by boron, which is extremely corrosive to most metals. Effort was focused on the behavior of Pt/B with Re due to the preliminary success of HRL in achieving a 30-hour source of B using these materials. Wetting studies of Pt/B to C (virgin) yielded results similar to those reported above for wetting of Ni/B to C (virgin). In both cases, a poorly-wetted droplet of alloy was formed which was characterized by large surface concentrations of C and N which appeared to prevent wetting.

Figure 6-22 shows scanning electron micrographs of a specimen of Pt/B alloy prewetted by the HRL group to a thin ribbon of Re. The front of the ribbon is well-wetted, while no evidence of wetting to the backside of the Re is observed as yet. The interior of the alloy shows evidence of widespread inhomogeneity and foreign particles which Auger studies later verified to contain the contaminants Ca, Mg, N, O, and C. Such particles were found in a number of cases during this work, and were often observed to float atop the molten alloy and follow the liquid turbulence created within the alloy during heating. We have invariably found liquid metal alloys of boron and arsenic to exhibit excellent wetting to metallic substrates.

Auger analysis of four points of the "as received" alloy surface are shown in Figure 6-23. Major impurities are C and O, with small concentrations of N, Mg, Ca, and Cs. The Cs is due to a previous, unrelated use of the vacuum chamber. It is difficult in Pt-containing alloys to positively establish the existence of BN due to the peak overlap of Pt and B near 180 eV. However, the B peak shape and energy are quite reminiscent of the boron nitride chemical shift discussed earlier.

During heating, alloy melting was found to occur at 1067 K (794 C), a temperature 4 degrees above the binary eutectic temperature for this system. That the melting point was so close to the system eutectic in spite of the large amount of surface contamination lends support to the notion that what was observed was bulk melting and not true surface melting. We had suspected this from the start of our investigations.

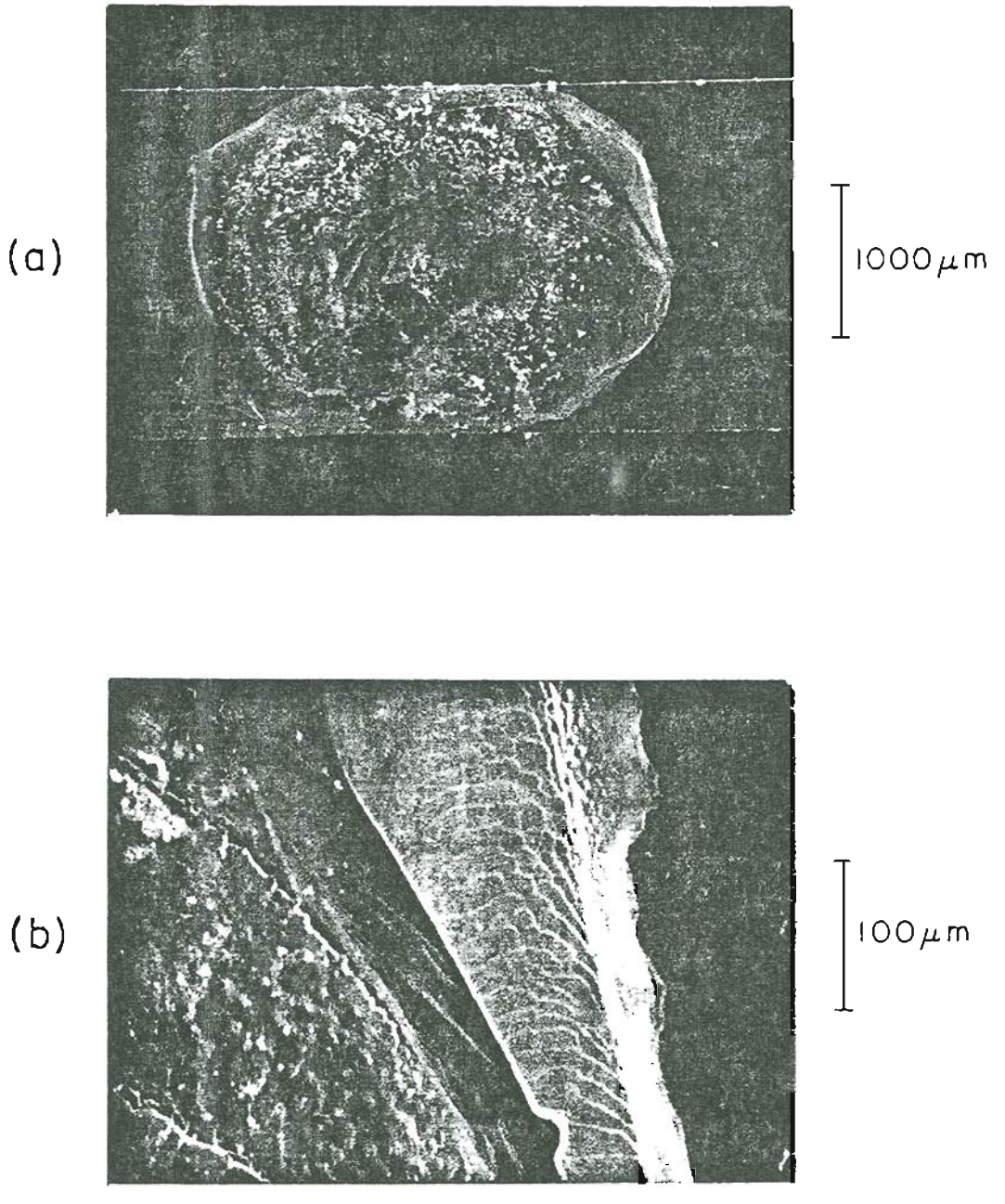

Figure 6-22. Images of the Pt/B on Re alloy in its "as received" condition at 300 K. (a) Overall view; (b) View at the right alloy/substrate boundary.

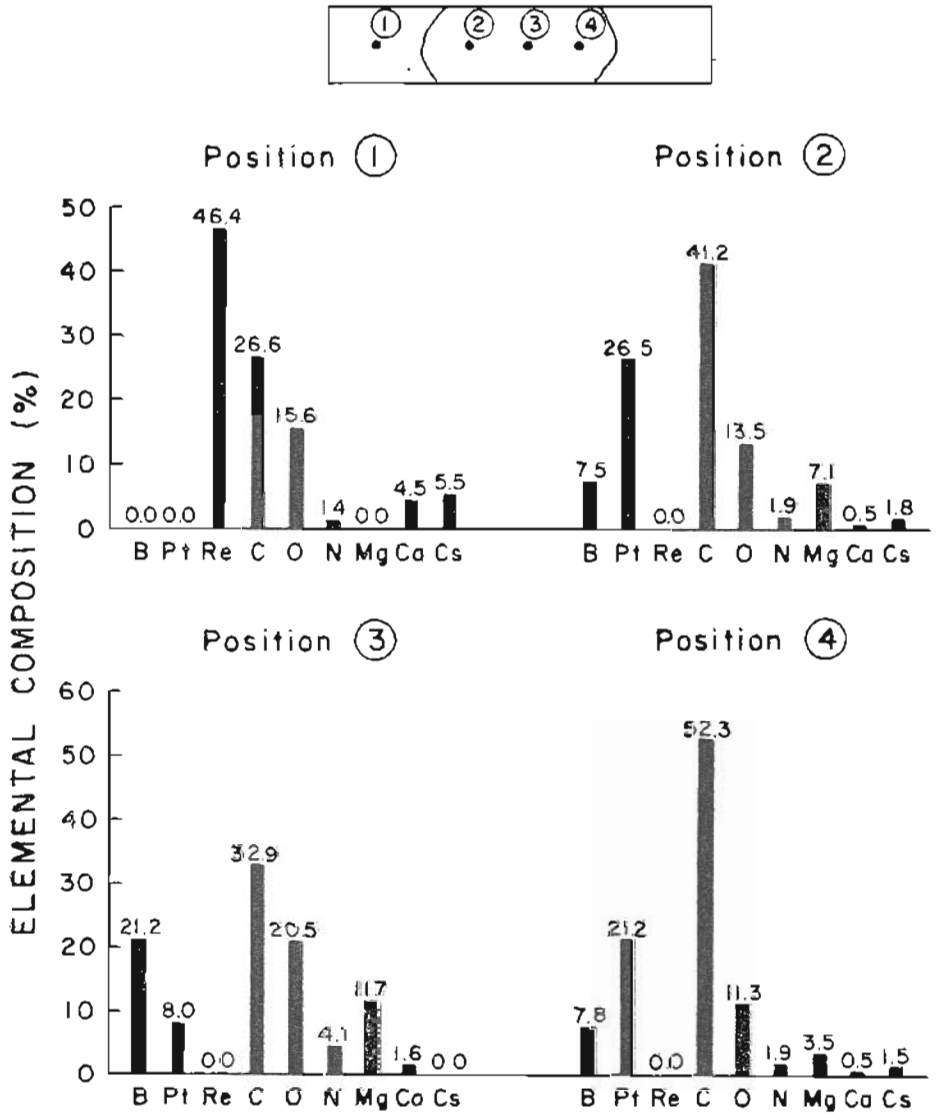

Figure 6-23. Auger surface elemental composition vs position for the Pt/B on Re alloy in its "as received" condition at 300 K.

Figure 6-24 displays the alloy surface composition vs position at a temperature 5 degrees below the melting point. The alloy surface impurities are nonvanishing at this temperature, although the C signal is reduced relative to the situation at 300 K. A first indication of the reaction speed for this contact system was found during an increase in temperature to 30 degrees above the melting point. After 10 minutes at this temperature, the alloy had resolidified. An Auger scan of the surface after resolidification revealed no unusual differences in surface composition from the situation at startup; in particular, no Re was found. A further increase in temperature to 60 degrees above the original melting point was necessary to remelt the alloy, but then the surface resolidified in about 15 minutes. Unusual changes in alloy brightness were observed during this period, indicative of large changes in substrate resistivity as the chemical reaction between alloy and substrate proceeded. During a further increase in temperature to remelt the alloy, the brightness of the right side of the alloy increased by nearly 150 degrees, which was followed by a rapid increase in the system pressure. The temperature at the time of this unusual behavior was about 100 degrees above the original melting point. Subsequent Auger analysis (Figure 6-25) showed that most of the surface contaminants found at lower temperatures had vanished, leaving mostly alloy components and nitrogen. Temperature cycling did not remove the bright region. The surface had resolidified again after about an hour, so it was necessary to increase the temperature to remelt the alloy. This time, a

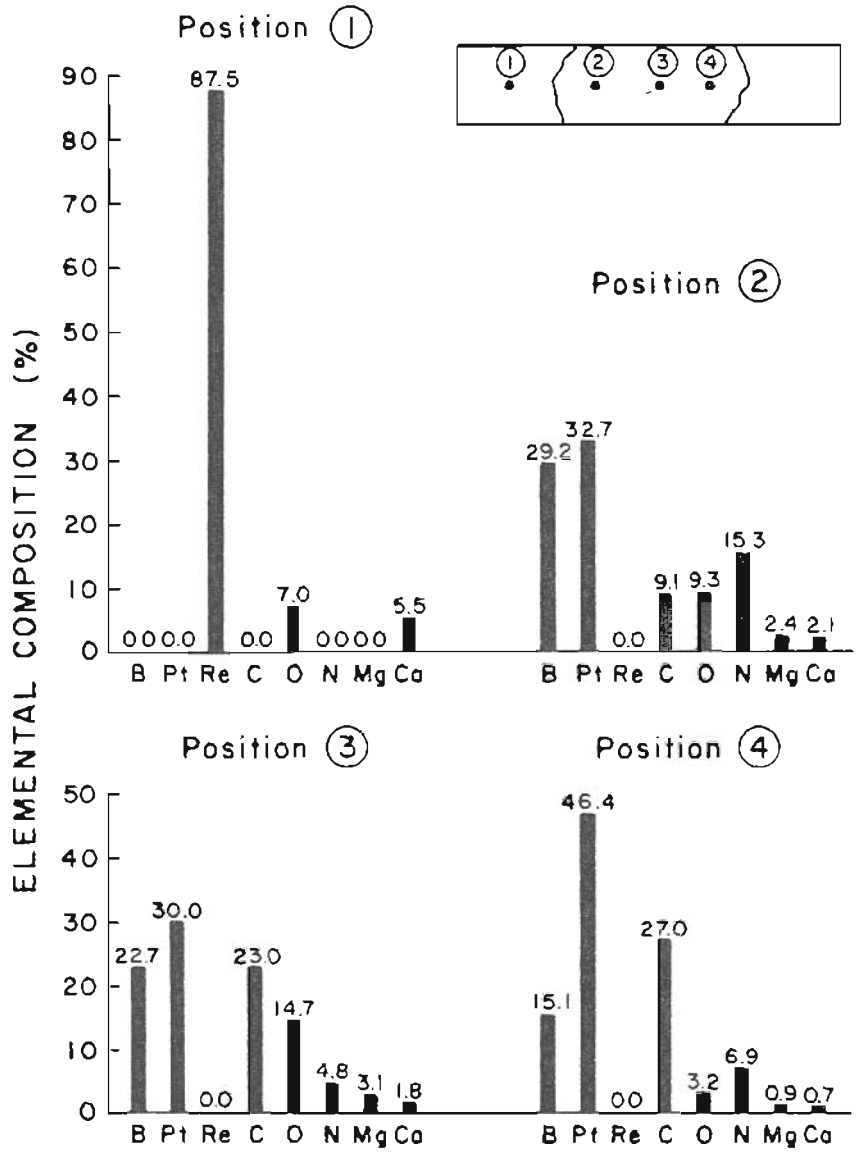

Figure 6-24. Auger surface elemental composition vs position for the Pt/B on Re alloy at T = 1060 K = T_R - 5°.

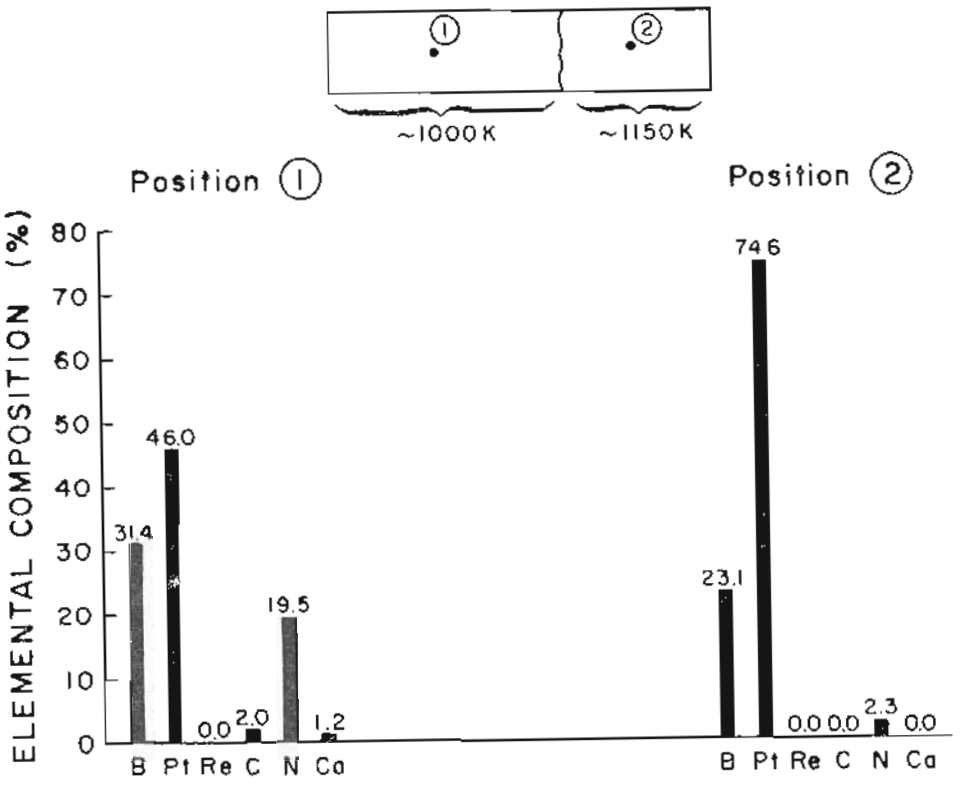

Figure 6-25. Auger surface elemental composition vs position for the Pt/B on Re alloy after the occurence of large resistivity changes in the ribbon.

temperature of 1400 K was necessary. A few minutes at this temperature resulted in catastrophic breakdown of the alloy as the ribbon began to volatilize away. Several SEM photographs of the resulting contact system are shown in Figure 6-26. The behavior displayed indicates that chemical reactions between alloy and substrate are sufficiently intensive to destroy the source at high temperatures.

Figure 6-27 shows the surface composition of the alloy at room temperature after catastrophic attack. The low concentrations of surface Re support the thesis that the alloy is dissolving into the substrate. In order to qualitatively measure the rate of dissolution, two positions on the surface were monitored by Auger spectroscopy for a few hours each to determine the degree of interdiffusion of alloy and substrate. The results are reported in Figures 6-28 and 6-29. For both positions investigated, the B concentration monotonically decreases which results in a similar trend upward for the Pt concentration.

This view of the reaction mechanism for Pt/B on Re is reinforced by scanning Auger investigations of a fractured cross-section of the contact system. The ribbon above was fractured and mounted edgewise facing the excitation beam. The perspective is revealed in Figure 6-30, which shows the cross-section and the positions of three characteristic areas which were studied. A central region exists that is primarily Re and Pt, with no trace of B. Surrounding this on both sides (it is important to note that the alloy had wet both sides of the Re ribbon) is a second region which contains relatively

(a)

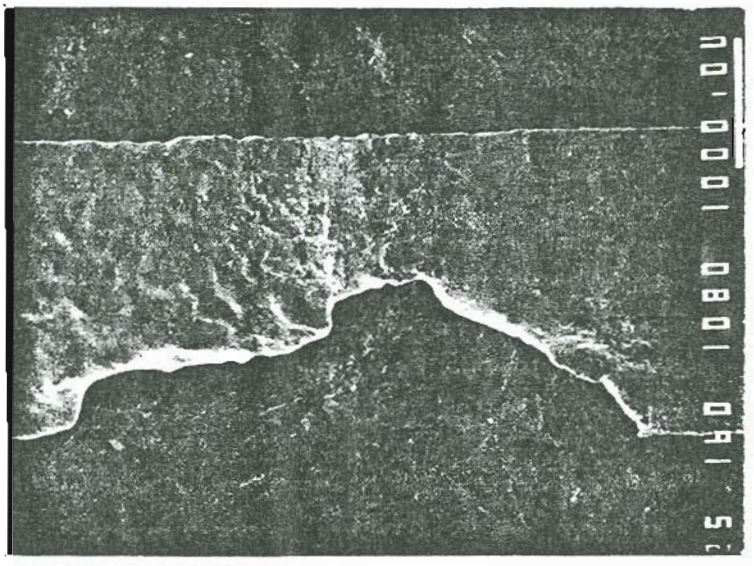

(b)

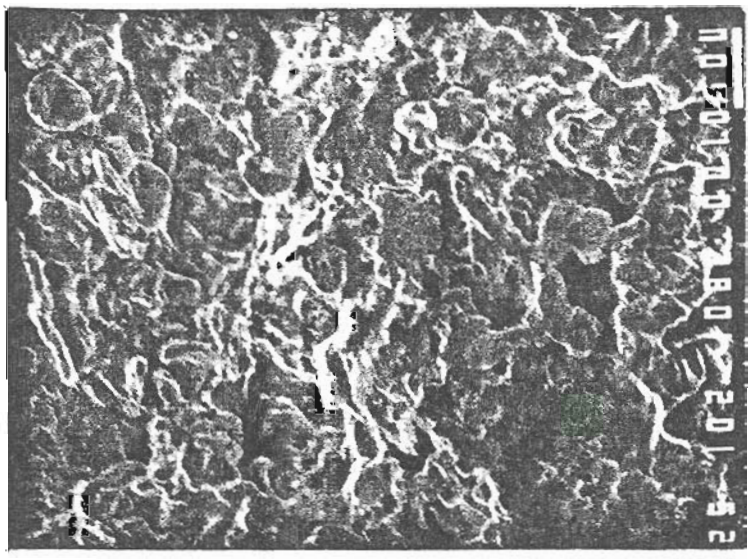

Figure 6-26. Post-mortem views of the Pt/B on Re alloy after catastrophic failure. (a) Overall view of the failure zone; (b) High magnification view of the microstructure within the failure zone. Notice that the wetting is excellent.

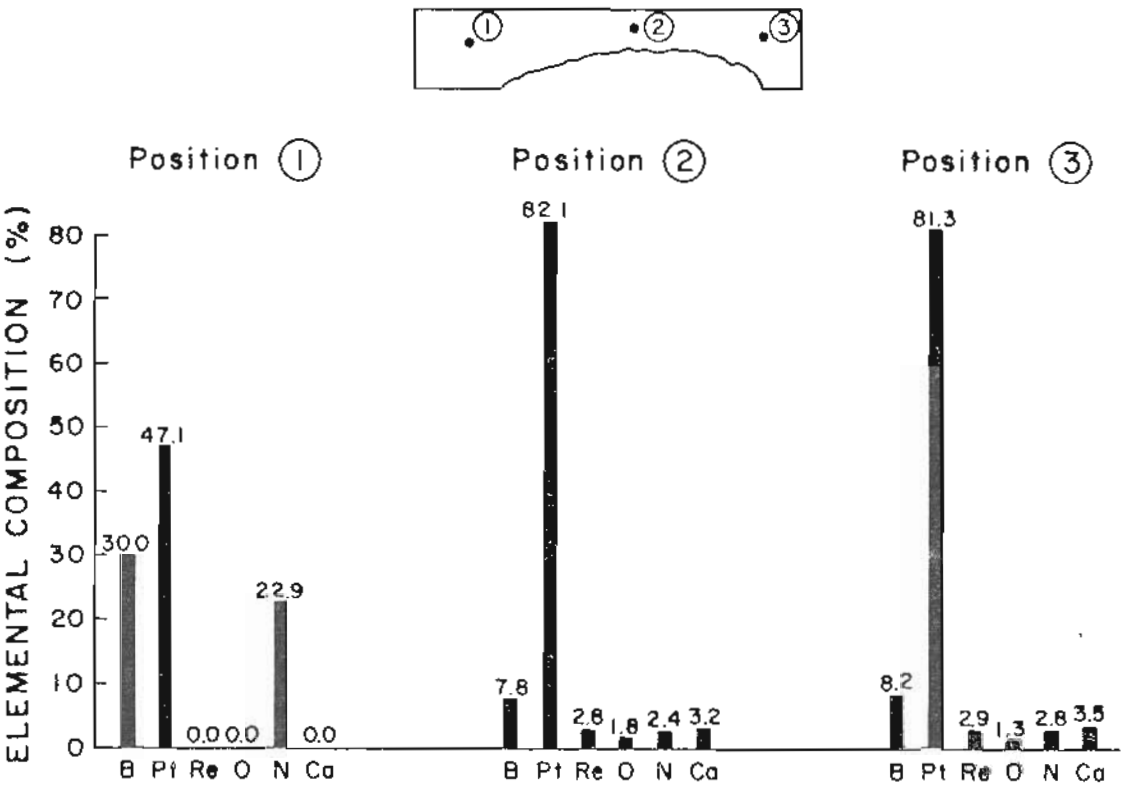

Figure 6-27. Auger surface elemental composition vs position for the Pt/B on Re alloy at 300 K following catastrophic failure.

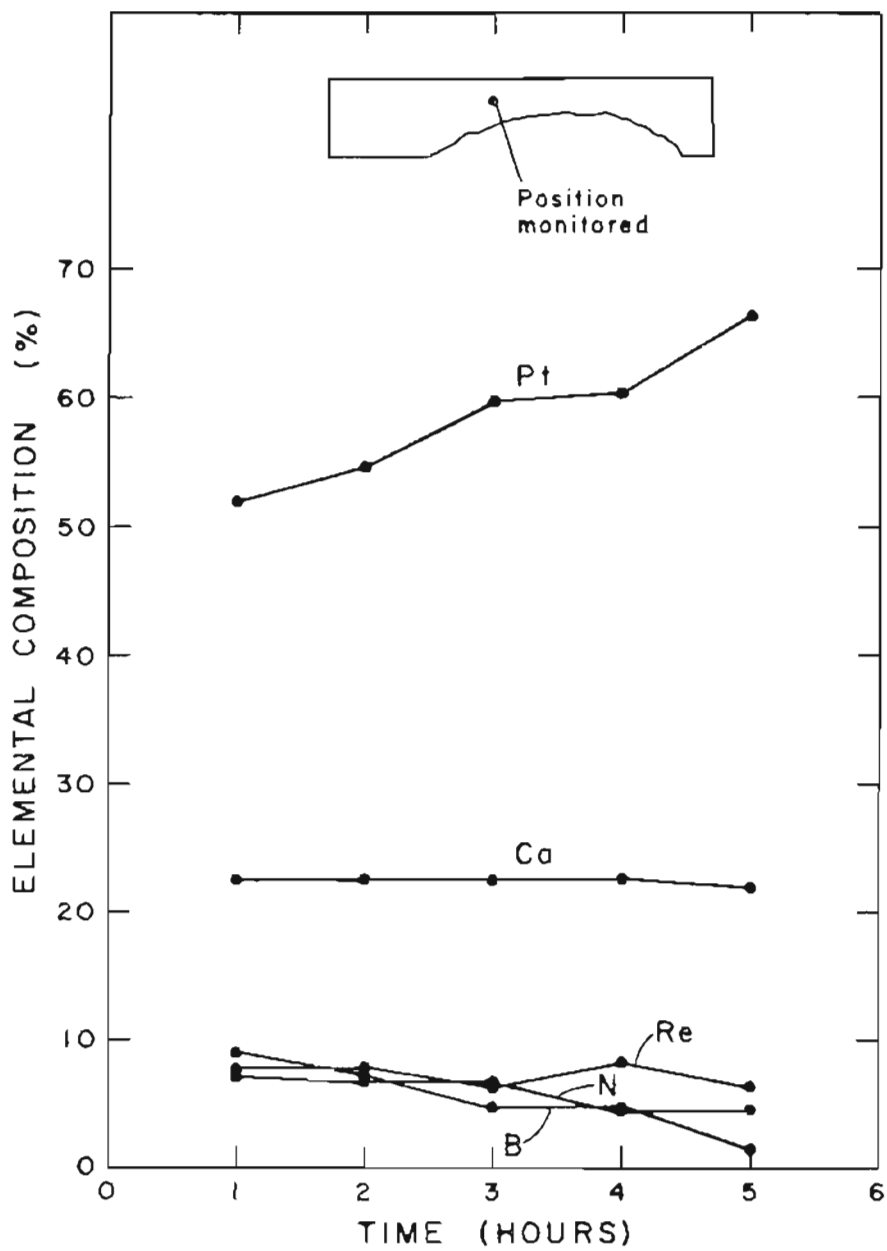

Figure 6-28. Auger surface elemental composition vs time for a single position on the failed alloy. The temperature is 1000 K. The alloy is solid at this temperature.

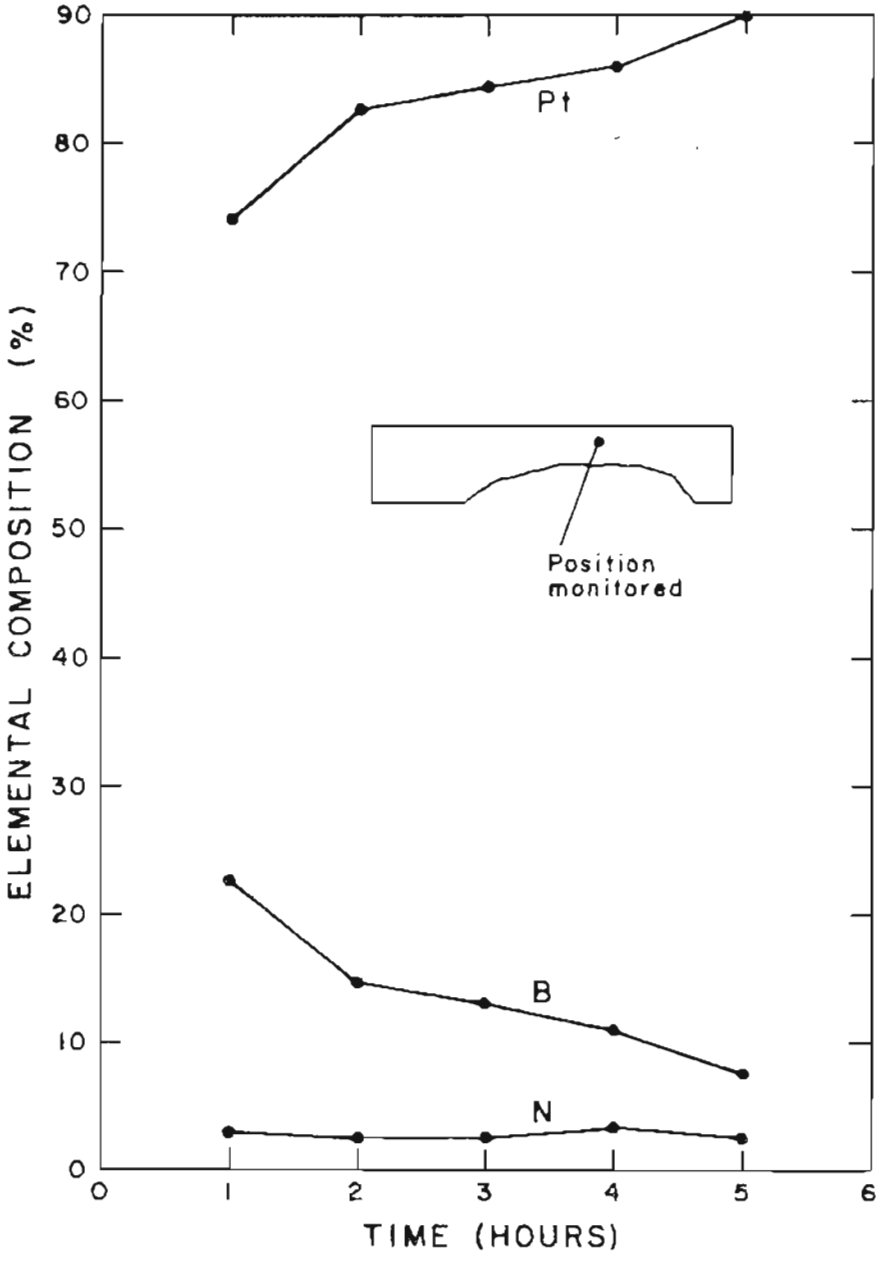

Figure 6-29. Auger surface elemental composition vs time for a single position on the failed alloy. The temperature is 1080 K. The alloy is solid at this temperature.

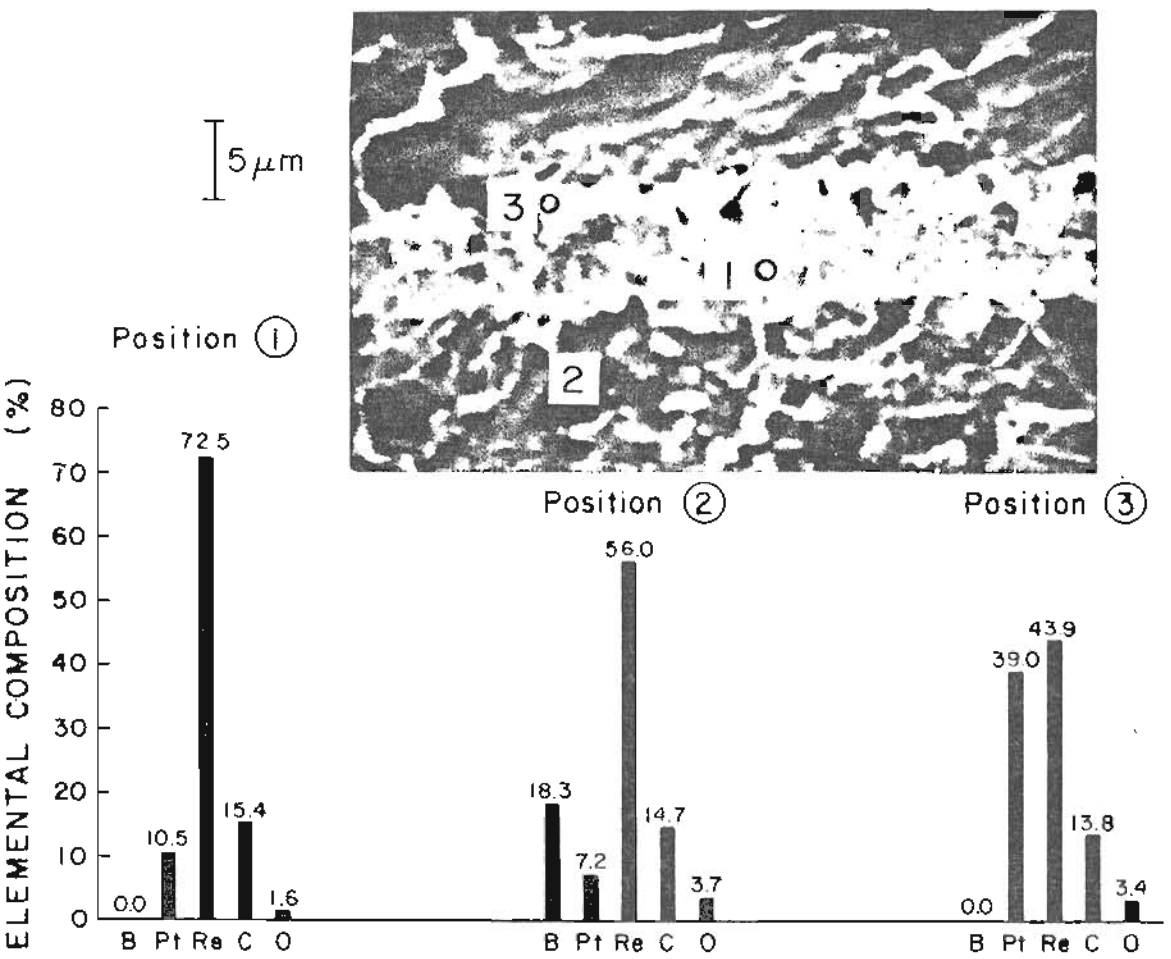

Figure 6-30. Auger surface elemental composition of three positions within the cross-section of the failed Pt/B on Re alloy.

smaller amounts of Pt and significant concentrations of B. The C and O signals appear because because the ribbon was not sputtered after reintroduction into the vacuum environment.

Scanning Auger maps of the cross-section, displayed in Figure 6-31, show that Re appears to be concentrated near the center of the original ribbon rather than distributed uniformly throughout the cross-section, as would be the case for an unreacted strip of metal. The Pt signal is strongest at the edges of the central Re concentration, indicating that the Pt is preferentially attacking the Re. These regions are relatively B-free. The boron concentration within the Re-rich center is probably spurious, as the point analyses shown earlier indicate that no B exists in this region. The discrepancy occurs because of the overlap of B and Re peaks in the energy window used to obtain the map. The map of B is therefore more accurately a map of B + Re. We have routinely subtracted out the contribution of the Re overlap in the elemental compositions reported in this study, but this cannot be done for Auger maps.

The wetting characteristics of this particular contact system were irregular but excellent, probably due to a temperature gradient across the sample due to unequal electrical and thermal contacts in the support mechanism. In particular, the right side of the ribbon wetted first, and appeared to be covered with a thin layer of alloy material that was Pt-rich, probably corresponding to the loss of B to Re reported above. The wetting behavior improved with rising temperature, and eventually the alloy spread from front to back of the Re ribbon with a near-zero contact angle. At temperatures near

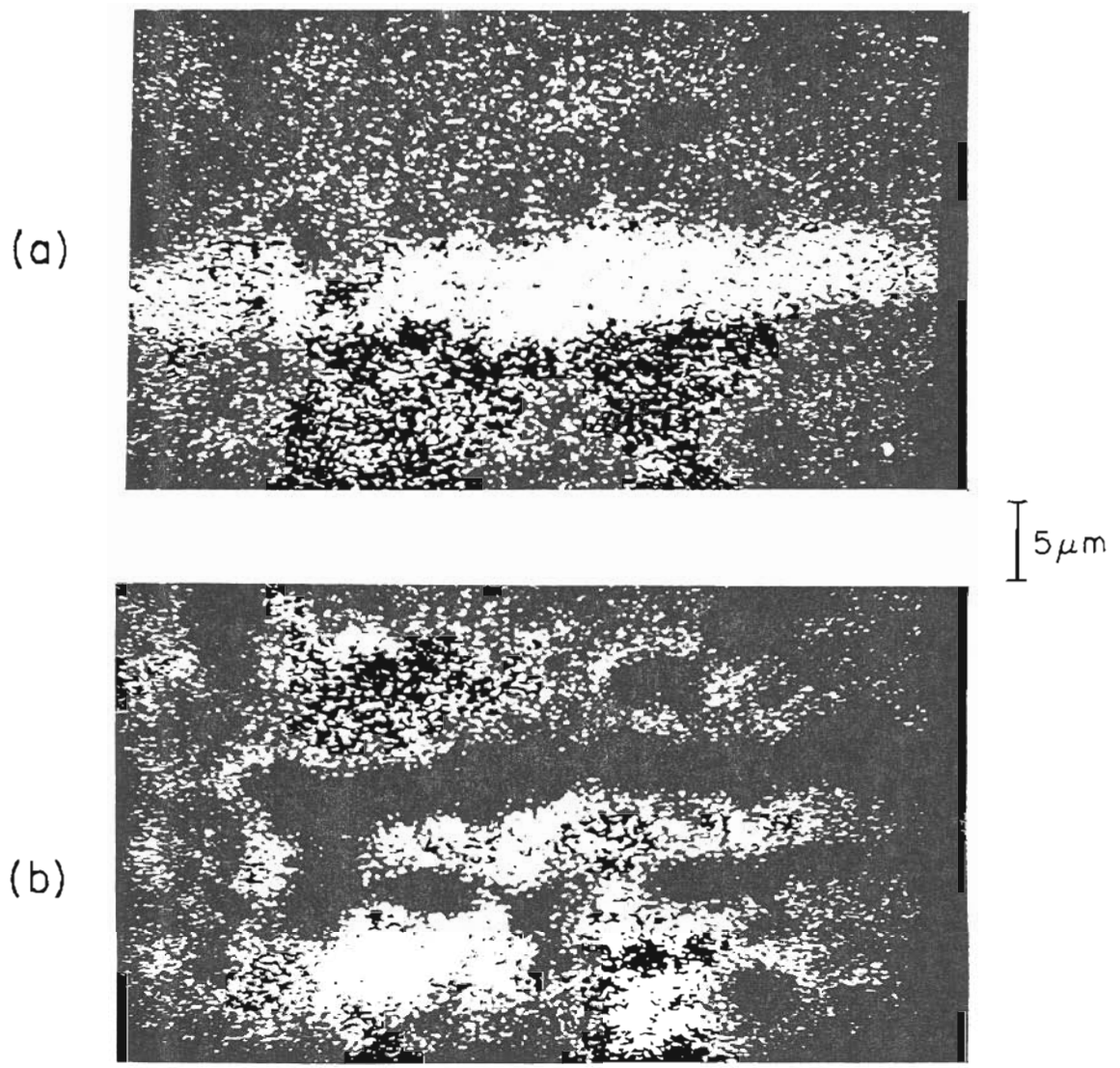

Figure 6-31. Scanning Auger elemental maps of the Pt/B on Re cross-section. For orientation, see the photograph of Figure 6-30. (a) Re map; (b) B (+ Re) map.

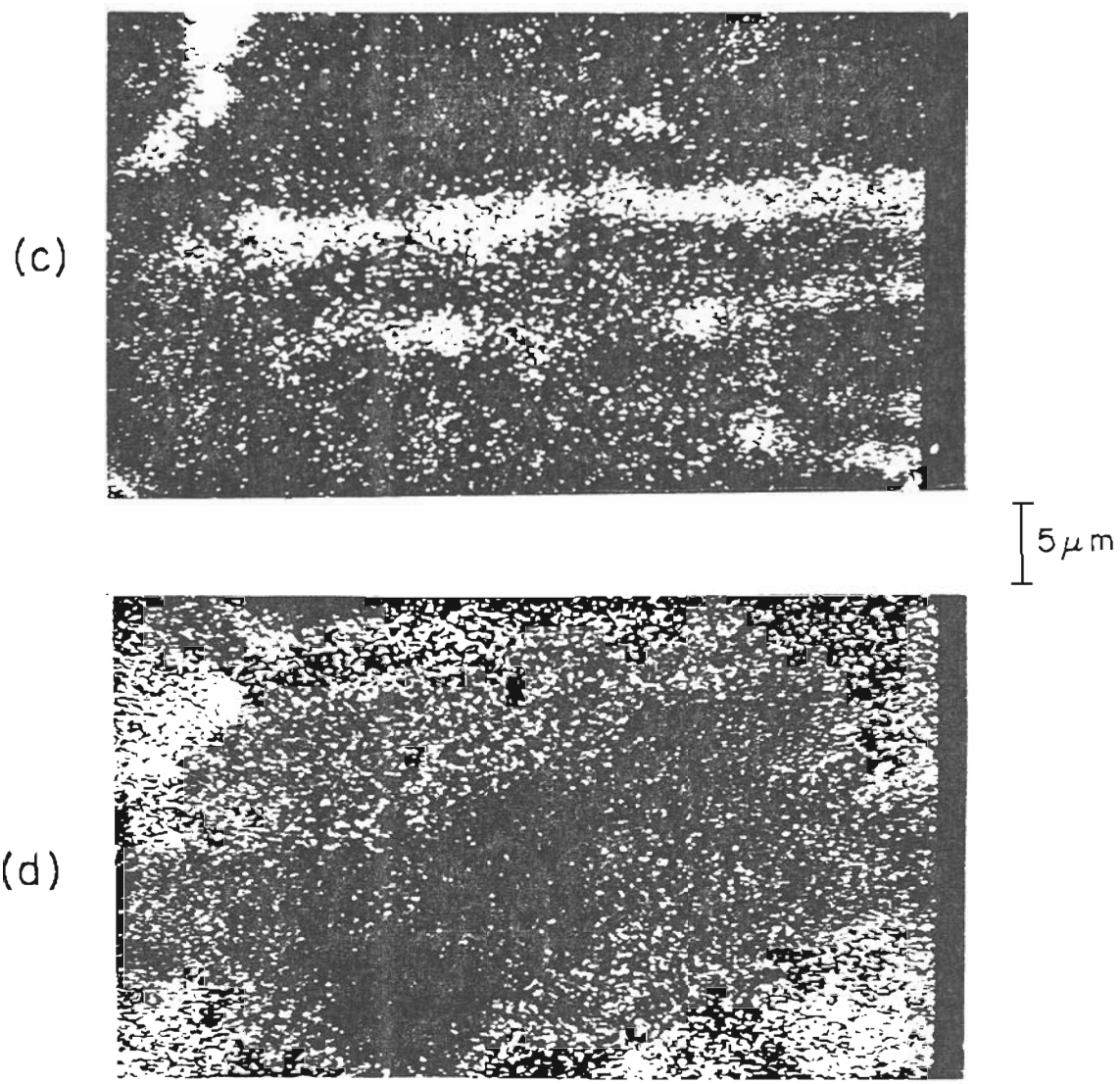

Figure 6-31 (continued). (c) Pt map; (d) O map.

the melting point of the Pt/B system and other low melting liquids, the surface retains significant amounts of undesorbed contaminants due to the low temperatures involved. As shown above, significant cleanup of the Pt/B alloy, for example, did not occur until temperatures near 100 degrees above the binary melting temperature. It would be interesting to investigate the behavior of these contaminants in a working ion source, addressing such questions as whether the contaminants are field evaporated in the first instant of operation, and how their presence affects the initial turn-on characteristics of the source.

2. Wetting Studies of Pt/B (LANL) to Re

The success of the HRL group in producing a 30-hour source of Pt/B on Re prompted further thermochemical studies of this contact system. In particular, questions concerning the potential role of Re impurities on the rate of chemical attack and the influence of induced strains in the material were considered sufficiently important to warrant additional study.

Auger surface analysis of the Re used by HRL in their emitters (Alfa, Lot #040583) showed that the Re was highly impure, even at high temperatures. As shown in Figure 6-32, significant surface concentrations of S, Mg, and Si persisted at temperatures as high as 1400 K. At the highest temperature tested, well above the melting point of Pt/B, the surface was only 63% pure.

The wetting of Pt/B (LANL: #273-5A; Pt = .72, B = .28) to a thin

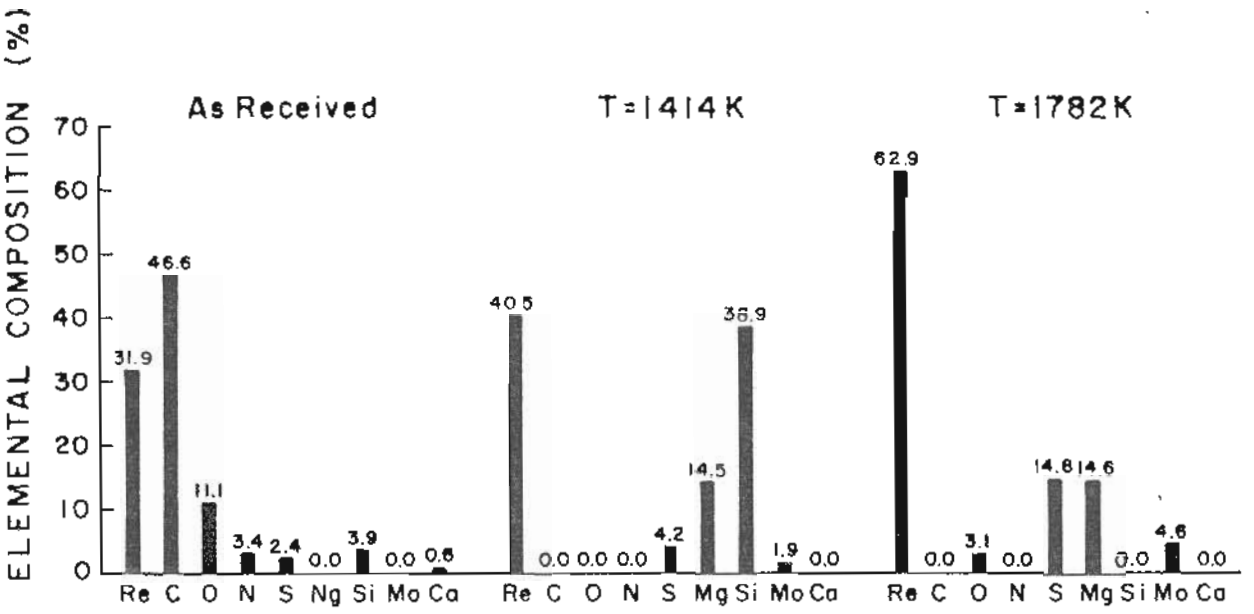

Figure 6-32. Auger surface elemental composition vs temperature for the Re substrate (HRL: Alfa, Lot # 040583). The Re is very impure.

ribbon of this Re was excellent, with the alloy spreading onto the backside of the ribbon with a near-zero contact angle. This study was different from the analysis described above in that the wetting was performed at our laboratory using well-characterized materials. The first system was pre-wetted at HRL. Tests to reveal the long-term effects of heating at the melting point of Pt/B are shown in Figure 6-33. In this figure, the alloy surface composition and melting point vs time are plotted. The sample was observed closely in order to record the changing melting point of the system and therefore the positions monitored by the Auger beam are different from spectrum to spectrum. Nevertheless, a number of tendencies which correspond favorably with the first experiment are noteworthy. First, the alloy melting point increased by about 100 degrees in 7 hours. Second, the Pt signal increased with time, while the B signal decreased. Third, Ca and O appeared to vanish simultaneously with rising melting point, suggesting that the Ca in the alloy existed as calcium oxide. Fourth, C and N persisted in the alloy, even after all O had vanished. We will find later that these are surface segregated species which reside as low-level impurities in the alloy.

The contact system suffered catastrophic failure between 11 and 20 hours of operation. Auger analysis of the failed surface is shown in Figure 6-34, showing significant C and N concentrations in addition to a small amount of Ca. The BN chemical shift indicative of BN formation in the alloy surface is found at all sampled locations, a likely result of the excessive temperatures caused by the changing resistivity of the Re ribbon during alloy attack. No Re

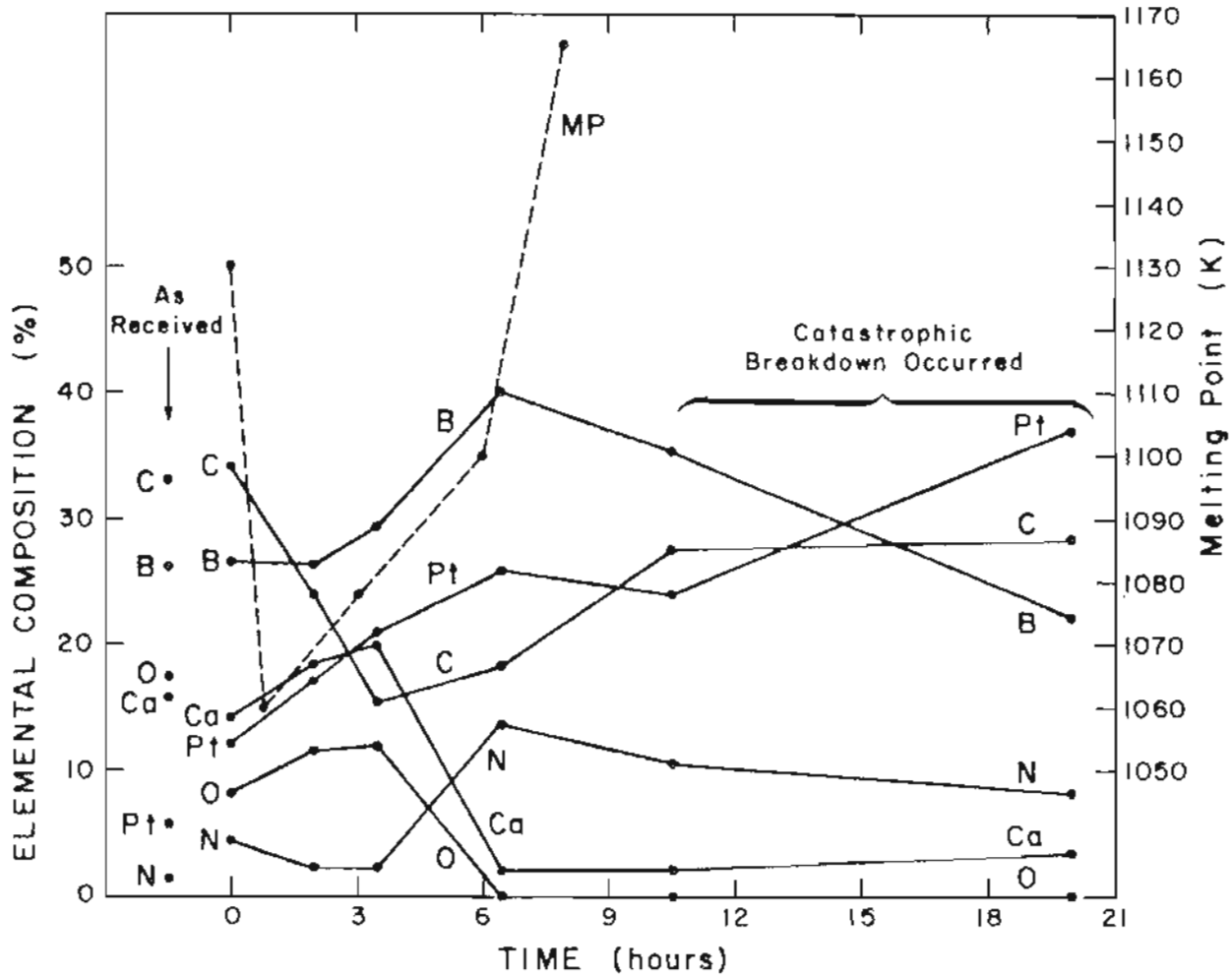

Figure 6-33. Auger surface elemental composition and melting point vs time for Pt/B (LANL: #273-5A; Pt=.72, B=.28) on Re (HRL: Alfa, Lot # 040583). The spectra were taken at T = T_m, which was found to increase with time.

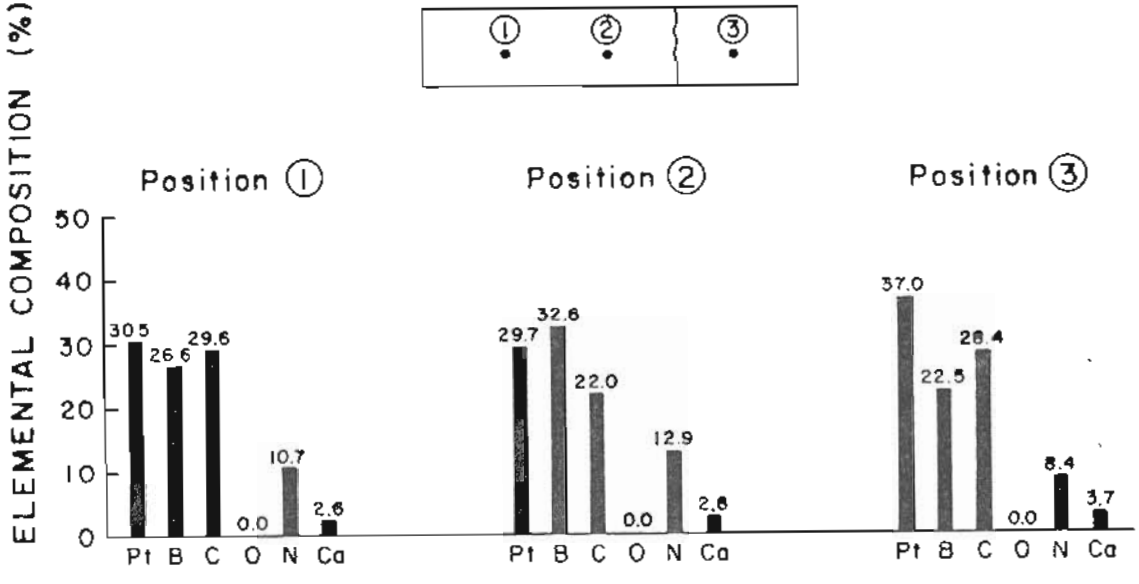

Figure 6-34. Auger surface elemental composition vs position for Pt/B (LANL: #273-5A; Pt=.72, B=.28) on Re (HRL: Alfa, Lot # 040583) after catastrophic failure. The temperature is 300 K. BN chemical shifts occur at each position.

is found at the surface. A micrograph of the system after failure is provided in Figure 6-35. An excessive amount of reaction has occurred. The Re ribbon was strained before the addition of alloy to see if attack occurred along the line of stress. No correlation could be attached to this mechanism of failure, in agreement with extensive tests by A. Bell [3] with stressed Re.

The results of both studies of Pt/B indicate that only limited success may be expected from this choice of alloy and substrate. As time progresses, both Pt and B are found to attack the Re, but since the rate of B dissolution is faster than Pt dissolution, the surface shows an enriched concentration of Pt. Concurrently, the melting point of the alloy continually increases, forcing an increase in heater current to retain the alloy in a molten state. This acts to accelerate the rate of attack, and increases the melting point further. Once the cycle of temperature increases is entered, there is no escape, and emitter lifetimes greater than 30 hours are the exception rather than the rule.

3. Evidence from Mass Spectrometer Studies of Pt/B on Re

The results of a mass spectrometric study of a liquid metal ion source of $Pt_{72}B_{28}$ eutectic on Re is consistent with the mechanism of alloy behavior discussed in the previous section. The details of this study will be reported in future publications of the OGC group. Here, we concentrate on those parts of the investigation dealing with the alloy thermochemistry.

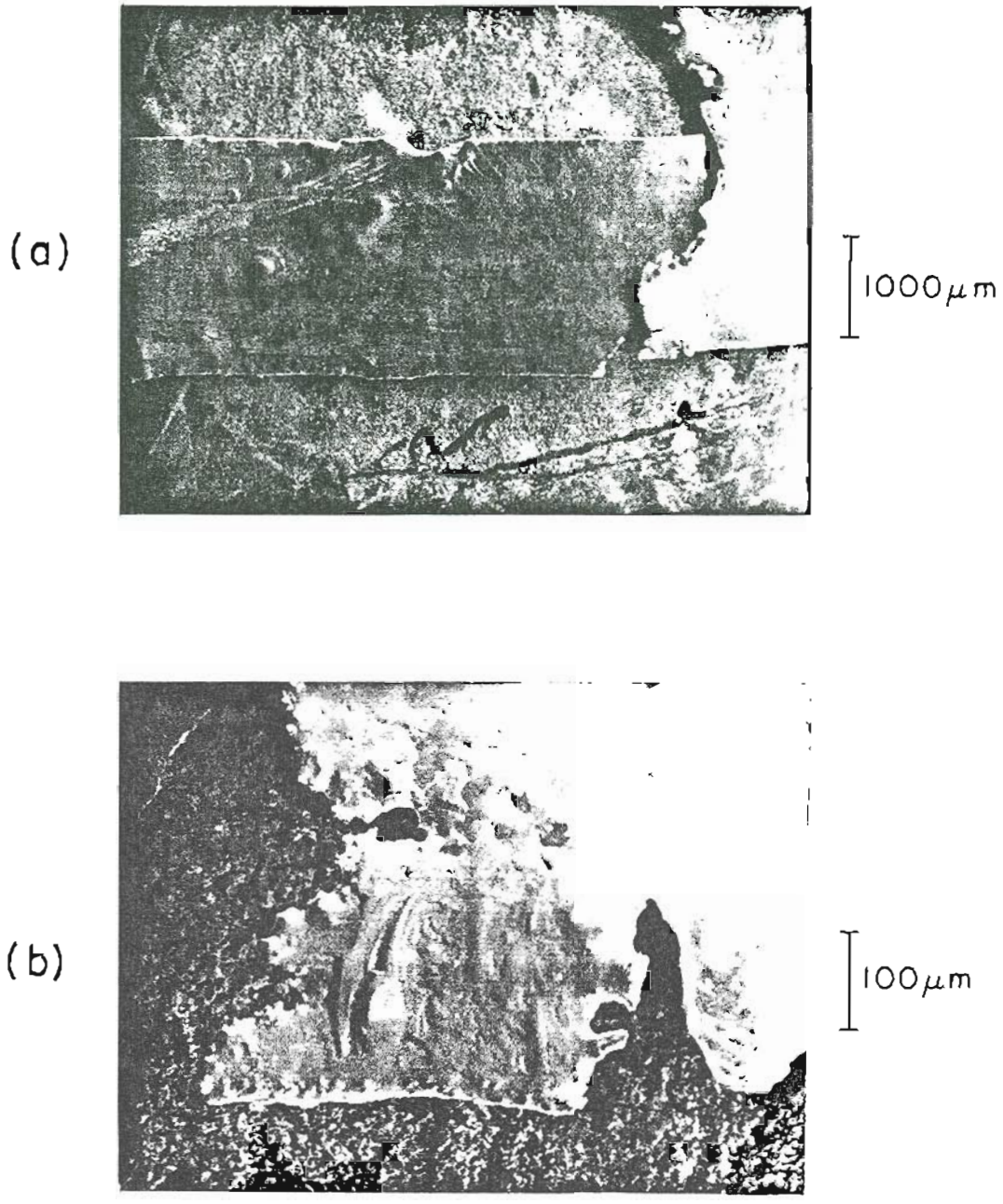

Figure 6-35. Views of the failed Pt/B (LANL: #273-5A; Pt=.72, B=.28) on Re (HRL: Alfa, Lot #040583).

The emitter assembly with prewetted alloy was supplied by the HRL group, and was studied by the Hitachi RMU-7 magnetic sector mass spectrometer at OGC, which has an entrance slit of 2 mr angle measured at the emitter. Relative amounts of the various mass species as a function of total current were determined by measuring the area under the respective mass peaks. No correction was made for the mass dependence of the spectrometer sensitivity.

Figure 6-36 gives the relative abundance of the various species observed in the Pt/B on Re LMI source as a function of current after several hours of operation. By summing the contribution of the various Pt and B species, a plot of the relative abundance of total B and Pt vs current is given in Figure 6-37. Surprisingly, the percent of B in the range of normal operating source current is only 10% whereas the original alloy contained 28% atomic weight of B. This result was confirmed at different source operating times and for two different sources.

Auger studies described above showed a decrease in B surface composition with time when a Pt/B liquid film on Re was heated at the melting point. This has been determined to be due to rapid diffusion and/or dissolution of B into the Re substrate. We speculate that during source activation when the Pt/B liquid film flows along the emitter that the Pt/B ratio increases due to B take-up by the substrate. Significant canges in the Pt/B ratio will force a higher temperature to maintain operation in the liquidus range of the phase diagram. This corresponds favorably with the experience reported from earlier Pt/B on Re ribbon studies. Interestingly, the measured

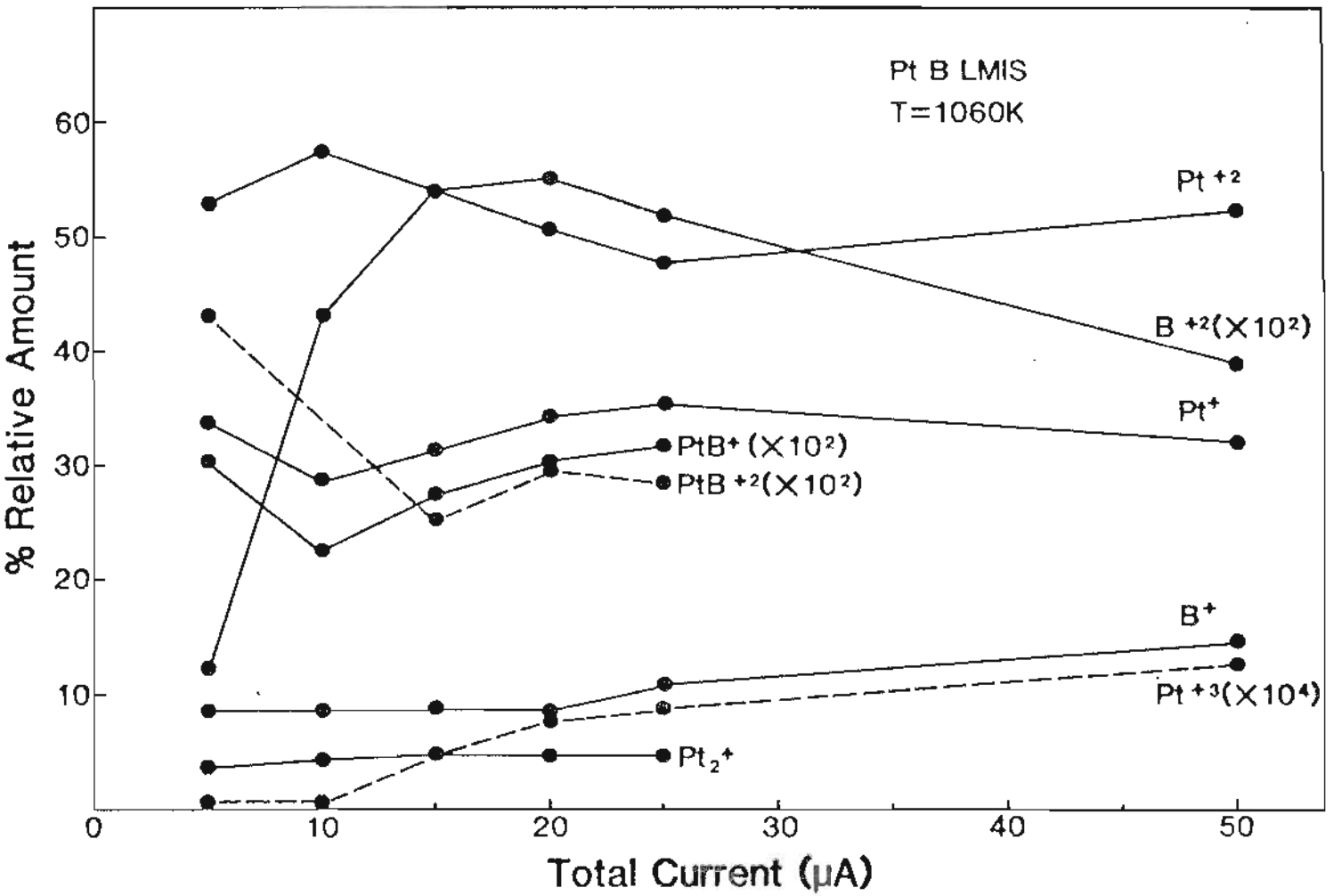

Figure 6-36. Relative abundance of various species in the ion beam vs total emission current for a $Pt_{72}B_{28}$ LMI source.

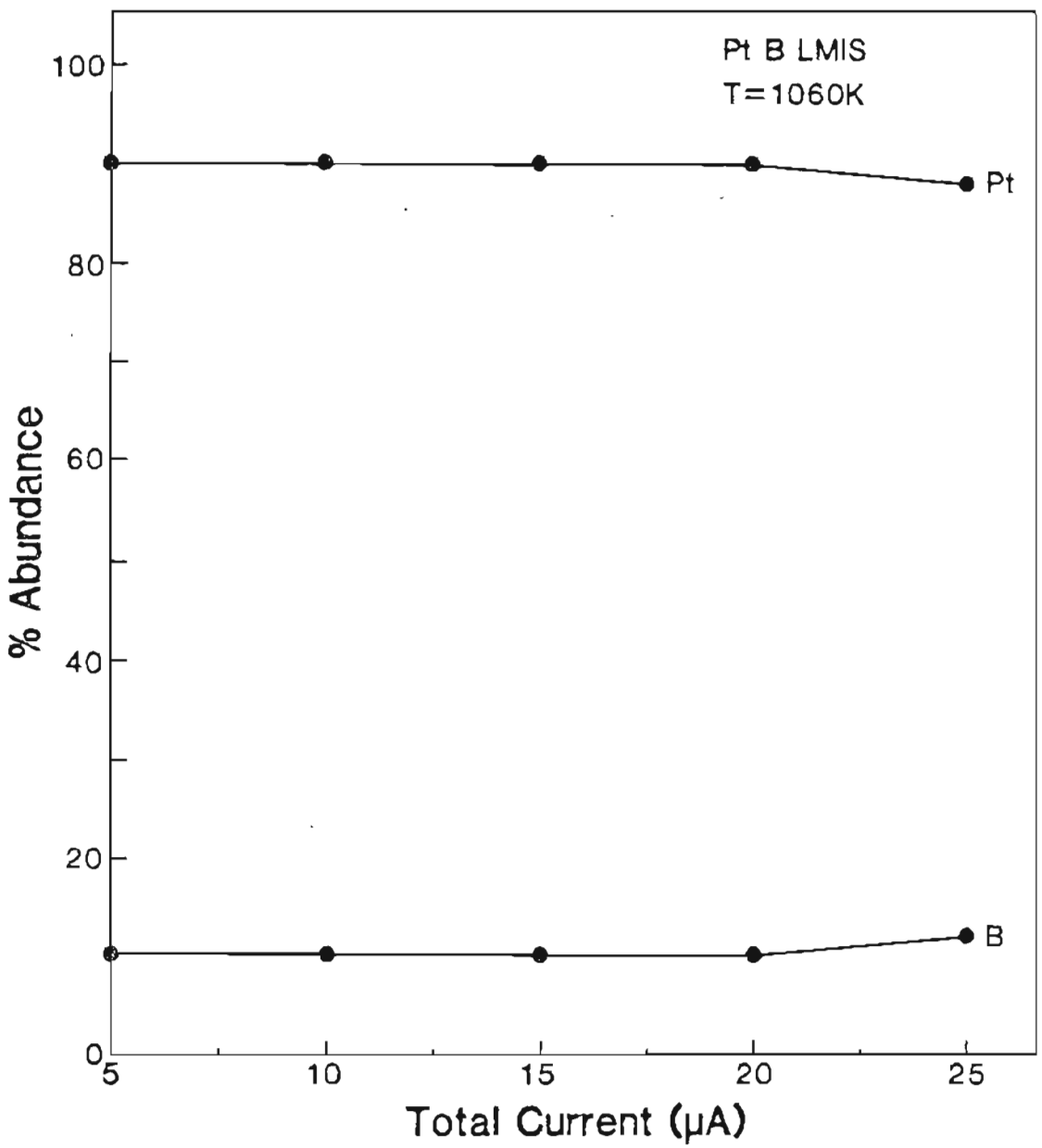

Figure 6-37. Relative abundance of total Pt and B vs total emission current for a $Pt_{72}B_{28}$ LMI source. The source was operated for several hours before measurement.

initial turn-on temperature of the LMIS was within experimental error of the eutectic melting point for $Pt_{72}B_{28}$.

4. The Formation of Rhenium Oxides on Emitter Structures

Emitter structures of Pt/B on Re manufactured by HRL were frequently found to possess precipitated second phase material, shown in Figure 6-38. These precipitates were usually found after a few hours of source operation, and occurred predominantly on the wetted Re support which held the alloy charge. In view of the importance of understanding the thermochemistry of this contact system, an attempt was made to identify these precipitates.

Figure 6-39 reports the results of a high resolution Auger analysis of several positions on the crystalline material and underlying wetted substrate. The perspective is shown in photo (b) of Figure 6-38. It appears that the crystalline material is a precipitated phase of rhenium oxide. The most stable rhenium oxide is ReO_2, which decomposes at ~ 1000 C. The underlying subsurface, by contrast, is composed of Pt-rich material with no indication of B.

The existence of precipitated second phase material on the emitter structure of Pt/B on Re uncovers another potential source of failure for this contact system, and reinforces the extent of chemical interaction between alloy and substrate discussed above. We saw earlier that the Pt/B on Re failed due to excessive reaction between B and Re, which subsequently enriched the surface with Pt. Apparently, the reaction has proceeded to such an extent here that no

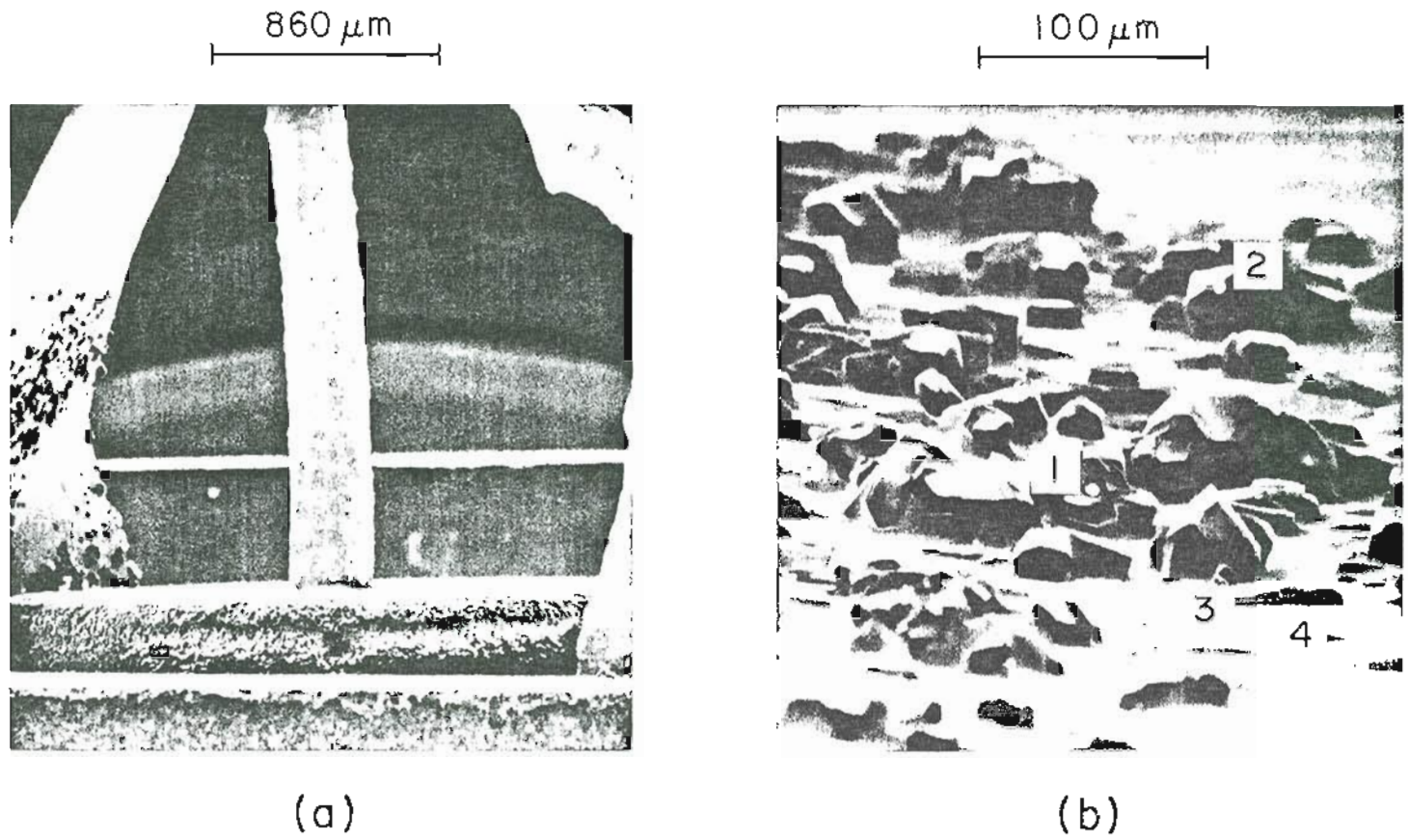

Figure 6-38. Views of the Pt/B on Re emitter structure with second phase material evident. (a) Overall view; (b) Closeup of the wetted left-hand holder, showing the crystalline precipitates. The numbers refer to analysis positions discussed ahead.

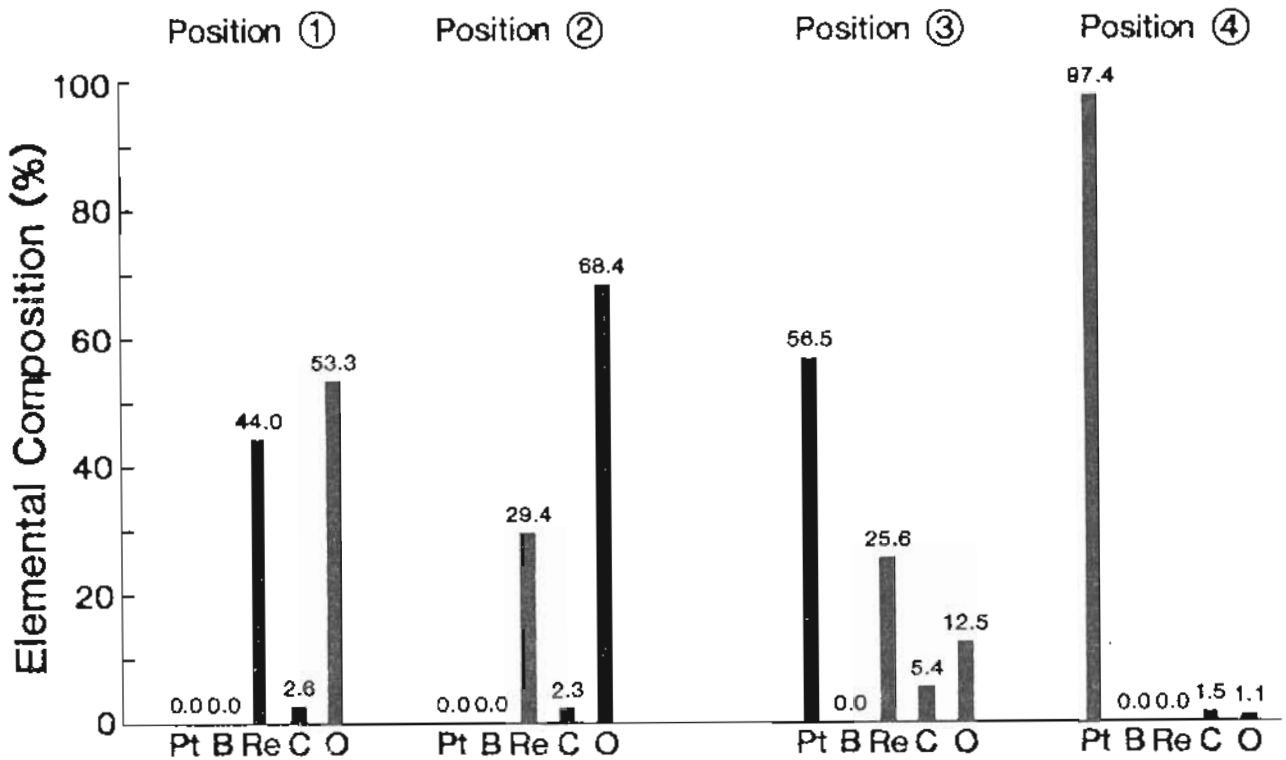

Figure 6-39. Auger surface elemental composition vs position for the failed Pt/B on Re (HRL: PW5-14) alloy containing precipitated second phase material. The temperature is 300 K. The precipitated structures appear to be rhenium oxide.

B at all remains at the surface. Where then does the oxygen originate? A number of possibilities exist. Results reported above show that at the low melting temperature of the Pt/B alloy, significant surface contamination still exists because the temperature is simply not high enough to effectively clean the alloy surface. In particular, oxygen is quite abundant. Second, the oxygen may arise as a result of poor vacuum conditions during wetting. It is unclear what vacuum existed in the HRL apparatus. Third, the oxygen may originate from impure starting materials. In any case, formation of rhenium oxides is not unexpected, as Table VIII shows that the Gibbs free energies of formation of nearly all existing oxides of rhenium are thermodynamically favorable.

TABLE VIII

GIBBS FREE ENERGY OF FORMATION OF RHENIUM OXIDE COMPOUNDS

Compound	T(K)	G (kcal/mole)	Reference
Re_2O_7	1100	-167.5	Wicks [4]
ReO_3	1100	-95.5	"
Re_2O_8	600	-209.0	"
ReO_2	300	-88.0	Lange [5]
ReO_3	300	-127.9	"

Formation of calcium oxide phases were indicated to form in the alloy in previous work, and are also not unexpected because CaO has a very high affinity for oxygen (see Figure 6-40). A possible solution in dealing with these oxide phases is to flash the emitter to a

temperature of about 100 degrees above the melting point of Pt/B for a couple of seconds after wetting. Earlier results showed that little residual contamination existed on the Pt/B molten surface after heating to this temperature.

Table 2 Oxygen Affinity of Metals

Oxide	pO*	Oxide	pO*
Au_2O_3	−5.5	RaO	46.3
Ag_2O_3	−3.3	Al_2O_3	47.2
PtO	−1.3	ZrO_2	47.2
PdO	−1.1	HfO_2	48.1
Air	0.7	Li_2O	48.5
IrO_2	0.9	BaO	48.6
Rh_2O	4.2	Sc_2O_3	50.3
TeO_2	7.2	SrO	51.2
Cu_2O	9.6	BeO	52.0
BiO	11.4	MgO	52.0
PbO	12.7	Y_2O_3	52.0
TcO_2	13.6	$(RE)_2O_3$	~53.0
ReO_2	13.6	ThO_2	55.5
H_2-H_2O ($F = 10^3$)	13.6	CaO	55.5
CO-CO_2 ($F = 10^3$)	14.6	Ac_2O_3	56.4
As_2O_3	15.3		
CoO	16.2		
NiO	16.2		
CdO	16.6		
GeO_2	18.4		
SnO_2	19.7		
H_2-H_2O ($F = 1$)	20.1		
MoO_2	20.1		
FeO	20.6		
CO-CO_2 ($F = 1$)	20.6		
WO_2	21.2		
K_2O	23.2		
In_2O_3	24.1		
ZnO	25.8		
H_2-H_2O ($F = 10^{-3}$)	26.0		
Ga_2O_3	26.2		
CO-CO_2 ($F = 10^{-3}$)	26.8		
Na_2O	28.9		
P_2O_3	29.7		
Cr_2O_3	30.1		
MnO	32.6		
Ta_2O_5	33.2		
NbO	33.7		
VO	34.5		
B_2O_3	35.4		
SiO_2	36.3		
TiO	44.2		

*$pO = -\log p_{O_2}$ for oxygen in equilibrium at 1000°K.

Figure 6-40. The Oxygen Affinity of Metals. From T. B. Reed, Free Energy of Formation of Binary Compounds (Cambridge: MIT Press, 1971), p. 67.

REFERENCES

1. C. L. Mantell, Carbon and Graphite Handbook, Interscience Publishers, 1968.

2. Union 76 Poco graphite reference sheet, 1-1-78.

3. A. E. Bell, Oregon Graduate Center, private communication.

4. C. E. Wicks and F. E. Block, Thermodynamic Properties of 65 Elements--Their Oxides, Halides, Carbides, and Nitrides (Washington: U.S. Government Printing Office, 1963).

5. J. A. Dean, ed., Lange's Handbook of Chemistry, 11th edition (New York: McGraw-Hill, 1973).

CHAPTER 7

THE SURFACE SEGREGATION MODEL OF WETTING BEHAVIOR AND THE TRUE NATURE OF BORONIZATION

A. A Summary of Results to Date

The outlook for development of a long-lived ion source of boron looked extremely pessimistic when viewed against the failure of several liquid metal alloys of boron to wet graphite. A no-win situation appeared to exist where the mutually exclusive requirements of minimal chemical reactivity and good wetting offered little hope for success. On the one hand, the lowest melting boron alloy (Pt/B) exhibited unacceptable levels of chemical reactivity with the metallic substrate (Re) best known to offer resistance to boron attack. On the other hand, poor chemical affinity of the boron alloys to one of the most chemically inert surfaces known (C) resulted in unacceptably poor wetting characteristics. The status of the experimental effort at this point may be summarized in five observations: (1) Pure Ni/B and Pt/B alloys wet and spread over virgin amorphous graphite; (2) Ni/B and Pt/B alloys containing high concentrations of C and/or N wet virgin amorphous graphite reluctantly or not at all; (3) Boronization of amorphous graphite facilitates wetting of Ni/B and Pt/B alloys to carbon; (4) Ni/B and

Pt/B alloys wet metallic surfaces such as Re, Zr, and W, but with excessive, lifetime limiting reactivity; and (5) Although Ni/B and Pt/B alloys are expected to wet substrates such as graphite, it is prevented in nearly all cases studied.

The expectation that Ni/B should wet graphite is based upon reported evidence [1] that metallic Ni by itself wets graphite with a contact angle of 45 degrees. Further, B is often used as an additive to metals to promote wetting on graphite. For example, pure Cu has a contact angle of 140 degrees on graphite, but Cu with 5% B added has a contact angle of 36 degrees [2]. Since the Ni/B eutectic is lower melting than pure Ni, it is less stable than pure Ni, and in addition has B for its second component. One therefore anticipitates that Ni/B should wet graphite. Reasons for the frequent failure of Ni/B to wet graphite are provided below.

B. The Problem: Surface Segregation of Low-Level Impurities in the Alloys

The wettability of solids by liquid metal alloys is governed by surface segregation of low-level C and N impurities in the molten alloys. Segregation of these elements to the surface of the molten droplet has been found in every alloy system we have studied, and allows an integration of the diverse results into a coherent model. Further, the influence of surface segregation on wetting casts doubt on many previous studies of this phenomena, as the existence of ppm impurities in the wetting materials can radically affect the

results. The evidence for segregation is extensive. In support of this idea, we offer five key examples.

1. Wetting Studies of Ni/B (OGC) to Aluminum Oxide

Perhaps the key experimental result of this study concerned wetting of Ni/B to aluminum oxide. Wetting of Ni/B to Al_2O_3 was attempted due to evidence from Lugscheider [3] which indicated that certain nickel boride alloys were found to wet aluminum oxide. In addition, use of this substrate served to isolate the alloy from outside sources of carbon. Locating the origin of C in the alloys proved to be a pivotal issue, as previous studies of this question were unable to determine whether carbon signals in the alloys originated from dissolution of the substrate or impure materials.

Figure 7-1 shows the wetting behavior of Ni/B to aluminum oxide. A solid specimen of Ni/B (OGC) was laid atop a ribbon of aluminum oxide made by filling an appropriately shaped mold with Aremco 552 high-temperature adhesive. The composition of this material was verified by Auger analysis to consist primarily of Al and O. The ribbon was laid atop a second ribbon of W, and the combination was loaded into the vacuum chamber and resistively heated until the alloy melted. The wetting was poor, and consisted of a contact angle of about 130 degrees. More significantly, however, were the large concentrations of C and N at the surface of the poorly-wetted droplet. These elements could only arise from the droplet itself, as

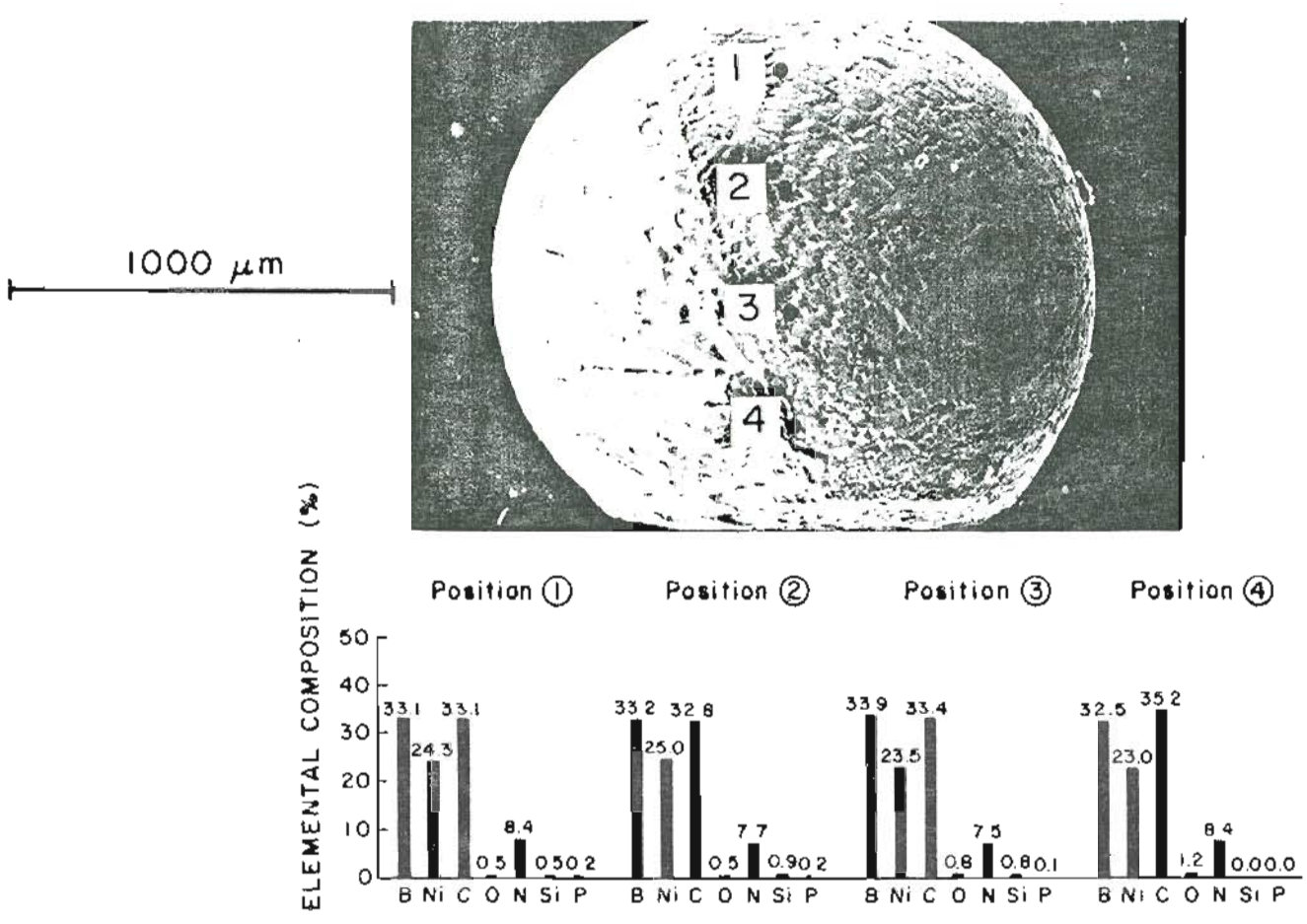

Figure 7-1. Auger surface elemental composition vs position for wetting of Ni/B (OGC) on Al_2O_3. Surface segregation of C and N are evident. The temperature is 1355 K = T_m + 60°.

the alloy is completely isolated from carbon and the droplet shows little or no oxygen, which rules out the contribution from adsorbed CO. Surface segregation of C and N which occurs coincident with melting is indicated as the source of the contaminants.

2. Wetting Studies of Pt/B (LANL) to Re

We have already discussed the behavior of this contact system. Here, the attention is focused on the character of the Pt/B alloy surface during a 20-hour study of surface composition. Recall from Figure 6-33 that the surface of the alloy was found to contain about 30% C throughout the experiment, even after all oxygen had vanished. The situation after catastrophic breakdown of the contact system is shown again in Figure 7-2. Strong C and N signals are found at all monitored locations. Since there is no carbon anywhere in this system except for the low level of bulk impurities in the alloy (the Re is C-free at the melting temperature of Pt/B--see Figure 6-32), we deduce that the C and N originate from surface segregation during alloy melting. Hence, both OGC and LANL alloys display similar behavior regarding segregation of low-level alloy impurities.

3. A Calculation of C Segregation in Ni/B Alloys

A theoretical calculation of surface enrichment was made to determine whether the low levels of C impurity found in the OGC alloy could be responsible for the high concentrations of this element found at the surface of Ni/B and Pt/B alloys. In particular,

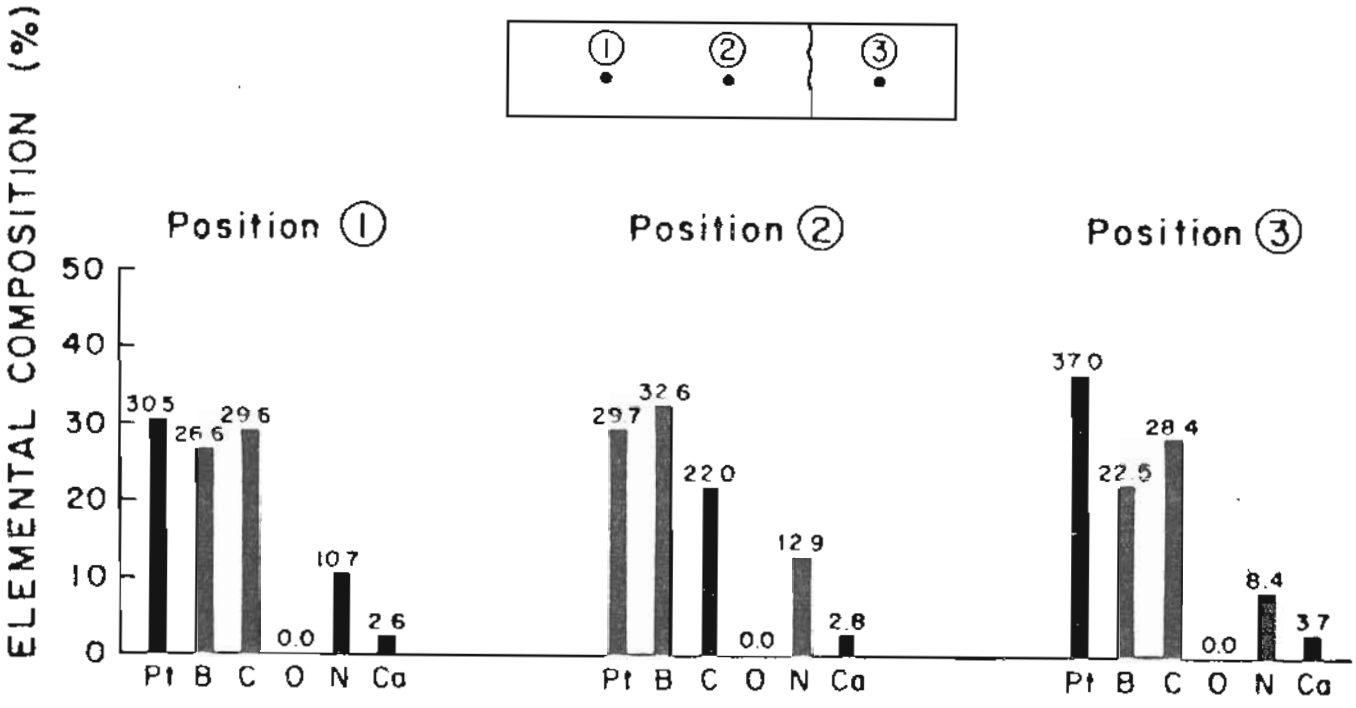

Figure 7-2. Auger surface elemental composition vs position for Pt/B (LANL: #273-5A; Pt=.72, B=.28) on Re (HRL: Alfa, Lot #040583) after catastrophic failure. The temperature is 300 K. BN chemical shifts occur at each position.

emission spectroscopic analysis of Ni/B (OGC) showed the OGC material to contain 0.019 w% C. Assuming the entire weight percent of C to segregate to the surface of a spherical droplet of alloy 0.5 mm in radius, the thickness T of the C layer formed is calculated to be:

$$T = 3.17 \times 10^{-6} D(Ni/B)/D(C) \quad cm$$

where D(Ni/B) and D(C) are the densities of Ni/B and C respectively. Assuming the density of graphite to be 2.0 gm/cm^3, and calculating the density of Ni/B (7.2 gm/cm^3) from values given in the literature [4,5] produces a value for t of 1140 A. Since the Auger beam probes the top 5 - 20 A of a surface, it is reasonable that the high concentrations of C observed at the surface of poorly-wetted droplets is due to surface segregation of C impurities within the alloy. The impurities are characteristic of the bulk concentration since the alloy fragments used in wetting are fractured from the interior of the original melt.

4. Cross-sectional Examinations of Poorly-wetted Droplets

Further evidence for surface segregation is given by analysis of cross-sectional slices of poorly-wetted droplets. Figure 7-3 shows one example of many we have examined. In this experiment, an attempt was made to wet Ni/B (LANL: #273-7A; Ni = .62, B = .38) on a surface of amorphous graphite with added Zr. The wetting was poor, with a contact angle of about 140 degrees. Auger analysis of the droplet while molten showed high amounts of surface C. The view at room temperature, shown in the left photo of the figure, shows that the

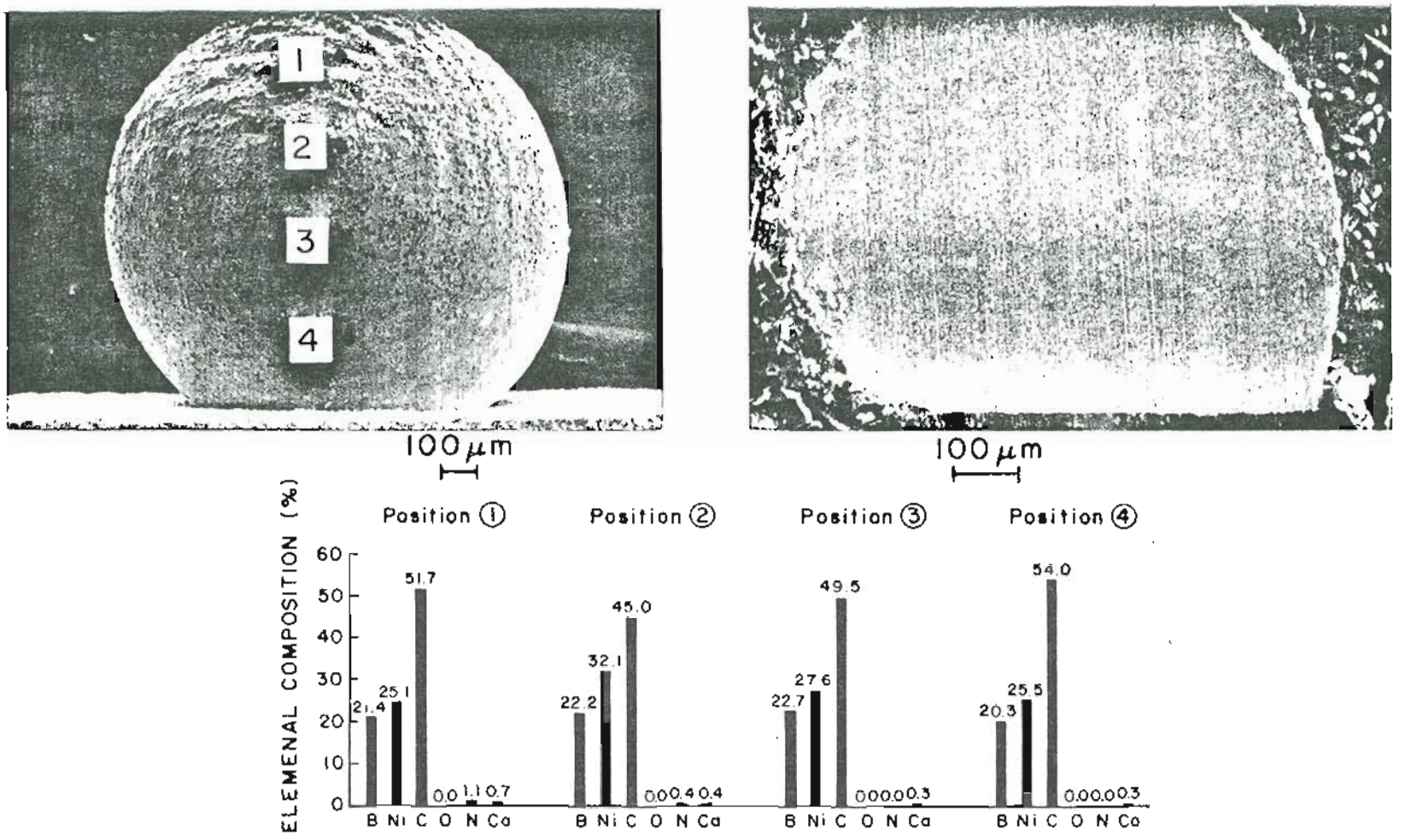

Figure 7-3. Wetting of Ni/B (LANL: #273-7A; Ni=.62, B=.38) on graphite with a Zr overlayer (surface: 11% Zr, 89% C). (Top left) Side view of wetting with monitored locations. (Top right) Cross-sectional slice through the droplet, showing segregated material. (Bottom) Auger surface elemental composition of 4 positions on the droplet at T = T_m + 60° = 1350 K. High concentrations of C are present.

droplet surface is covered with recrystallized precipitates of hexagonal material that later analysis proved to be graphite. Micrographic examination of several cross-sections through the droplet show evidence of second phase material at the droplet surface. By contrast, the interior of the droplet is smooth and uniform, characteristic of pure alloy material.

A second example is provided in Figure 7-4. In this case, Ni/B (OGC) was heated atop virgin amorphous graphite and formed the usual poorly-wetted droplet. A second graphite ribbon at the same temperature was then brought into contact with the top hemisphere of the droplet to investigate whether the alloy would wet this ribbon. The results have been detailed above during the discussion of carbon ruboff. In brief, the alloy droplet was found to yield to thrusts from the second ribbon. When the second ribbon was positioned to lightly touch the alloy droplet, formation of a bright zone along the contact developed that remained when the ribbon was pulled away from the droplet. This is direct evidence that the alloy dissolves carbon. Figure 7-4 shows the droplet profile at room temperature after a series of such experiments. The droplet surface shows large areas of carbon-containing material originating from segregation and the extreme treatment described above. The interior of the droplet is relatively uniform, consisting primarily of alloy components.

5. The Composition of Alloy Material Flowing from the Interior of the Earliest Poorly-Wetted Droplets

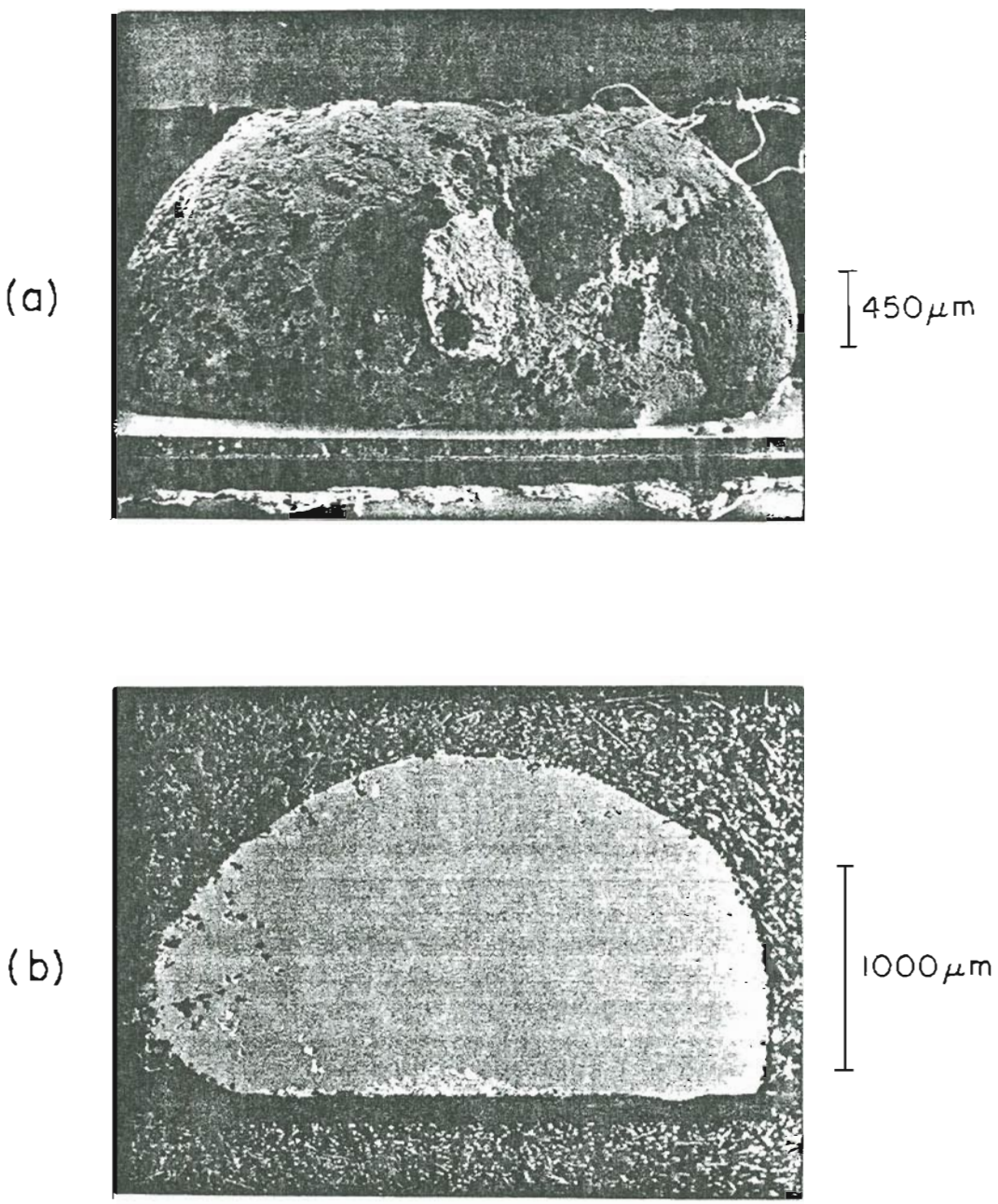

Figure 7-4. The Ni/B (OGC) on C (virgin) alloy after puncture by a second graphite ribbon. The interior of the alloy is remarkably clean, given the appearance of the droplet surface in (a). Photograph (b) shows a cross-sectional slice through the alloy.

It was reported above that most of the earliest, prewetted contact systems contained poorly-wetted droplets from which pure alloy could be made to flow by heat treatment. The pure alloy material flowed from the inside of the droplets and wetted the virgin graphite. Auger analysis showed the surfaces of the poorly-wetted droplets to invariably consist of high concentrations of C and N, which remained behind in inert form after the fracture of the surface skin. For prewetted systems that were well-wetted, little evidence of such surface C was found. This is further support for the existence of segregated material that arises during the wetting process as the alloy is melted.

6. The Theory of Surface Segregation

Segregation refers to the redistribution of elemental components from the bulk of an alloy to a free surface or grain boundary. That is, the equilibrium concentration of an alloy surface is not necessarily identical to its bulk composition. Since there are no grain boundaries in molten liquids, segregation occurs entirely at the interface between contacting phases. The first rigorous theoretical description of surface segregation was formulated by Gibbs [6]. In this formalism, Gibbs argued that the driving force for segregation is the decrease in the total free energy of the contact system when segregation occurs. In terms of the Gibbs adsorption isotherm, the excess surface concentration of one component of an alloy over its bulk concentration, E, is related to

the compositional dependence of the surface tension d@/du by:

$$E(2) = - d@/du(2)$$

where @ is the surface tension of the solution, u(2) is the chemical potential of the solute, and E(2) is the surface excess of the solute with respect to the Gibbs equimolar dividing surface for the solvent. If the dependence of the chemical potential on the composition obeys Henry's law (i.e., the system is a dilute binary system), this equation may be rewritten as [7]:

$$E(2) = -[X(2)/kT] d@/dX(2)$$

where X(2) is the concentration of the solute. This means that one component of the alloy should segregate to its surface if the surface tension decreases with increasing concentration of that component. In addition, the surface will become depleted of solute that raises the surface tension. The problem in applying this equation to surface segregation is that, experimentally, little is known about the dependence of surface tension on chemical potential or composition. Therefore, a number of alternate approaches have been cast to alter the Gibbs adsorption isotherm in such a way that experimentally accessible quantities may be correlated. Although the approaches contain a number of simplifying assumptions not necessarily applicable to the complicated systems studied here, it is useful to discuss briefly two of the more well-established results in light of the physical principles involved.

Assuming that the surface consists of only the topmost atomic layer (the monolayer assumption), Somorjai [8] and Defay and Prigogine [9] derived an equation relating the surface composition of

an ideal binary solution to the bulk composition:

$$X(S,1)/X(S,2) = [X(B,1)/X(B,2)] \exp [a(\Theta(2) - \Theta(1))/kT]$$

where X(S,1), X(S,2), and X(B,1), X(B,2) are the surface and bulk atom fractions, respectively, for the two components 1 and 2 of the alloy, $\Theta(1)$ and $\Theta(2)$ are the surface tensions of the pure components, a is the average surface area occupied per atom, and the other symbols have their usual meanings. According to this equation, the surface will be enriched by the component which has the smaller surface tension. This is sensible, because the lower the surface tension, the easier it is for that component to form new surface.

The exponential dependence of the ratio of surface-to-bulk composition can result in impressive enrichment factors. For example, for a surface tension difference of only 0.05 N/m (50 dyn/cm), the enrichment factor at 1000 K and a = 10^{-19} m^2/atom is 1.44. As the temperature is lowered, the excess increases. The surface tensions of the alloy components we have studied are not fully documented at all temperatures. There are such large differences between the surface tension of metals and nonmetals, however, that segregation of the nonmetallic component of the alloy (or nonmetallic impurities) is virtually assured (e.g., at the melting point, the surface tensions of our alloy components are: Ni = 1750 dyn/cm, Pt = 1860 dyn/cm, Pd = 1480 dyn/cm, and B = 1060 dyn/cm). The surface tension of graphite could not be found, but is likely to be near 1000 dyn/cm. The magnitudes of surface enrichment we have seen in our studies here are therefore not unexpected. In fact, enrichment factors of 100-10000 have been reported [10].

A second and very successful semiempirical theory of surface segregation has been developed by Miedema [11]. Miedema argued that the Somorjai expression fails to account for the effects of elastic size mismatch energy in cases where the atoms of the alloy are of different size, and in addition, that Somorjai neglects the heat of solution of component 1 in 2. To extend the monolayer expression, Miedema postulates that three terms are necessary to explain the phenomenon of surface segregation. The first is the difference in surface tensions of the alloy components, the second is the size mismatch energy, and the third is the heat of solution.

The size mismatch energy is necessary because the inclusion of a large atom of one component amidst a regular array of atoms of the other component produces an elastic stress energy which may be lowered by segregation to a free surface or grain boundary. The heat of solution is necessary because as the heat of solution of a system of solvent and solute increases, the solute tends to come out of solution and segregate. The dominant contribution in alloys of two transition metals is the surface tension term. In alloys consisting of a metallic and nonmetallic component, the difference in surface tensions is so large that the other two terms can be treated as second order effects or ignored completely.

The formula suggested by Miedema is [12]:

$$C(S,1)/C(B,1) = \exp\{fdH - g[J(1) - J(2)]V^{.66}/3RT\}$$

where $C(S,1)/C(B,1)$ represents the ratio of the concentration of the solute atoms in the first atomic layer to that in the bulk, dH is the partial molar heat of solution of metal 1 in metal 2, V is the molar

volume of the solute, J(1) and J(2) are surface enthalpies, f and g are constants, and the other parameters have their usual meanings. Chelikowsky [13], in discussing the ability of this formalism to predict which component will segregate in systems of dilute transition metals, believes the theory is accurate to 90% or better.

C. The Solution: Boronization and Siliconization

Boronization refers to the process of forming a boron layer on a virgin graphite ribbon. This was carried out by depositing a slurry of B powder and acetone on graphite, and then flash heating the combination to temperatures above the melting point of B (2300 K). Previous studies of prewetted HRL contact systems has shown that the surface resulting from this process, although difficult to reproduce, promotes wetting of B-containing alloys to graphite. To clarify this issue, and to integrate the results with the fact that impurity-free alloy appears to wet virgin graphite, a detailed series of experiments involving boron films was performed which are discussed in this section.

1. Wetting of 3% B-Fluxed Ni/B Alloy on Flashed and Unflashed Boronized Substrates

The first study in the series addressed the effect of high temperature flashing in the boronization process. Figure 7-5 displays the Auger surface elemental composition of a slurry of 325 mesh red B (Alfa) and acetone before and after high temperature

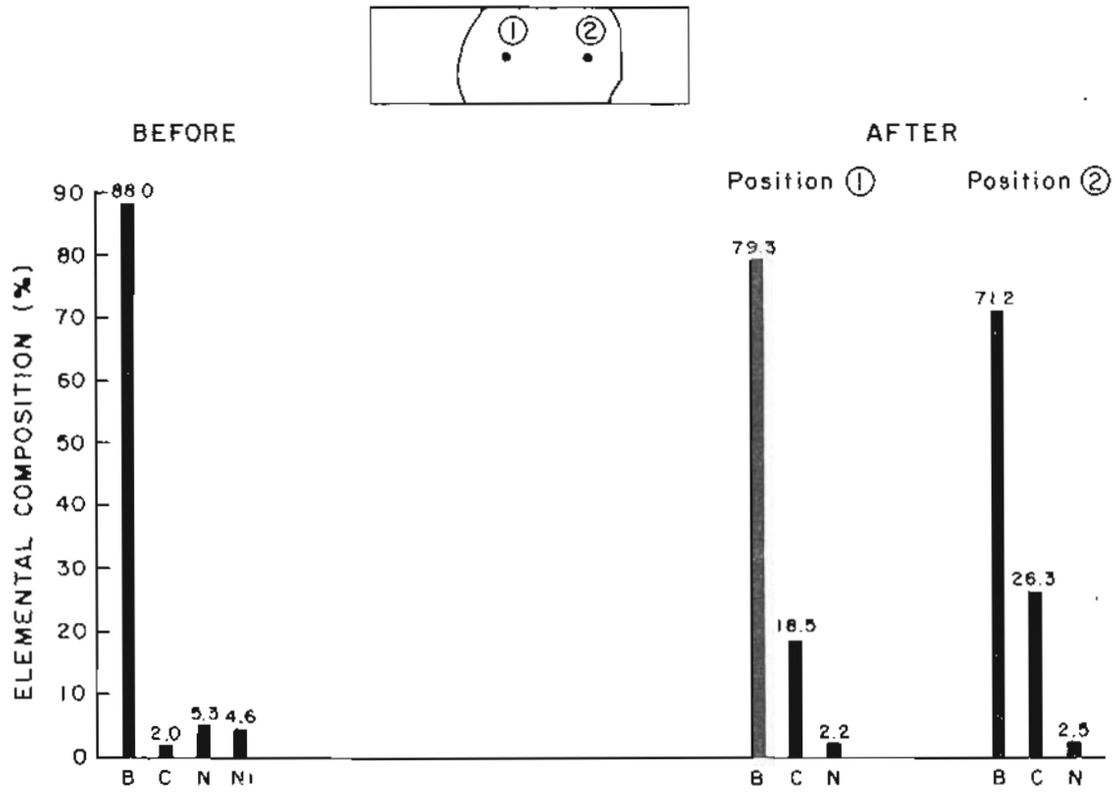

Figure 7-5. Auger surface elemental composition for a slurry of 325 mesh red B and acetone before and after high temperature flashing (HTF). The spectra were taken at a temperature of 1396 K.

flashing (HTF). The HTF was performed by setting the ribbon heating supply (a variac) to full power with the switch off, and then switching the supply on for a couple of seconds. The experiment was performed in the UHV chamber. Before flashing, the surface consisted mostly of B with small amounts of C, N, and Ni. After the HTF, shown in the "after" histograms, the surface has reduced amounts of B and the red boron has turned dull grey in color. Experiments performed later to determine the maximum graphite temperature attained during the HTF showed this temperature to be well below the melting point of B, at most about 2000 K.

Subsequent wetting of 3% B-fluxed Ni/B powder (HRL) to this boronized surface was excellent, as demonstrated in Figure 7-6. The contact angle is near-zero, and the alloy has wet and spread to the nonboronized backside of the graphite ribbon. Auger compositions of the Ni/B surface at wetting show reduced C concentrations (and increased N concentrations) compared to the situation immediately prior to wetting. This behavior was observed throughout the series of experiments in this section, and indicate that C is depleted from the surface in the process of wetting. This result will be discussed further in a moment.

An identical experiment was prepared using the same materials and boronization technique. Rather than flashing the substrate, however, the temperature of the boronized ribbon was increased to only 1400 K during the experiment. An Auger spectrum of the boronized layer was then recorded, which is displayed in Figure 7-7. Again, the boronized surface is primarily composed of B powder which has turned

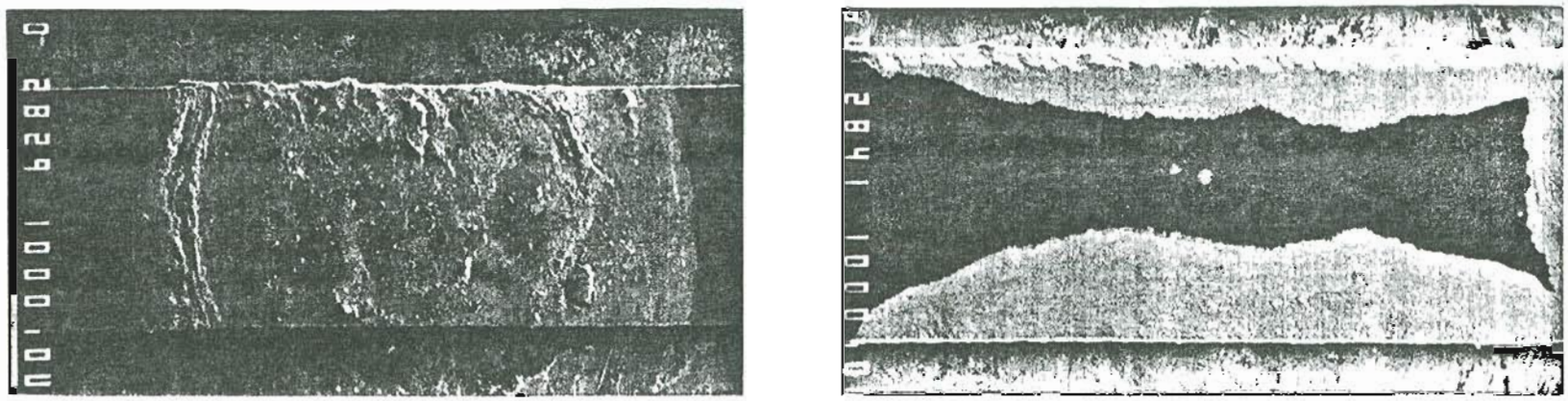

Figure 7-6. Wetting of 3% B-fluxed Ni/B powder on a HTF boronized (325 mesh red B) substrate. (Top left) View of the frontside wetting. (Top right) View of the backside wetting. (Bottom) Auger surface elemental composition of the substrate and alloy at a temperature near the melting point of Ni/B.

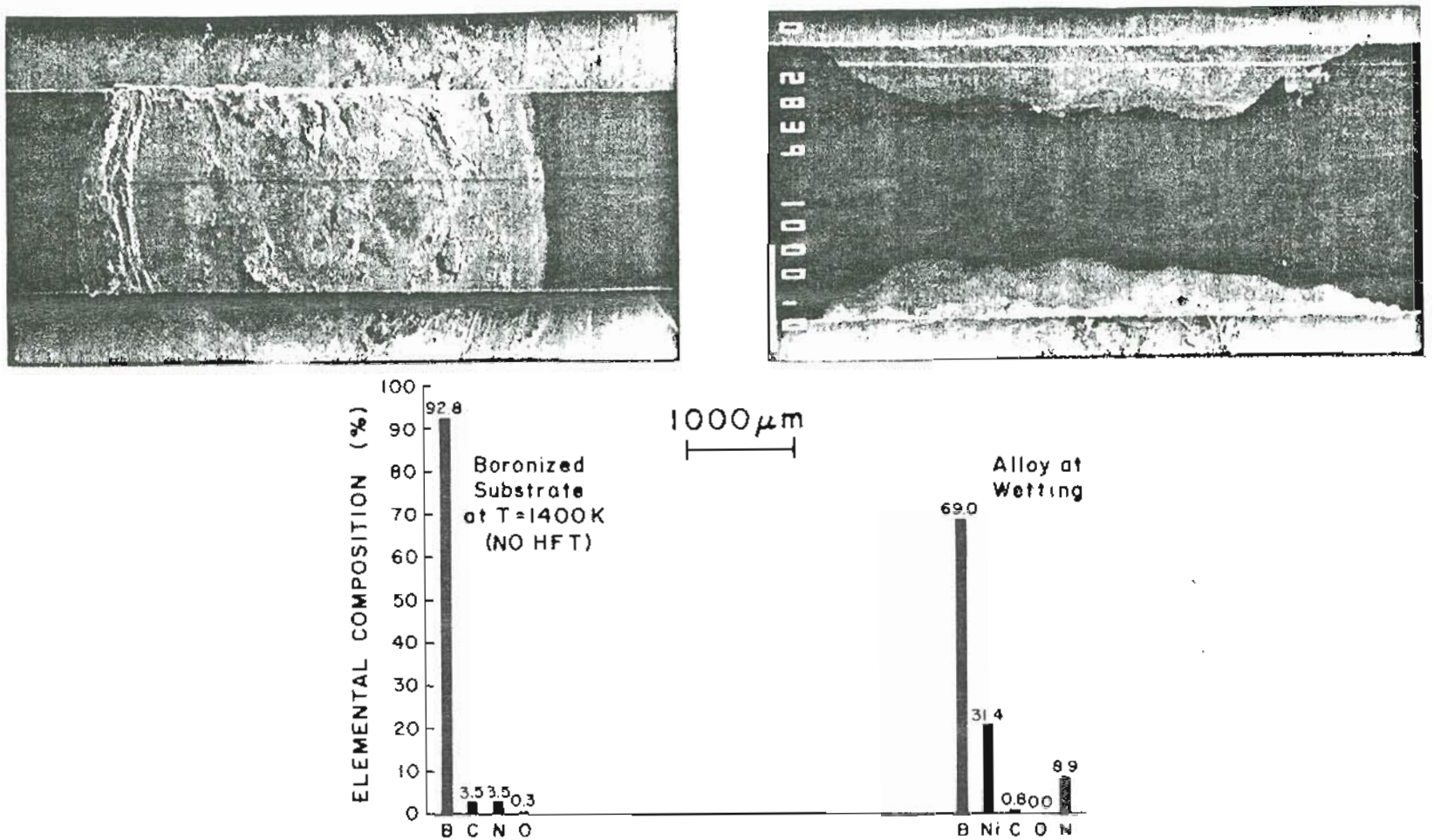

Figure 7-7. Wetting of 3% B-fluxed Ni/B powder on a boronized (325 mesh red B) substrate prepared by heating to T = 1400 K (no HTF). (Top left) View of the frontside wetting. (Top right) View of the backside wetting. (Bottom) Auger surface elemental composition of the substrate and alloy at the melting point of Ni/B.

grey in color. Wetting of 3% B-fluxed Ni/B powder (HRL) to this surface produced results identical to the flashed surface, consisting of a near-zero contact angle and wetting and spreading to the nonboronized backside of the graphite ribbon. Similar behavior was found for the C and N concentrations of the alloy surface at wetting--the C signal decreased and the N signal increased. These results show that a HTF is not required to produce a well-wetted surface. Indeed, as shown below, flashing can readily produce a poorly-wetted surface corresponding to the extent to which the boron is flashed away. It is not the flashing that is important in the wetting process, but rather the presence of a uniform layer of boron. Further studies to deduce whether heating the boronized layer was necessary showed that better wetting behavior resulted after heating the graphite to a temperature of about 1300 K where the red to grey color transition occurred. We believe that heating enhances the adhesion of the boron powder to the graphite, but does little else by way of improved wetting.

2. Surface Composition vs Temperature for 325 Mesh Red Boron and OGC Boron on Virgin Graphite

The previous experiment showed that it is possible to retain boron on the surface of a flashed substrate if the temperature reached during the flash is well below the melting point of boron. To further characterize the temperature behavior of boronized graphite, surface composition vs temperature was studied for ribbons

boronized with two different sources of boron. The goal of this exercise was to determine the temperature at which most boron has volatilized from the surface. Previous results using a thin covering of B showed that nearly all B had vanished at a temperature of 1660 K.

Figure 7-8 is a plot of Auger surface elemental composition vs temperature for a slurry of 325 mesh red boron (Alfa) on virgin graphite. Data was taken at a single point on the boronized surface. Boron is found to persist at this position up to a temperature of about 2200 K before being rapidly volatilized. The true situation is more complicated than this, however, as shown in Figure 7-9. In this figure, a plot of composition vs position for the boronized surface after heating to 2300 K is shown. It is found that the volatilization of B has been highly nonuniform, with portions of the surface containing large concentrations of B and other portions containing almost no B.

Repeating the experiment using a thick layer of red boron obtained at OGC whose origin is unknown resulted in similar behavior. At the position monitored, the B begins to rapidly volatilize at a temperature of about 2000 K, well below the melting point of B. This is plotted in Figure 7-10. Admixtures of B-rich and C-rich regions are found on the ribbon after heating to 2100 K, and the surface is highly nonuniform compositionally.

The important conclusion to be drawn from this work is that high temperatures produce an irreproducible and inhomogeneous wetting layer when the starting slurry of red boron is relatively thick. For

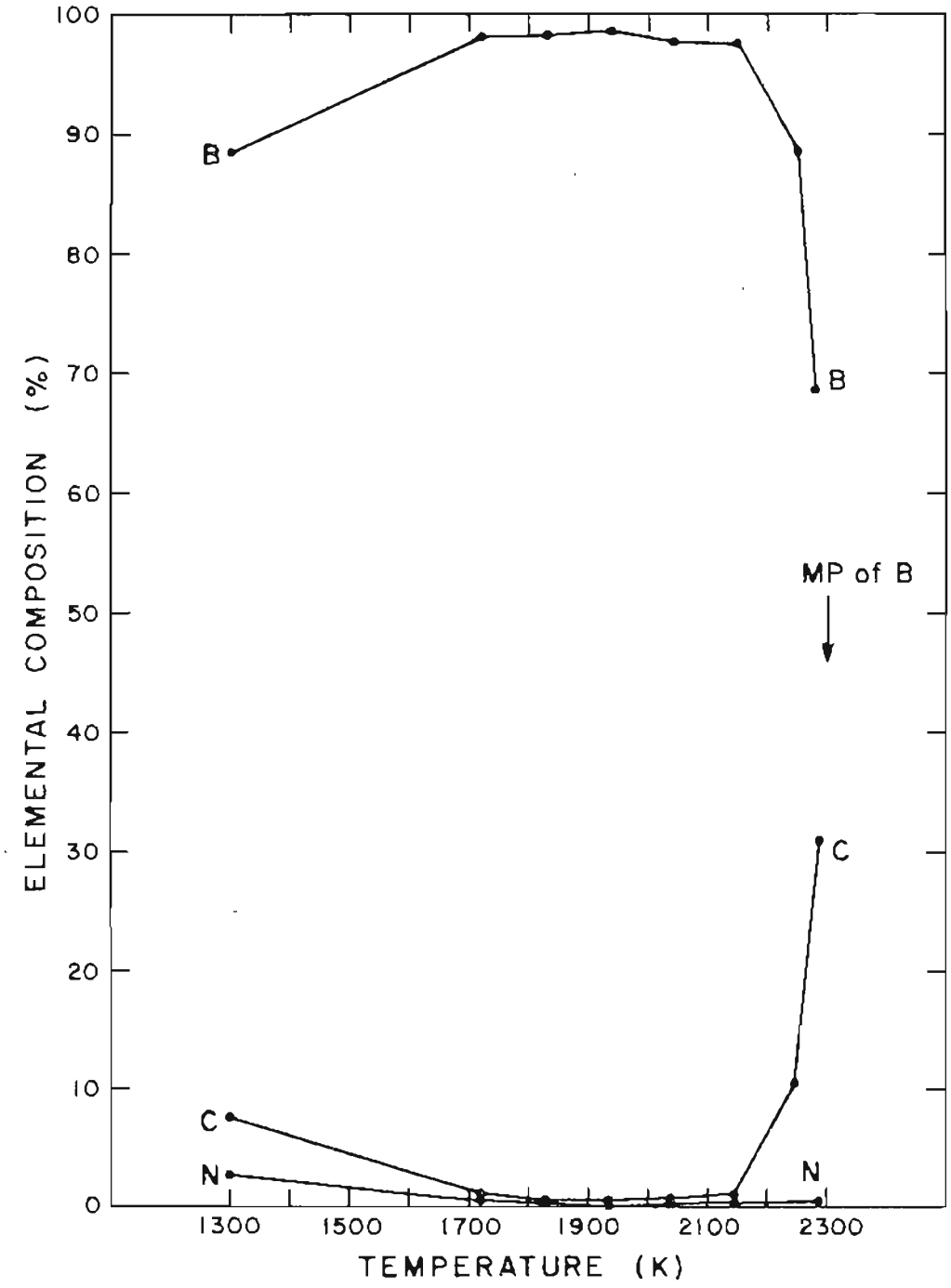

Figure 7-8. Auger surface elemental composition vs temperature for a slurry of acetone and 325 mesh red B on graphite. The time between points is about 7 minutes.

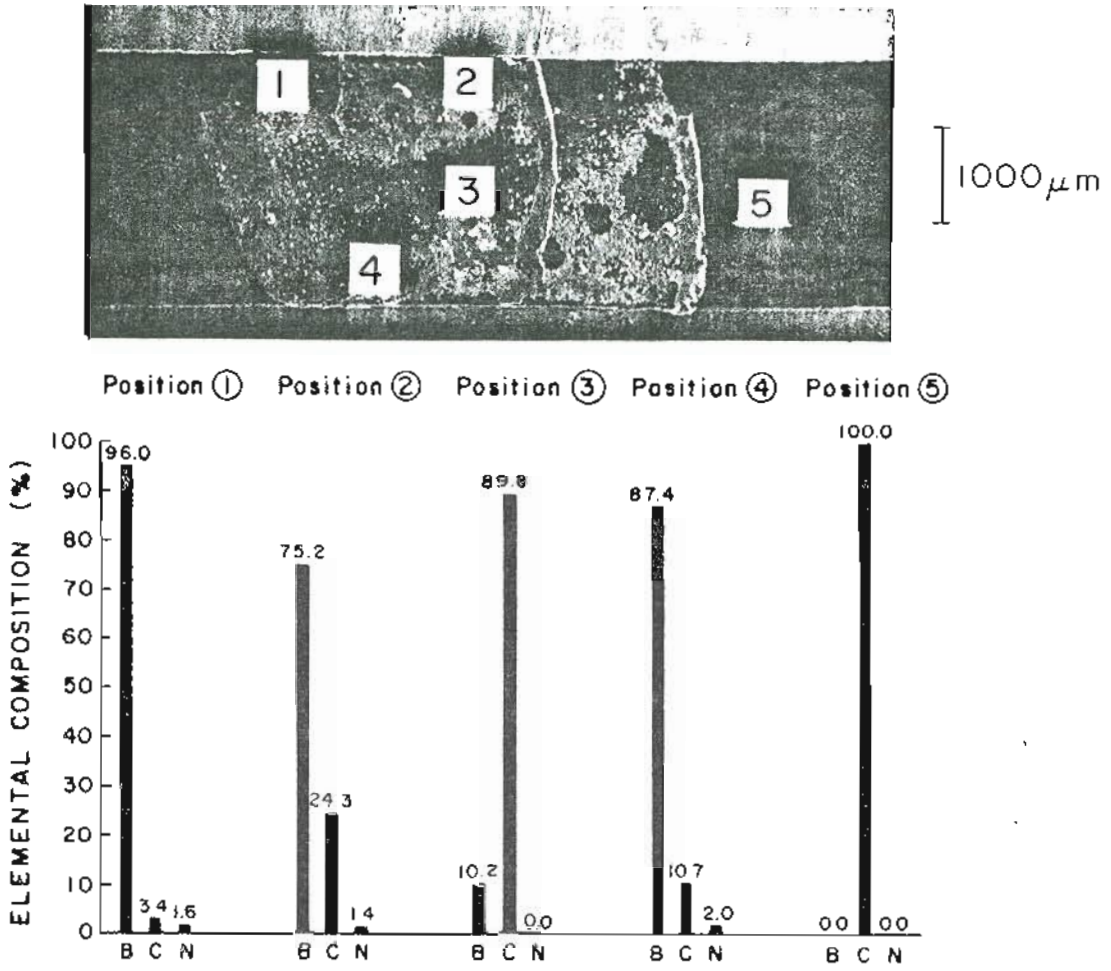

Figure 7-9. Auger surface elemental composition va position after heating to 2300 K for a slurry of 325 mesh red B powder and acetone on graphite. Volatilization of B is found to highly nonuniform.

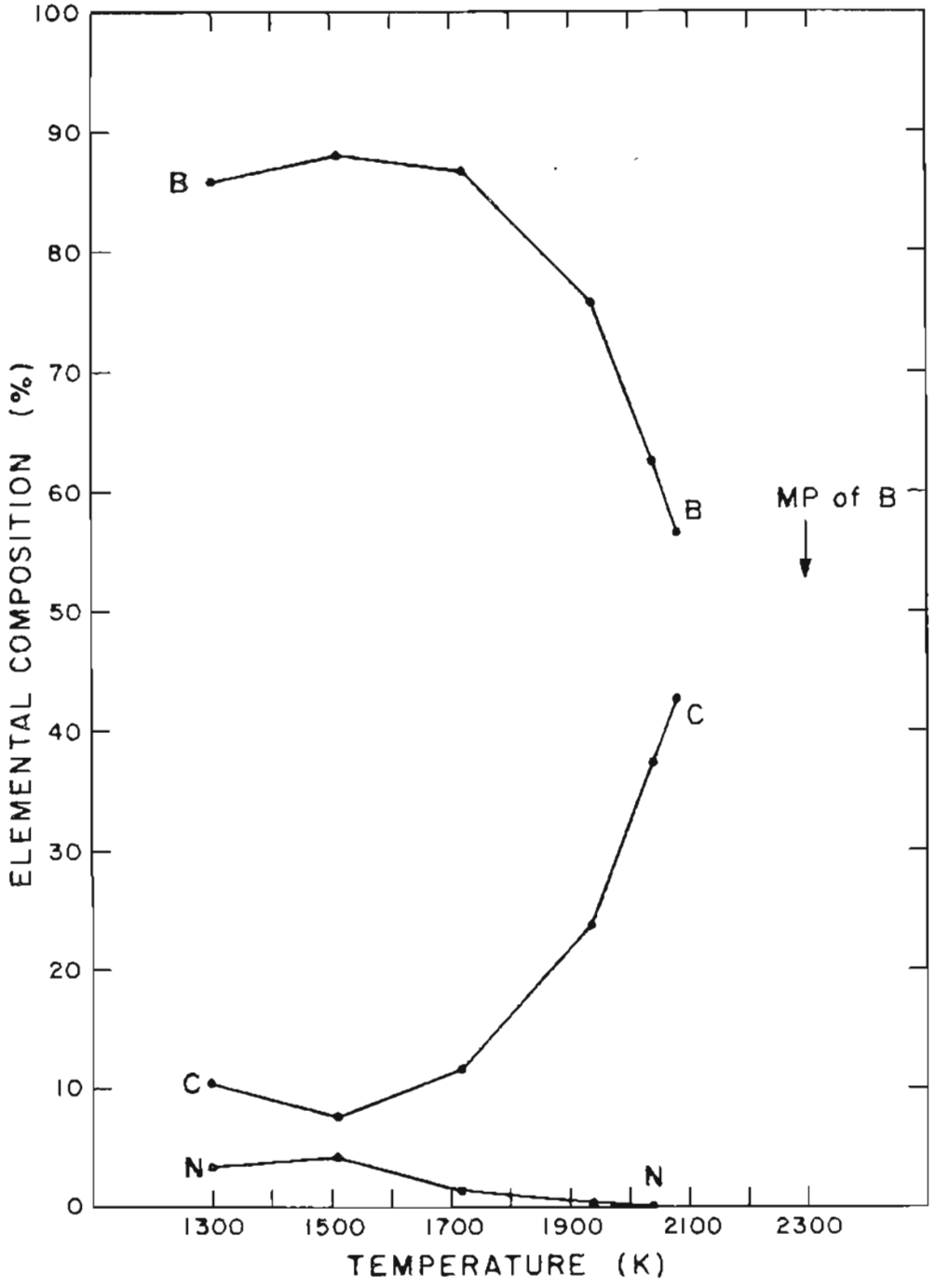

Figure 7-10. Auger surface elemental composition vs temperature for a slurry of acetone and OGC boron on graphite. The time between points is about 7 minutes.

thin coatings, the boron may be flashed off completely. This provides an explanation for the differing degrees of wetting success found in the earlier work. The wetting is poor when the alloy sees a predominantly C substrate, and improves as less B is flashed away. It has been difficult to reproduce "ideal" boronization with a HTF because one cannot reproduce such a surface by flashing. Only by maintaining low temperatures during the heating of a boronized surface can the integrity of the boron layer be preserved.

3. Wetting Studies of Fluxed and Nonfluxed Ni/B to Virgin Graphite

Early work by the Hughes group suggested that the best wetting of B-containing alloys occurred when the substrate was "ideally" boronized and 3% additional B powder was mechanically mixed with the alloy. In order to verify this assertion, fluxed and nonfluxed powdered alloys were applied to both virgin and boronized graphite. This section details the wetting behavior on virgin graphite.

The wetting of nonfluxed Ni/B powder to virgin graphite has been attempted several times in the course of our investigations, and was discussed earlier. Invariably, the wetting behavior has been poor, with the contact angle well over 90 degrees. In these experiments, the attraction of the alloy for itself is much greater than the attraction of the alloy for the graphite. A slurry of nonfluxed Ni/B powder spread over a large area of graphite will be drawn into the rapidly forming droplet of poorly-wetted material before sticking to

the graphite. A number of photographs of the resulting droplets may be found thoughout this report.

In contrast, wetting of 3% B-fluxed Ni/B powder to virgin graphite is better than wetting of nonfluxed material to virgin graphite, but still leaves much to be desired. Figure 7-11 provides photographs and Auger compositions of the surface after wetting. The wetting is characterized by an irregular mixture of contact angles and the surface is rich in carbon. High magnification views of the resolidified alloy droplets on the surface show the presence of dark hexagonal structures that previous analysis has shown to be precipitated graphite. An explanation for the difference in wetting of fluxed and nonfluxed is offered below.

4. Wetting Studies of Fluxed and Nonfluxed Ni/B on Identically Boronized Graphite

In contrast to the difference in wetting of fluxed and nonfluxed Ni/B to virgin graphite, we could find no significant differences in wetting of the same materials to boronized graphite. Wetting of 3% B-fluxed Ni/B powder to boronized graphite is shown in Figure 7-12. The alloy was found to wet and spread over both boronized and nonboronized sides of the ribbon with a contact angle of near-zero. The elemental composition of the alloy surface at wetting behaves in a manner similar to that described above, with low percentages of C. Figure 7-13 depicts the wetting of the nonfluxed Ni/B powder to boronized graphite. Little difference is noted in wetting behavior

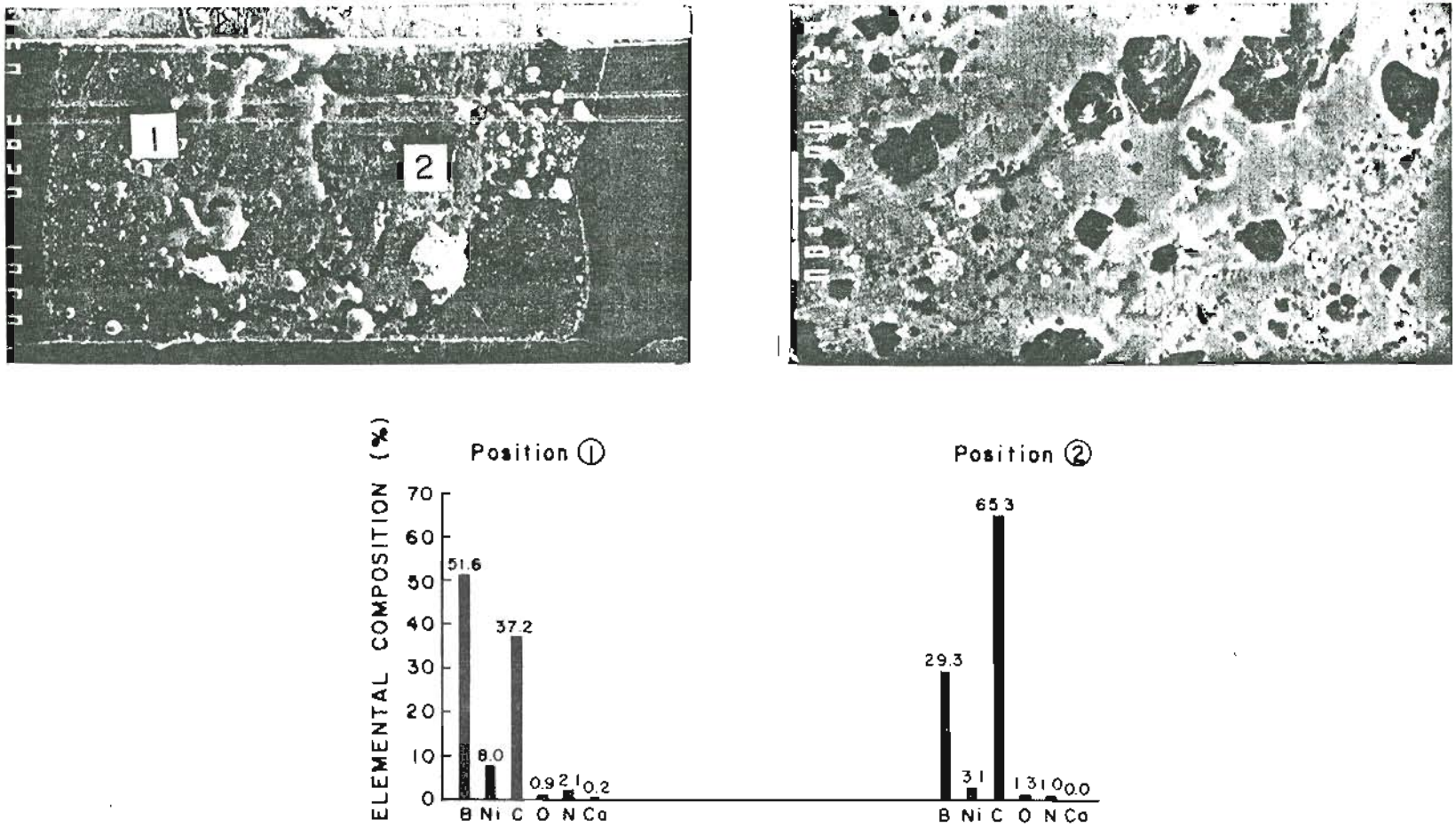

Figure 7-11. Wetting of 3% B-fluxed Ni/B powder to virgin graphite. (Top left) Overall view of the wetting behavior. (Top right) A high magnification view of the wetted alloy. (Bottom) Auger surface elemental composition at 1255 K of two positions within the alloy after wetting.

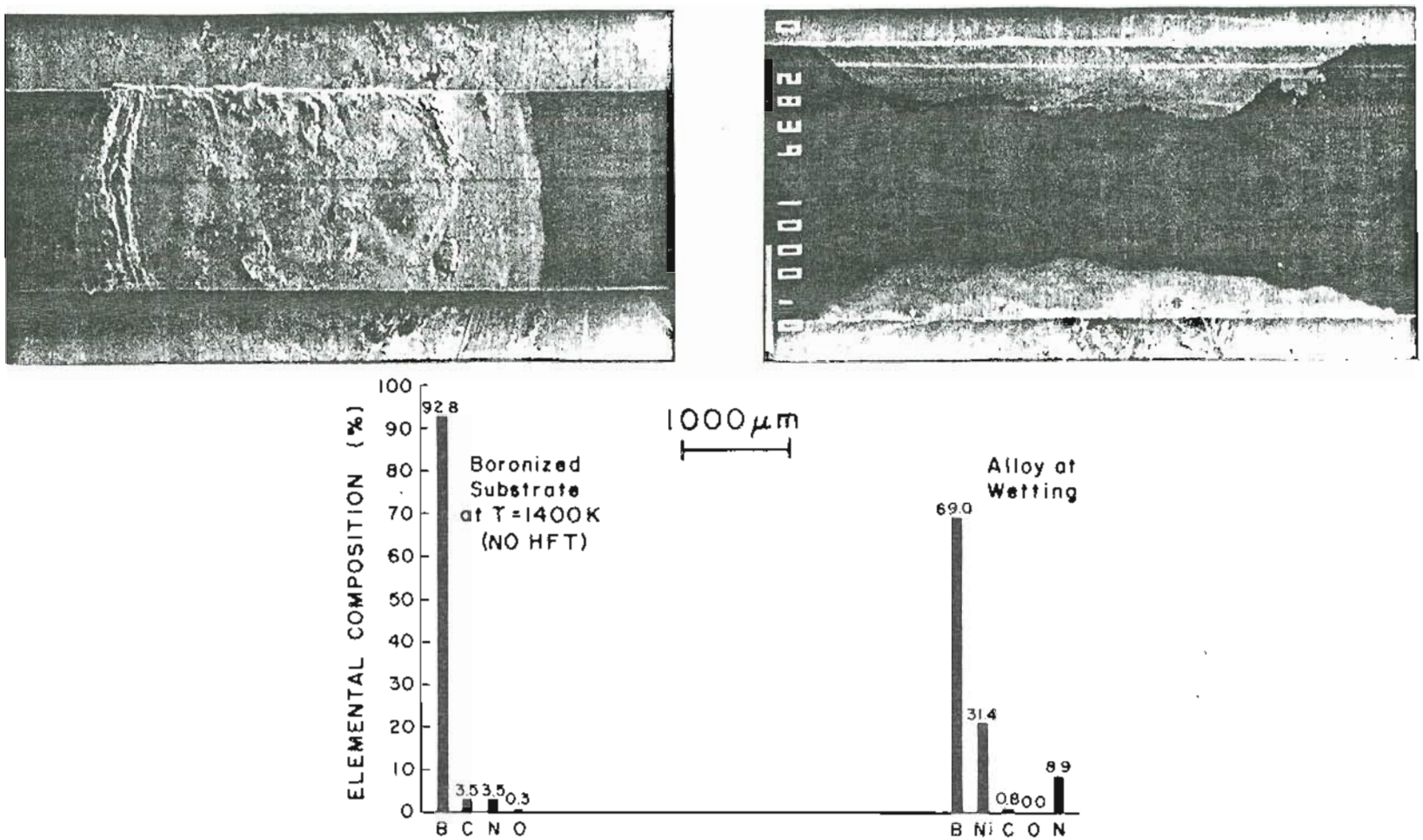

Figure 7-12. Wetting of 3% B-fluxed Ni/B powder on a boronized (325 mesh red B) substrate prepared by heating to 1400 K (no HTF). (Top left) View of the frontside wetting. (Top right) View of the backside wetting. (Bottom) Auger surface elemental composition of the substrate and alloy at the melting point of Ni/B.

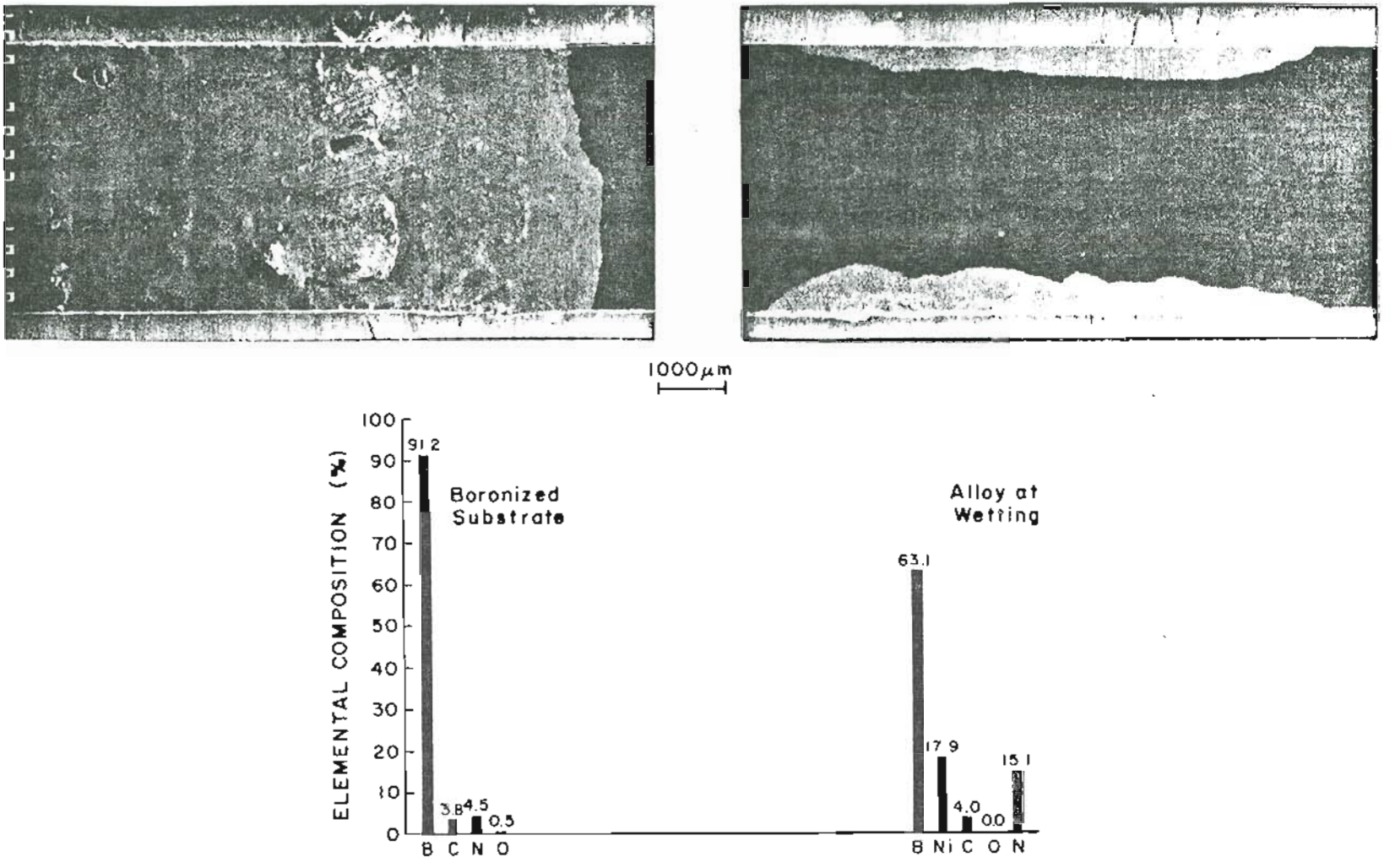

Figure 7-13. Wetting of nonfluxed Ni/B powder on a boronized (325 mesh red B) substrate. (Top left) View of the frontside wetting. (Top right) View of the backside wetting. (Bottom) Auger surface elemental composition of the substrate and alloy at the melting point of the alloy.

or surface composition. The results suggest that fluxing helps the wetting of Ni/B to virgin graphite, but does little if anything to improve the wetting on boronized graphite.

5. Wetting Studies of Ni/B to Crystalline Boron

The surface of boronized graphite was determined above to consist largely of boron. It is therefore natural to presume that Ni/B would wet a pure boron surface. To verify this assertion experimentally, a solid specimen of Ni/B (OGC) was mounted above a disk of pure, single-crystal B rod (99.999% zone refined) which in turn was mounted above a graphite ribbon. The combination was then heated resistively by passing current through the graphite until the alloy melted. The wetting was excellent, consisting of a near-zero contact angle with spreading over the side and bottom of the boron disk (see Figure 7-14). Given the results above, this behavior is not unexpected, but nonetheless required verification.

6. Wetting Studies of Ni/B to B_4C and B_5C

This series of experiments were performed to determine whether a boronized surface could be simulated by a surface consisting of a B-rich compound. Three wetting substrates were investigated: single-crystal B_4C, CVD deposited B_4C, and single-crystal B_5C.

Wetting of Ni/B (LANL #273-7B; Ni = .55, B = .45) to single-crystal boron carbide resulted in a poorly-wetted droplet of alloy containing large islands of bright material in the upper

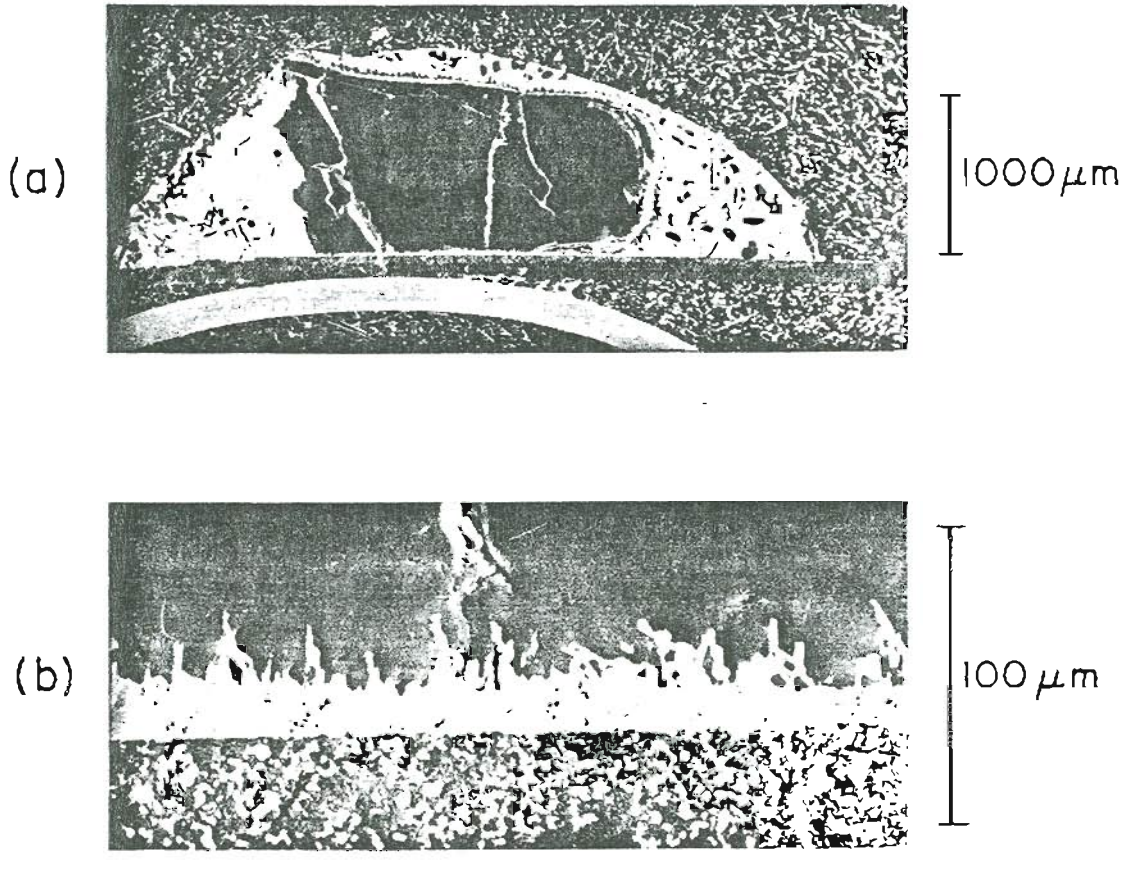

Figure 7-14. Wetting of Ni/B (OGC) to a disk of single-crystal B. (a) Alloy surrounding the boron disk, shown at center; (b) The alloy-filled boundary between the boron and the graphite ribbon.

hemisphere. A line of brightness contrast separating upper and lower hemispheres of the droplet also developed. SEM photographs of the situation are provided in Figure 7-15; the alloy droplet had broken away from the substrate during removal from the vacuum chamber. Auger analysis of the droplet while molten are given in Figure 7-16. The exact analysis locations could not be determined, and positions shown are indicative only. The outstanding feature is the large amount of N present in the spectra at all sampled locations. Further, there is evidence of competing chemical shifts due to formation of BN and B_4C in the alloy surface. Although the boron carbide surface was found to contain a small, nonvanishing concentration of N, there is little likelihood that the large concentrations of N found at the alloy surface originate from diffusion from the substrate. This is because for N to exist at high temperatures on the substrate, it must be bound as BN. Few other options exist for the origin of boron carbide and nitride in the alloy. These materials have been formed either during alloy synthesis or during the wetting process as a result of the complicated segregation forces that exist during alloy melting.

Wetting of Ni/B (OGC) to the surface of a boron carbide layer (LANL:"M") formed by chemical vapor deposition (CVD) onto a substrate of graphite showed little improvement (see Figure 7-17). Auger analysis of the molten droplet surface revealed high concentrations of C at all sampled positions, and a N signal that increased as the bottom of the droplet was approached. The bright/dark boundary was again observed, which may be formed by the presence of BN in this

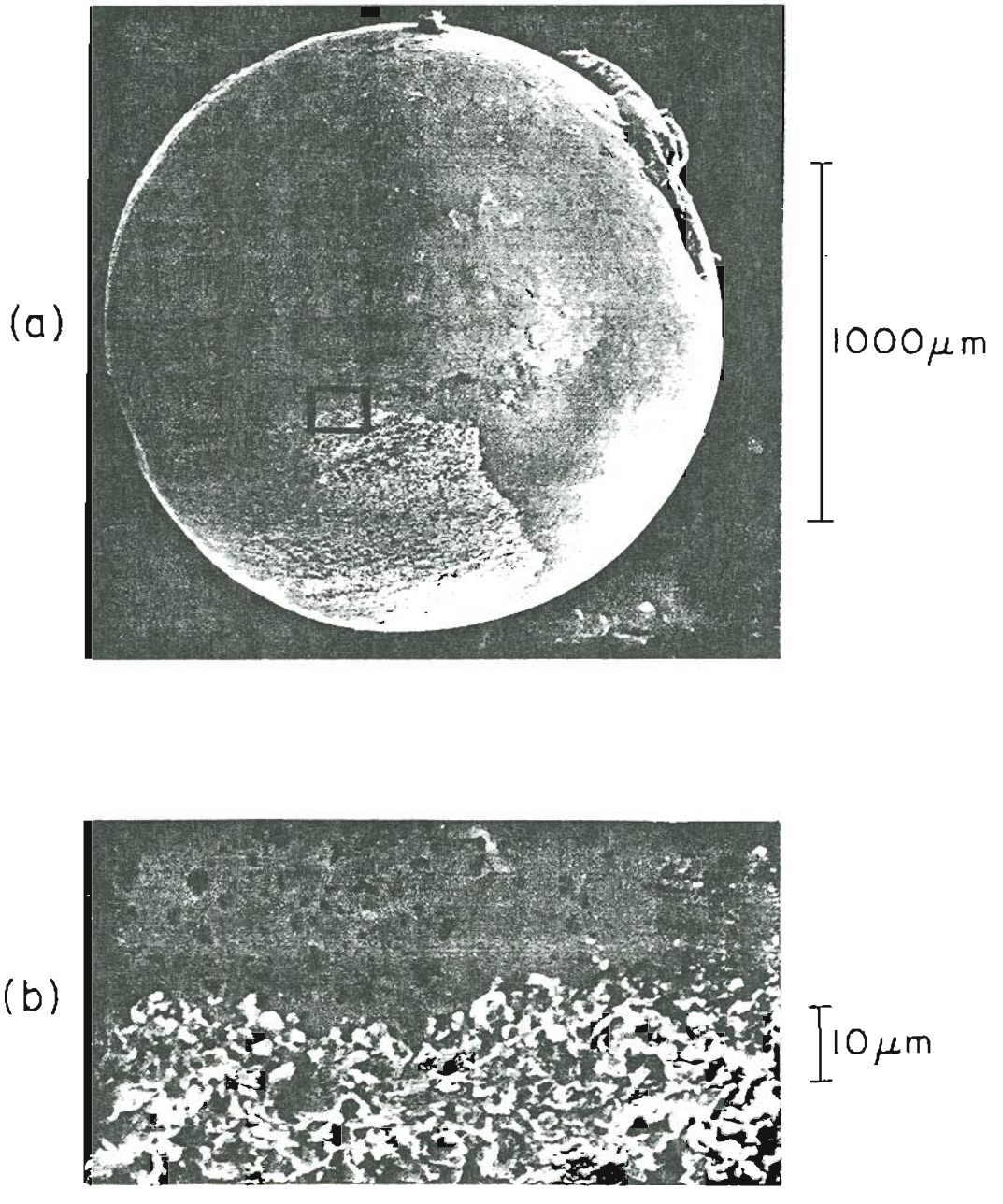

Figure 7-15. Ni/B (LANL) after wetting to B_4C (virgin). (a) Overall view of the poorly-wetted droplet; (b) An enlargement of the boxed area of photo (a).

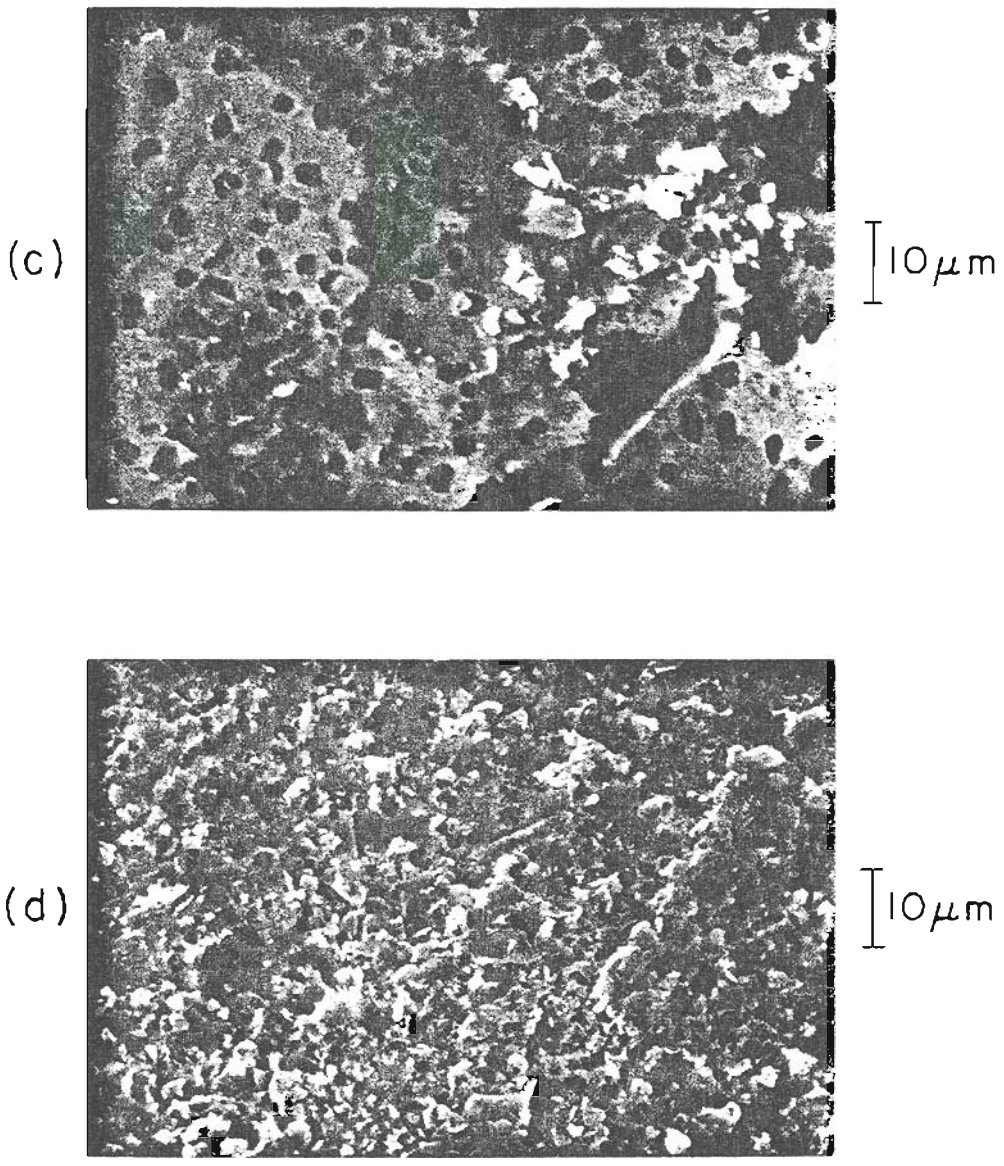

Figure 7-15 (continued). (c) A close-up of the upper half of photo (b); (d) A close-up of the lower half of photo (b).

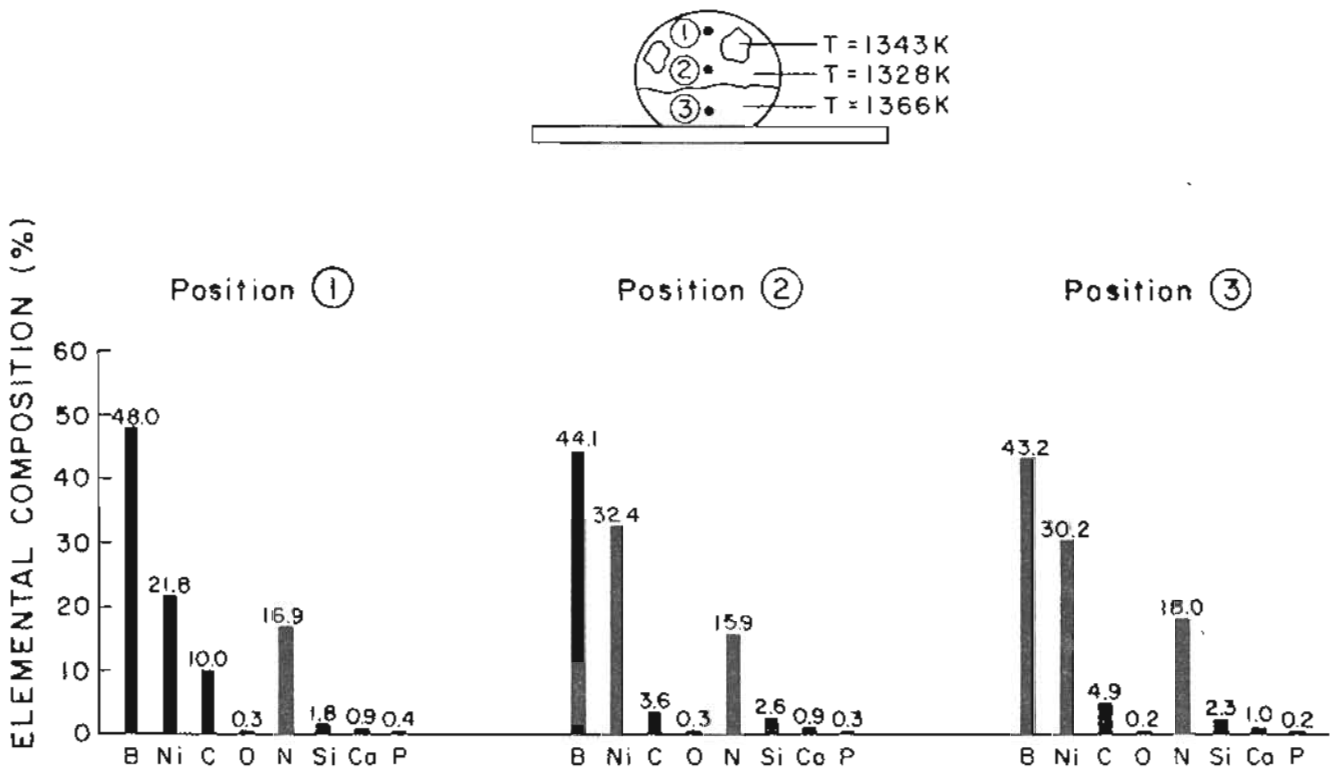

Figure 7-16. Auger surface elemental composition vs position for the poorly-wetted Ni/B (LANL) on B_4C (virgin) alloy during heating to 1350 K. Presence of both B_4C and BN are indicated in the Auger spectra.

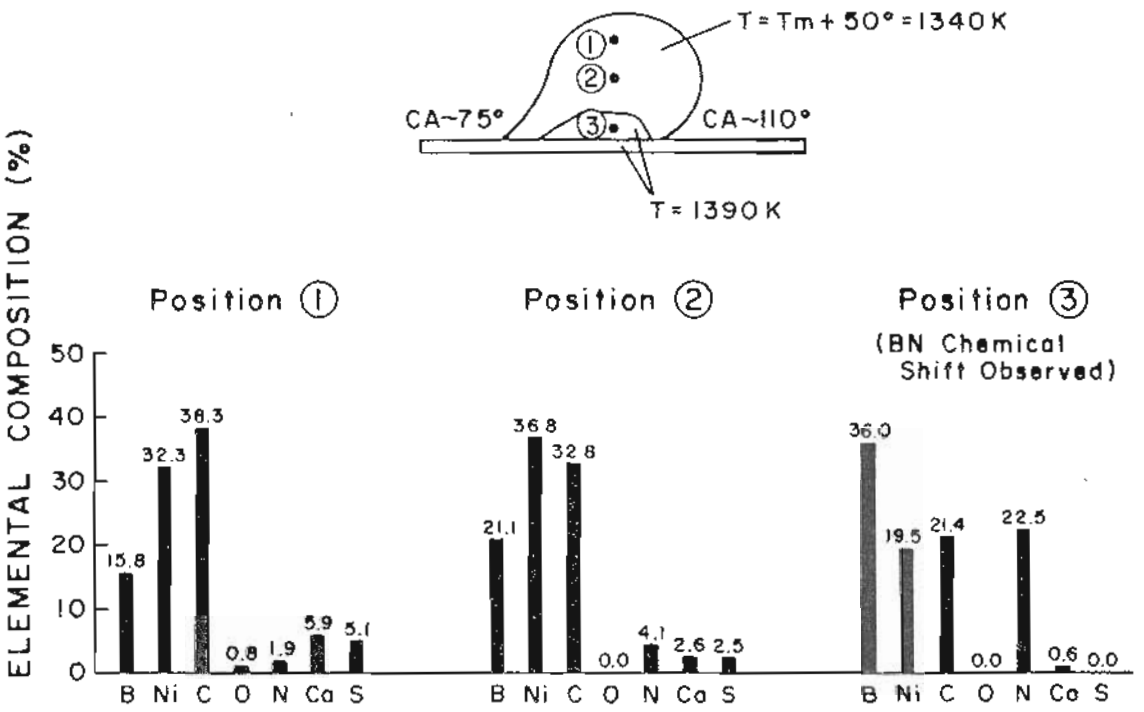

Figure 7-17. Auger surface elemental composition vs position for wetting of Ni/B (OGC) on CVD B_4C (LANL: "N").

case. Scanning electron micrographs of the droplet before and after sectioning are shown in Figure 7-18. Photos (c) and (d) are closeups of the microstructure, showing the presence of fractured blocks of material that appear to have formed during cooling.

Wetting of Ni/B (OGC) to single-crystal B_5C resulted initially in the establishment of a poorly-wetted droplet of alloy. The surface of the slab-shaped substrate before wetting is characterized in Figure 7-19. A position typical of the surface was probed by Auger spectroscopy as the temperature was increased. As more heat was applied, the surface approached the stoichiometric ratios, but nowhere was the ratio near 5 to 1. At approximately the melting point of Ni/B, the alloy sees a surface with near equal ratios of B and C. Chemical effects characteristic of carbide formation appear in the Auger spectra. Analysis of the molten alloy droplet (Figure 7-20) show large C concentrations over the entire surface of the droplet, accompanied by small amounts of N and Ca. Chemical shifts indicative of carbide formation are found at positions 2 and 3. The bright/dark boundary was observed. This situation remained for about 2 hours at the melting point.

At the end of this time, a sudden reduction in contact angle occurred, decreasing from about 130 degrees to 45 degrees. This is shown in Figure 7-21. A surface probe of the top hemisphere of the collapsing droplet showed nearly pure alloy components, while the lower half of the droplet still contained large concentrations of C with accompanying chemical shift. Once again it is found that

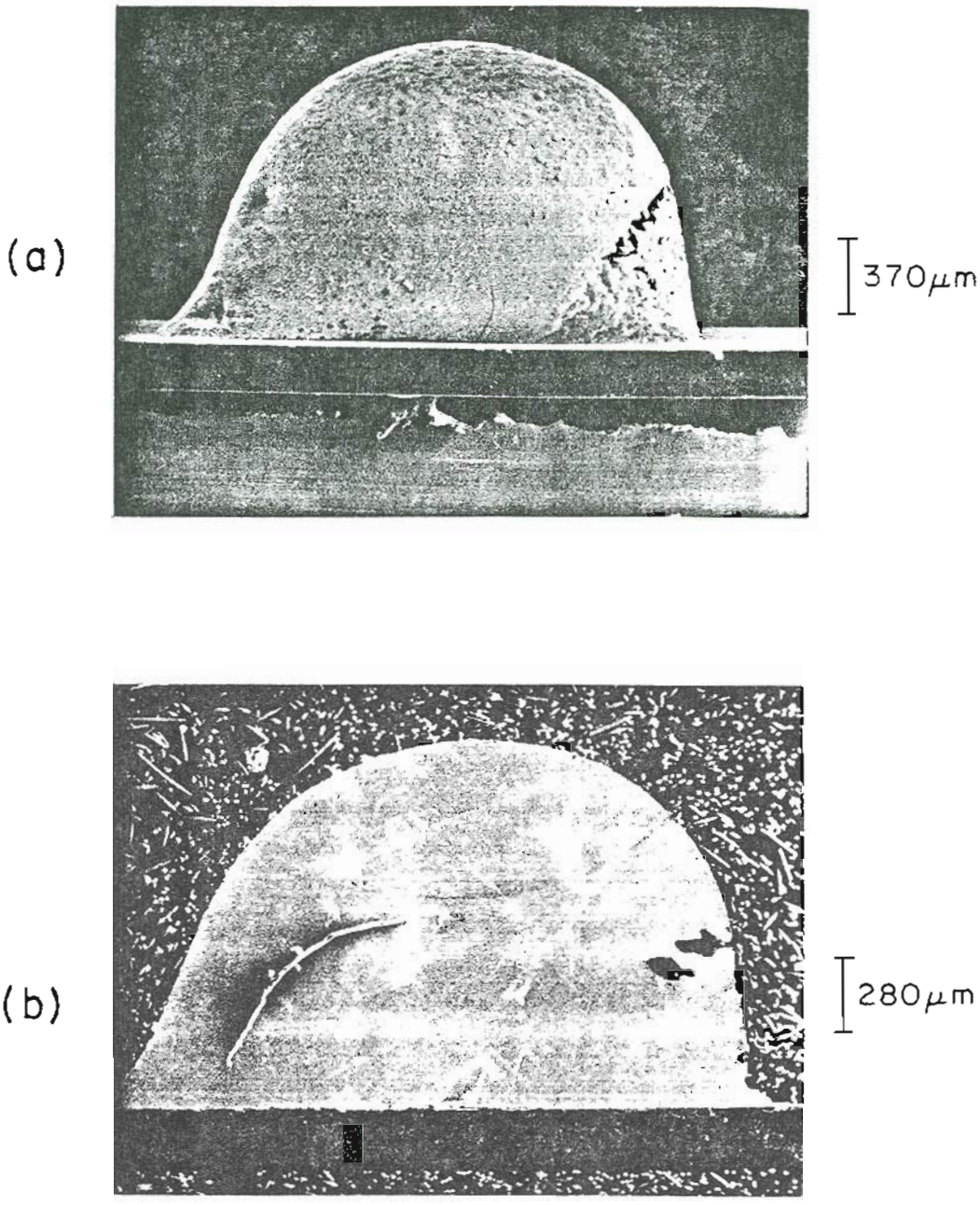

Figure 7-18. Wetting of Ni/B (OGC) to CVD B_4C (LANL: "M"). (a) Side view of wetting profile; (b) Cross-sectional slice through the droplet.

(c)

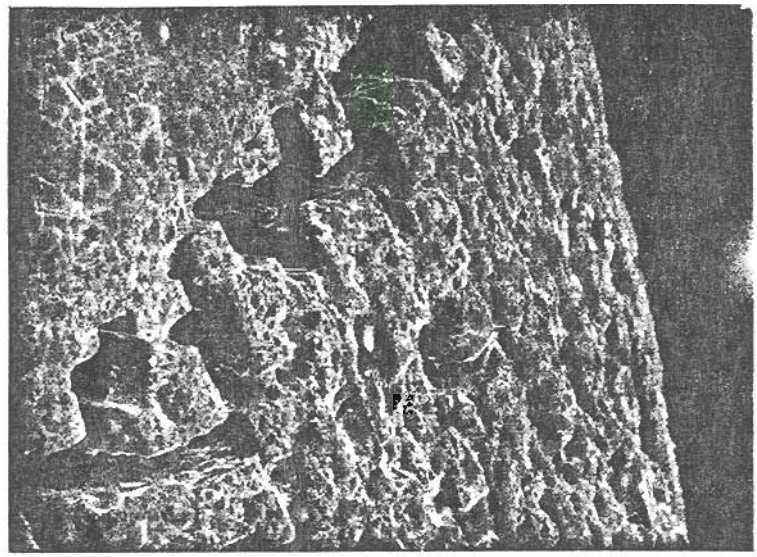

(d)

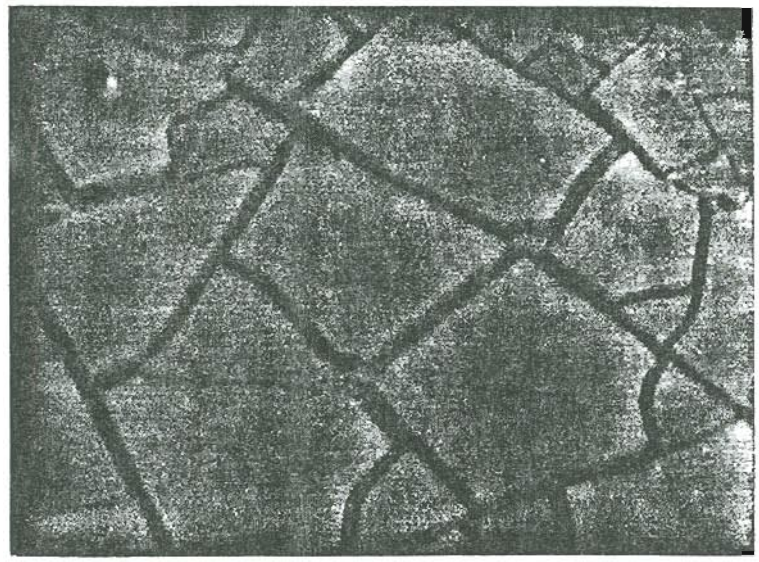

Figure 7-18 (continued). (c) View at the side of the poorly-wetted droplet; (d) High-magnification view of the fractured structure seen in (c).

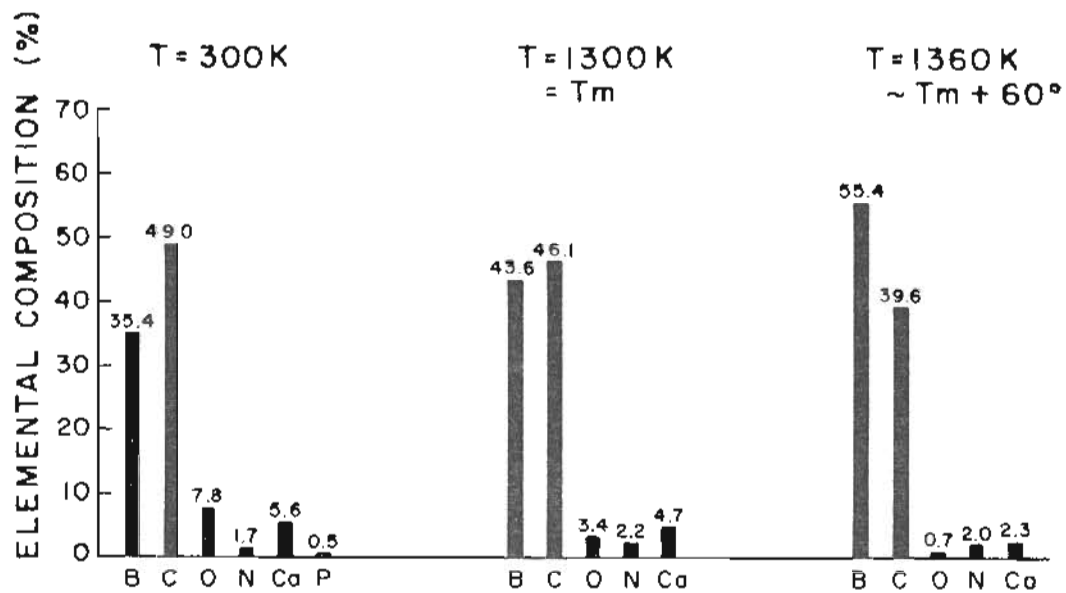

Figure 7-19. Auger surface elemental composition vs temperature for B_5C.

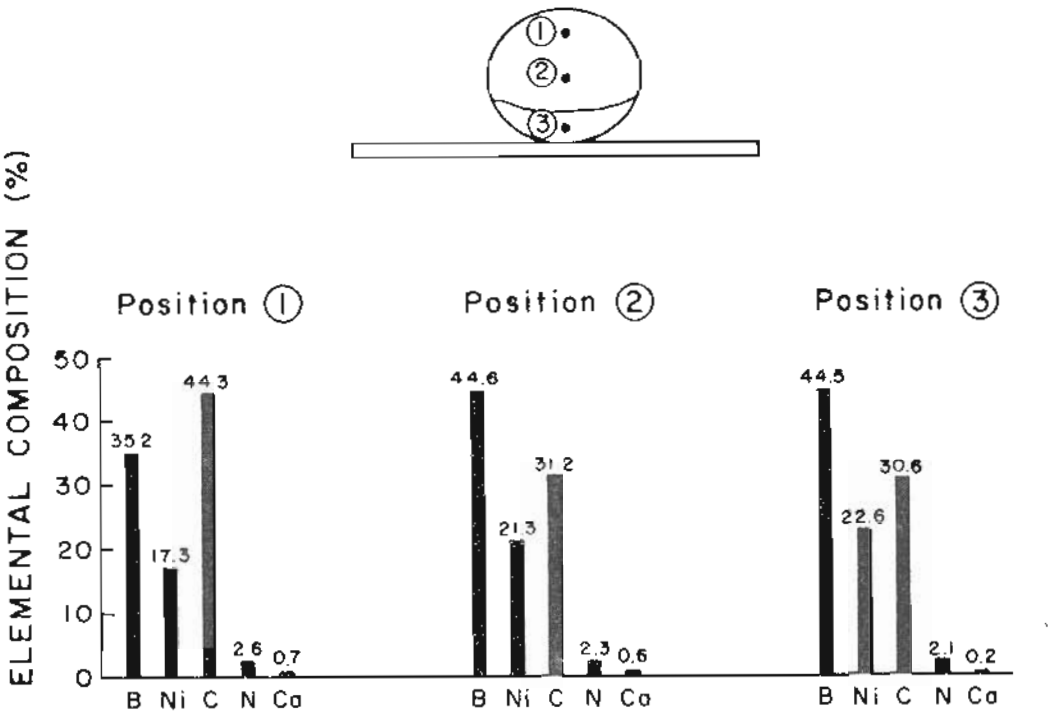

Figure 7-20. Auger surface elemental composition vs position for Ni/B (OGC) on B_5C. The temperature is $T = T_R + 10^o = 1302$ K. Carbide chemical shifts are found at positions 2 and 3.

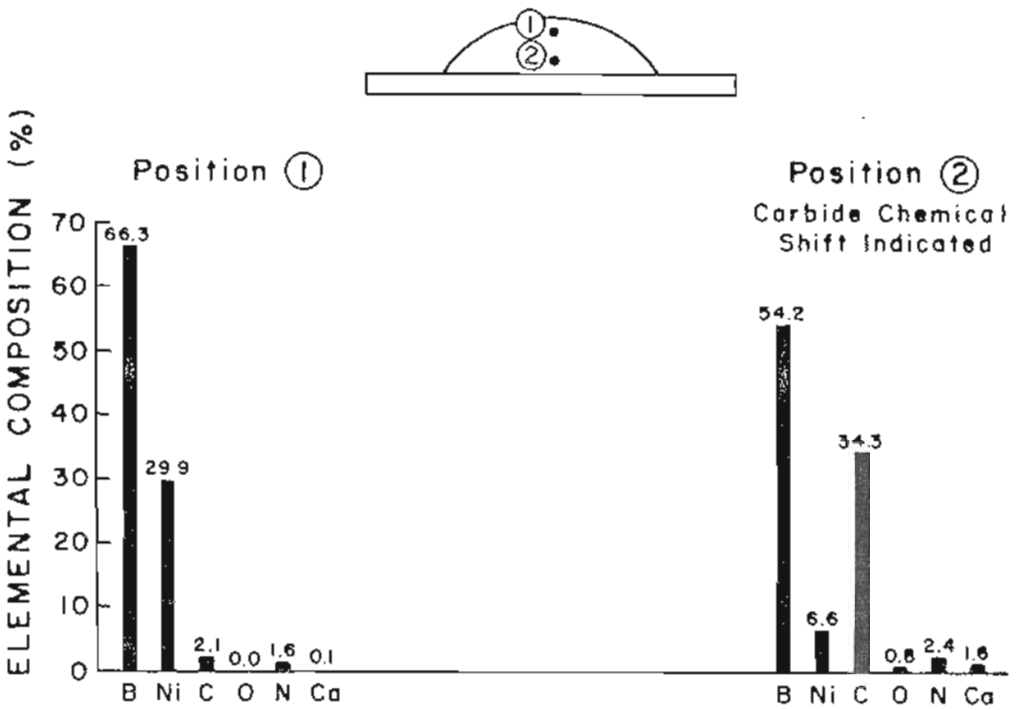

Figure 7-21. Auger surface elemental composition vs position for Ni/B (OGC) on B_5C after 2 hours at $T = T_m + 10^{\circ} = 1302$ K. The alloy contact angle has changed dramatically, with a decrease in C at the top of the droplet.

depletion of C from the droplet surface and wetting appear to be connected.

A final piece of information from this experiment concerns alloy wetting to the backside of the B_5C ribbon. On this surface had been painted a slurry of nonfluxed Ni/B powder in order to compare the wetting of a solid specimen of alloy (on the frontside) to a powdered specimen of alloy (on the backside). Scanning electron micrographs of the results are shown in Figure 7-22. In like fashion to the frontside wetting, the initial wetting behavior of the powdered alloy was poor. As time progressed, however, the powders displayed increasing adhesion to the substrate and the wetting was qualitatively better than that displayed by the solid specimen of alloy. Perhaps a higher temperature during the initial wetting would have facilitated faster results.

In summary, the results of these experiments are generally mixed with respect to using compounds of boron as a viable wetting surface. Wetting is substantially better on B_5C than on B_4C, but not as good as wetting on the single-crystal of B nor on the boronized graphite surface of nearly 100% B. Further, it is difficult to envision a feasible method for machining B_5C into usable emitter shapes, as this material is extremely hard and nearly impossible to grind using conventional techniques. We show below that, for wetting to occur, it is necessary that substrates contain free boron in order to tie up the segregated carbon. Boron which is chemically bound, such as exists in the case of carbides of boron, requires additional energy to dissociate and reform bonds with the

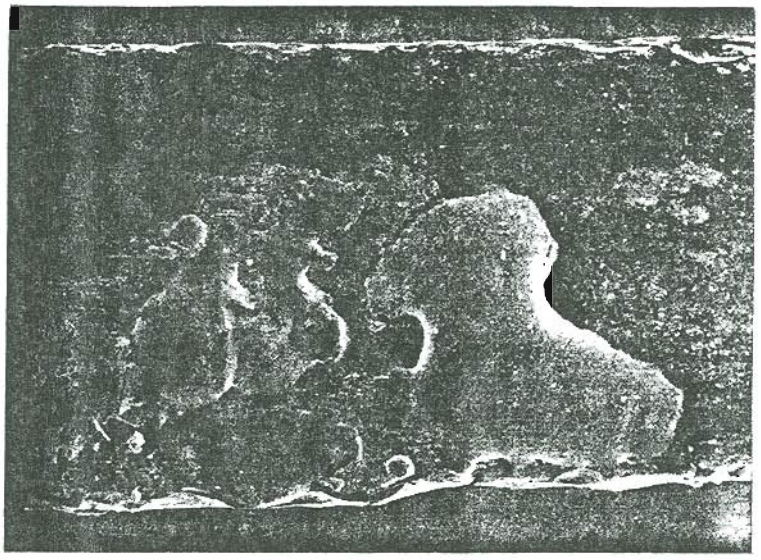

Figure 7-22. Wetting of Ni/B (OGC) to B_5C. (a) Wetting of Ni/B (fragment) to the topside; (b) Wetting of Ni/B (powder) to the backside.

segregated carbon, B_4C, and BN. Wetting is facilitated in contact systems where this additional expenditure of energy is not required.

7. Wetting of Pd/B to a Siliconized Graphite Emitter

Experiments using a thin coating of silicon rather than boron were performed to determine whether the improvement in wetting by way of a coating of boron is specific to boron alone. In other words, may another element with similar thermochemical properties be utilized to facilitate wetting of liquid metal alloys with segregated surfaces of carbon, BN, and B_4C? This question is more than casually interesting, as identification of such a material would provide an optional method by which to facilitate wetting of boron-containing alloys to graphite-based substrates. Further, Ishitani [14] has reported preliminary measurements of the emission characteristics of a LMI source of B using a ternary alloy of Ni, B, and Si.

Figure 7-23 shows several SEM micrographs of a carbon emitter wetted with a $Pd_{72}B_{28}$ (LANL: #273-24) alloy. The photos were taken after 100 hours of heating at a temperature of 30 degrees above the alloy melting point. The wetting procedure consisted of coating a graphite emitter with a slurry of powdered Si and propanol, which was then heated to the melting point of Si. At melting, the Si wets and spreads superbly over the graphite substrate, forming a thick layer that Auger spectroscopy demonstrated to be predominantly Si. The interfacial compound which forms during wetting is SiC, which was

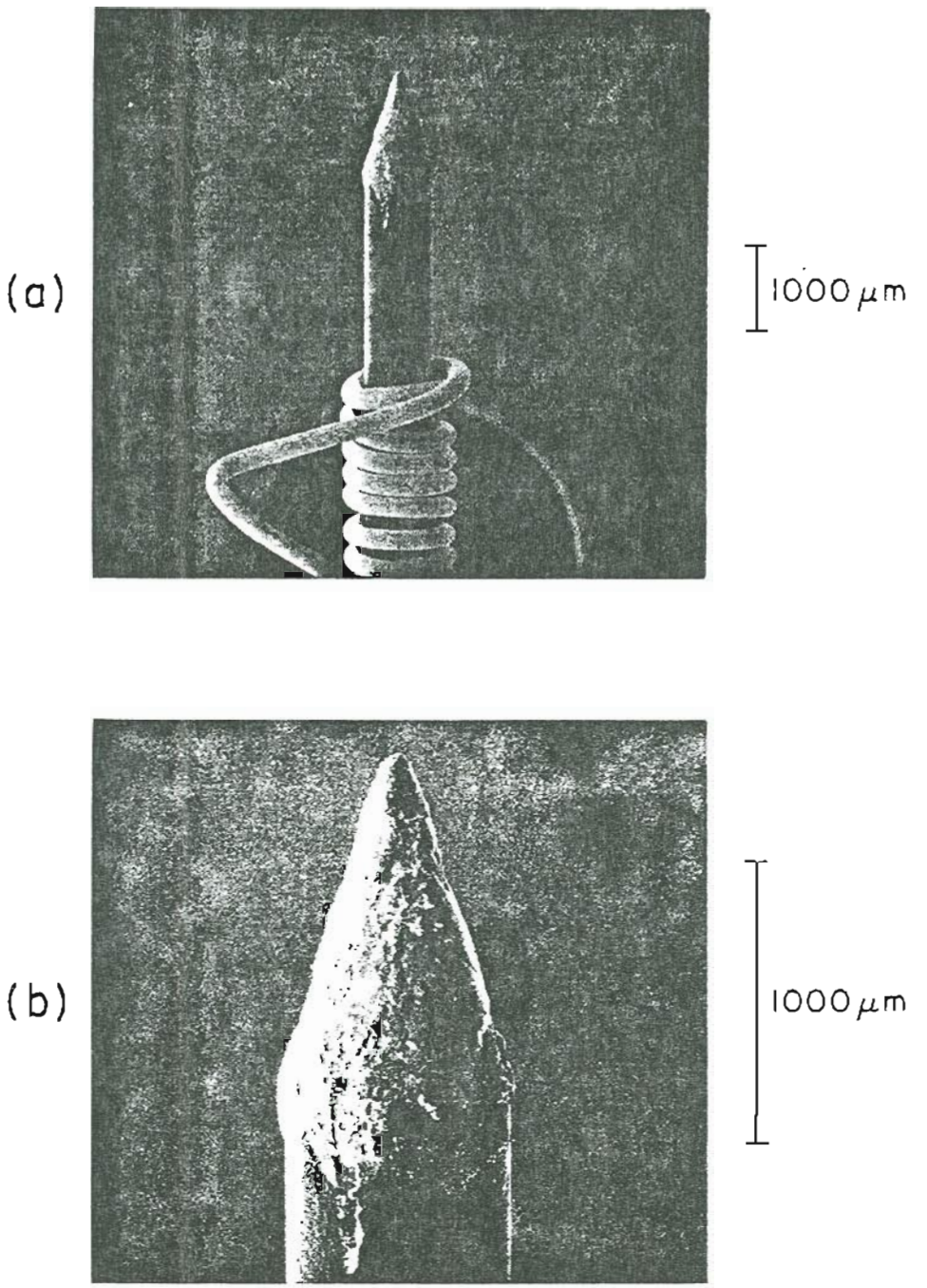

Figure 7-23. The wetting of a siliconized graphite emitter with $Pd_{72}B_{28}$ (LANL: #273-24) after 100 hours of heating at a temperature of $T = T_m + 30^{o} = 1200$ K.

verified by flashing off the free Si. The wetting surface therefore consists of an interfacial compound of SiC covered by a thick layer of free Si. At this point, the Pd/B alloy was added in powdered form with propanol, and then electron bombarded until the alloy melted. Frequently, this latter step was repeated to elicit best wetting. Electron bombardment heating yields superior results to resistive heating, probably because the side of the alloy away from the substrate melts first.

The melting point of Pd/B on Si proved to be about 150 degrees lower (1165 K) than the melting point of Pd/B alone (1310 K). Apparently, the dissolution of silicon in the binary results in formation of a lower-melting ternary composition. As may be seen in Figures 7-24, the wetting characteristics of this solution are excellent on the siliconized graphite, consisting of a uniform coverage over the wetted tip. Although the alloy does not appear to have spread beyond the location of the siliconized layer, we have found this to be true for other cases we have studied.

Figure 7-25 shows the results of an experiment designed to investigate the alloy surface as a function of temperature. The alloy surface elemental composition was monitored by Auger spectroscopy as the temperature of the alloy was first increased, then decreased. Numerous observations may be noted. First, the Si concentration at the surface is surprisingly low, considering the reduction in melting point. That larger amounts of Si are present in the bulk is verified by mass spectrometer studies of the emission characteristics of this contact system, which reflect the bulk

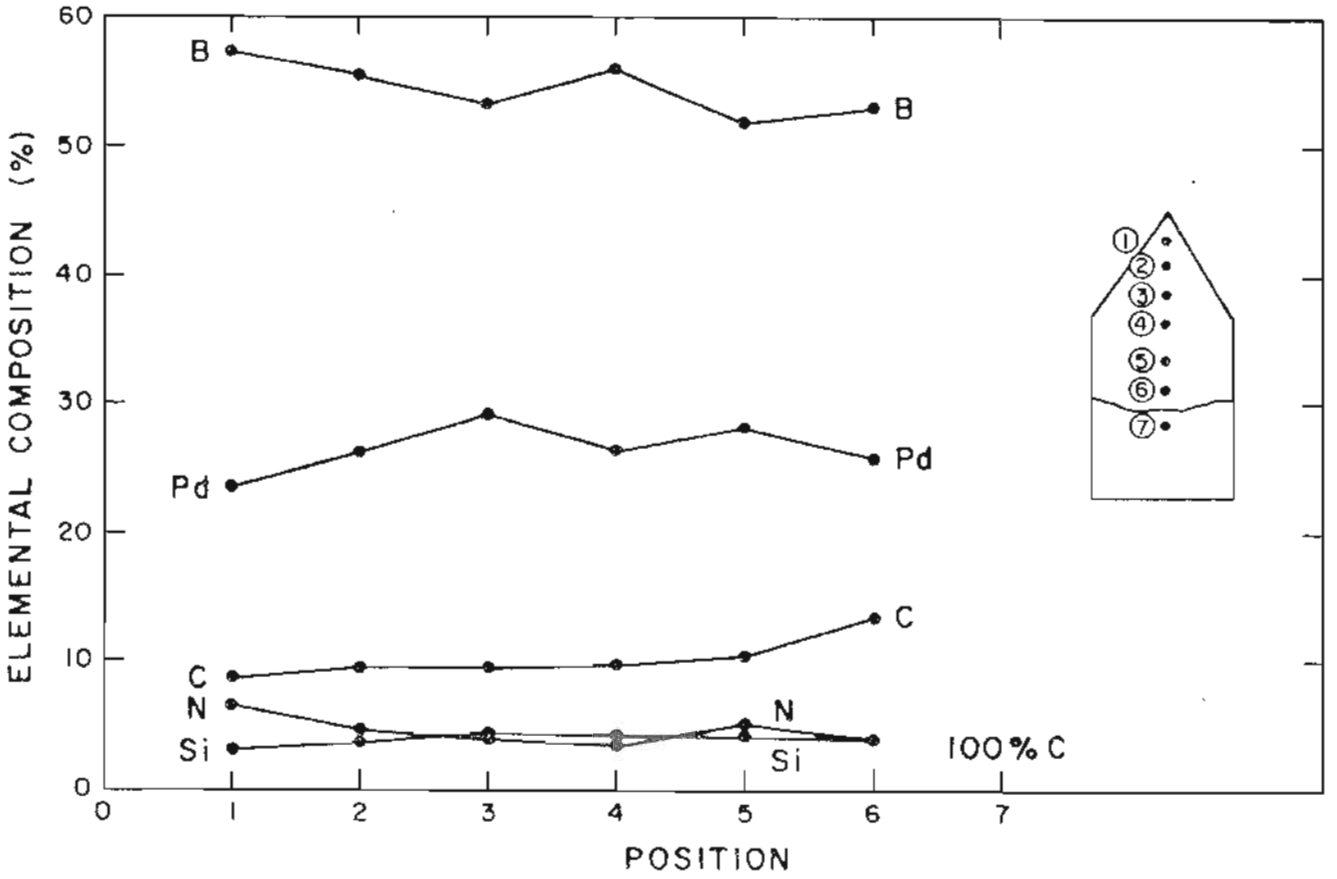

Figure 7-24. Auger surface elemental composition vs position along a siliconized graphite emitter wetted with $Pd_{72}B_{28}$ (LANL: #273-24). The temperature is $T = T_m + 50^o = 1220$ K.

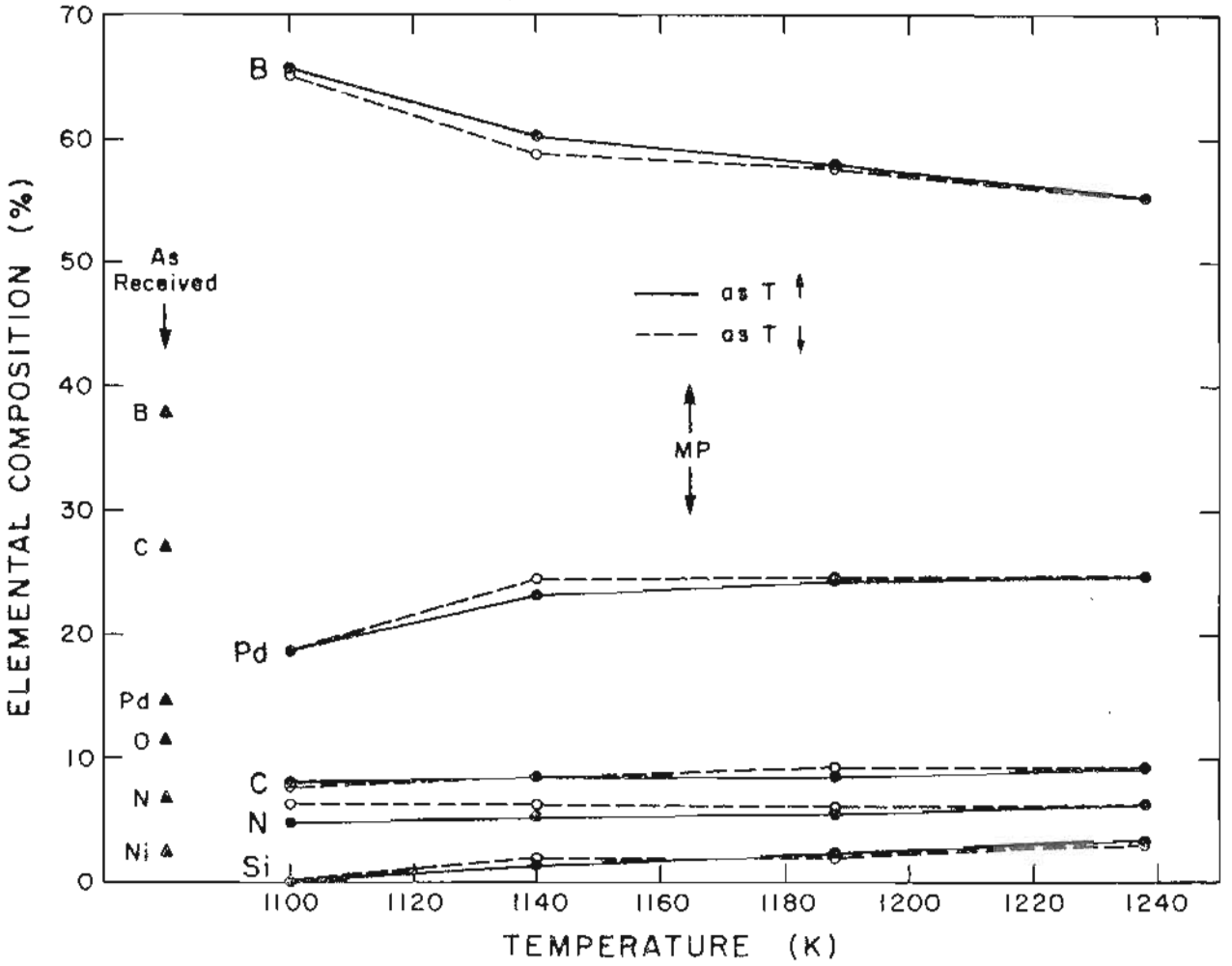

Figure 7-25. Auger surface elemental composition vs temperature for $Pd_{72}B_{28}$ (LANL: #273-24) on a siliconized graphite emitter. The position monitored remained fixed. Oxygen and nickel remained less than 5% throughout the temperature range and are not plotted.

stoichiometry. Significant amounts of Si are found (see Table IX). Second, the boron surface concentration is significantly enriched relative to the stoichiometric ratios for this alloy. This arises from surface segregation of boron, which is expected because boron is a nonmetal and has a much lower surface tension than palladium. Third, no significant changes occur in the surface composition as the melting point of the alloy is crossed, and the composition is highly reversible. Fourth, the C and N surface concentrations are substantially lower than the concentrations which result when Pd/B is wetted to virgin graphite. This means that the Si is tying up the segregated C at the liquid-solid interface in much the same way that the free B in boronized layers ties up C. This is not unexpected, since boron carbide and silicon carbide have nearly identical Gibbs free energies of formation at these temperatures. Hence, silicon appears to react with segregated C in a way similar to boron in the contact systems.

TABLE IX

RELATIVE AMOUNTS OF VARIOUS ELEMENTS IN THE ION BEAM OF $Pd_{72}B_{28}$ AT 20 MICROAMPS TOTAL CURRENT AND 1165 K

Species	% of Total	FWHM (eV)
Pd^+	66.9	32.8
PdB^+	16.2	
Pd^{++}	6.39	20.16
B^+	3.74	9.68
Si^{++}	3.74	14.0
Pd_2Si^+	1.67	
Si^+	1.20	15.4
Pd_2B^+	0.279	
BO^+	0.223	
$PdSi^+$	0.197	
Si_2^+	0.167	20.12
$PdSiB^{++}$	0.0149	
B^{++}	0.0055	6.98
SiB^+	0.0054	32.7

Peaks identified, but not measured: B_2^+, $PdSi^+$, Pd_2^+, Pd_3^+

Total Pd = 77.4; Total B = 16.5; Total Si = 6.0.

Long-term heating of the emitter at a temperature of 50 degrees above the melting temperature of the alloy shows little change in surface composition vs time (see Figure 7-26). In particular, no evidence of substrate attack or variation of heating power requirements were observed. In addition, little dissolution of the alloy into the graphite is indicated. This contact system therefore possesses low chemical reactivity and good wetting behavior and offers a potentially long-lived source of B. An added advantage is that the addition of the silicon layer lowers the melting point of

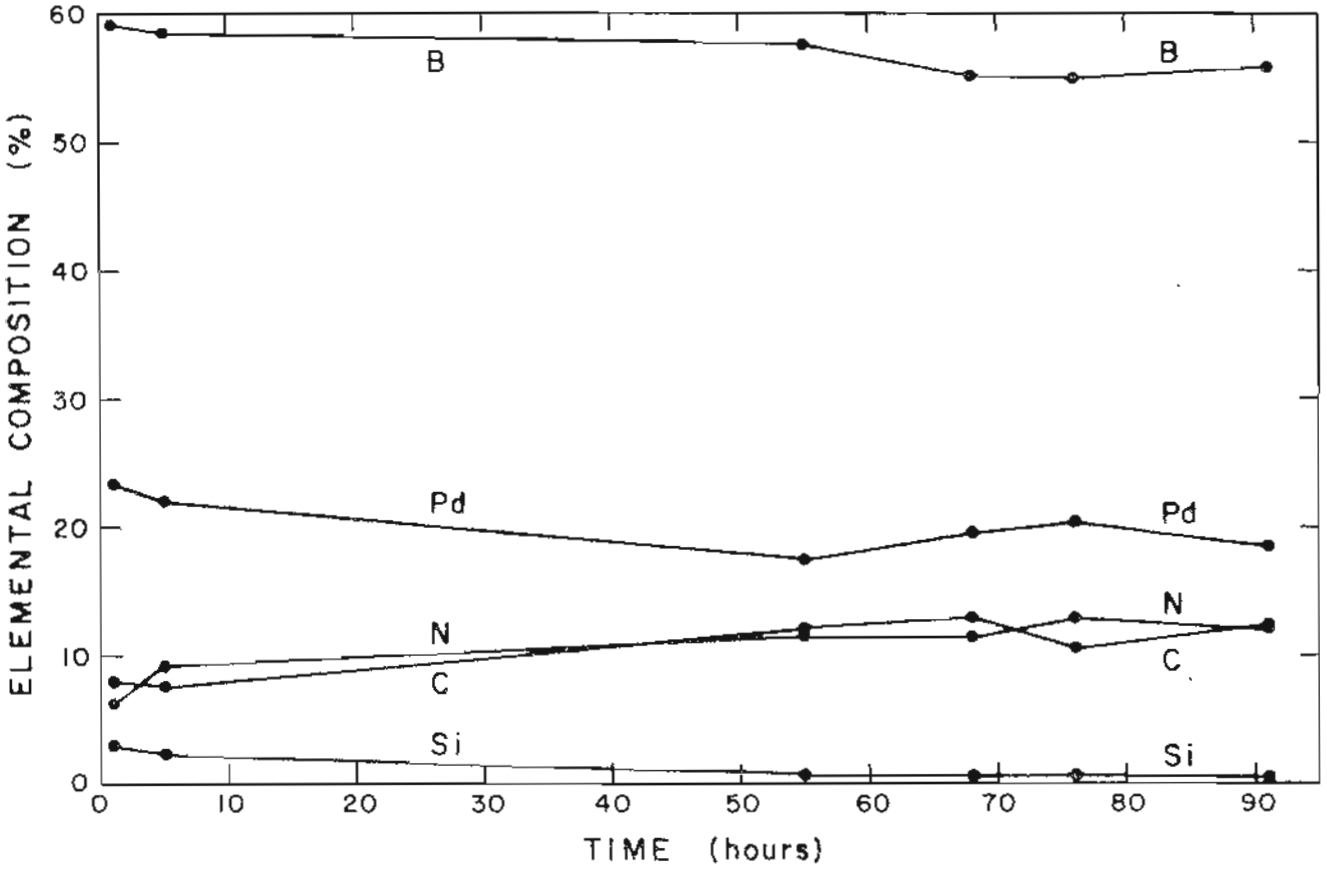

Figure 7-26. Auger surface elemental composition vs time at a fixed analysis position for $Pd_{72}B_{28}$ (LANL: #273-24) on a siliconized graphite emitter. The temperature remained constant at $T = T_m + 50^o = 1220$ K.

the alloy. Whether the ion emission contains adequate amounts of B^{+} and B^{++} species for most implantation applications remains to be answered. Preliminary mass spectrometer results indicate that a significant fraction of the B is tied up as PdB^{+}.

D. The Reason: An Explanation of Boronization and Siliconization and its Effect on Wetting

Enough information presently exists to enable substantial progress to be attained by way of understanding the complex thermochemistry governing the wetting of solid substrates by liquid metal alloys. The formidable variety of diverse phenomena observed throughout this study may now be elucidated through proper understanding of the roles of boron and surface segregation. The resultant model of surface behavior elucidates the mechanism of boronization, and explains the various classes of wetting behavior found in the early work. The results and model details are summarized in the answers to a series of pertinent questions. In short, the existence of surface segregation explains nearly all of the wetting phenomena observed throughout this study.

1. Question #1: What Prevents B-Containing Alloys from Wetting Virgin Amorphous Graphite?

Surface segregation of carbon and nitrogen in the form of C, B_4C, and BN is the primary cause for wetting failure in contact systems composed of liquid metal alloys and graphite. We say that

nitrogen in the form of BN segregates because it is unlikely that N exists in the alloys in its elemental form. When the melting temperature of the alloy is reached during the initial wetting process, carbon and nitrogen present as low-level alloy impurities immediately segregate to the surface. The resulting surface layer of carbon, boron nitride, and boron carbide inhibits interaction between the alloy components and the substrate, and results in an unfavorable combination of surface tensions. Wetting is subsequently prohibited. We saw earlier that the small amount of C impurity present in the OGC alloy material is enough to create a surface layer of over 1000 A around an alloy droplet of typical dimensions if it all segregated. The experimental evidence supports this view, as many of the poorly-wetted alloy droplets were found to contain a surface film of C surrounding the relatively pure alloy material. Carbon which enters the alloy due to dissolution from an outside source such as the substrate also appears to segregate, as numerous instances exist which show that most of the dissolved C ends up at the surface of poorly-wetted droplets in contact systems which have been heated to high temperatures. In only one case have we found significant boron carbide formation within the bulk of the alloy, and in that case, a large fraction of the graphite substrate had been dissolved by the alloy.

Boron nitride and boron carbide possess favorable Gibbs free energies of formation and may be expected to form during the arc melting process and at temperatures near the melting points of Pt/B and Ni/B (see Chapter 9). Once formed, these materials segregate as

the alloy is liquified. This is the primary reason why many of the alloy droplets in the early HRL work were covered with hard shells of boron nitride and carbide. Surface segregation of low-level C and N impurities further explains why the interior of most of the poorly-wetted droplets of alloy contained alloy material of high purity which was found to wet virgin graphite as the droplet film was penetrated by pure alloy after prolonged heat treatment. This is because carbon and nitrogen were tied up in the surface shell and not in the bulk of the alloy. When the alloy is rid of these materials, it wets virgin graphite.

A second possible mechanism contributing to wetting failure is mechanical "ruboff" of carbon, described earlier. This hypothesis was originally proposed to explain the discontinuity in brightness temperature found in many poorly-wetted alloy droplets, which were often found to contain larger concentrations of C in the bottom (bright) regions of the droplets than in the top (dark) regions. Later work, however, showed that lines of brightness discontinuity exist in droplets having uniform distributions of C, and in alloys such as Pt/B on vitreous carbon which display so little affinity for the substrate that it is difficult to believe that substrate carbon is mechanically pulled up into the alloy droplet. Further, carbon ruboff is unable to explain why alloys that wet virgin graphite do not also suffer carbon ruboff. The postulate of mechanical ruboff is therefore an unlikely explanation for the behavior of most contact systems. From the present perspective, the mechanism of surface segregation is adequate to explain nearly all of the observed

phenomena found in the alloy systems.

2. Question #2: How do Boronization and Siliconization Facilitate Wetting?

Free boron and silicon act in similar ways to facilitate wetting of liquid metal alloys of boron to graphite. We use boron as the example for the explanation. When a uniform layer of boron is applied to a graphite substrate, the effect is to replace the graphite substrate with a more chemically reactive boron substrate at the point of wetting. This acts to tie up alloy carbon (and, to a lesser extent, nitrogen) which would otherwise segregate, by formation of interfacial boron carbide and nitride. The resultant chemical reaction is precisely what is necessary for wetting. It has been shown above that during wetting on a boronized layer, the C Auger signal from the alloy surface characteristically drops to near-zero in comparison to the situation on unboronized graphite, where the surface of the alloy is typically covered with a thick layer of segregated carbon. Further, Auger analysis of the interior of a number of alloy specimens after heating shows that the interior of the alloys are nearly impurity-free. If the low level of carbon inherent in the alloy is not at the surface nor in the bulk of the alloy, the only other place for it to exist is at the interface between alloy and substrate. Boronization therefore works because the alloy chemically reacts with the boron surface. A C-C nonreaction is replaced by a C-B or C-Si reaction. That the process

is not specific to boron is further support of this view.

Thermodynamically, the energetics for such a mechanism are favorable. The Gibbs free energies of formation for boron carbide, boron nitride, and silicon carbide are all favorable at the melting point of B-containing alloys. Further, assuming the following reaction mechanism, an increase in the boron activity at the interface will shift the reaction to the right, which reduces the dissolved and precipitated carbon in the alloy:

$$C'' + 4B' = B_4C'' \qquad K = K(B_4C'')/K(C'') = 1/A(B')^4$$

where single primes refer to "in solution" and double primes refer to the solid phase, A is the activity, and K is the equilibrium constant. The carbon that has been shown to surface segregate on an unboronized substrate is instead tied up at the interface to form boron carbide or silicon carbide. Together, these mechanisms act to promote wetting.

This theory of the role of surface segregation on wetting has been criticized by Storms [15] of the Los Alamos group, who suggested that it may be the presence of small impurities in the boronized layer that promotes the wetting, not the interaction of C at the interface to form boron carbide. In response, we cite three observations which support our position: (1) No evidence has been found to indicate the existence of such contaminants in Auger spectra of the boron used to form the boronized layer; (2) The wetting action is independent of the source of boron. It is unlikely that the same contaminants exist in the four different sources of boron we have tested in our experiments; (3) The wetting action is not

specific to boron. Other elements such as silicon with similar thermochemical properties can be substituted which result in similar wetting behavior. A weakness of our position has been the inability to characterize the interface between alloy and substrate experimentally. We have been unable to effectively analyze the complex structure of the interlayer due to the roughness of the boronized layer and the resolution limitations of accessible instrumentation.

3. Question #3: Why does the Alloy Subsequently Wet and Spread Over Virgin Amorphous Graphite?

Numerous instances exist where the alloy has been found to spread far past the boronized layer and onto virgin material with no change in wetting behavior. In other words, the alloy needs a boronized surface during the initial stages of wetting, but then is able to wet an unboronized surface. This peculiar behavior may be explained by the action of the segregated carbon with the boron layer. In essence, the presence of free boron at the interface provides a gettering action for the segregated surface carbon which develops at melting. We have seen above that the thermochemistry is favorable for reaction of carbon with boron and silicon to form stable compounds at the interface. This mechanism acts to purify the alloy and tie up the carbon shell that would otherwise prevent wetting. When the alloy is pure, it wets virgin graphite because there is no more segregated material to contend with and direct interaction of

the alloy components and the substrate is possible. Further, at temperatures near the melting point of the alloy systems, there is little dissolution of C from the substrate. We showed above that the wetting of metallic alloys of Ni and B is expected both from the point of view of existing experimental evidence and present theories of wetting.

4. Question #4: What Prevents B-Containing Alloys from Wetting Substrates that they "Should"?

We can now provide reasons for wetting failure of alloy/substrate systems which both theory and experiment predict should possess low contact angles. The answer is that surface segregation of low-level impurities in the alloy inhibits the reaction between alloy and substrate and creates an unfavorable combination of surface tensions. Recall that in the chemical wetting process, a chemical reaction is required to occur which forms chemical bonds between one or more components of the alloy and substrate. If a segregated layer of carbon forms at the interface, these reactions are inhibited, and the alloy does not wet at the melting point. Only by increasing the temperature can the reaction eventually succeed, but then the rate of carbon dissolution in the alloy increases. The addition of boron, on the other hand, acts to tie up the carbon that would otherwise segregate. Examples of substrates which are expected to possess favorable contact angles with alloys of Ni and B are chromium carbide, zirconium carbide, graphite, aluminum oxide, and others (see

the Appendix). Our work with these materials has shown that the systems possess poor wetting characteristics with droplets of material covered with carbon and nitrogen. In short, the phenomenon of surface segregation is the dominant mechanism affecting the wettability of solid substrates by liquid metal melts.

5. Question #5: Why do the Alloys Begin to Wet, but then Form Poorly-Wetted Dropleta?

The behavior referred to here concerns the action of solid specimens of alloy at the point of wetting. At the melting point, the alloy typically acts as though it intends to wet the substrate. It begins to collapse toward the substrate, but then immediately pulls back into itself and forms a poorly-wetted droplet. The entire process is extremely rapid, occurring in a span of time of the order of a second. This behavior may be explained by the speed of surface segregation in the liquid alloys. During the first instant that the alloy is molten, segregation is incomplete and the chemical reaction between the alloy components and the substrate begins to occur. The result is that the alloy starts to wet the substrate. During the next instant of time, however, the segregated species are sufficiently concentrated and alter the surface tension of the system. The alloy then draws back into itself. If, rather then surface segregation of carbon, dissolution of carbon from the substrate is the dominant thermodynamical mechanism at the melting point of the alloy, then a similar result is expected. It was shown

earlier that during dissolution of the substrate in the alloy, the liquid-solid surface tension first decreases and then increases; this could also explain the observed results.

6. Question #6: Why does Boron Fluxing Appear to Facilitate Wetting?

Our results indicate that mechanical addition of 3% B to the powdered alloys has no effect on wetting to boronized substrates. In the case of alloy wetting to virgin graphite and mixtures of C and B (nonideal boronization), however, 3% B-fluxing does appear to cause a slight improvement in the wetting. This may be explained in a fashion similar to that described above. During surface segregation of carbon in the alloy, the excess boron reacts with the carbon impurities and improves the wetting by reducing the segregated carbon. We have shown that both LeChatelier's principle and the free energies of formation of B_4C and BN are consistent with this interpretation. When the carbon content of the alloy is lowered, wetting improves. This has been observed experimentally on several occasions. A related question concerns the spatial distribution of the added boron in the contact system. We have seen above that the addition of boron to the bulk of the alloy provides a small improvement in wetting on carbon, but a thick layer at the interface dramatically improves the wetting. Why does it matter where the boron is placed? In answer, the location of boron is important because wetting is an interfacial phenomenon. When added to the

interface between alloy and substrate, boron is located precisely where chemical reactions are required for wetting and spreading. When boron is added to the bulk of the alloy, a small improvement is seen because of its gettering effects with segregated carbon, but reaction at the interface is what is needed for large improvements in wetting.

7. Question #7: What is the Cause of the Differing Degrees of Wetting Success Found in the Early HRL Work?

Our evidence suggests that the various degrees of wetting found in the early experiments correspond to how closely the HTF technique came to producing a uniform B layer. It has been demonstrated above that flashing to high temperatures produces a type of boronized layer that is not only unnecessary, but also impossible to reproduce. It is not necessary to melt the boron to promote the wetting, nor is high temperature processing required. A uniformly distributed boron layer is the key expedient. Flashing merely increases the risk that most of the boron will be evaporated during the process, creating the uncontrollable wetting observed in the early work. "Ideally" boronized substrates correspond to surfaces where little B was evaporated. "Non-ideally" boronized substrates correspond to surfaces with mixtures of C and B which were created by irreproducible factors inherent in the flashing process. These factors include the thickness of the boronized layer, the dwell time and temperature of the HTF, the degree of boron vaporization, and the

uniformity of the resulting layer. Not one of these factors was easily controllable in the HRL procedure.

8. Question #8: Why do Alloy Powders Wet Better than Solid Alloy Specimens?

The behavior here refers to the ability of powdered specimens of alloy to wet better than single alloy fragment on identical surfaces. Several contact systems showed improved wetting when the alloy was first ground into fine powder in a mortar and pestle before application to the substrate. The best evidence is provided by wetting of Ni/B alloy to B_5C, described above. In this experiment, a single alloy fragment was applied to the top of the substrate, while powdered alloy was painted on the backside. Although wetting was reluctant for this system, the powdered alloy possessed the more favorable contact angle. On the microscopic scale, this behavior is easy to understand, because powders possess a larger surface area in contact with the substrate. A larger surface area provides a larger catalytic potential for interaction, and promotes reaction between alloy and substrate.

On the other hand, the impurity segregation to the surface of an alloy fragment depends upon the volume to surface ratio of the fragment. Assuming spherical fragments, this ratio is proportional to the radius of the fragment, meaning that the smaller the fragment, the smaller the coverage of contaminant on the surface. More of the pure alloy is then exposed to the substrate, and better wetting results.

9. Question #9: Why are Surfaces of Free B and Si Necessary to Promote Wetting?

It has been shown that surfaces with uniform coatings of free B and Si are necessary to facilitate wetting. Surfaces where these elements are largely flashed away, or surfaces consisting of carbides of B or Si result in poor wetting. Experiments documenting this behavior have been reported above. Wetting of Ni/B to surfaces of B_4C and B_5C resulted in formation of poorly-wetted droplets of alloy. In contrast, when wetting Ni/B to surfaces of crystalline boron and boronized carbon, excellent wetting was observed. Similar behavior was found for wetting to an interface of SiC and siliconized carbon. The explanation of this behavior lies in the energetics of the two situations. Recall that wetting is dependent upon the relative magnitudes of cohesion and adhesion in the contact system. In particular, good wetting results when the adhesion between substrate and alloy is greater than the cohesion of either material. This means that the wetting of B_4C and SiC substrates cannot occur since no free boron or silicon is available to react with carbon impurities.

10. Question #10: What is the Relative Importance of C Segregation and C Dissolution on Wetting Behavior?

A definitive answer cannot be given, but the end result of both substrate dissolution and bulk impurity segregation appears to be the same. Experiments indicate that whether carbon originates from the alloy or from dissolution of the substrate, it segregates to the surface. In one case, as a result of high temperature heating, it was found that the alloy dissolved a small portion of the graphite substrate. Subsequent examination of the alloy showed that an enormous "icecap" of C had formed at the top surface of the material, but that the interior of the droplet was remarkably free of carbon. In a second case, where the alloy had dissolved a substantial portion of graphite, a significant amount of B_4C formed throughout the interior of the alloy. These results suggest that the mechanism of surface segregation predominates at low carbon activities, but in light of the complex nature of binary and ternary alloys, the issue requires further study before a positive answer may be given.

A number of key questions concerning the behavior of the alloy systems have therefore been answered by the model of surface segregation of low-level impurities in the alloys. One highly visible type of behavior of the alloys, however, has resisted explanation. This behavior is the formation of the light-dark boundary observed in numerous cases of poorly-wetted droplets of alloy. The bright-dark boundary nearly always forms during wetting of Ni/B to virgin graphite, and may be associated there with C ruboff or dissolution. An indication of this was seen when a second graphite ribbon was inserted into the side of a poorly-wetted droplet. After removing the ribbon, a bright region existed along the puncture zone. There also is evidence that the boundary is associated with BN formation in the alloys. A third piece of evidence suggests that it may be associated with segregation itself. During the wetting process, it was found that the boundary often occurred concidently with formation of poorly-wetted droplets, but as wetting proceeded, the boundary collapsed toward the substrate and disappeared. Whatever its origin, the collapse of the boundary seems to be associated with the onset of wetting in initially poorly-wetted droplets. It appears to be localized at the droplet surface, as fractured cross-sections of poorly-wetted droplets which contained the boundary show no evidence of it in the droplet interior. The best explanation one can give at present is that the bright-dark boundary is probably due to a combination of several factors, including reflection of the heated substrate from the lower half of the alloy droplets.

REFERENCES

1. Ju. V. Naidich, Prog. Surf. Membrane Sci. 14 (1981) 420.
2. Ibid., p. 421.
3. E. Lugscheider, H. Zhuang, and M. Maier, Welding Research (Supplement), October 1983, 295s.
4. M. Hansen and K. Anderko, Constitution of Binary Alloys, 2nd Edition, 1958, p. 256.
5. A. J. Frueh, Acta Cryst. 4 (1951) 66.
6. J. W. Gibbs, The Collected Works of J. Willard Gibbs, Vol 1 (New Haven: Yale University Press, 1948).
7. R. Defay, I. Prigogine, A. Bellemans, and D. H. Everett, Surface Tension and Adsorption (New York: Wiley, 1966).
8. G. A. Somorjai, Principles of Surface Chemistry (Englewood Cliffs: Prentice-Hall, 1972), p. 63.
9. Defay, Surface Tension.
10. M. P. Seah and C. Lea, Philo. Mag. 31 (1975) 627.
11. A. R. Miedema, Z. Metall. 69 (1978) 455.
12. Ibid., p. 457.
13. J. R. Chelikowsky, Surf. Sci. 139 (1984) L197.
14. T. Ishitani, K. Umemura, S. Hosoki, S. Takayama, and H. Tamura, J. Vac. Sci. Technol. A 2 (1984) 1365.
15. E. K. Storms, private communication.

CHAPTER 8

WETTING AND SURFACE STUDIES OF LIQUID METAL ALLOYS OF ARSENIC

A. The Challenge Presented

The major problem to be faced in the development of a liquid metal ion source of As is to establish an alloy combination possessing a favorable vapor pressure. The problem can best be illustrated by reference to Table X, which shows the temperature at which elemental arsenic has the indicated vapor pressure.

TABLE X

VAPOR PRESSURE OF ARSENIC

Temperature (C)	Vapor Pressure (torr)
380	1
440	10
510	100
580	400
610	760
808 (MP, 28 atm)	$> 10^4$

It is seen that the vapor pressure of pure As at the relatively low temperature of 600 C is nearly 1 atmosphere. Since a successful ion source requires vapor pressures of near 10^{-7} torr or lower, this is clearly an unacceptably high volatility. The challenge is therefore to identify materials which lower the As vapor pressure by

over ten orders of magnitude. This is not an easy task, particularly when set against the additional requirements of good wettability and low rates of chemical reaction. Nonetheless, the experience gained through study of boron alloys allowed the choice of a successful combination of materials in a relatively short period of time.

In general, there are three ways to lower the vapor pressure of a liquid. The first is to choose a simple, deep eutectic of As with as low a melting point as possible. This lowers the As pressure by simple reduction in operating temperature. It is doubtful that appropriate materials could be identified to bring about the needed reduction of ten orders of magnitude in vapor pressure. The second way is by formation of an ideal solution of As with a second component M, which results in a vapor pressure lower than that for elemental As by a factor equal to the mole fraction of As in the liquid solution. There is little to gained by this measure, however, since even extreme cases (e.g., M = 99% and As = 1%) produce too small a reduction to significantly lower the vapor pressure of As. The third way to reduce the the vapor pressure of a volatile species is to select a compound with a low (i.e., high negative) Gibbs free energy of formation. For example, for a given arsenic compound such as AsX_n, where X is a low volatility element, the equilibrium condition between vapor and liquid is:

$$AsX_n(l) = n\ X(g) + As(g)$$

The equilibrium constant for this reaction is

$$K(p) = P(As)\ P^n(X)$$

and the Gibbs free energy is

$$dG = - R T \ln K(p)$$

Hence, if dG has a large negative value, K(p) and P(As) will typically be smaller than the case of an ideal solution (no compound formation) of the same elemental constitutents. This is true because nonideal (compound) solutions are more stable than ideal solutions due to the existence of chemical bonding forces between the chemical species. In the case of ideal solutions, interactions are assumed to be negligible.

B. The Palladium-Arsenic Binary System

Based upon the familiarity of Storms with the phase diagram of Pd/As and subsequent analysis by members of the ion source project, the determination of a number of favorable palladium arsenide compounds was made. The compound Pd_2As appeared to offer the most promise, as a SOLGASMIX [1] calculation by Santandrea [2] indicated that it was congruently vaporizing. Several palladium arsenide compounds were manufactured by Behrens [3] of the Los Alamos group by the combustion synthesis technique and distributed to the OGC group for surface studies. These studies are discussed below.

There have been few investigations of the Pd/As binary system. The most authoritative work is the 1964 study of Saini, Calvert, and Heyding [4], who remarked that they were aware of only four previous studies of the palladium arsenides. An independent study was performed in 1963 by Raub and Webb [5]. Both sources provide phase

diagrams, with Shunk [6] deriving a composite of both studies which is reproduced in Figure 8-1.

A number of eutectics and several congruently melting compounds appear in the phase diagram. Seven intermediate phases exist: Pd_5As, Pd_3As, $Pd_{2.65}As$, Pd_5As_2, a-Pd_2As, b-Pd_2As (<455 C), and $PdAs_2$. The compound PdAs does not exist. While Saini assigned a singular stoichiometry to $PdAs_2$, Raub and Webb found evidence for a range of homogeneity which is reflected in the phase diagram of Figure 8-1. Crystal structures for the solid phases of each of these compounds are discussed in the references.

C. Wetting and Surface Studies of Pd_2As on W

Tungsten was selected as an appropriate first choice for wetting studies due to its ease of use and proven capabilities with elemental low-melting liquid metals such as Ga. A solid specimen of Pd_2As was mounted atop a thin ribbon of W within the vacuum chamber and resistively heated until melting occurred. The experimental melting point of this compound was determined to be 1075 K by comparison to W, whose temperature-brightness characteristics are well-documented.

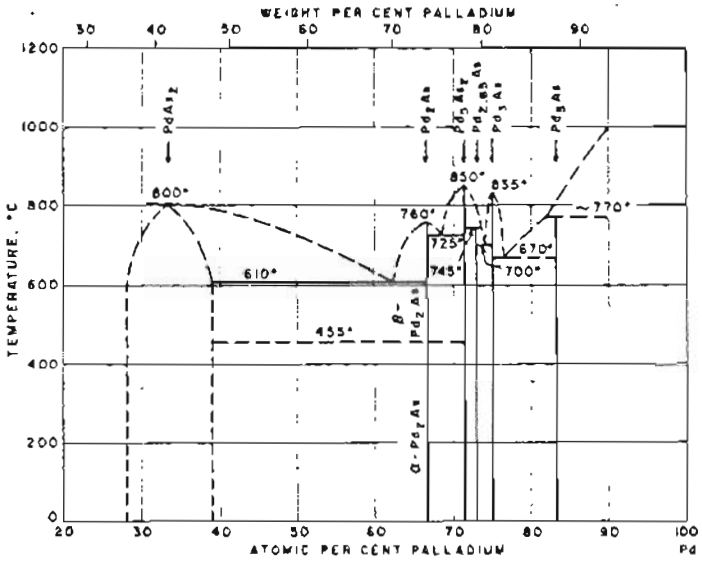

Figure 8-1. The phase diagram of the Pd-As system. From reference [6].

Initially, the wetting was poor. At the melting point, a poorly-wetted droplet of alloy formed with contact angle of about 130 degrees. The surface of the droplet was covered by large masses of material whose brightness was considerably less than that of the interior of the droplet. Later analysis showed that the dark masses were carbon. The interior of the droplet was visible through "cracks" between the large masses.

Heating to a temperature of nearly 300 degrees above the melting point was necessary to cause substantial changes in wetting. At this temperature, the dark shell surrounding the droplet fractured and a rapid effusion of alloy material from the droplet interior occurred which wetted the W ribbon with a near-zero contact angle. The fractured shell was left behind as an inert mass of material which floated atop the liquid alloy surface. At this point, the system was vented and the specimen remounted to enable study by the Auger beam.

The elemental composition of the alloy surface at 300 K after reinsertion into the vacuum chamber is shown in Figure 8-2. The shell remnant was located at T = 300 K on the left side of the alloy surface. A large amount of carbon is indicated. The right side of the alloy consisted of material which formerly occupied the interior of the initially poorly-wetted droplet. It is primarily composed of alloy components with a small amount of contaminating species. Auger analysis of the unwetted substrate, shown in Figure 8-3, shows that the surface is only 50% W at temperatures near the melting point of Pd_2As. Significant amounts of oxygen and calcium are also present, but no sign of carbon is found.

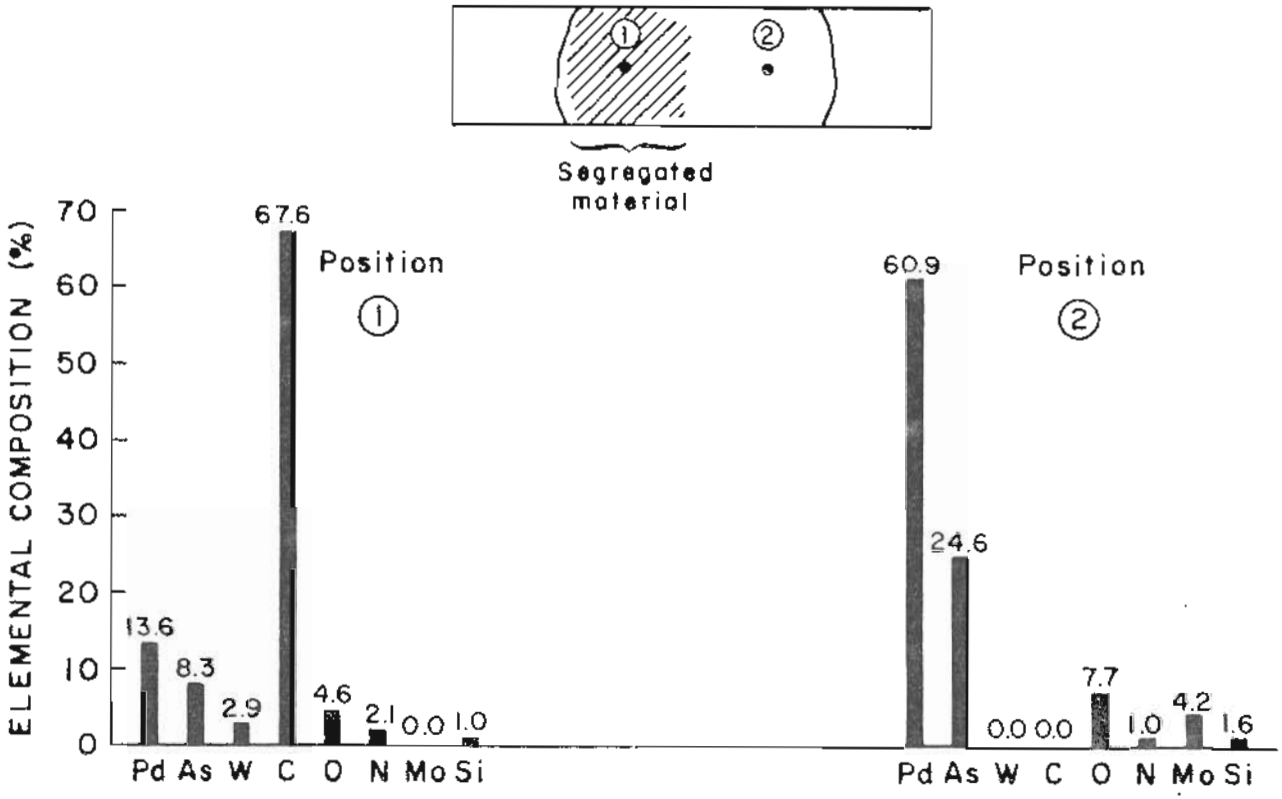

Figure 8-2. Auger surface elemental composition vs position for the Pd_2As (LANL: #273-20A) alloy on W. The alloy was wetted and reinserted into the vacuum chamber. The temperature is 300 K.

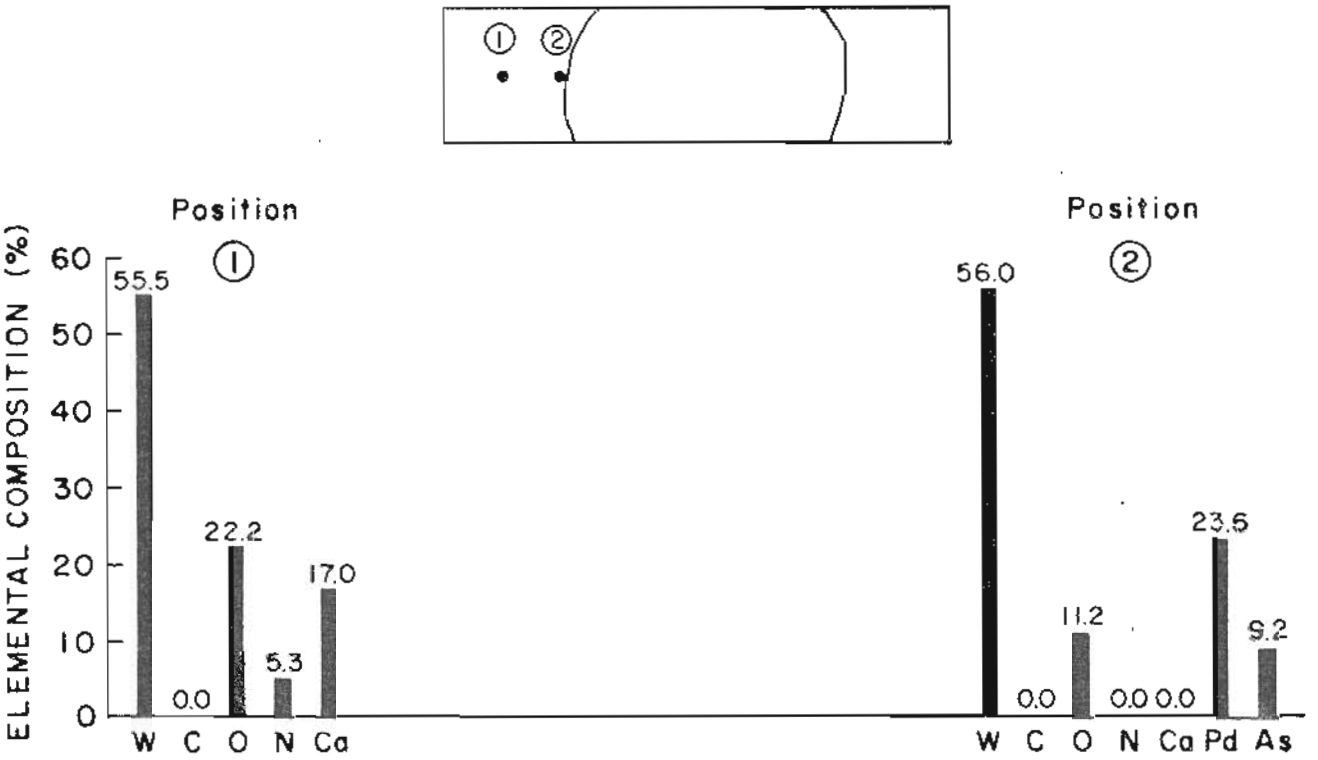

Figure 8-3. Auger surface elemental composition vs position for the W and near-W substrate. The temperature is $T = T_R + 50^{o} = 1125$ K.

The alloy surface composition was found to be essentially unchanged after heating the alloy to a temperature above the melting point. This is seen in Figure 8-4. However, as the surface became molten, the shell remnant floated atop the molten alloy and moved to the other side of the W ribbon. Again it was found that the underlying alloy was quite pure and consisted prodominantly of alloy components, while the shell was mostly carbon. The wetting of arsenic alloys appears to be governed by the same mechanism as was discovered in the case of boron alloys. The wetting is controlled by surface segregation of low-level carbon impurities inherent to the alloy. Surface segregation of carbon is indicated because there is no carbon anywhere in the contacting materials and the experiment was performed under good vacuum conditions. Similar results were found in previous experiments with boron alloys. The important conclusion is that the mechanism preventing the wetting of liquid metal alloys to solid substrates appears to be alloy and process independent. It is difficult to find alloy systems which are more materially different than the boron and arsenic alloys investigated here. Further, the alloys are manufactured by two entirely different processes. Nonetheless, segregated carbon has proved to be present in both cases.

Long-term heating of the Pd_2As on W contact system showed little change in surface composition after 150 hours at a temperature of 50 degrees above the melting point. In particular, no evidence of W is found in the alloy surface, in spite of the fact that temperatures in excess of $T_m + 300^o$ were required to produce

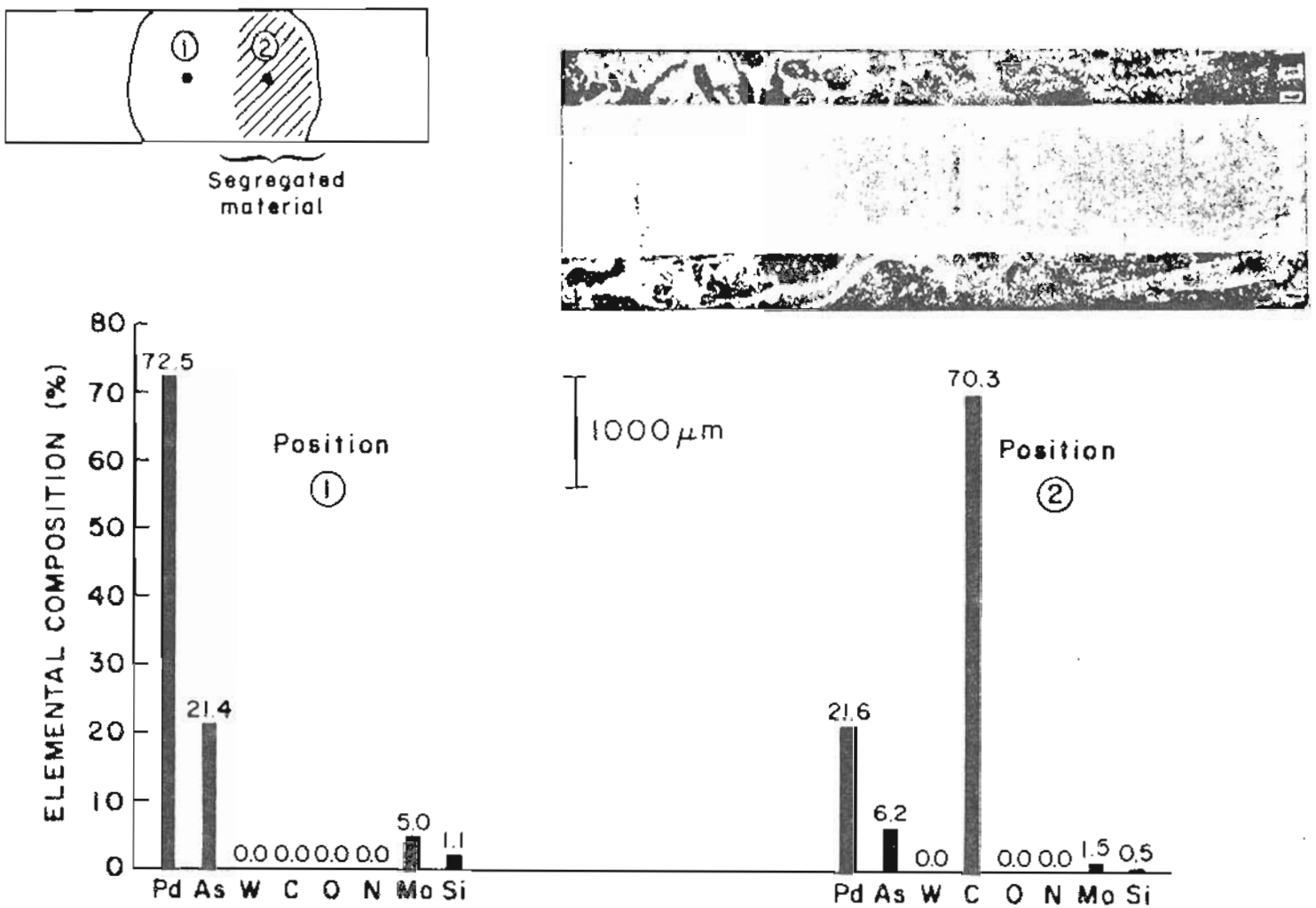

Figure 8-4. Auger surface elemental composition vs position for Pd_2As (LANL: #273-20A) on W. The temperature is $T = T_m + 50^o = 1125$ K. Upon melting, the segregated material moved to the right-hand side of the liquid surface.

wetting. This is seen in Figure 8-5. The elemental compositions of Pd and As remain constant throughout the experiment, and no indication of excessive attack of the W substrate is found. More significantly, little change in the system pressure was observed during heating this alloy to temperatures far in excess of those required to volatilize elemental arsenic. The alloy possesses stability sufficient to lower the vapor pressure of arsenic to low values at the melting point of the alloy. This is a remarkable achievement, and a testimony to the ability of thermodynamic functions to predict the behavior of complex material systems.

D. Wetting and Surface Studies of $Pd_{50}B_{25}As_{25}$ on Re

In view of the dramatic success of Pd_2As on W, a first step toward development of a LMI source containing both B and As is to use an alloy containing Pd, As, and B. Such an alloy has been synthesized, and the results are discussed in this section.

Surface studies of $Pd_{50}B_{25}As_{25}$ on Re revealed excessively high levels of chemical reaction occurring between alloy and substrate. The alloy was manufactured by the combustion synthesis method at Los Alamos, and supplied to OGC as a solid fragment of material broken from the original melt. The alloy was dull grey in color with no metallic sheen, in contrast to the Pd_2As alloy which exhibited a shiny, smooth appearance typical of most metallic alloys. Examination in an optical microscope revealed evidence of multiphase structure, which was later verified by microprobe and

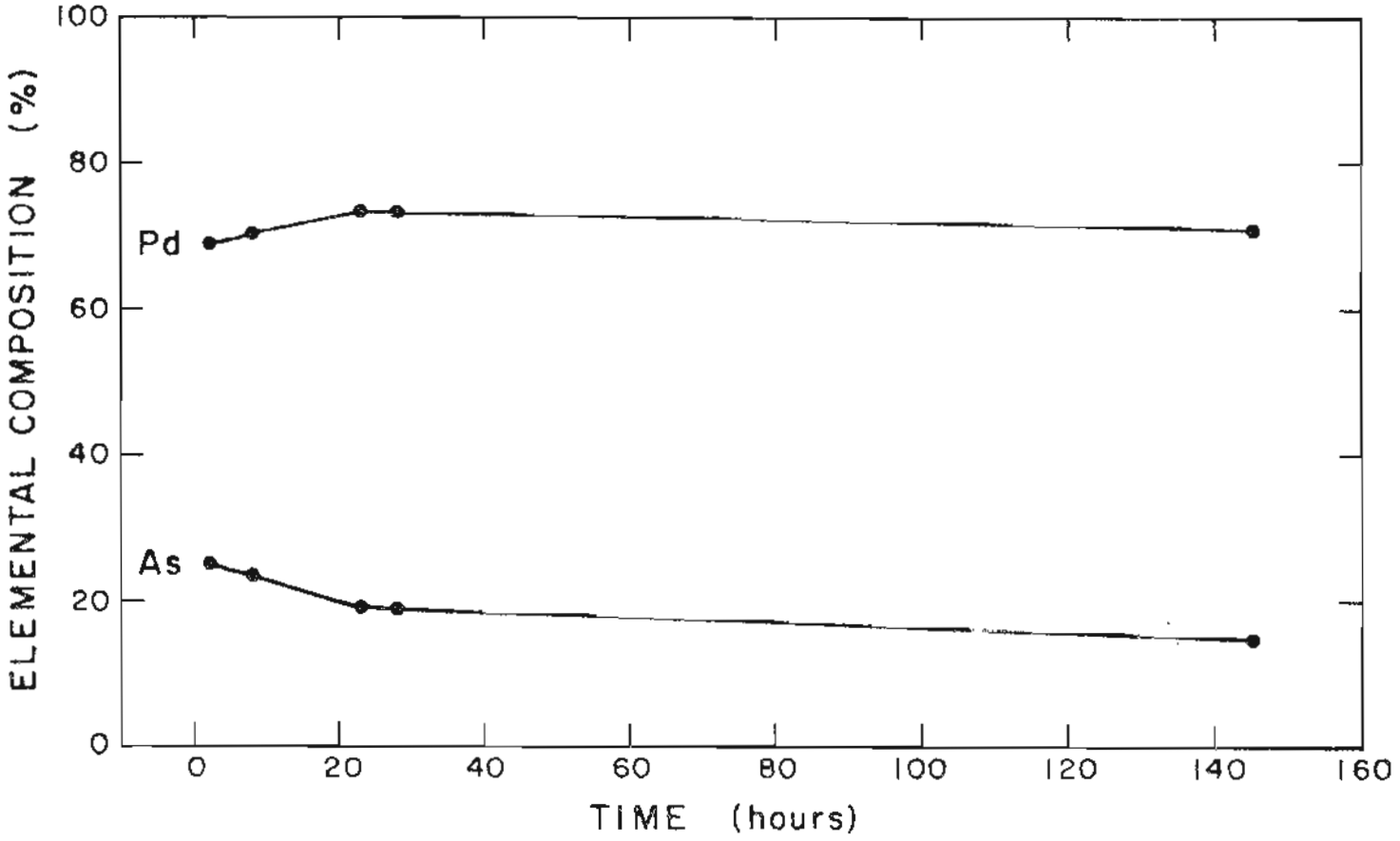

Figure 8-5. Auger surface elemental composition vs time for Pd_2As (LANL: #273-20A) on W. The temperature is $T = T_R + 50^{\circ} = 1125$ K. Small, unplotted percentages of Si and Mo remained less than 5% throughout the test.

metallography studies.

The alloy was mounted on a Re substrate and wetted in the usual fashion. Re was selected as the substrate because of its documented ability to resist boron diffusion at high temperatures. The melting point of the Pd/B/As alloy was difficult to determine with certainty because the melting behavior of this material was highly nonuniform. A large mound of alloy near the center of the Re ribbon took nearly 30 minutes to fully melt. We estimate the melting point to be about 1050 K by observation of significant liquid flow over the substrate.

The wetting behavior of this contact system was excellent once the liquid phase was predominant. The contact angle was near-zero, and some of the alloy spread to the backside of the Re. The Auger surface elemental composition of the liquid surface at melting is given in Figure 8-6. The main feature of the analysis is the large concentration of carbon. As we showed above in the case of Pd_2As, this carbon can only originate from within the alloy because there are no other sources for it in this contact system. It arises from surface segregation of low-level impurities in the alloy.

The $Pd_{50}B_{25}As_{25}$ on Re system failed after 16 hours at a temperature of 50 degrees above the melting point. The mutual attack of the alloy and ribbon were excessive. Figure 8-7 shows the surface composition of the alloy just prior to catastrophic breakdown. The alloy surface contains large concentrations of Re at all monitored positions, and the Re has warped considerably at the center (hottest) part of the ribbon. This behavior was observed to begin during the first 0.5 hour of operation.

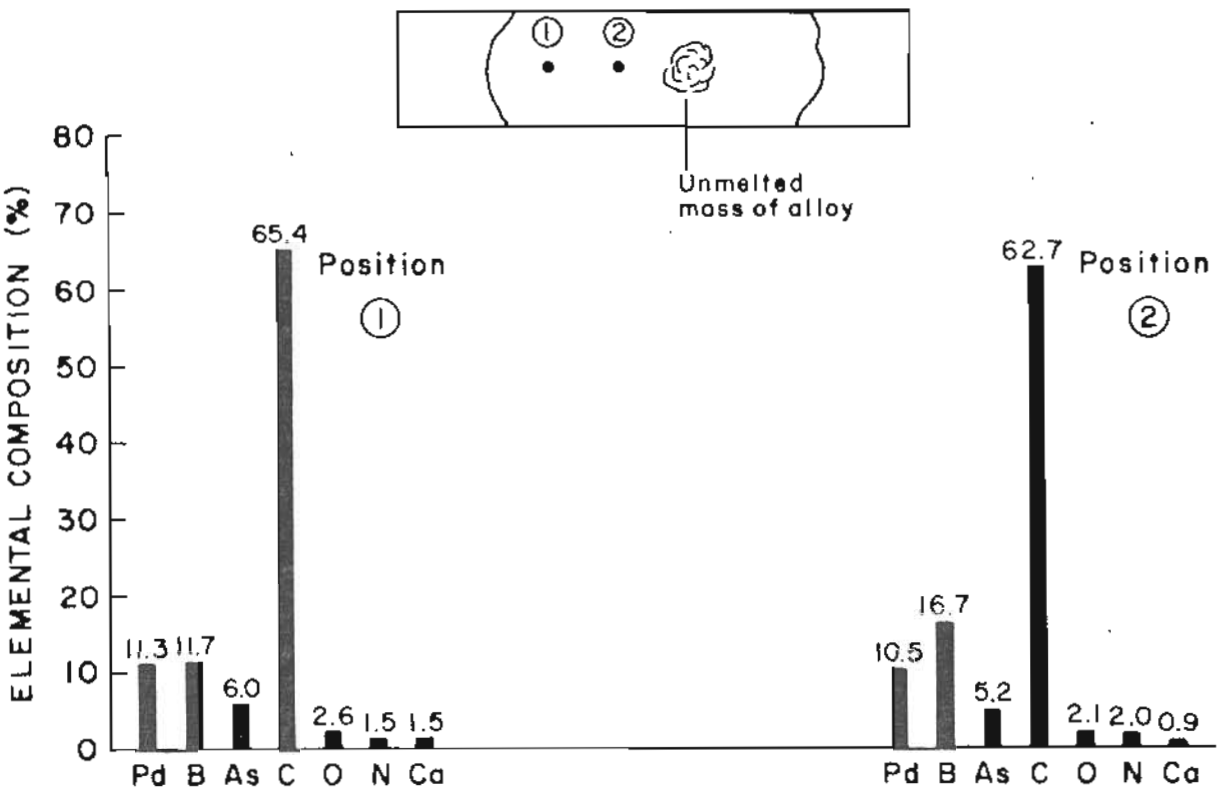

Figure 8-6. Auger surface elemental composition vs position for the $Pd_{50}B_{25}As_{25}$ alloy (LANL: #273-26A) on Re (Cross: Lot # X1-401777-7) just after melting. The temperature is $T = T_m + 50^o = 1115$ K.

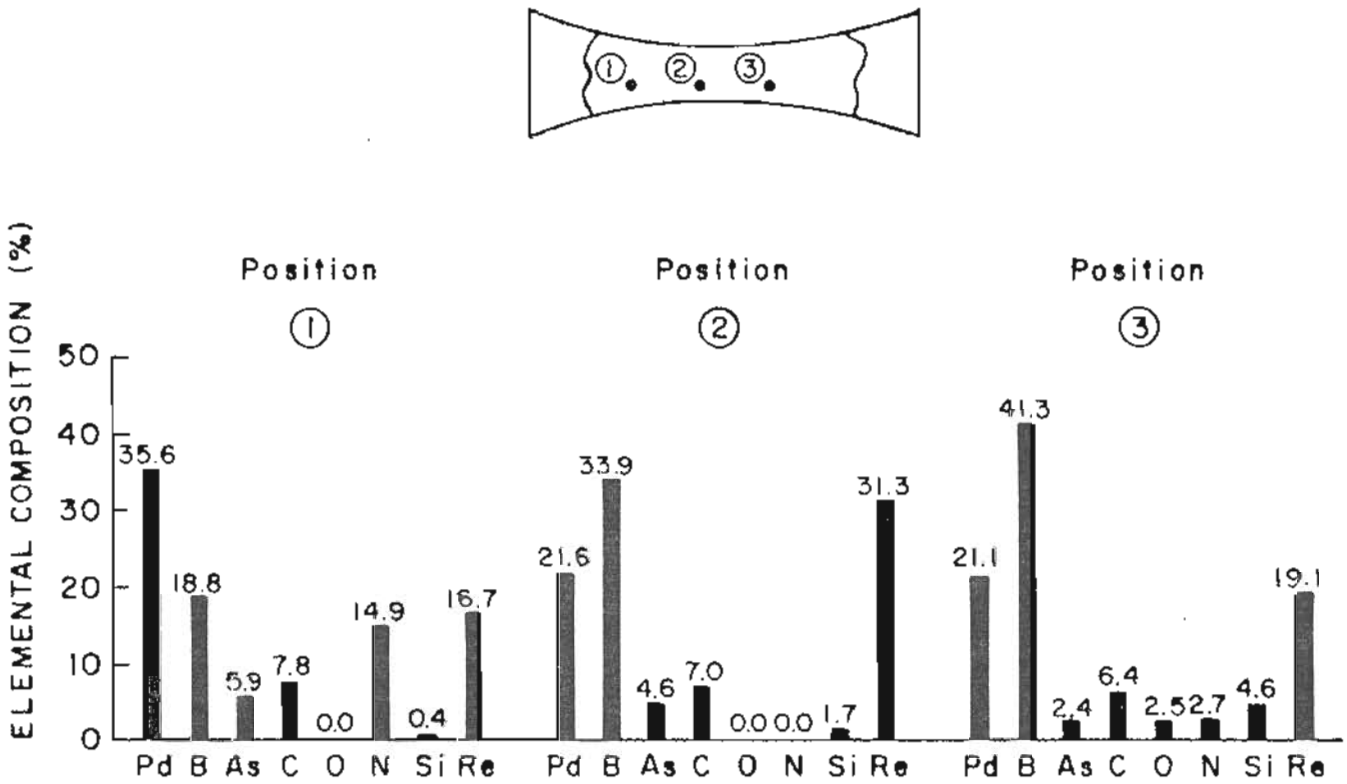

Figure 8-7. Auger surface elemental composition va position for the $Pd_{50}B_{25}As_{25}$ alloy (LANL: #273-26A) on Re (Cross: Lot # X1-401777-7) after 16 hours at T = T_m + 50° = 1115 K. The attack of the substrate is excessive.

Scanning electron micrographs of the surface after breakdown are shown in Figure 8-8. The distortion of the contact system is readily visible in the upper photo, while the bottom view shows a blowup of the central part of the ribbon where the attack is greatest. It appears as though the chemical attack may be occurring along grain boundaries. In any case, the morphological structure of the central, distorted region of the contact is radically different from the view in an area far away from the attack zone. In summation, the potential of this contact system for use as a LMI source of B and As is doubtful. A nonmetallic substrate may be preferable, as would an alloy with more uniform melting characteristics. Present evidence suggests that lowering the stoichiometric fraction of B has a beneficial effect on wetting to metallic substrates. This is not unexpected, as lowering the B and increasing the Pd content reduces the risk of excessive reactivity. It remains to be seen, however, whether such a source can generate sufficient amounts of B and As in the beam.

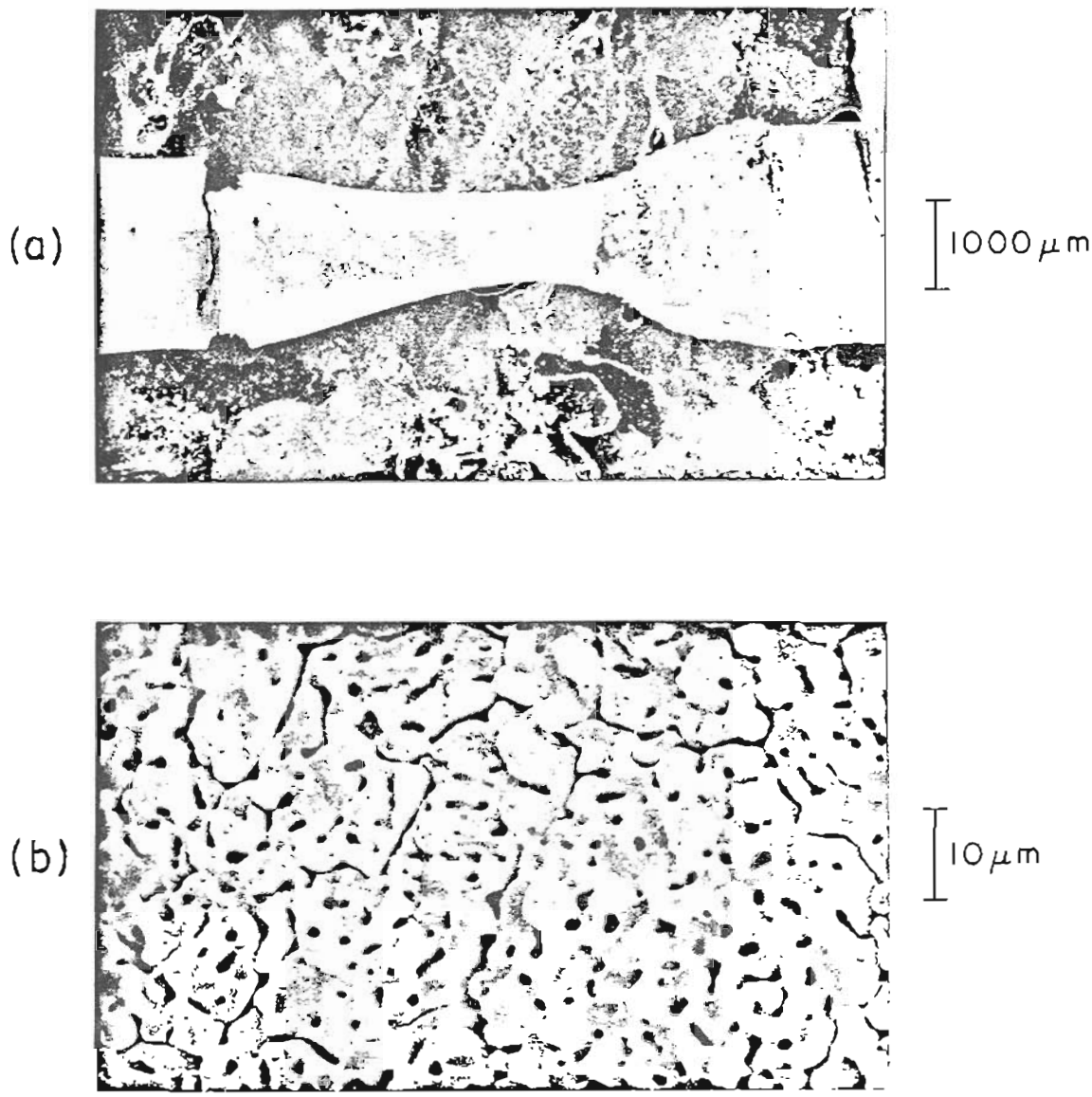

Figure 8-8. Views of the $Pd_{50}B_{25}As_{25}$ on Re alloy after catastrophic breakdown. The view in photo (b) is near the center of the ribbon shown in (a).

REFERENCES

1. G. Eriksson, Chemica Scripta 8 (1975) 100.

2. R. Santandrea, Materials Chemistry Group, Los Alamos National Laboratory, private communication.

3. R. G. Behrens, Materials Chemistry Group, Los Alamos National Laboratory, private communication.

4. G. S. Saini, L. D. Calvert, R. D. Heyding, and J. B. Taylor, Can. J. Chem. 42 (1964) 620.

5. C. J. Raub and G. W. Webb, J. Less-Common Met. 5 (1963) 271.

6. F. A. Shunk, Constitution of Binary Alloys, 2nd supplement (New York: McGraw-Hill, 1969), p. 59.

CHAPTER 9

MISCELLANEOUS WETTING STUDIES

A. The Formation of High-Melting Carbides and Nitrides and Dissolution of C by Ni/B at High Temperatures

There have been several instances of surface carbide and nitride formation in our studies. Further, a number of cases exist where high temperatures have produced significant dissolution of carbon into the alloys. This section summarizes the important conclusions of these studies, with emphasis on the importance of temperature control in the study of liquid metal contact systems.

The first key experiment concerns the wetting of Ni/B to a boronized graphite substrate. The wetting of this substrate was excellent, as described previously (see Figure 7-13 and accompanying text). However, during a temperature increase from $T_m + 50^o$ to $T_m + 150^o$, boron carbide was formed at the alloy surface. That boron carbide has formed is shown in Figure 9-1 by the small oscillation on the low energy side of the C (272 eV) peak.

A second example concerns Pt/B on Re, described in detail above (Chapter 6, Section C). After 10 hours of operation, the alloy surface was found to contain large amounts of BN. It is difficult to unambiguously determine when this material formed, because the

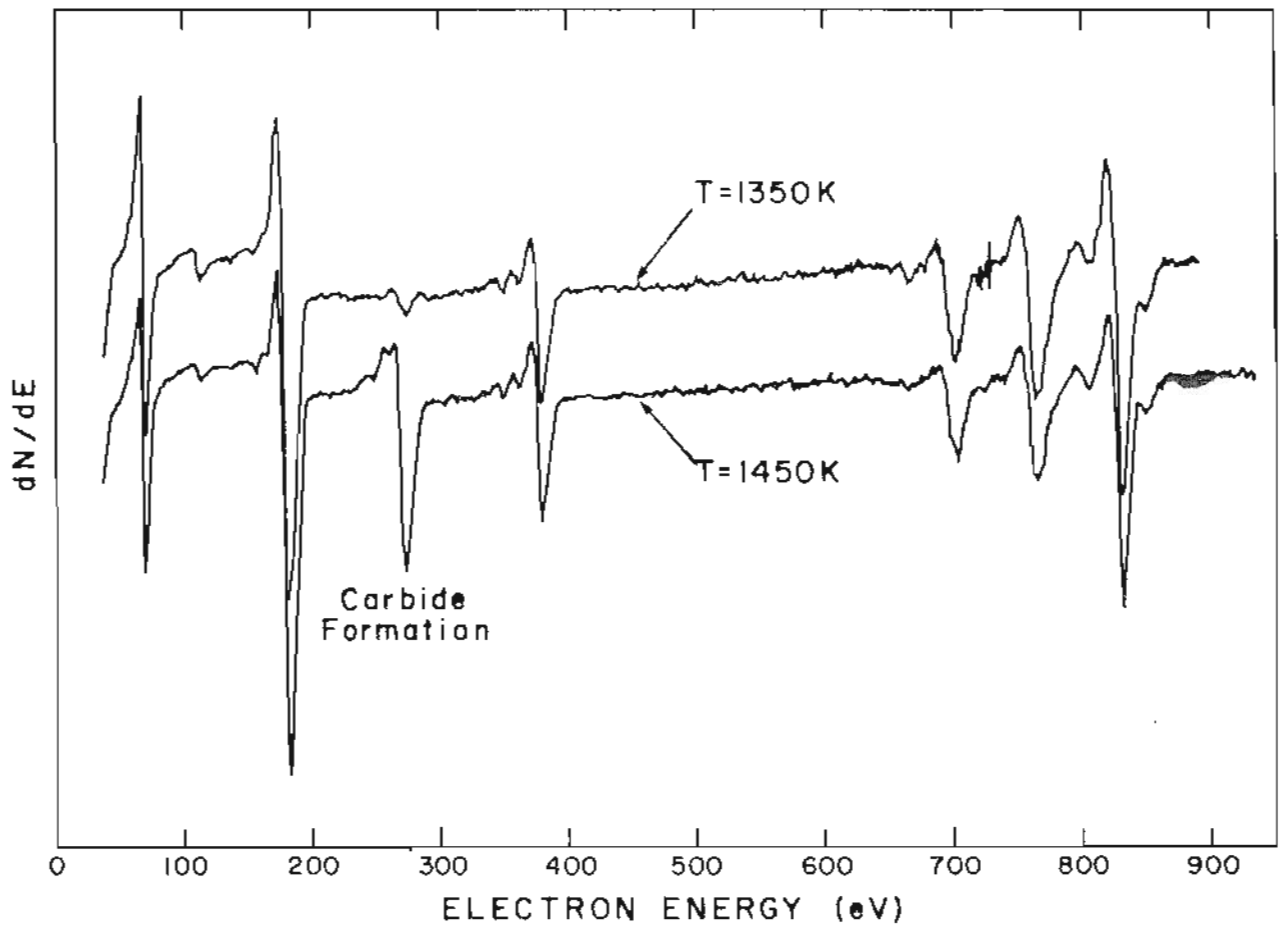

Figure 9-1. Auger spectra describing the wetting of nonfluxed Ni/B powder to a boronized substrate. Boron carbide is observed to form on the surface after a temperature increase from T = T_m + 50° (1350 K) to T = T_m + 150° (1450 K).

temperature was raised by nearly 100 degrees during the experiment to keep the alloy molten. Sudden changes in substrate resistivity resulting from alloy attack may also have occurred, creating sudden increases in temperature. In any case, it is the combination of excessive temperature and surface segregation of C and N that creates the problem of formation of high-melting carbides and nitrides in the alloy surface.

The final evidence for the effect of high temperatures on formation of BN and B_4C is given by the totality of poorly-wetted droplets found in the HRL prewetted material. Nearly every poorly-wetted droplet contained these compounds, resulting from the high temperatures utilized during the wetting process.

A dramatic instance underscoring the effects of high temperatures on carbon dissolution is shown in Figure 9-2. Here, an attempt was made to wet Ni/B (OGC) to a surface of C with an overlayer of Cr. The wetting was poor. Subsequently, the temperature of the system was increased to $T_m + 300^o$. A large mass of pure C developed in the upper hemisphere of the droplet. Notice also that the wetting characteristics of the droplet improved little as a result of this procedure. A cross-sectional slice through the droplet after the experiment showed that the C originated from dissolution of the substrate. The alloy has attacked the graphite and nearly penetrated it. That the C is concentrated at the top hemisphere of the alloy droplet indicates that C segregates to the surface regardless of how it is introduced into the alloy. Other samples we have analyzed have displayed similar behavior.

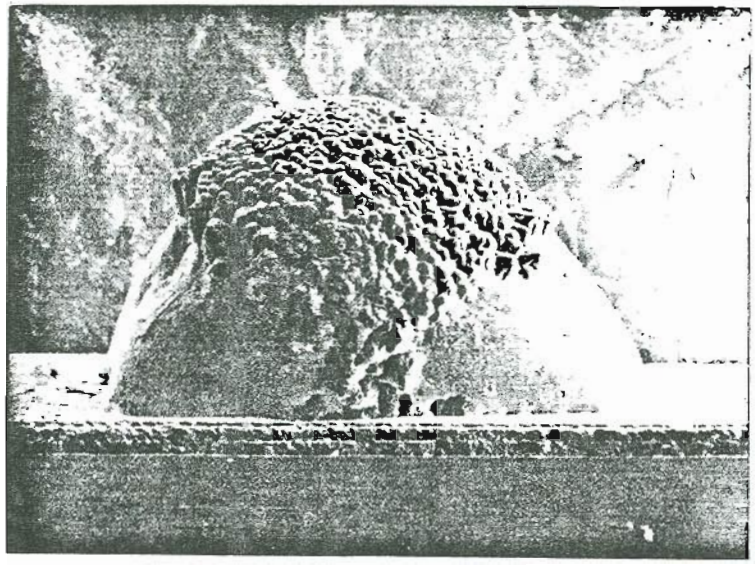

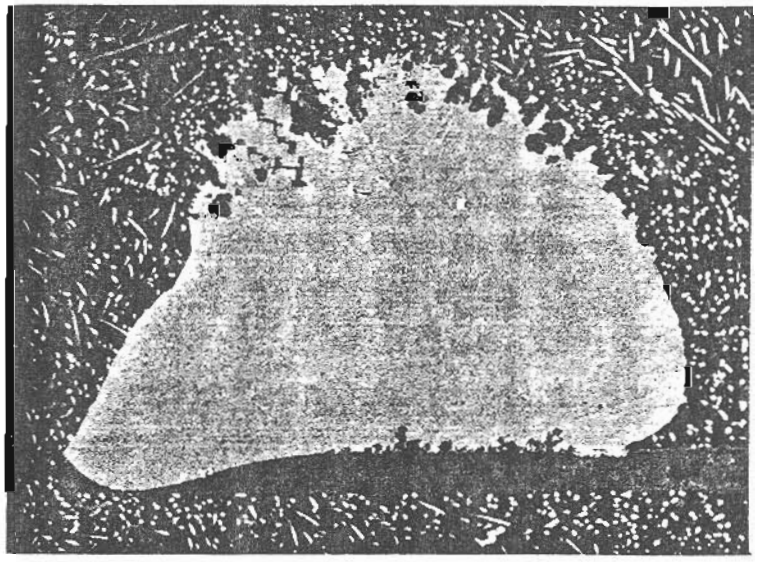

Figure 9-2. Wetting of Ni/B (OGC) to graphite with a Cr overlayer. The alloy had been heated to $T = T_m + 300^{\circ} = 1600$ K. The mound on the top of the droplet in (a) is 100% C. Photo (b) is a cross-sectional slice through the droplet. Attack of the graphite is observed.

B. The Wetting of B-Containing Alloy to Vitreous Carbon

1. Auger and Resistive Heating Study of Vitreous Carbon

Vitreous carbon is a glassy form of carbon that is less thermodynamically stable than polycrystalline graphite. As a result, it is expected that wetting will be better on this material than on the polycrystalline surfaces of carbon we have investigated up to this point. A number of samples of vitreous carbon were manufactured by the OGC and LANL groups for use in wetting studies. This subsection reports on the heating characteristics and surface composition of vitreous carbon.

Scanning electron micrographs of the LANL material before and after annealing are shown in Figure 9-3. The surface consists of a smooth glassy layer of carbon with evidence of localized patches of contamination. Little change in morphology is observed after annealing to 1300 K. The elemental composition of the surface "as received" and during heating at 1100 K is reported in Figure 9-4. The surface is quite pure, with a small amount of S, O, and N contamination.

The electrical power required to heat vitreous carbon ribbon, as a function of time, is shown in Figures 9-5 to 9-6. In this experiment, the vitreous ribbon was resistively heated by a constant current D.C. power supply while the voltage across the ribbon was monitored for 5 hours. The power consumption monotonically decreased during this period, as the brightness temperature of the ribbon dropped by about 20 degrees. Repeating the experiment at a higher

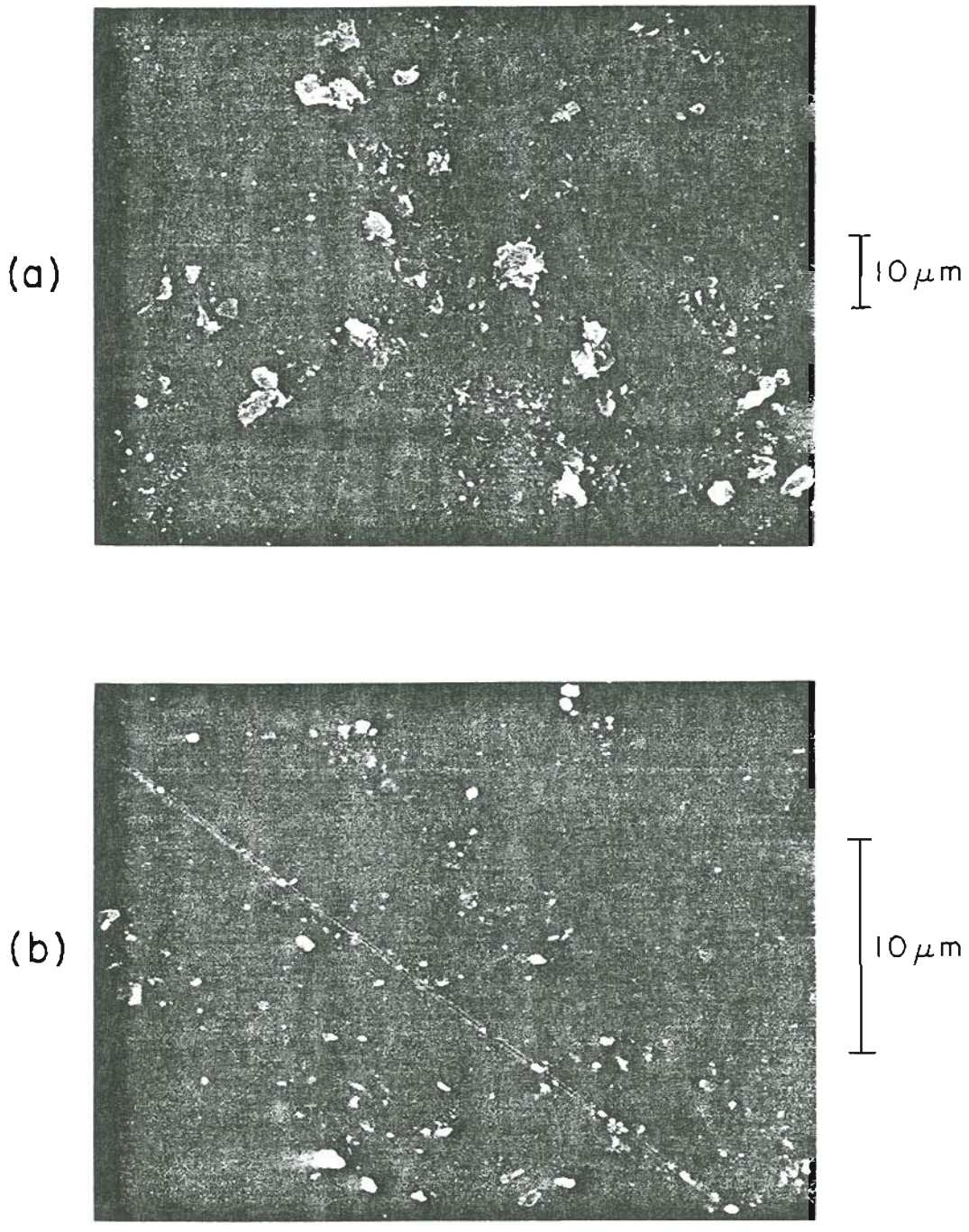

Figure 9-3. Views of the vitreous carbon (LANL) surface. (a) The "as received" surface; (b) After annealing to 1300 K. Little change in surface morphology is evident.

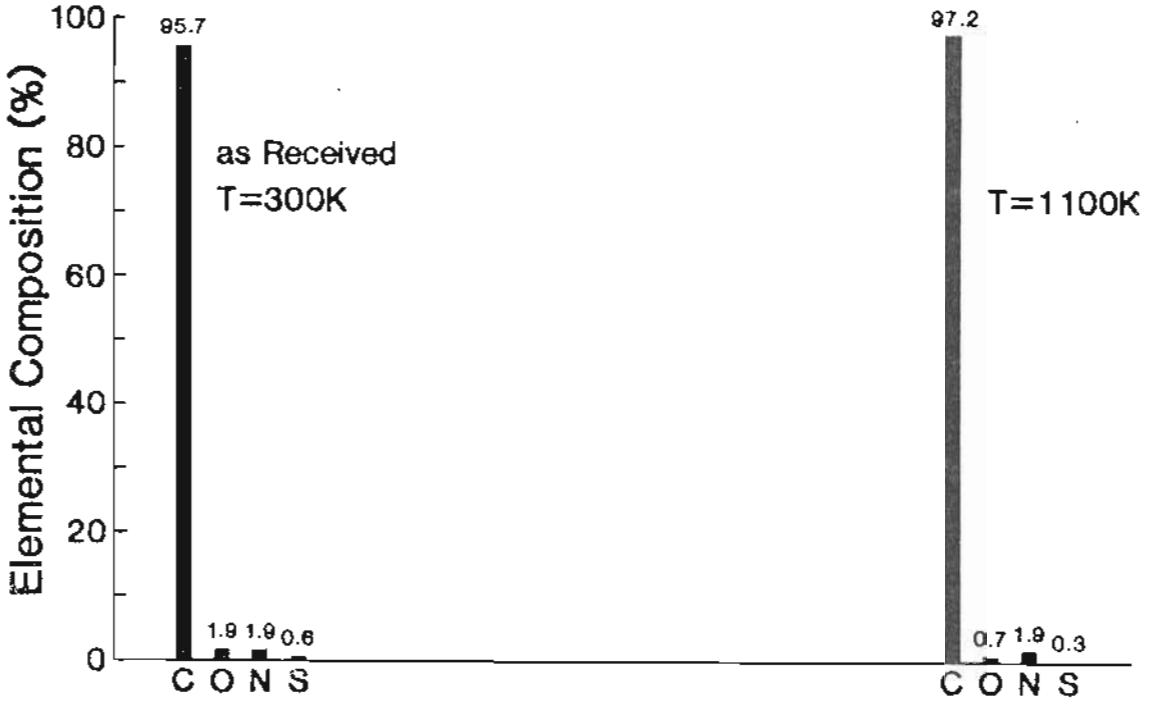

Figure 9-4. Auger surface elemental composition vs temperature for vitreous carbon (LANL).

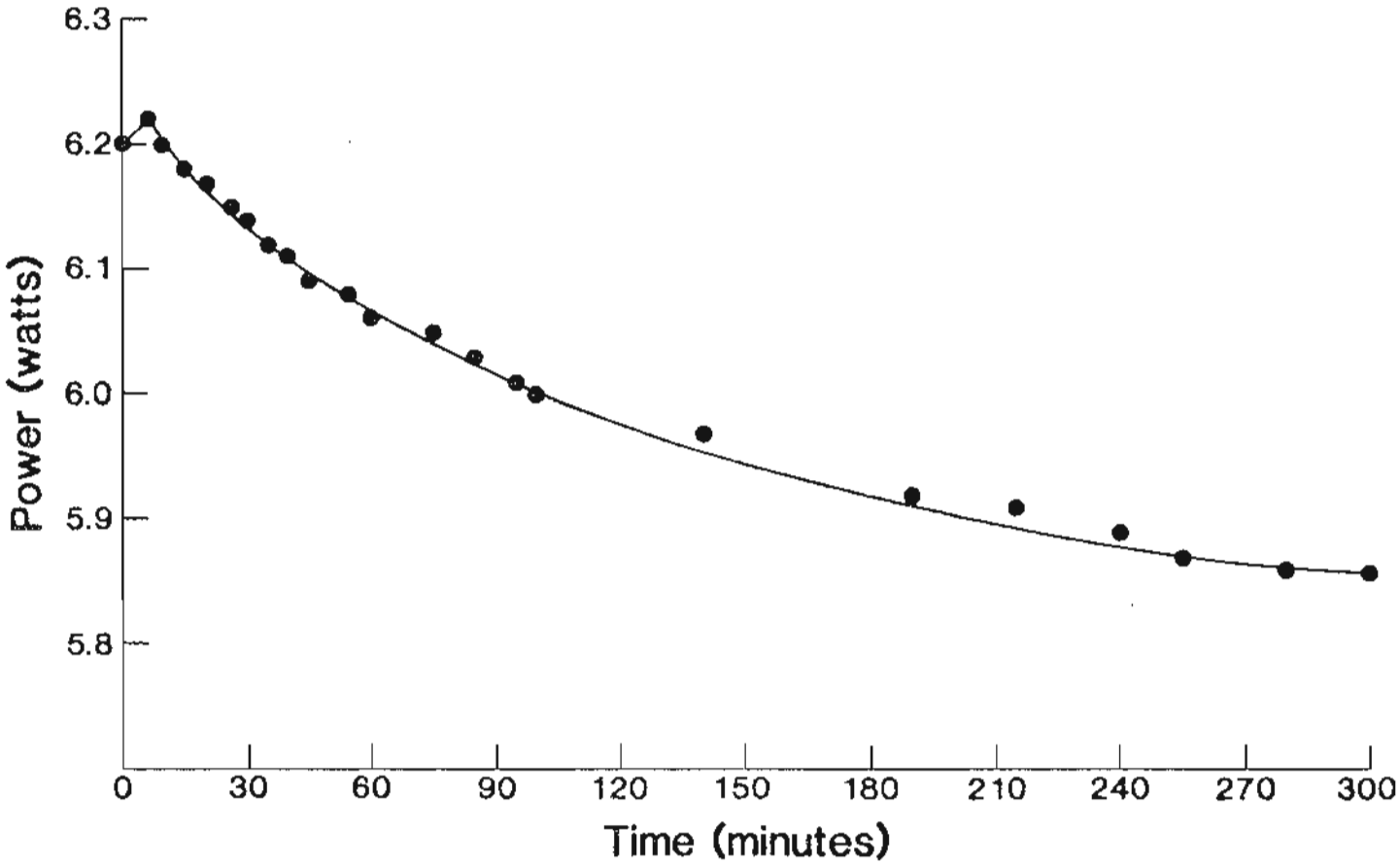

Figure 9-5. Electrical power vs time for heating of vitreous carbon (LANL). The current was constant throughout the test. The temperature was 1100 K at the beginning of the heating, and dropped about 20 degrees in 5 hours.

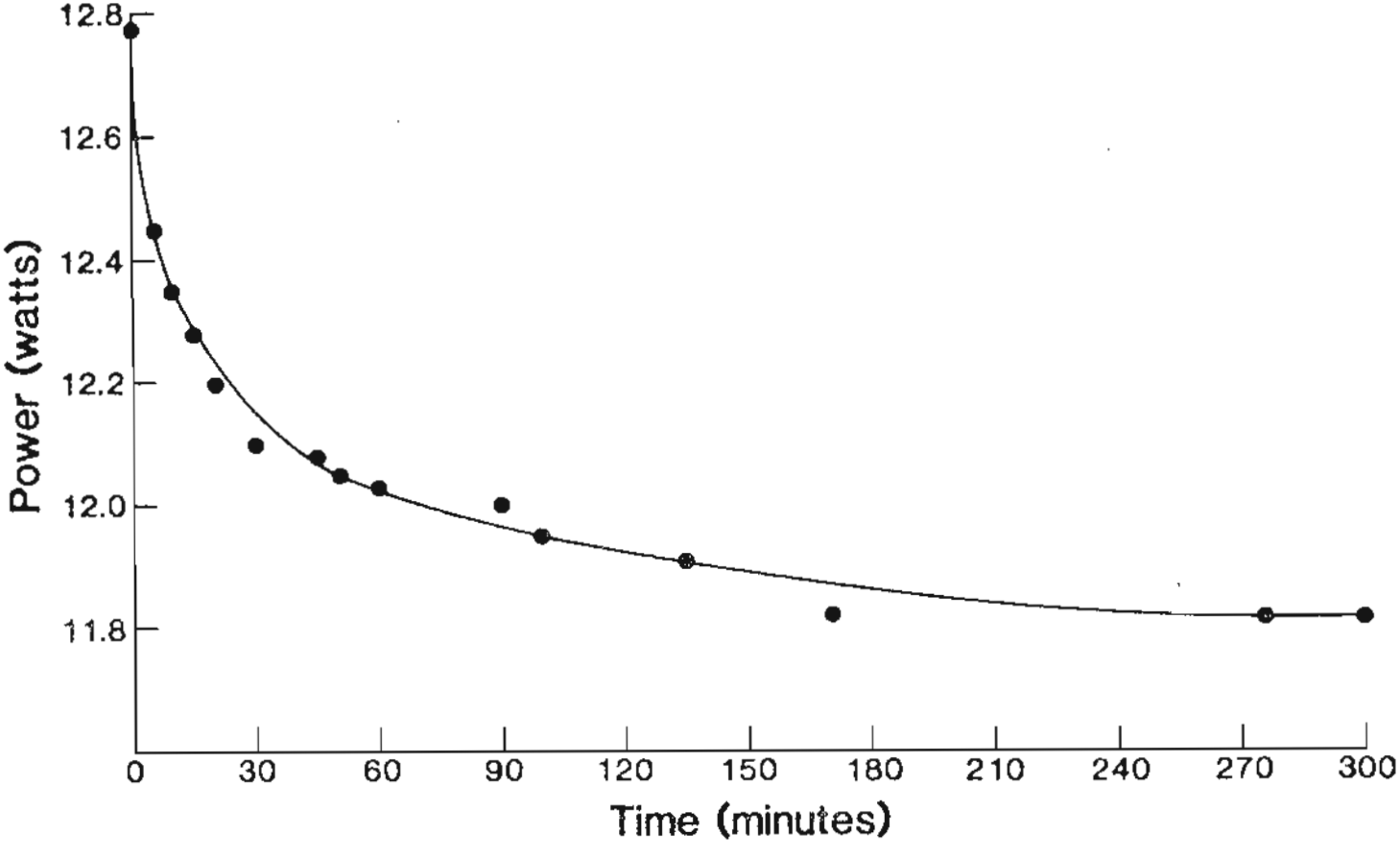

Figure 9-6. Electrical power vs time for heating of vitreous carbon (LANL). The current was constant throughout the test. The temperature was 1300 K at the beginning of heating, and dropped about 40 degrees in 0.5 hour.

starting temperature (1300 K) revealed a faster power dropoff and temperature decrease (see Figure 9-6). Returning to the lower temperature (1100 K), no change in power consumption was observed over a 5 hour period. These results indicate that the resistivity of vitreous carbon changes during initial heating at 1300 K, but then is stable at 1100 K. Thus, vitreous carbon possesses sufficient electrical stability for use as a contact material for liquid metal alloys of B and As.

2. Wetting Studies of Ni/B to Vitreous Carbon

Wetting of Ni/B alloy to both LANL and OGC vitreous carbon ribbons was studied. We first discuss the results on LANL specimens. Wetting of Ni/B (OGC) to vitreous carbon (LANL) resulted in the establishment of a poorly-wetted droplet of alloy with a contact angle of about 120 degrees. Auger analysis of the molten droplet at $T = T_m + 50^o$ is shown in Figure 9-7. Large amounts of surface carbon are readily apparent, in addition to lower concentrations of N, Ca, and S. After leaving the system at this temperature for a couple of hours, it was found that part of the alloy had wet and spread over a substantial portion of the substrate. As shown in Figure 9-8, it is clear that the wetted portion of alloy has attacked the vitreous ribbon and penetrated to the backside, forming a mirror-image of the frontside wetting. Side and cross-sectional views of the poorly-wetted droplet are given in Figure 9-9. It appears that the right side of the droplet has

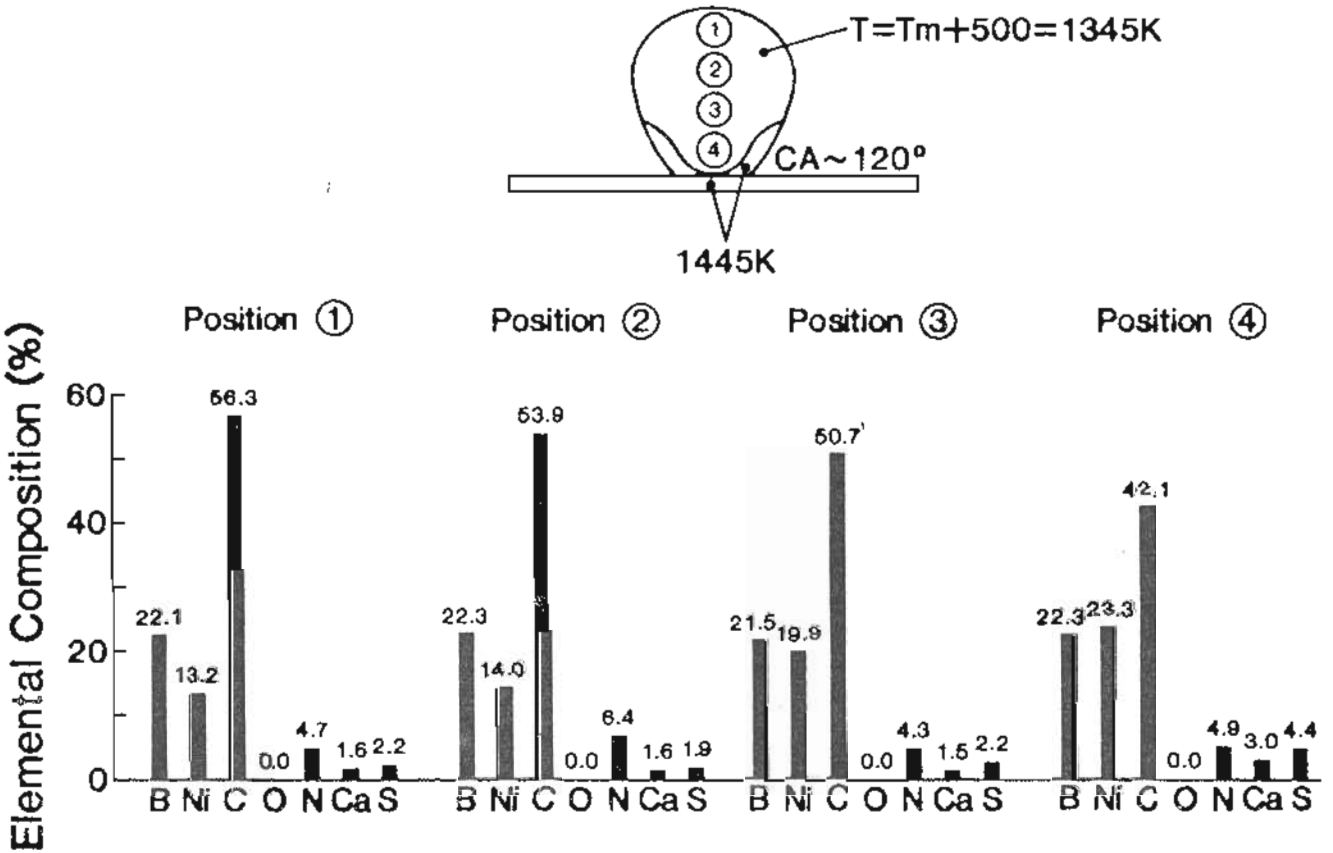

Figure 9-7. Auger surface elemental composition vs position for Ni/B (OGC) on vitreous carbon (LANL) at T = T_m + 50° = 1342 K.

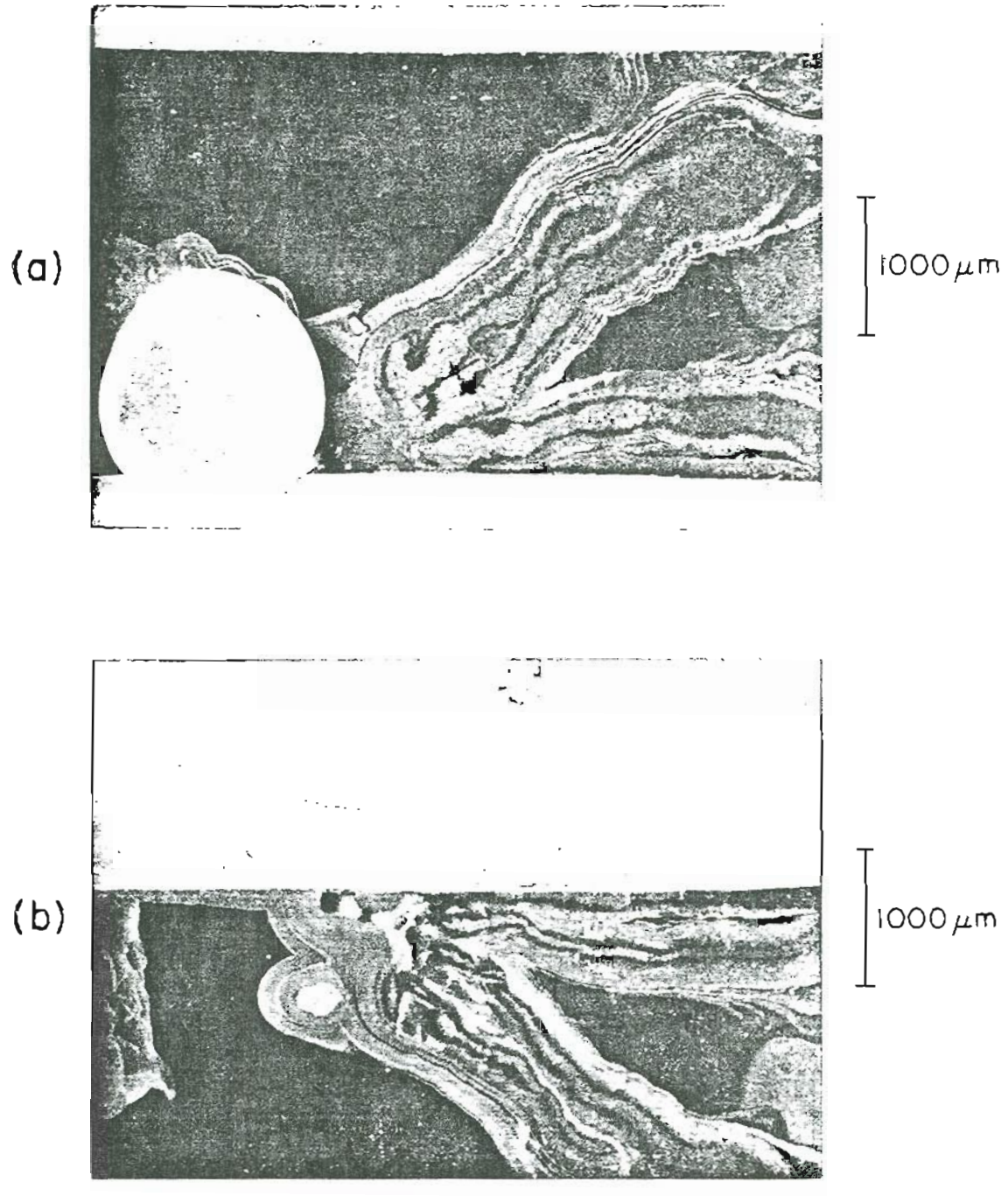

Figure 9-8. Wetting of Ni/B (OGC) to vitreous carbon (LANL). (a) Top view of the wetting, showing a well-wetted alloy front proceeding from the side of the poorly-wetted droplet; (b) View of the backside wetting.

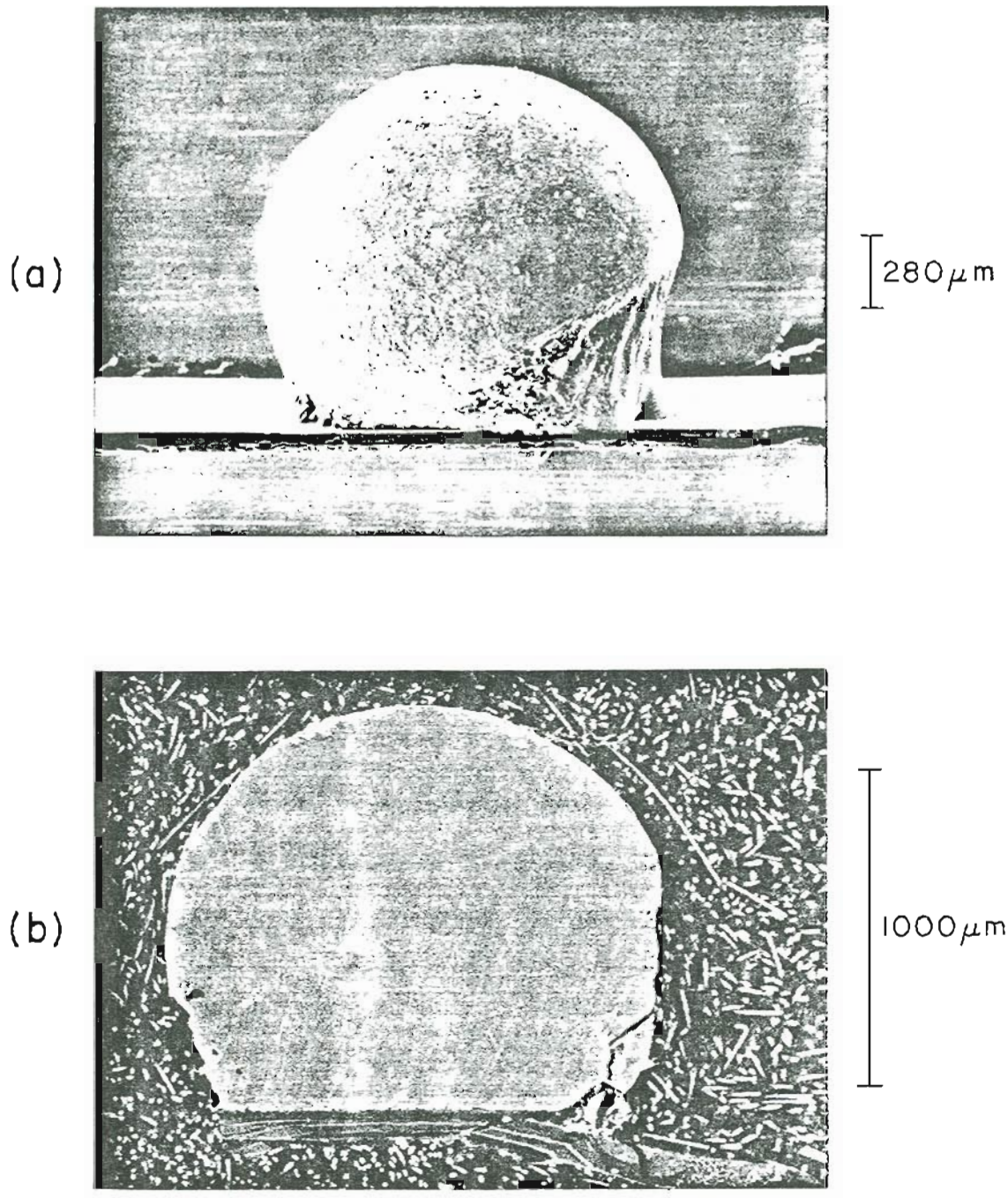

Figure 9-9. Wetting of Ni/B (OGC) to vitreous carbon (LANL). (a) Side view of the poorly-wetted droplet; (b) A cross-sectional slice through the alloy droplet.

collapsed during supply of the alloy to the ribbon. The results of this experiment are therefore discouraging regarding the use of vitreous carbon as a viable substrate for the nickel boride alloy.

Wetting of Ni/B (LANL: #273-7B; Ni=.55, B=.45) to the OGC sample of vitreous carbon was better than wetting to the vitreous LANL sample, but not significantly so. At melting, the alloy formed a droplet with a contact angle of about 90 degrees, which decreased to about 45 degrees over a period of 0.5 hour. Auger analysis of the molten droplet (see Figure 9-10) shows the usual amounts of segregated C and N. Position 3 of this figure shows evidence of boron carbide. Figure 9-11 characterizes the wetting photographically. The left rim of the alloy droplet (view a) consists of material which is uniform, while the rest of the droplet is covered by dark precipitates (view b). Further, there is evidence of wetting and flow of some kind, as part of the glassy carbon is covered with a thin layer of material that could only have originated from the droplet (view a). Figure 9-12 provides an Auger analysis of these features. The uniform material consists of Ni-rich alloy with a small amount of C, while the wetting front is composed of C with 5% alloy coverage. A possible interpretation of this behavior is that it corresponds to monolayer diffusion of alloy out over the vitreous carbon. A blowup of the dark features atop the alloy is shown in Figure 9-13. These structures are hexagonal in nature, and therefore are probably precipitated graphite resulting from the C which has segregated to the molten surface. The alloy material surrounding the graphite consists of B, Ni, and C. The Ni-richness of this material

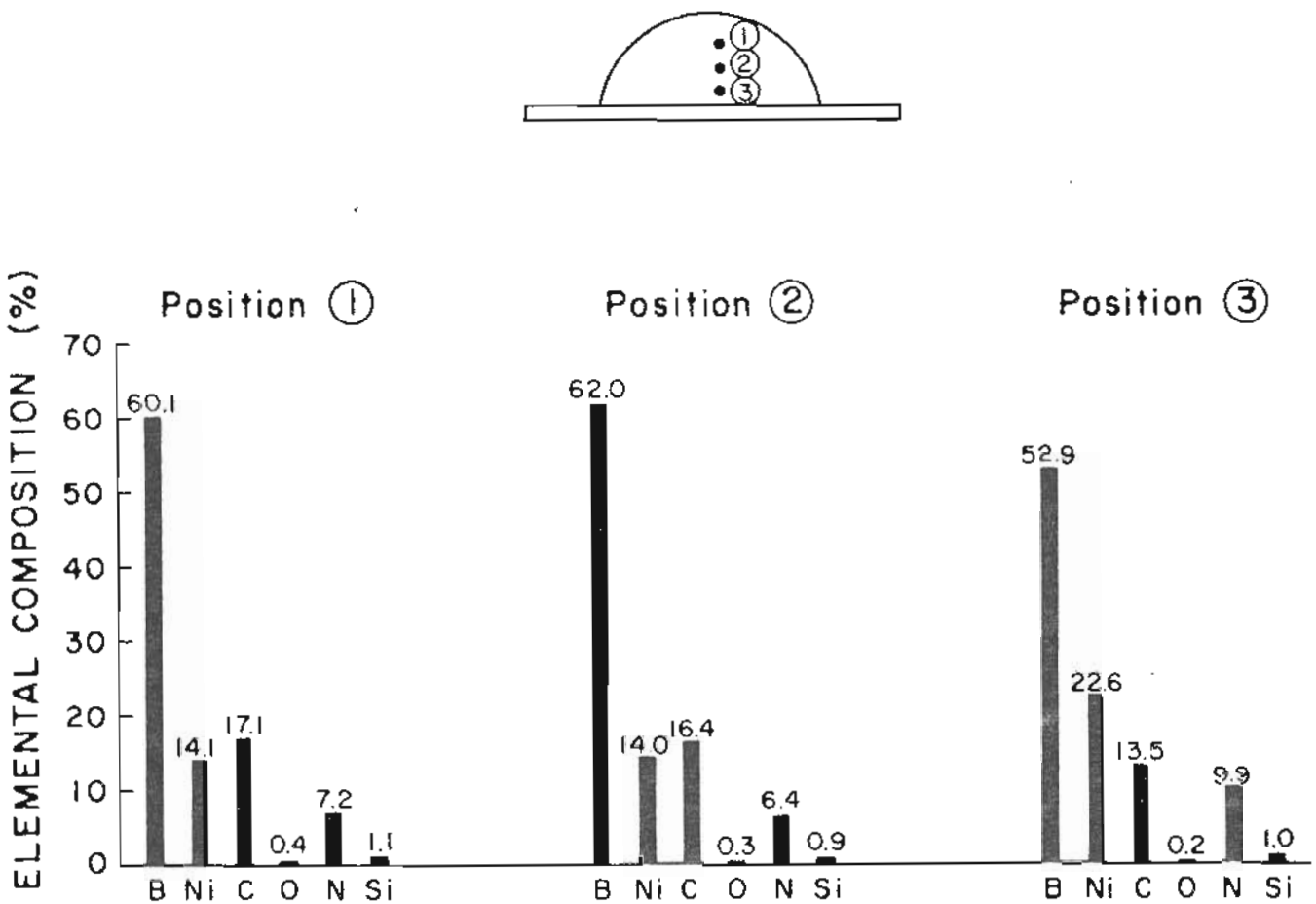

Figure 9-10. Auger surface elemental composition vs position during wetting of Ni/B (LANL: #273-7B; Ni=.55, B=.45) to vitreous carbon (OGC). Significant signals of C and N are present. The temperature is $T = T_R = 1300$ K.

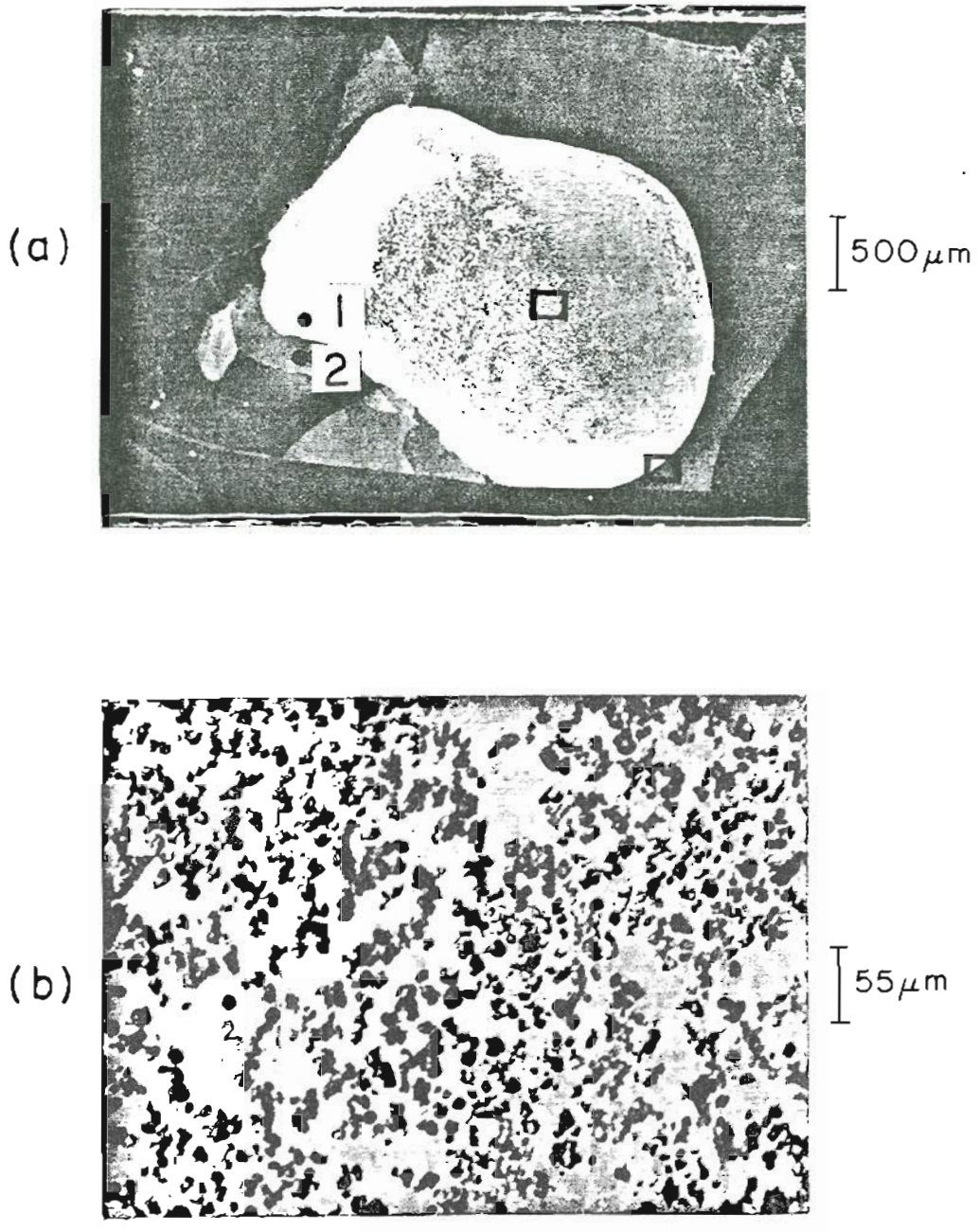

Figure 9-11. Views of the wetting behavior of Ni/B (LANL) on vitreous carbon. The temperature is 300 K. (a) Top view of the wetting; (b) A high magnification view of the boxed region of photo (a).

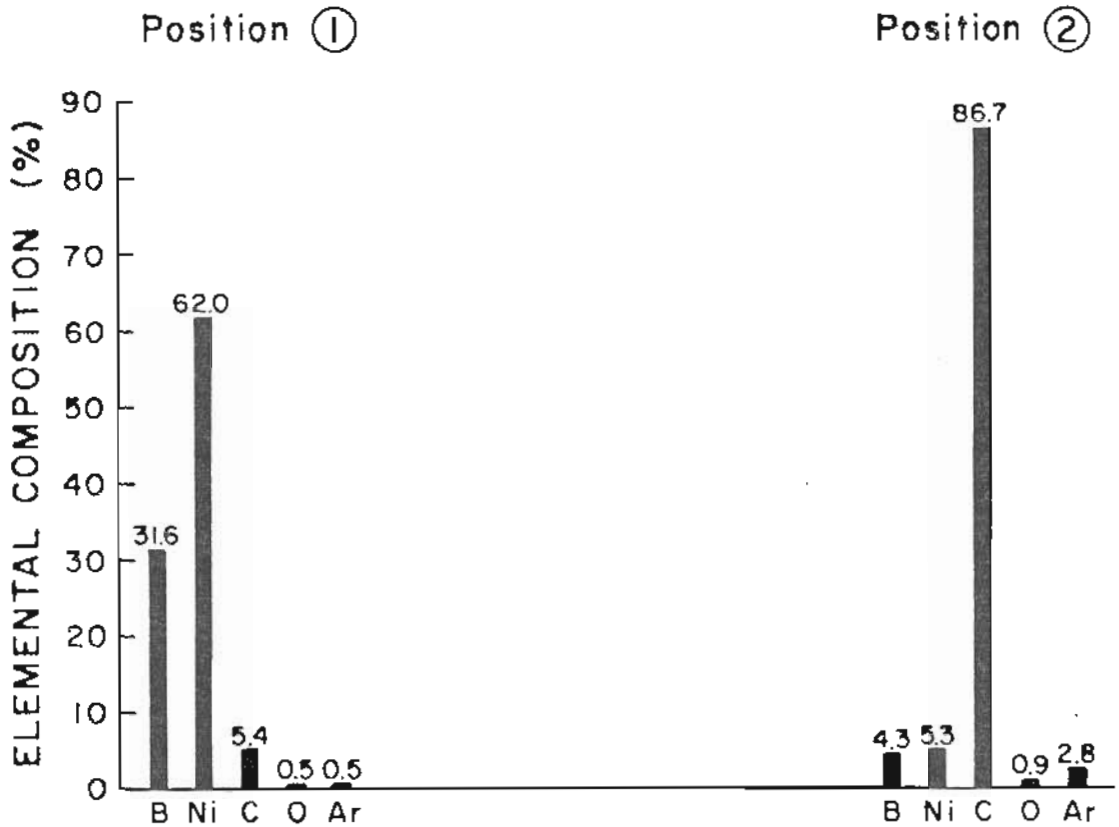

Figure 9-12. Auger surface elemental composition of 2 positions near the expanding alloy front of the Ni/B (LANL) on vitreous carbon. The positions monitored are shown as points 1 and 2 of photo (a) of Figure 9-11. The surface has been cleaned by 100 A Ar^+ sputtering.

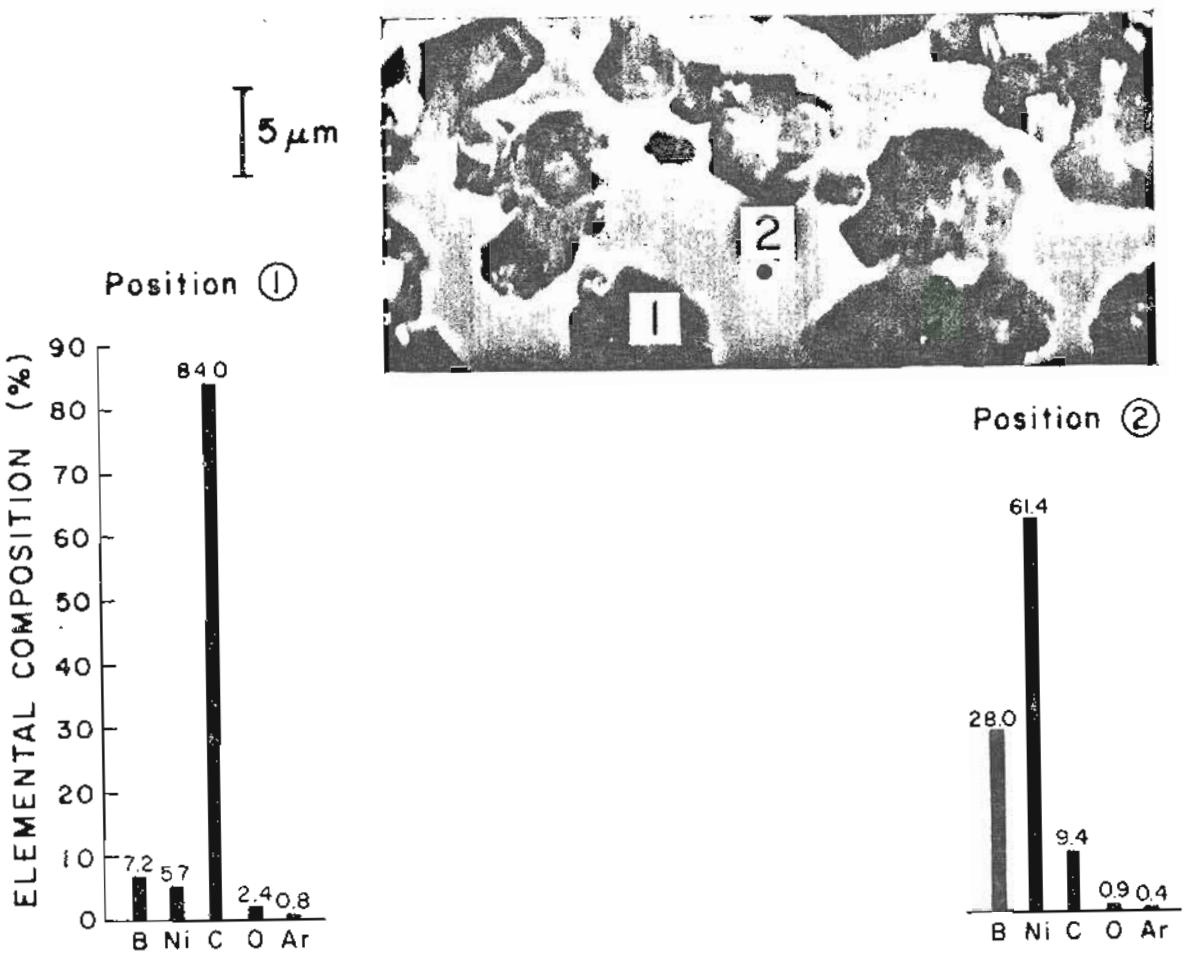

Figure 9-13. Auger surface elemental composition of 2 positions within the microstructure atop Ni/B (LANL) on vitreous carbon. The view shown is a blowup of the structures seen in photo (b) of Figure 9-11, after 100 Å Ar^+ sputtering. The hexagonal structures are precipitated graphite.

indicates that the surface boron is being removed. A probable mechanism is B_4C formation, as the Auger spectra of the surface at melting showed boron carbide to have formed in the lower part of the droplet. It is likely that further analysis of the droplet would reveal the presence of boron carbide.

3. Wetting Studies of Pt/B to Vitreous Carbon

Wetting of Pt/B (LANL: #273-5A; Pt=.72, B=,28) to vitreous carbon (LANL) was extremely poor. So little adhesion existed between alloy and substrate that the alloy droplet rolled off the vitreous ribbon during system venting. The Auger surface elemental composition for the poorly-wetted molten droplet is shown in Figure 9-14. High concentrations of segregated C and N are found at all sampled locations. Photos of the resulting droplet and substrate are provided in Figure 9-15. The circular morphology on the bottom of the droplet in photo (a) is where the alloy contacted the substrate. Photo (b) is a high magnification view of the substrate at the position where the alloy contacted the substrate. Small particles of alloy are seen, along with a thin film which marks the location where the alloy sat. It is this kind of evidence which leads us to question the validity of carbon ruboff in the contact systems. So little affinity for the alloy and substrate exists here that it is difficult to believe that carbon has been mechanically brought up into the alloy during wetting.

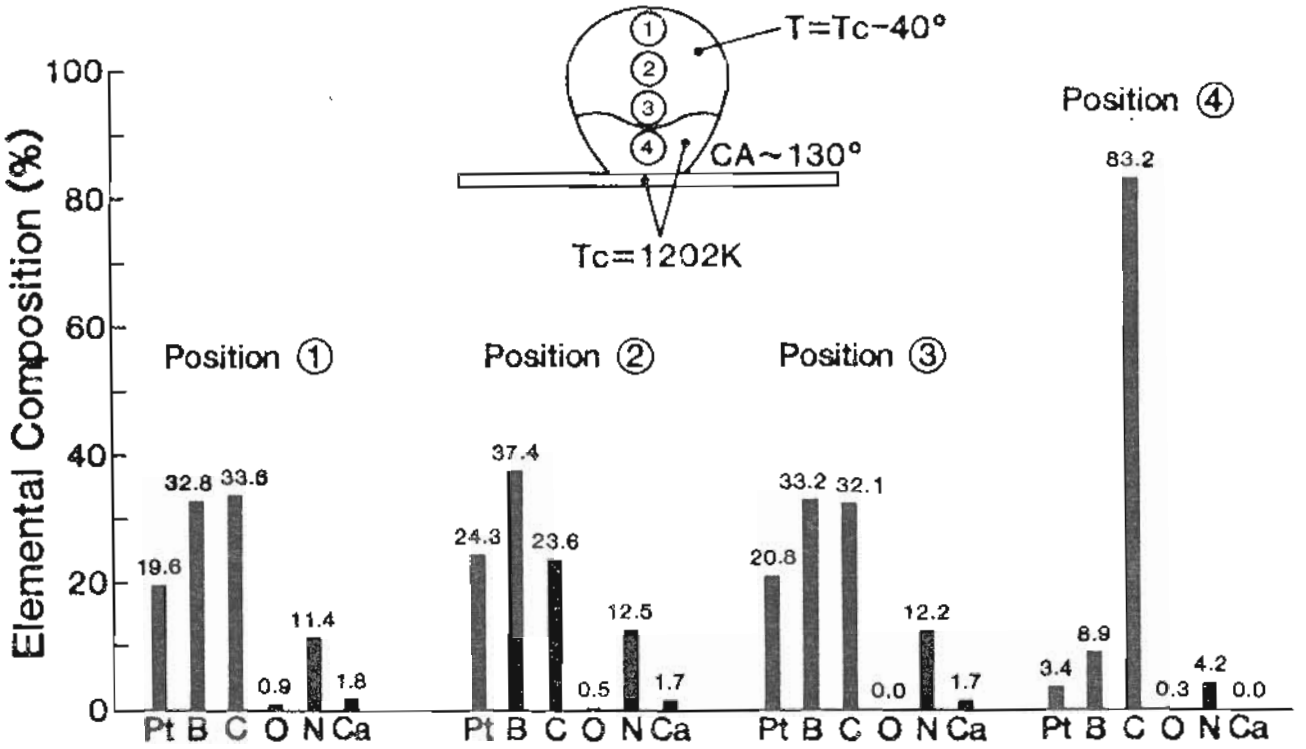

Figure 9-14. Auger surface elemental composition vs position for Pt/B (LANL: #273-5A; Pt=.72, B=.28) on vitreous carbon (LANL) while molten. High concentrations of C and N are present, and the BN chemical shift is found at all sampled locations.

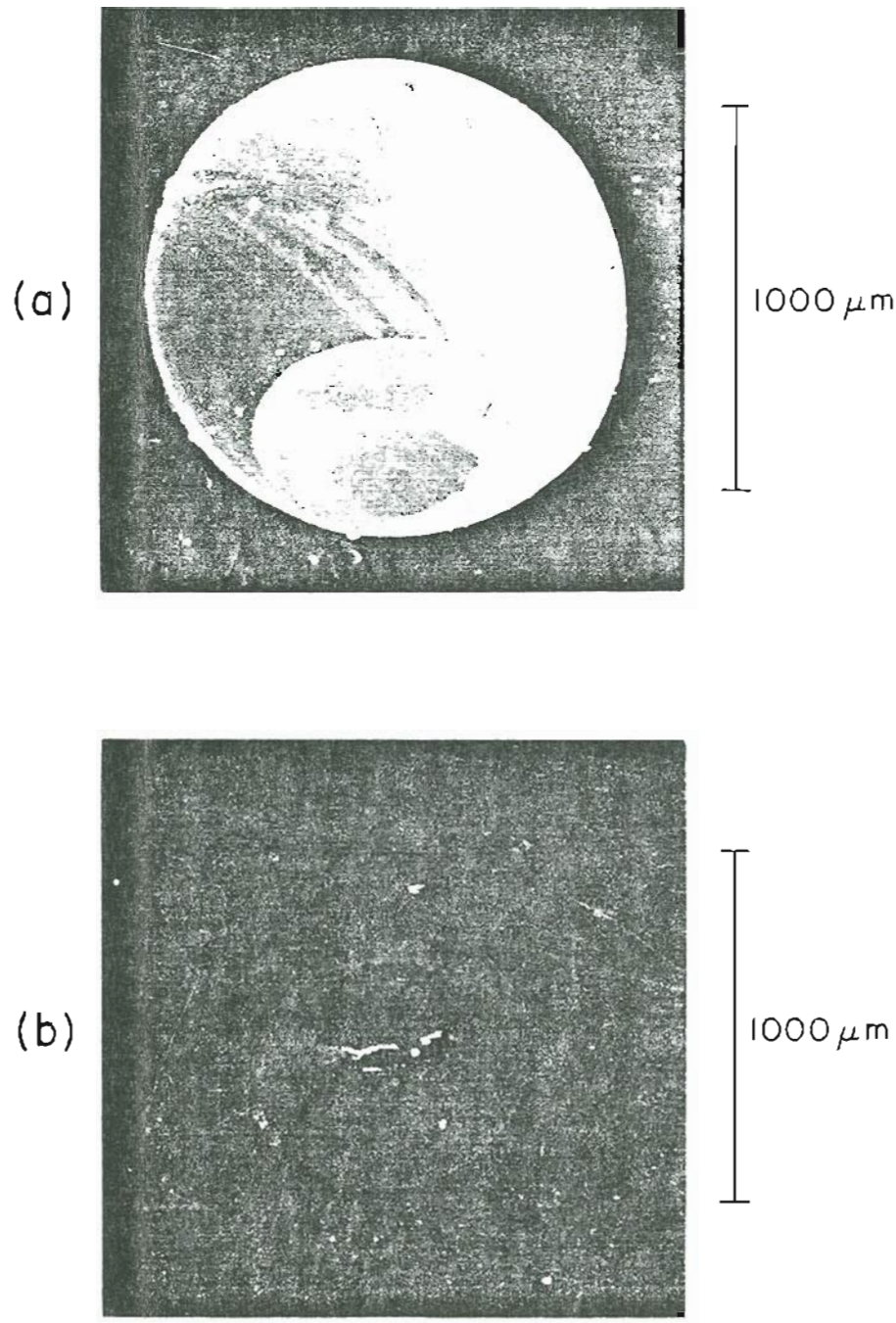

Figure 9-15. Views of the Pt/B alloy on vitreous carbon. (a) View of the alloy droplet which had rolled off the substrate; (b) The vitreous carbon surface where the alloy droplet had contact.

C. Wetting Studies of Ni/B to an Overlayer of W_6Co_7

Storms [1] suggested a series of wetting agents to improve the wetting of B-containing alloys to graphite. This section details a series of experiments which investigated the feasibility of using one of these agents in a liquid metal ion source.

The wetting agent offering the best promise of success was a tungsten-cobalt alloy. A slurry of W_6Co_7 alloy + acetone was painted atop a ribbon of polycrystalline graphite and an Auger spectrum of the surface layer was recorded. As seen in Figure 9-16, the tungsten-cobalt overlayer at temperatures near the melting point of the Ni/B alloy is heavily contaminated with O and Ca. This is not unexpected, as Table XI. shows that a number of compounds of W, O and Ca are strongly favored to form at 1300 K.

TABLE XI

GIBBS FREE ENERGIES OF FORMATION OF W, CO, AND CA OXIDES AT 1300 K

Compound	dG (kcal/mole)
WO_2	-83.5
WO_3	-123.9
CoO	-34.6
Co_3O_4	-100.0
CaO	-119.9

Wetting of Ni/B powder (Alfa) to this overlayer was excellent, consisting of a contact angle of near-zero. However, an Auger analysis of the alloy surface showed it to consist heavily of BN

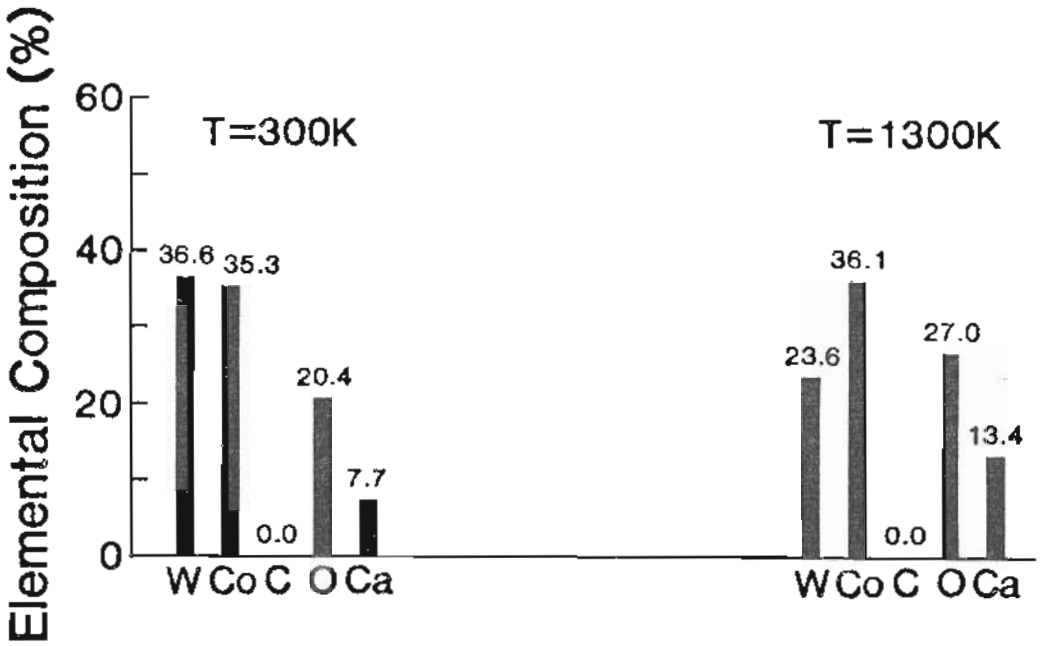

Figure 9-16. Auger surface elemental composition vs temperature for a slurry of W_6Co_7 (LANL) and acetone. The spectra were taken at the same position on the surface.

(Figure 9-17). As a result, the surface was solid during most of the experiment and did not flow past the W/Co overlayer and onto the virgin graphite. It is interesting that the W/Co overlayer causes wetting to occur despite its inability to tie up the segregated C and N in the same way that a boronized layer does. We have found this to be the case for wetting to most metallic substrates. In the absence of this gettering action, it appears that high-melting carbides and nitrides have a greater propensity to form at the top surface of the alloy, which is precisely where they cause the greatest harm. A boronized layer, by contrast, causes formation of these compounds at the interface instead of at the liquid-vacuum interface.

Figure 9-18 shows the wetted surface after system venting. The wetting is excellent, but the alloy has not spread to the virgin graphite. After 1.0 hour at temperatures near the melting point, no sign of either W or Co appeared at the alloy surface.

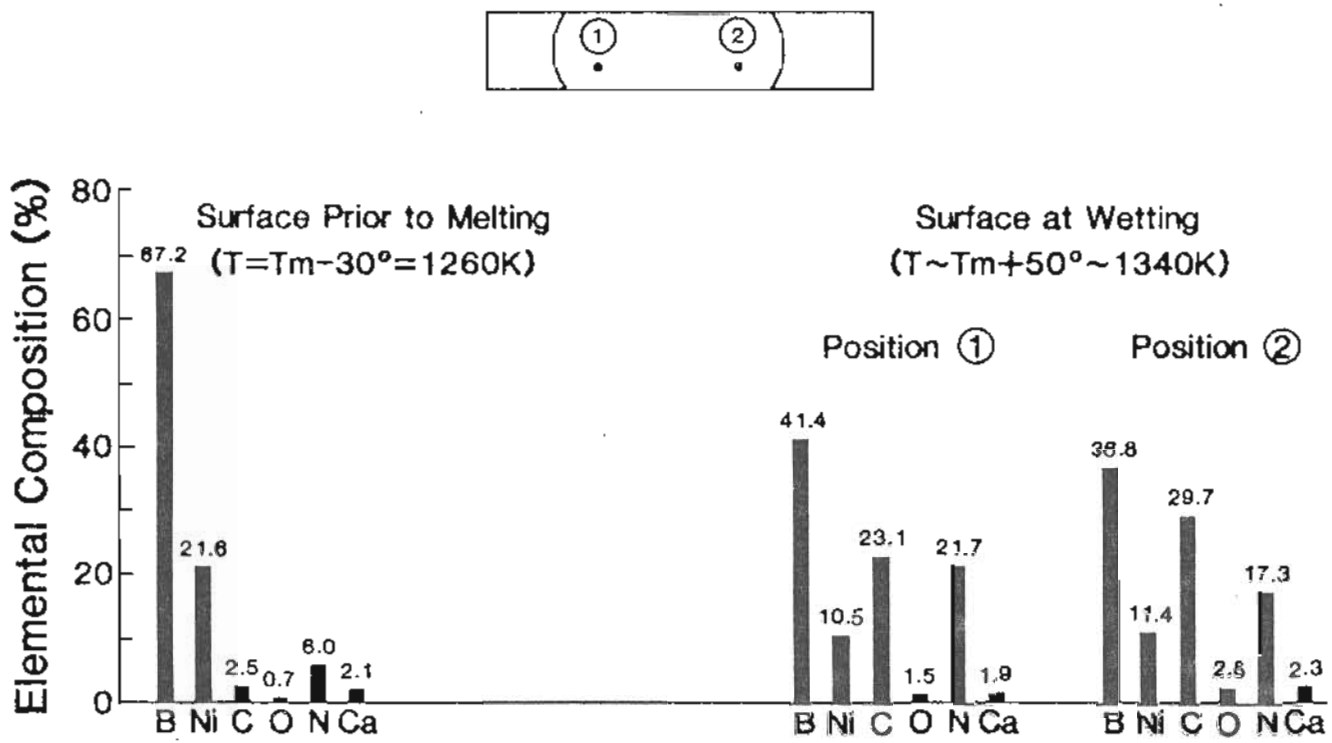

Figure 9-17. Auger surface elemental composition before and after wetting Ni/B powder (JD&M; #3) atop W_6Co_7. BN chemical shifts are found throughout the wetted surface. The surface composition changed little after 1 hour at T = 1340 K.

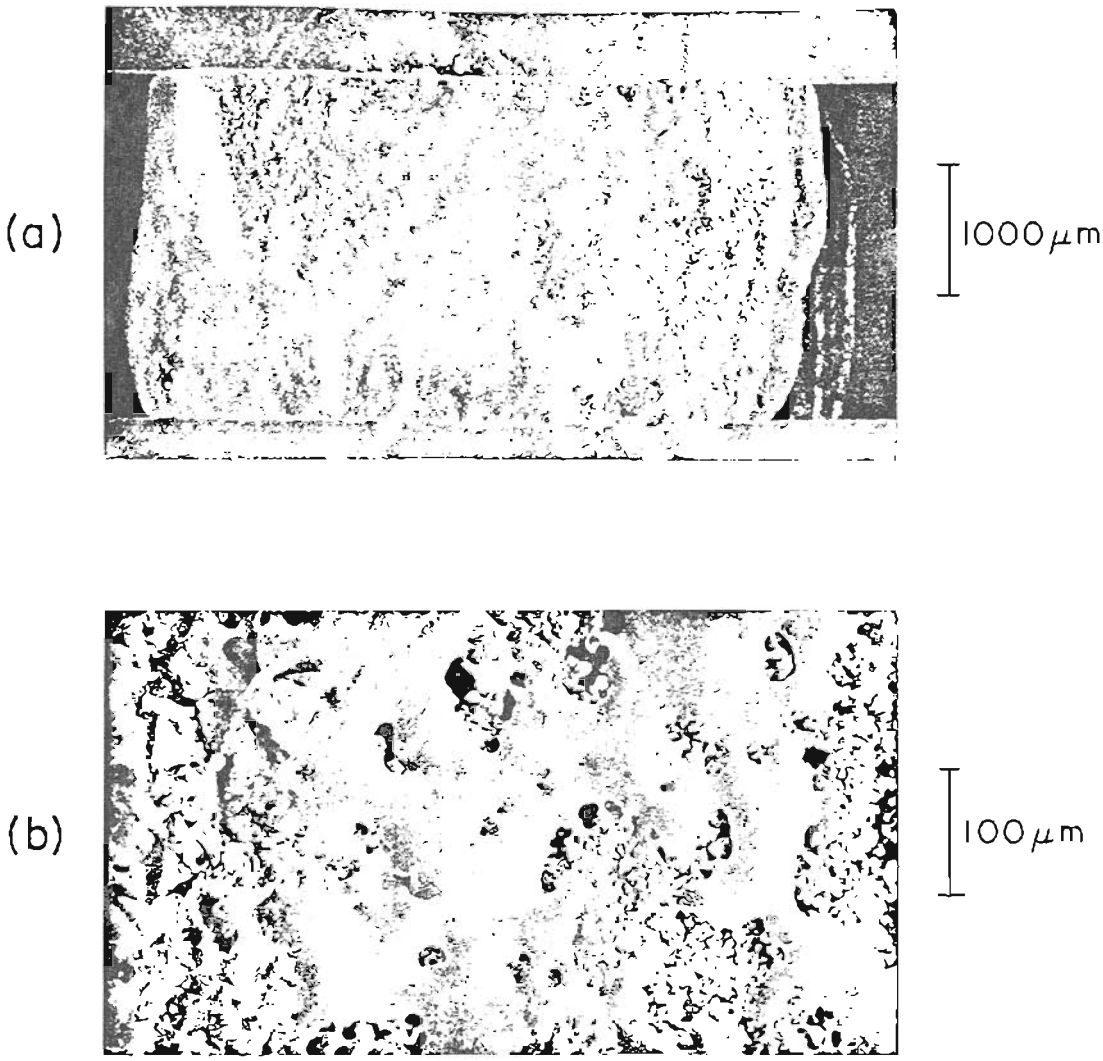

Figure 9-18. Views of the wetting of Ni/B powder (JD&M; #3) to W_6Co_7. (a) Overall view of the wetting; (b) A blowup of the alloy near the left-hand alloy/substrate boundary in (a).

REFERENCES

1. Edmund K. Storms, Los Alamos National Laboratory, private communication.

CHAPTER 10

CONCLUSIONS

Significant progress in our understanding of liquid alloy wetting has been attained as a result of this dissertation research. A number of contact systems have been identified which show excellent promise as liquid metal ion sources of B. Further, the problem of high vapor pressures in As-based contact systems has been completely solved, resulting in the first beam of As ions.

Thermochemical considerations are key to understanding the phenomenon of wetting in liquid metal contact systems containing B. The initial act of wetting is governed by the existence of rapid surface segregation of low-level nonmetallic impurities present in the alloys. These materials form a reaction barrier which inhibits contact between alloy and substrate and results in a poorly-wetted system. There are two obvious solutions to this problem. The first is to rid the alloy of these contaminants in the first place. The second is to break down the surface segregated material by chemical bonding to a surface coating with high affinity to the offending elements. This is precisely what happens when a graphite substrate is coated with free boron or silicon. Both of these elements form stable compounds with carbon, which is tied up at the interface between alloy and substrate. Direct contact between substrate and alloy is then possible, and wetting proceeds along normal thermochemical lines.

The existence of surface segregation in the alloys casts an air of suspicion on many previous studies of wetting, because low levels of carbon and nitrogen have been observed to segregate in every alloy system we have studied. This includes both As and B based materials, which were manufactured under entirely different processes and whose metallurgical properties are substantially different. Therefore, it appears that the use of pure materials and surface analytical techniques is imperative to the study of wetting. As we noted in the introduction, however, there have been very few studies of the liquid surface with surface sensitive instrumentation. This creates a situation where it is difficult for the researcher to defend the purity of his materials, and in particular, the purity of the surfaces of his materials. Since wetting is an interfacial phenomenon, assurances regarding the integrity of the surfaces of contacting phases are absolutely essential.

The first necessity in developing a liquid metal ion source of As in to lower the vapor pressure of As by as much as 10 orders of magnitude. This has been accomplished by use of a liquid compound rather than a liquid alloy. The compound lowers the vapor activity of As by way of chemical bonding, which is reflected through the Gibbs free energy function. A compound with a low Gibbs free energy is more stable than another form having a high Gibbs free energy. The vapor pressure of As is lowered because it is more energetically favorable for As to exist in the bound, compound liquid state than in the free gaseous state. In addition, As-based alloys have excellent contact properties with metals, since As is not so aggressive in

attacking refractory metals. Boron, on the other hand, attacks nearly all refractory metals.

Results for the most important contact systems we have studied and their potential for use in liquid metal ion sources of B or As are given in the Appendix.

APPENDIX

SUMMARY OF ALLOY PROPERTIES

Alloy: $Y_{62}Ni_{23}B_{15}$

Experimental Melting Point:	1102 K
Work Function:	3.5 eV
Volatility:	Minimal at the MP
Alloy Solubility in Substrate (@ MP):	Minimal on Re
Substrate Solubility in Alloy (@ MP):	Substantial dissolution of Re
Surface Percentage of B at MP:	40%. Lowers to 20% with Re dissolution.
Wetting Behavior:	Excellent on Re
Potential as LMI Source:	Poor. B tied up with Y and O. Little B in beam. Melting point increases with Re dissolution.

Alloy: $Ni_{55}B_{45}$

Experimental Melting Point:	1292 K (on C) 1192 K (on Si)
Work Function:	5.1 eV
Volatility:	Minimal at the MP
Alloy Solubility in Substrate (@ MP):	Minimal on C
Substrate Solubility in Alloy (@ MP):	Minimal on C 20% on C with Si overlayer Minimal on C with B overlayer
Surface Percentage of B at MP:	60%

Wetting Behavior:

Substrate	Comments
C (virgin)	Nonwetting. Large amounts of C and N on droplet surface. Excellent wetting when alloy is rid of contaminants.
C (with B overlayer--100%)	Excellent wetting. Little C at alloy surface.
C (with Si overlayer--100%)	Excellent wetting. 20% Si at alloy surface.
C (vitreous)	Fair wetting. In case one, CA* was 90 at wetting, lowering to 45 in 0.5 hour. In case two, CA > 90 with no decrease.
Al_2O_3	Nonwetting. Large amounts of C and N on droplet surface.
B (single-crystal)	Excellent wetting.
Boron carbide (B_4C)	Nonwetting on both CVD and single-crystal specimens. BN found near interface.

* Contact angle

B_5C	Fair wetting. CA initially 130, lowering to 45 in 2 hours. Better than B_4C, but not as good as pure B.
C (with Zr overlayer--20%)	Nonwetting. CA lowers slightly with time. Large amounts of C on droplet surface.
C (with Cr overlayer)	Mixed wetting. For surface of C with Cr overlayer (20%), CA was initially 130, lowering slightly with time. For surface of Cr carbide, CA was 75 with usual large amounts of C and N.
C (with Ni overlayer-70%)	Nonwetting. 20-40% C on droplet. BN and B_4C detected.
C (with Ti overlayer-10%)	Slight wetting. CA = 80.
C (with B overlayer-60%)	Nonwetting. Initially CA was 170, lowering to 90 in 5 minutes.
C (with B overlayer-80%)	Fair wetting. CA initially 160, lowering to 45 in 30 seconds.
C (with W_6Co_7 overlayer)	Excellent wetting. Substantial BN at surface. No sign of W after a few hours.
Potential as LMI Source	Good. Pure alloy wets C with minimal chemical reaction. Impure alloy wets C with B or Si layer similarly.

Alloy: $Pt_{72}B_{28}$

Experimental Melting Point:	1196 K
Work Function:	4.8 eV
Volatility:	Minimal at the MP
Alloy Solubility in Substrate (@ MP):	Minimal on C Substantial dissolution on Re
Substrate Solubility in Alloy (@ MP):	Minimal on C Minimal on Re
Surface Percentage of B at MP:	50%

Wetting Behavior:

Substrate	Comments
C (virgin)	Nonwetting. Droplet rolls off substrate.
C (with B overlayer--100%)	Good wetting. Powdered alloy has CA of near-zero. Solid alloy fragment has CA of 45.
Re	Excellent. However, B attacks Re and limits lifetime to < 20 hours.
C (vitreous)	Nonwetting.

Potential as LMI Source:	Good. Wets and spreads over C with boronized layer. Has low melting point. No C found in 100 hours of heating near MP.

Alloy: $Pd_{40}Ni_{40}B_{20}$

Experimental Melting Point:	Too contaminated to determine.
Work Function:	Too contaminated to determine.
Volatility:	Low. System pressure found to increase only at high temperatures
Alloy Solubility in Substrate (@ MP):	Minimal on C
Substrate Solubility in Alloy (@ MP):	Minimal on C
Surface Percentage of B at MP:	45%
Wetting Behavior:	Excellent on C when the alloy is rid of carbon.
Potential as LMI Source:	Difficult to determine, but suspected to be good.

Alloy: $Pd_{72}B_{28}$

Experimental Melting Point:	1310 K on C 1165 K on Si
Work Function:	-------
Volatility:	Minimal at the MP
Alloy Solubility in Substrate (@ MP):	-------
Substrate Solubility in Alloy (@ MP):	On C (with Si overlayer): 2% Si at surface and 6% in bulk
Surface Percentage of B at MP:	70%
Wetting Behavior:	Excellent on C (with Si overlayer)
Potential as LMI Source:	Good. Source structure has been made and tested. No Si observed after 70 hours at MP. Good heating characteristics, good wetting characteristics.

Alloy: Pd_2As

Experimental Melting Point:	1075 K
Work Function:	-------
Volatility:	Minimal at MP
Alloy Solubility in Substrate (@ MP):	Minimal on W
Substrate Solubility in Alloy (@ MP):	Minimal on W (for 150 hours)
Surface Percentage of As at MP:	20%
Wetting Behavior:	Excellent on W
Potential as LMI Source:	Excellent. Emitter has been manufactured and tested to 50 hours. Stable emission of As.

Alloy: $Pd_{50}B_{25}As_{25}$

Experimental Melting Point:	1050 K
Work Function:	-------
Volatility:	-------
Alloy Solubility in Substrate (@ MP):	Significant on Re
Substrate Solubility in Alloy (@ MP):	Excessive reaction with Re. Failure after 16 hours.
Surface Percentage of As at MP:	5%
Wetting Behavior:	Excellent once alloy has fully melted.
Potential as LMI Source:	Doubtful.

VITA

Michael J. Bozack was born in Lansing, Michigan and attended Lansing Eastern High School. He earned his B.S. and M.S. degrees in physics at Michigan State University, and then went on to receive an M.A. in systematic theology from Western Conservative Baptist Theological Seminary, where he was the 1979 valedictorian. He has been a research assistant at the National Superconducting Cyclotron Laboratory, a teaching assistant at Michigan State University, an instructor at Carnegie-Mellon University, and a research physicist with the Electron Devices Group at Tektronix, Inc. While at Michigan State, he served as a consultant for the self-paced physics program. Having a strong interest in physics education, he has completed a number of courses in science education, and was the highest rated physics instructor among faculty and graduate assistants at Michigan State and Carnegie-Mellon.

The author believes strongly in the dissemination of scientific research to the public, and has given several talks and seminars throughout the Northwest. He has taught a class in Practical Astronomy in the Saturday Academy, a program for gifted secondary students in the Portland metropolitan area, and has written several articles concerning the interrelation of science and theology.

The author is a member of the American Vacuum Society (AVS), the American Society of Metals (ASTM), the American Association of Physics Teachers (AAPT), and the American Physical Society (APS).